

Synthesis of Bicyclic Sulfones: Inhibitors of Neuraminidase

by

Michael Glenn Brant
B.Sc., University of Victoria, 2009

A Dissertation Submitted in Partial Fulfillment
of the Requirements for the Degree of

DOCTOR OF PHILOSOPHY

in the Department of Chemistry

© Michael Glenn Brant, 2015
University of Victoria

All rights reserved. This dissertation may not be reproduced in whole or in part, by
photocopy or other means, without the permission of the author.

Supervisory Committee

Synthesis of Bicyclic Sulfones: Inhibitors of Neuraminidase

by

Michael Glenn Brant
B.Sc., University of Victoria, 2009

Supervisory Committee

Dr. Jeremy Wulff, Department of Chemistry
Supervisor

Dr. Lisa Rosenberg, Department of Chemistry
Departmental Member

Dr. Peter Wan, Department of Chemistry
Departmental Member

Dr. Martin Boulanger, Department of Biochemistry and Microbiology
Outside Member

Abstract

Supervisory Committee

Dr. Jeremy Wulff, Department of Chemistry

Supervisor

Dr. Lisa Rosenberg, Department of Chemistry

Departmental Member

Dr. Peter Wan, Department of Chemistry

Departmental Member

Dr. Martin Boulanger, Department of Biochemistry and Microbiology

Outside Member

The lithiation of 3-sulfolene followed by subsequent treatment with an alkyl halide electrophile has been previously established as a method to produce 2-substituted-3-sulfolenes. Tandem reactivity with bis-alkyl halides has been observed to afford relatively simple bicyclic products. We hypothesized that it may be possible to access more complex bicyclic systems through use of bis-vinyl ketones as the electrophilic component. Herein, we present the outcome and mechanistic insights for the reaction between a variety of 3-sulfolene and substituted-3-sulfolene anions with bis-vinyl ketones to afford a variety of stereochemically complex fused, bridged and spiro bicyclic archetypes. The potential of these bicyclic-sulfone frameworks to act as molecular scaffolds for the generation of conformationally-restricted enzyme inhibitors is explored.

Potent monocyclic small molecules that inhibit influenza's neuraminidase enzyme have been developed as commercially successful antivirals. Similarly potent inhibitors against prokaryotic or eukaryotic neuraminidases have yet to be described. Selective inhibitors of these latter neuraminidase isozymes may provide useful treatments for bacterial infections (such as cholera and pneumonia) as well as a variety of cancers and metabolic disorders. A conformationally-restricted scaffold may prove ideal for designing selective (and potent) inhibitors against these underexplored enzymes. As a proof of principle, one of our rigid bicyclic-sulfone archetypes is elaborated to a drug-like scaffold that is shown to inhibit viral, bacterial and human neuraminidase enzymes.

Table of Contents

Supervisory Committee	ii
Abstract	iii
Table of Contents	iv
List of Schemes	vii
List of Figures	viii
List of Tables	xi
List of Abbreviations	xii
Acknowledgments	xvi
Dedication	xvii
Chapter 1 – Influenza and Neuraminidase	1
1.1.0. Influenza: The Disease and the Virus	1
1.2.0. Combating Influenza: Vaccines and Antivirals	4
1.3.0. Neuraminidase: Structure and Function	6
1.4.0. Viral Neuraminidase and the Generation of Potent Inhibitors	10
1.4.1. The Dihydropyran Scaffold: DANA, Zanamivir and Beyond	12
1.4.2. Oseltamivir and the Cyclohexene Scaffold	13
1.4.3. Peramivir: The Cyclopentane Scaffold	16
1.4.4. The Pyrrolidine Scaffold: A Hydrophobic S2 Subsite	17
1.4.5. Aromatic Inhibitors of Neuraminidase	19
1.4.6. Mechanism-Based Inhibitors and 150-Cavity Binders	20
1.5.0. Emergence of Mutation-Induced Resistance	22
1.6.0. Inhibitors of Human and Bacterial Neuraminidases	24
1.6.1. Human Neuraminidases (NEU1-4)	24
1.6.2. Bacterial Neuraminidases	27
1.7.0. Chapter Summary and Thesis Objectives	29
Chapter 2: Tandem Reactions of Bis-Vinyl Ketones and 3-Sulfolene	31
2.1.0. Introduction	32
2.1.1. The Anion of 3-Sulfolene	34
2.1.2. Applications of 3-Sulfolenes to Natural Product Synthesis	41
2.2.0. Reaction of 3-Sulfolene with Bis-Electrophiles	42
2.3.0. Origin of Diastereoselectivity of 2-5a and 2-7a	48
2.4.0. Variation of the Bis-Vinyl Ketone Coupling Partner	50
2.5.0. Application of the 2-7 Core Towards Neuraminidase Inhibition	52
2.6.0. Chapter Summary	53
Chapter 3. Bicyclic Inhibitors of Neuraminidase	55
3.1.0. Introduction	56
3.2.0. Synthesis of a Bicyclic S1, S2 Viral Neuraminidase Subsite Binder	61
3.3.0. Synthesis of a Bicyclic S1, S2, S3 Viral Neuraminidase Subsite Binder	72
3.4.0. Chapter Summary	80
Chapter 4. Tandem Reactions of Bis-Vinyl Ketones and 3-Substituted-3-Sulfolenes	82
4.1.0. Rationale and Literature Review:	83
4.2.0. Reactivity of 3-Substituted-3-Sulfolenes with Bis-Vinyl Ketones	87
4.3.0. 1,3-Diene Formation from the Bicyclic Sulfone Archetypes	94
4.4.0. Chapter Summary	95

Chapter 5. Targeting the S4 Subsite of Viral Neuraminidase.....	96
5.1.0. Introduction.....	97
5.2.0. C2 Alkylation.....	99
5.3.0. 1,3-Dipolar Cycloaddition of Vinyl Sulfones and Azomethine Imines.....	102
5.4.0. Tandem Reactivity of 2-Substituted 3-Sulfolenes and Bis-vinyl Ketones	104
5.5.0. Future Work:.....	105
Chapter 6. Experimental	107
6.1.0. General Remarks.....	107
6.1.1. Enzyme Assay Protocol	108
6.2.0. Chapter 2 Experimental	110
6.3.0. Chapter 3 Experimental:	121
6.4.0. Chapter 4 Experimental:	141
6.5.0 Chapter 5 Experimental:	150
Bibliography	161
Appendix A: NMR Data for Selected Compounds.....	178
Figure A-1. ¹ H NMR (CDCl ₃ 500 MHz) of vinyl-sulfone 2-7a	178
Figure A-2. ¹³ C NMR (CDCl ₃ 500 MHz) of vinyl sulfone 2-7a	178
Figure A-3. ¹ H NMR (D ₂ O 300 MHz) of amino-acid 3-34	179
Figure A-4. ¹³ C NMR (D ₂ O 300 MHz) of amino-acid 3-34	179
Figure A-5. ¹ H NMR (D ₂ O 500 MHz) of guanidino-acid 3-27	180
Figure A-6. ¹³ C NMR (D ₂ O 500 MHz) of guanidino-acid 3-27	180
Figure A-7. ¹ H NMR (CDCl ₃ 300 MHz) of [3.2.1]bicycle 4-5b	181
Figure A-8. ¹³ C NMR (CDCl ₃ 300 MHz) of [3.2.1]bicycle 4-5b	181
Figure A-9. ¹ H NMR (CDCl ₃ 300 MHz) of [5.4]spirocycle 4-6f	182
Figure A-10. ¹³ C NMR (CDCl ₃ 300 MHz) of [5.4]spirocycle 4-6f	182
Figure A-11. ¹ H NMR (CDCl ₃ 500 MHz) of benzyl-sulfone 5-4	183
Figure A-12. ¹³ C NMR (CDCl ₃ 500 MHz) of benzyl-sulfone 5-4	183
Appendix B: Crystallographic Parameters.....	184
Table B-1. Crystallographic parameters for 2-7a , 2-9b and 3-20	184
Table B-2. Crystallographic parameters for 3-29 , 3-33 and 3-37	185
Table B-3. Crystallographic parameters for 4-4c , 4-5b and 4-4e'	186
Table B-4. Crystallographic parameters for 4-6f , 5-5 and 5-10	187
Appendix C: Complete Listing of Bond Lengths and Angles	188
Figure C-1: ORTEP diagram of 2-7a with thermal ellipsoids shown at the 50% probability level.	188
Table C-1: Bond Lengths (Å) and Angles (°) for 2-7a	188
Figure C-2: ORTEP diagram of 2-9b with with thermal ellipsoids shown at the 50% probability level.	189
Table C-2: Bond Lengths (Å) and Angles (°) for 2-9b	189
Figure C-3: ORTEP diagram of 3-20 with thermal ellipsoids shown at the 50% probability level.	190
Table C-3: Bond Lengths (Å) and Angles (°) for 3-20	191
Figure C-4: ORTEP diagram of 3-29 with thermal ellipsoids shown at the 50% probability level.	192
Table C-4: Bond Lengths (Å) and Angles (°) for 3-29	192

Figure C-5: ORTEP diagram of 3-33 with thermal ellipsoids shown at the 50% probability level.	194
Table C-5: Bond Lengths (Å) and Angles (°) for 3-33	194
Figure C-6: ORTEP diagram of 3-37 with thermal ellipsoids shown at the 50% probability level.	195
Table C-6: Bond Lengths (Å) and Angles (°) for 3-37	195
Figure C-7: ORTEP diagram of 4-4c with thermal ellipsoids shown at the 50% probability level.	197
Table C-7: Bond Lengths (Å) and Angles (°) for 4-4c	197
Figure C-8: ORTEP diagram of 4-5b with thermal ellipsoids shown at the 50% probability level.	199
Table C-8: Bond Lengths (Å) and Angles (°) for 4-5b	199
Figure C-9: ORTEP diagram of 4-4e' with thermal ellipsoids shown at the 50% probability level.	202
Table C-9: Bond Lengths (Å) and Angles (°) for 4-4e'	202
Figure C-10: ORTEP diagram of 4-6f with thermal ellipsoids shown at the 50% probability level.	204
Table C-10: Bond Lengths (Å) and Angles (°) for 4-6f	204
Figure C-11: ORTEP diagram of 5-5 with thermal ellipsoids shown at the 50% probability level.	206
Table C-11: Bond Lengths (Å) and Angles (°) for 5-5	206
Figure C-12: ORTEP diagram of 5-10 with thermal ellipsoids shown at the 50% probability level.	208
Table C-12: Bond Lengths (Å) and Angles (°) for 5-10	208

List of Schemes

Scheme 1. Reaction of bis-vinyl ketone 2-2a with the 3-sulfolene anion to form 2-5a through a tandem γ -1,2 addition/anionic oxy-Cope.....	45
Scheme 2. Formation of the [3.3.0] bicycle 2-7a through a γ -1,2 addition.	47
Scheme 3. Formation of tricyclic sulfones using cyclic bis-vinyl ketones.....	51
Scheme 4. Synthesis of α - β -unsaturated ketone 3-6 from vinyl sulfone 2-7c	62
Scheme 5. Synthesis of carbamate 3-10 from vinyl sulfone 2-7c	63
Scheme 6. Conversion of vinyl sulfone 2-7e to carboxylic acid 3-16	65
Scheme 7. Synthesis of guanidino-ester 3-20 from carboxylic acid 3-16	66
Scheme 8. Conversion of vinyl sulfone 2-7e to ketone 3-30 ; installation of the S3 probing <i>N</i> -acetyl function.....	75
Scheme 9. Synthesis of S1, S2, S3 binder 3-34 from ketone 3-30	76
Scheme 10. Synthesis of guanidino-acid 3-27 and carbamido-amide 3-37	79
Scheme 11. Reaction of 3-methyl-3-sulfolene and 3-chloro-3-sulfolene with 2-2e	87
Scheme 12. Synthesis of 3-substituted-3-sulfolenes 2-1d and 2-1e	89
Scheme 13. Reaction of 3-thiophenyl-3-sulfolene and 3-phenyl-3-sulfolene with 2-2e . .	90
Scheme 14. Reaction of 3-carboxymethyl-3-sulfolene and 3-cyano-3-sulfolene with 2-2e	91
Scheme 15. Reaction of 3-bromo-3-sulfolene and 3-sulfonyltolyl-3-sulfolene with 2-2e	92
Scheme 16. Reaction of 3,4-diphenyl-3-sulfolene with 2-2e	93
Scheme 17. Cheletropic removal of sulfur dioxide from 3-sulfolenes and 2-sulfolenes..	94
Scheme 18. Successful C2-alkylation studies performed on reduced vinyl sulfones 5-3 and 3-12	99
Scheme 19. Alkylation study of 5-7 using previously optimized <i>t</i> -BuLi and THF.....	100
Scheme 20. Successful C2-methylation of globally protected sulfone 5-10	101
Scheme 21. Dipolar cycloaddition of cyclic azomethine imines with a variety of monocyclic and bicyclic vinyl sulfones.	103
Scheme 22. Tandem reactivity of 2-substituted-3-sulfolenes and bis-vinyl ketone 2-2e	105

List of Figures

Figure 1. Notable influenza pandemics and the two mechanisms of influenza evolution..	1
Figure 2. Structure of the influenza A virus. (NS1 is a gene product but not present in the assembled virions).	3
Figure 3. Therapeutics targeting the influenza A virus.....	5
Figure 4. Substrates and cleavage products of sialidases, where R = the rest of the glycoconjugate which is attached to the cell surface.	7
Figure 5. Comparison of active sites of N1 viral (PDB: 2BAT), hNEU2 human (PDB: 2F0Z), and NanA (PDB: 2YA7) bacterial neuraminidase. Putative catalytic residues are underlined.	8
Figure 6. Mechanism of <i>exo</i> -sialidase based hydrolysis of Neu5Ac from glycoconjugates.	9
Figure 7. Surface and ribbon view of a N2 neuraminidase complexed with Neu5Ac. (PDB: 2BAT).	10
Figure 8. Active site residues and active site map of an N2 viral neuraminidase. (PDB: 2BAT)	11
Figure 9. Dihydropyran inhibitors of neuraminidase.....	12
Figure 10. Longer duration of action analogs of zanamivir.....	13
Figure 11. Evolution of the dihydropyran scaffold.....	14
Figure 12. Optimization of the hydrophobic side-chain and conformation change upon binding of oseltamivir. Glu276 (yellow, apo form of the enzyme), Glu276 and Arg224 (green, bound oseltamivir).	15
Figure 13. Development of the cyclopentane based scaffold.	16
Figure 14. Development of pyrrolidine inhibitor A-315675.	18
Figure 15. Some aromatic inhibitors of viral neuraminidase.....	19
Figure 16. Mechanism-based covalent inhibitors of NA.	20
Figure 17. 150-cavity binders and a potent carboxylic-zanamivir analog. A: N1, B: N9. 21	
Figure 18. Bound structure of oseltamivir and zanamivir overlayed with the WT and H274Y mutant enzymes.....	22
Figure 19. A: Zanamivir complexed with N8 neuraminidase (PDB: 2HTQ). B: Zanamivir complexed with NEU2 (PDB: 2F0Z). C: Overlay of zanamivir co-structures.....	25
Figure 20. IC ₅₀ values of inhibitors designed to target the human neuraminidases (NEU1-4).	26
Figure 21. Cycloaddition reactions of sulfur dioxide and some representative dienes. ...	32
Figure 22. Origin of stereospecificity in the (4+1) cheletropic ring closure and retro-(4+1) ring opening of <i>cis</i> -2,5-dimethyl-3-sulfolene and <i>trans</i> -2,5-dimethyl-3-sulfolene.	33
Figure 23. Cheletropic removal of sulfur dioxide from the alkylated butadiene sulfone anion and ring-opening of the butadiene sulfone anion at -78 °C.....	34
Figure 24. Alkylation of cyclopentadiene-masked 3-sulfolene with <i>n</i> -BuLi where X = halogen.....	35
Figure 25. Alkylation of vitamin D-3 derivative with methyl iodide.	36
Figure 26. Alkylation of 3-sulfolene using alkyl halides and LiHMDS.....	37
Figure 27. Alkylation of 3-sulfolene using alkyl halides and NaH.	38
Figure 28. Acylation of 3-sulfolenes with <i>n</i> -BuLi.....	39

Figure 29. Use of 3-sulfolenes in the total synthesis of a few representative natural products.....	41
Figure 30. Numbering system employed for describing the reaction between bis-electrophiles and 3-sulfolenes.....	42
Figure 31. Formation of [3.3.0] and [3.2.1] ring systems from 3-sulfolene and bis-alkyl halides.....	43
Figure 32. Proposed retrosynthesis of cyclononenone precursor (2-3) and known reactions of the butadiene sulfone anion with methyl vinyl ketone.....	44
Figure 33. Reaction of 3-methyl-3-sulfolene with mono-vinyl ketones.....	46
Figure 34. Possible transition states leading to anionic oxy-Cope product 2-5	49
Figure 35. Possible transition state leading to γ -1,2-addition product 2-7 . The orange bracket indicates an unfavorable steric interaction.....	50
Figure 36. Overlay of 2-7a (solid phase) and peramivir (enzyme bound).....	53
Figure 37. Examples of some rigidification strategies.....	56
Figure 38. (A): The four conformations of peramivir found in the solid-state X-ray structure of the unbound molecule. (B): Enzyme-bound structure of peramivir in the active site of four influenza A neuraminidases, PDB 2HTU (grey), 1L7F (cyan), 1L7G (green), and 1L7H (magenta); (C): Overlay of computationally determined solution structure of peramivir (grey) overlaid with unbound peramivir (cyan). (D): Overlay of computationally determined solution structure of peramivir (grey) with enzyme-bound peramivir (1L7F, cyan) (E): Crystal structure of 2-7a (green) and overlay of crystal structure of 2-7a with enzyme bound peramivir (cyan, PDB 2HTU).....	58
Figure 39. Known bicyclic inhibitors of influenza neuraminidase.....	59
Figure 40. Sulfone 3-1 (R=H) in the neuraminidase active site. Overlay of sulfone 3-1 (green) with peramivir (cyan) docked in the neuraminidase active site.....	60
Figure 41. Retrosynthesis of guanidino-acid 3-1 from vinyl sulfone 2-7c via a Curtius rearrangement.....	61
Figure 42. Retrosynthesis of guanidino-acid 3-1 from vinyl sulfone 2-7e	64
Figure 43. Synthesis of guanidino-acid 3-1 from guanidino-ester 3-20 . Action of neuraminidase on the fluorescent substrate.....	67
Figure 44. Raw fluorescence data for guanidino-acid 3-1 (top) and IC ₅₀ curve for 3-1 (bottom).....	68
Figure 45. Comparison of monocyclic and bicyclic S1, S2 neuraminidase subsite binders.....	69
Figure 46. Michaelis-Menten plot (top) and Lineweaver-Burk plot (bottom) for guanidino-acid 3-1 against NP-40 inactivated H1N1 virus.....	70
Figure 47. Determination of K _i for guanidino-acid 3-1 against NP-40 inactivated H1N1 virus.....	71
Figure 48. Three subsite binding analogs of zanamivir, oseltamivir and peramivir.....	73
Figure 49. A regiochemical switch of guanidinium and carboxylate functions to achieve a three subsite binder derived from common precursor (+/-)- 2-7e	74
Figure 50. Activity of amino-acid 3-34 against H1N1 whole virus, recombinant N1 neuraminidase, an N1 H274Y mutant, bacterial neuraminidases <i>V. cholerae</i> and <i>C. perfringens</i> and human neuraminidases NEU1, NEU2, NEU3 and NEU4.....	77

Figure 51. Comparison of activities of S1, S2 and S3 subsite binders constructed from the [3.3.0]bicyclic (3-34), cyclopentane (1-15), dihydropyran (3-24), cyclohexene (1-11) and aromatic (BANA108) templates.	81
Figure 52. Use of 3-substituted-3-sulfolenes to access up to six bicyclic archetypes.	83
Figure 53. Regiochemical methylation of 3-substituted-3-sulfolenes.	84
Figure 54 Dialkylative couplings of 3-sulfolene (2-1a), 3-methyl-3-sulfolene (2-1b) and 3-chloro-3-sulfolene (2-1c) with bis-alkyl halides.	85
Figure 55. Dialkylative coupling of 3-thiophenyl-3-sulfolene with bis-alkyl halides.	86
Figure 56. Origin of diastereoselectivity during α -1,2 addition.	88
Figure 57. Summary of X-ray structures of each structural archetype prepared.	95
Figure 58. Targeting the S4 subsite (shaded green) of viral neuraminidase. 5-1a (yellow) peramivir (cyan).	97
Figure 59. Summary of approaches to arrive at C2 functionalized analogs of 3-34	98
Figure 60. Dipolar cycloaddition using an azomethine imine in order to access 5-2	102
Figure 61. Use of 2-substituted-3-sulfolenes as a way to access key intermediate 5-2	104
Figure 62. Bicyclic templates for the generation of conformationally-restricted enzyme inhibitors of neuraminidase.	106

List of Tables

Table 1. Clinically relevant mutations conferring resistance to NA inhibitors.	23
Table 2. Some properties of the human neuraminidases.	24
Table 3. Activities of potent influenza neuraminidase inhibitors against bacterial neuraminidases.	28
Table 4. Reaction of zinc-sulfenylate with a variety of electrophilic partners.	40
Table 5. Scope of the tandem γ -1,2 addition/anionic oxy-Cope, followed by a γ -1,2 addition.	51

List of Abbreviations

δ	chemical shift
μg	microgram
μM	micromolar
^{13}C NMR	Carbon Nuclear Magnetic Resonance
^1H NMR	Proton Nuclear Magnetic Resonance
\AA	angstrom
Ac	acetyl
aq.	aqueous
Bn	benzyl
Boc	<i>tert</i> -butyloxycarbonyl
br	broad
calcd	calculated
CBZ	carboxybenzoyl
CDC	Centers for Disease Control
cm^{-1}	wavenumbers
COSY	$^1\text{H} - ^1\text{H}$ correlation spectroscopy
d	doublet
dd	doublet of doublet
ddd	doublet of doublet of doublets
DPPA	diphenyl phosphoryl azide
DBU	1,8-diazabicyclo[5.4.0]undec-7-ene
DEPT	distortionless enhancement by polarization transfer
DFT	Density Functional Theory
DMAP	<i>N,N</i> -dimethylaminopyridine
DMF	dimethylformamide
DMSO	dimethyl sulfoxide
dq	doublet of quartets
<i>dr</i>	diastereomeric ratio
dt	doublet of triplets

E	enzyme
e.g.	for example
EI	enzyme-inhibitor complex
<i>epi</i>	epimer
eq.	equivalents
ES	enzyme-substrate complex
ESI	enzyme-substrate-inhibitor complex
Et	ethyl
NEt ₃	triethylamine
FT-IR	Fourier Transform Infrared
g	grams
HA	hemagglutinin (H)
HRMS	High resolution mass spectrometry
Hz	hertz, s ⁻¹
<i>i.e.</i>	that is
IC ₅₀	maximal inhibitory concentration
IR	infrared spectroscopy
J	coupling constant
k _{cat}	catalytic rate constant
K _d	dissociation rate constant
kDa	kiloDalton
KHMDS	potassium hexamethyldisilazide
K _i	inhibition constant
K _m	Michaelis-Menten rate constant
L	litre
LC-MS	liquid chromatography-mass spectrometry
LiHMDS	lithium hexamethyldisilazide
M	molar
m	multiplet (or multiple overlapping resonances)
<i>m</i> CPBA	<i>meta</i> -chloroperoxybenzoic acid
M ⁺	molecular ion

MD	Molecular Dynamics
mg	milligrams
MHz	megahertz
mM	millimolar
mmol	millimoles
mol	moles
mp	melting point
MS	mass spectrometry
Ms	methanesulfonyl
NA	viral neuraminidase
ng	nanogram
nM	nanomolar
NaHMDS	sodium hexamethyldisilazide
NMO	<i>N</i> -methylmorpholine <i>N</i> -oxide
NOE	nuclear Overhauser enhancement
NOESY	nuclear Overhauser enhanced spectroscopy
°C	degrees Celsius
<i>p</i>	<i>para</i>
Ph	phenyl
PMP	<i>p</i> -methoxyphenyl
q	quartet
R	generalized substituent
RNA	ribonucleic acid
RT	room temperature
s	singlet
S	substrate
<i>t</i> or <i>tert</i>	tertiary
t	triplet
THF	tetrahydrofuran
TLC	thin layer chromatography
TMS	trimethylsilyl

FDA	Food and Drug Administration
WHO	World Health Organization
WT	wild type
TBAB	tetrabutylammonium bromide

Acknowledgments

This thesis and the work presented within would have been impossible without the help of a vast number of individuals. Firstly, I would like to thank Dr. Jeremy Wulff for accepting this individual into his research group when I was an undergraduate student. I would like to secondly thank the legend Dr. Caleb Bromba for initially training me and providing frequent wisdom. Thirdly, the rest of the Wulff graduate students who entertained me, taught me a few things, and who have become some of my closest friends: Dr. Katherine Davies, Dr. Natasha “Little Buddy” O’Rourke, Dr. Jason Davy, Jun Chen and Ronan Hanley. In addition to these fine individuals, I would like to thank all of the Wulff group undergraduate students whom I have worked closely with over the years: Steven Wong, Jeremy Mason, Jordan Friedmann, Connor Bohlken, and many others. A big thanks to Dr. Emma Nicholls-Allison who has helped me more than anyone in this endeavor (especially getting to group meetings on time).

I would like to acknowledge my committee for their support and guidance: Dr. Martin Boulanger, Dr. Lisa Rosenberg and Dr. Peter Wan. Thank you also to Dr. Adrian Schwan for making the journey to UVic. On the research side of things, I would like to thank the collaborators for the neuraminidase project: Dr. Martin Boulanger and Dr. Christopher Cairo as well as Dr. Amgad Albohy. My job would be infinitely more difficult without the hard work of the UVic staff: Chris Greenwood, Chris Barr, Dr. Ori Granot, Dr. Tyler Trefz, Sean Adams, Andrew McDonald the entire staff at Sciences Stores, and many others.

On the personal side of things, the rest of the UVic graduate students have made this experience thoroughly enjoyable and memorable. Huge thanks to Dr. Dave Berry and Kelli Fawkes for their mentorship and igniting my inner teacher. Finally, I would likely not be here right now without the effort of Dr. Paul Steinbok and his colleagues, I am forever thankful.

Dedication

To my friends, family, HF, and my (formerly alive) pets

Chapter 1 – Influenza and Neuraminidase

1.1.0. Influenza: The Disease and the Virus

Sporadically occurring influenza A pandemics have plagued the human race for centuries (Figure 1).¹⁻³ The 1918 H1N1 Spanish flu infected an estimated one third of all humans and eradicated 3-5% of the total population.⁴ Unlike its less infectious relatives influenza B and C, the influenza A virus is able to infect a large variety of animals including birds, swine, equine and water mammals.⁵ Migratory aquatic birds are hypothesized to be the primary natural reservoir for the influenza A virus; the intermingling of influenza A carrying hosts with large populations of influenza harboring migratory birds is believed to be the mechanism for the arrival of new influenza strains into the human population.^{5,6} The influenza virus is spread through direct contact with an infected host, contaminated surfaces/objects or through aerosol droplets produced during coughing, sneezing or speaking.⁷ Once exposed, a broad range of illness can result ranging from symptomless infection, mild or severe respiratory syndromes as well as an increased susceptibility to bacterial infections (such as pneumonia).⁸ Between pandemic years, it is estimated by the WHO that seasonal strains of the virus (and localized epidemics of novel strains) contribute to the deaths of ~200,000 people annually worldwide.⁹

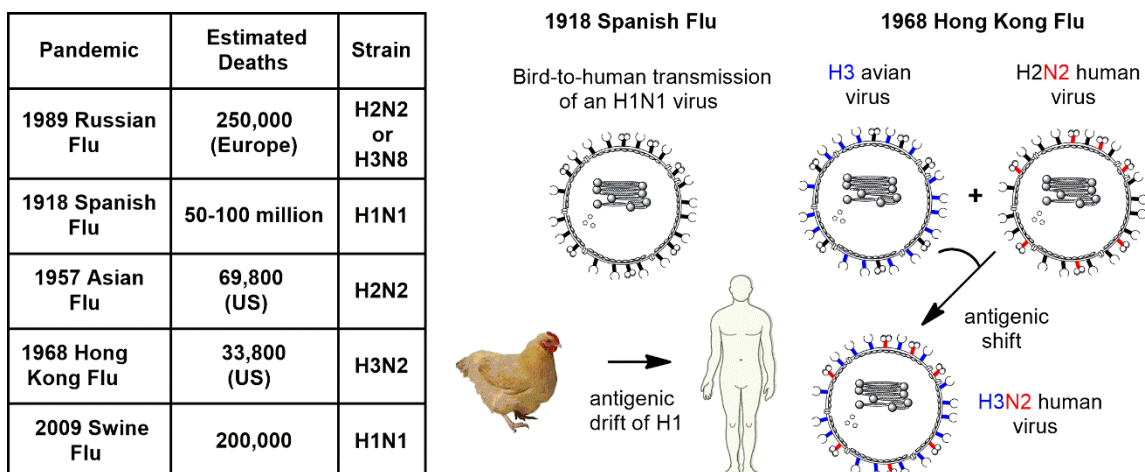


Figure 1. Notable influenza pandemics and the two mechanisms of influenza evolution.

The emergence of pandemic strains of influenza A can be attributed to the antigenic shift and antigenic drift of the genetic sequence that encodes for two proteins expressed by the influenza virus: hemagglutinin (HA) and neuraminidase (NA).¹⁰ HA and NA, both present on the surface of the virion, are under constant selective pressure from the host immune system. Each strain of influenza A is classified by its antigenic differences in HA and NA; sixteen subtypes of hemagglutinin have been characterized (H1-16), along with nine neuraminidases (N1-N9).¹⁰⁻¹² Recently, two novel strains (H17N10 and H18N11) from “influenza-like” viruses were isolated from Central and South American fruit bats.¹³ Of the many subtypes only N1 and N2, and H1, H2 and H3 have developed stable lineages in the human population, with the other strains mostly limited to aquatic birds. Antigenic drift involves the accumulation of mutations (insertions, deletions, and substitutions) in the viral genome allowing the virus to evade the host immune response. Each round of error-prone viral replication produces a diverse population of genetically diverse virions; the fittest virions gain a select advantage over their viral colleagues producing new mutant variants. The Spanish flu is believed to be caused by antigenic drift; a single point mutation to the hemagglutinin gene allowed the avian H1N1 virus (selective for Neu5Ac- α 2,3-galactose receptors, Figure 4) to more effectively bind to the human sialic receptors (Neu5Ac- α -2,6-galactose, Figure 4), and thus more efficiently infect humans.¹⁴ With no pre-existing antibodies to either surface antigen, the avian derived H1N1 strain was especially lethal to the human population. The second mechanism of viral evolution (antigenic shift) involves the mixing of genes from two viruses of different origins. For example the 1968 H3N2 Hong Kong influenza is believed to be caused by the reassortment of genes between a H2N2 human virus and an H3 from an avian virus (Figure 1).¹⁵

The influenza A virus is a very simple (but effective) packet of biological ferocity (Figure 2). Inside the host-derived 80-120 nm (in diameter) lipid bilayer envelope are 8 segments of single stranded negative-sense RNA which encode for ten major gene products: the surface proteins HA and NA, a matrix protein (M1), a proton ion channel (M2), a non-structural protein (NS1), three polymerase components (PB1, PB2 and PA), a nucleoprotein (NP) and a nuclear export protein (NEP).^{5, 16} HA recognizes the host cell by

weakly binding terminal *N*-acetylneuraminic acid (**1-1**, Neu5Ac) receptors in the respiratory tracts of the host, and is also responsible for inducing membrane fusion.¹⁷ NA cleaves Neu5Ac residues from glycoconjugates allowing release of the newly synthesized virions from the surface of the host cell after budding (via exocytosis) of the viral progeny.⁵ It is estimated that each virion contains approximately 100 copies of neuraminidase and 500 copies of hemagglutinin on its surface.¹⁸ The proton selective ion channel (M2) is involved in the uncoating of the endosome-entrapped virus during cell fusion.^{19, 20} The nucleoprotein (NP) encapsulates the RNA segments while the most abundant protein, a matrix protein (M1) surrounds the space between the viral envelope and NP-encapsulated RNA. PB1, PB2, PA constitute the RNA-dependent RNA polymerase (RdRp) complex responsible for the replication of the viral RNA. Four other gene products (PB1-F2,²¹ PB1-N40,²² PA-X,²³ and M42)²⁴ have been recently identified. Point mutations are extremely common during viral replication (1 per 1000-10,000 bases) since the influenza RdRp complex lacks the ability to proof read during transcription. Two non-structural proteins are involved with viral replication and signaling (NS1 and NEP): NEP mediates the nuclear export of the viral protein-RNA complex after replication occurs in the host cell while NS1 is involved in blockade of the host immune response by inhibiting interferon synthesis.²⁵

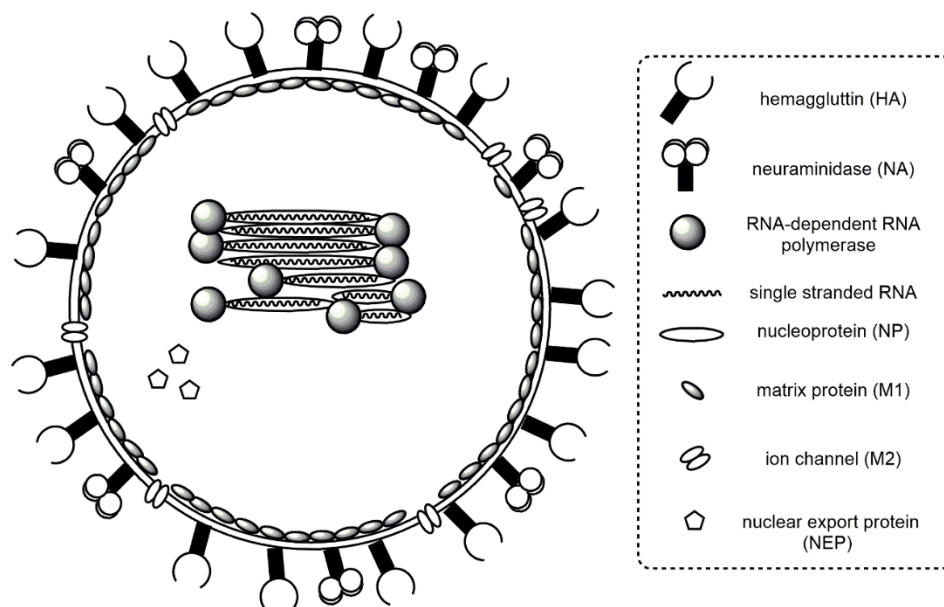


Figure 2. Structure of the influenza A virus. (NS1 is a gene product but not present in the assembled virions).

1.2.0. Combating Influenza: Vaccines and Antivirals

The inhibition of viral enzymes and proteins by substrate analogs, transition state analogs or allosteric compounds is a concept that is widely used in pharmacology to suppress the replication of disease causing pathogens. As of 2015, five antiviral therapies have been successfully approved by the FDA against two of the gene products produced by the influenza A virus. Despite these successes, vaccination remains the primary preventative measure in reducing infection by influenza.²⁶ The formulation of the vaccine contains either detergent inactivated whole-virus (split-product) or a mixture of partially purified virus HA and NA proteins.²⁶ The WHO GISN (global influenza surveillance network) identifies which strains may be especially problematic during the coming season and selects circulating version of H1N1, H3N2 and a B virus to include in the regional trivalent vaccines.²⁷ The effectiveness of the seasonal vaccine at preventing symptomatic laboratory-confirmed influenza has been estimated at the 70-90% level for healthy individuals.²⁸ Predicting which strains will be circulating often leads to delays with preparation of the yearly vaccine.²⁹ In order to combat non-seasonal influenza strains (which may lead to local epidemics or large scale pandemics) and to treat individuals who are already infected with the virus, significant research has gone into developing antivirals against nearly all of the influenza gene products.

Before 1999 and the approval of the neuraminidase inhibitors zanamivir (Relenza®) and oseltamivir (Tamiflu®), only two other antiviral treatments against influenza were approved by the FDA, amantadine (Symmetrel®, approved in 1966)³⁰ and rimantadine (Flumadine®, approved in 1994).³¹ Both of these compounds (Figure 3) bind in the *N*-terminal hydrophobic pore of the M2 channel, preventing the uptake of protons via electrostatic repulsion with the positively charged amino groups.^{20, 32} This interaction impedes the uncoating of the viral envelope after endocytosis, preventing the viral RNA from entering the cytoplasm.¹³ However, since the 2005-2006 flu season it has been estimated that >90% of all influenza strains are now resistant to rimantadine and amantadine due to antiviral induced point mutations S31N, V27A and L26F.^{33, 34} Some

success targeting these mutants has been achieved, though no new M2 inhibitors have entered clinical trials thus far.³⁵⁻³⁷

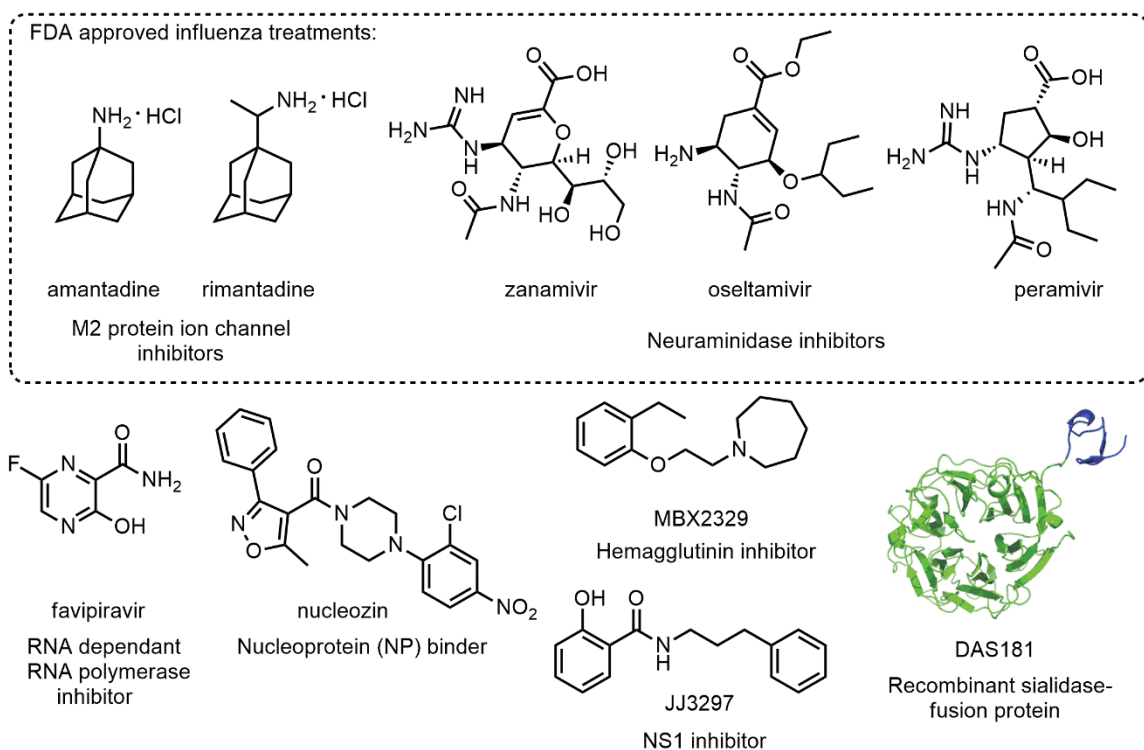


Figure 3. Therapeutics targeting the influenza A virus.

Other influenza therapies targeting other viral proteins are currently in pre-clinical or clinical development (Figure 3). An interesting strategy (currently in phase II clinical trials as of 2014)³⁸ is the administration via inhalation of a sialidase-fusion protein DAS181 (Fludase®).³⁹ DAS181 consists of a bacterial sialidase from *Actinomyces viscosus* fused to a human protein (amphiregulin, in order to assist in a epithelium-anchoring)³⁸ and acts to cleave off the Neu5Ac receptors in the upper respiratory tract; cells thus become less susceptible to influenza infection since hemagglutinin can no longer initiate contact.³⁹ Success has been achieved targeting the RNA-dependant RNA polymerase complex of influenza using the pyrazinecarboxamide favipiravir (phase III clinical trials as of 2014).⁴⁰ Favipiravir is also an inhibitor of viral replication of many other RNA viruses (including the influenza, West Nile, yellow fever and Ebola viruses).^{40, 41} It has been established that favipiravir induces a high rate of errors during viral replication, leading to nonviable viral

progeny.⁴² The nucleoprotein (NP) of influenza has also been shown to be a druggable target using nucleozin.⁴³ The binding of nucleozin causes NP to aggregate and antagonizes its nuclear accumulation, leading to cessation of viral replication.⁴³ Small molecules that target hemagglutinin (binding to the HA2 domain) prevent viral entry into the cell,⁴⁴ with one example depicted in Figure 3.⁴⁵ NS1 inhibitor JJ3297 has been reported to inhibit viral replication by restoring interferon production assisting with the cell's defense against the infection.⁴⁶

Inhibitors against nearly all of the gene products expressed by the influenza A virus are currently in clinical or pre-clinical development stages (Figure 3). Although encouraging, the only FDA approved drugs against influenza are currently the M2 inhibitors and neuraminidase inhibitors. Unfortunately, due to their widespread use amantadine and rimantadine are no longer approved by the CDC for the treatment of influenza.⁴⁷ Neuraminidase inhibitors are currently the only recommended antiviral medication approved for use today for the prophylaxis and treatment of influenza. However mutation-induced resistance now threatens the efficacy of all three currently approved NA inhibitors (Section 1.5).⁴⁸ The development of inhibitors of viral neuraminidase will be the subject of extensive discussion in Section 1.4, while the structure and function of neuraminidase will be discussed in the ensuing section.

1.3.0. Neuraminidase: Structure and Function

Exo-sialidases (also called neuraminidases, or commonly just sialidases) are glycosylase ("sugar cleaving") enzymes that catalyze the hydrolysis of terminal *N*-acetylneuraminic acid (**1-1**, Neu5Ac) residues linked in a α -(2,3), α -(2,6) or α -(2,8) fashion to glycoconjugates such as glycolipids and glycoproteins found on the surface of cells (Figure 4).⁴⁹ Sialidases with varied substrate and linkage specificity are encoded by organisms throughout the natural world including viruses,⁵⁰ mammals,⁵¹ bacteria,⁵² protozoa,⁵³ and fungi.⁵⁴ Anionic Neu5Ac residues have a wide range of functions in the cell ranging from stabilization of cell membranes, binding and transportation of ions and molecules, modulation of transmembrane signalling by masking or enhancing recognition

sites, protecting groups for glycoproteins, and stabilizing the conformation of nearby proteins.⁵⁵ Hydrolytic *exo*-sialidases such as viral neuraminidase and the human neuraminidases (NEU1-4) cleave terminal sialic acid residues with a net retention of the stereochemistry at the site of substitution (Figure 4). Two other types of *exo*-sialidases have been found in bacteria, leeches and protozoan: the *trans*- and IT *trans*-sialidases.⁵⁶⁻⁵⁸ *Trans*-sialidases enable the transfer of sialic acid to other glycoconjugates, while the intermolecular (IT) *trans*-sialidase releases 2,7-anhydro-Neu5Ac as the cleavage product (Figure 4).

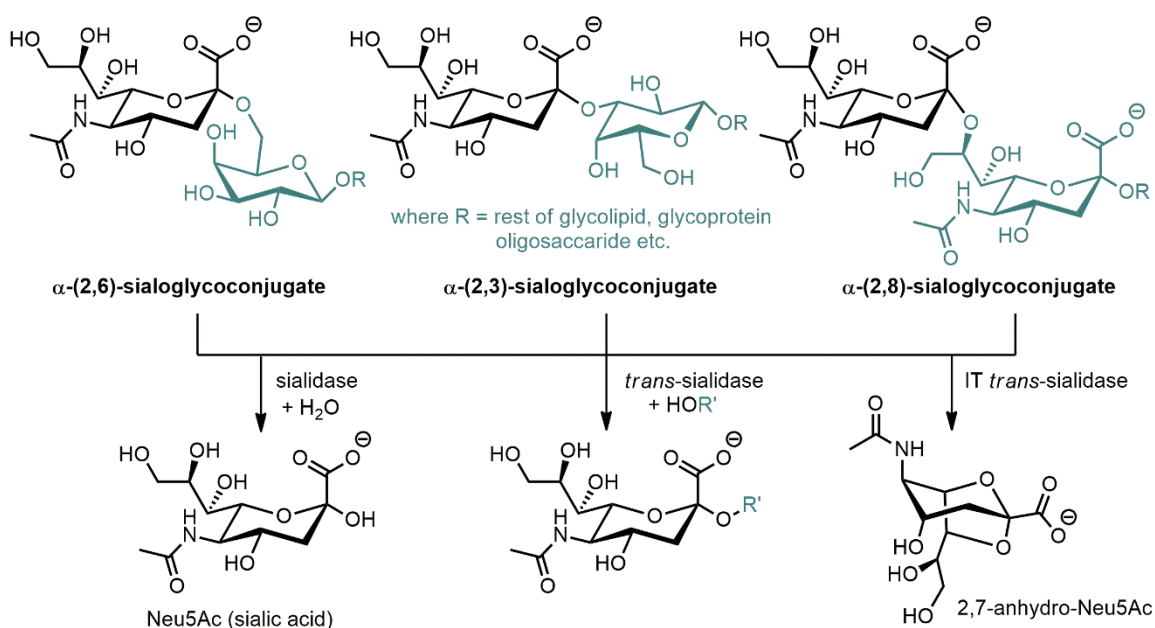
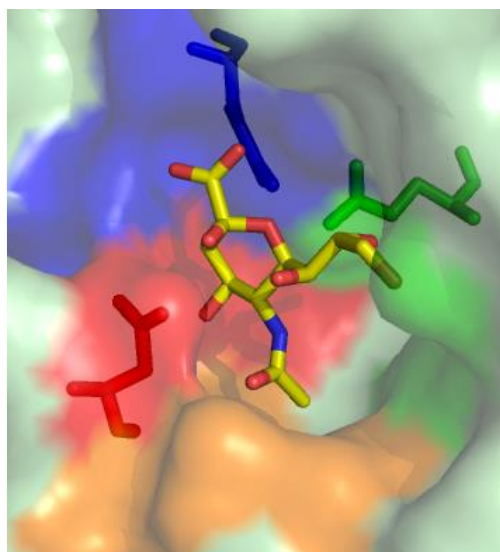
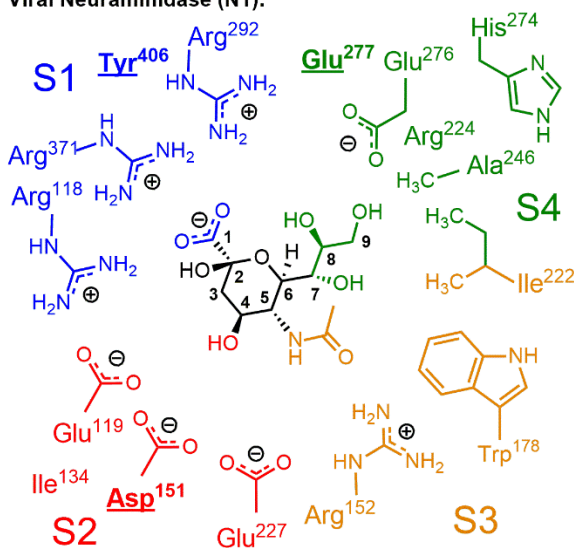


Figure 4. Substrates and cleavage products of sialidases, where R = the rest of the glycoconjugate which is attached to the cell surface.

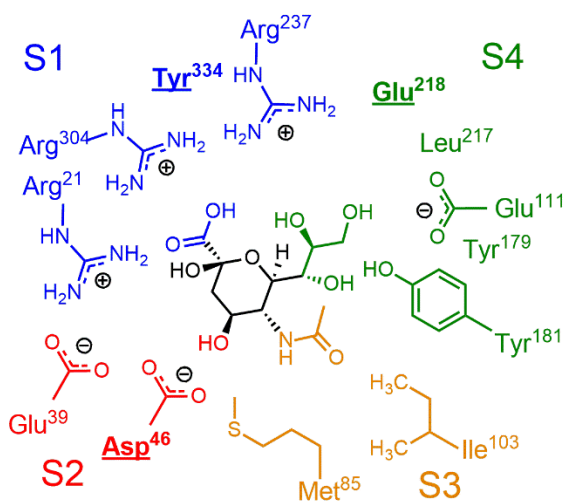
The active site of neuraminidase enzymes can be divided into four sub-sites, S1-S4 (Figure 5). The S1 sub-site consists of three positively charged arginine residues which engage the carboxylate function of Neu5Ac in electrostatic and hydrogen bonding interactions (salt bridging).⁵⁹ The S1 site also possesses a tyrosine residue which is essential to enzymatic activity.⁶⁰ The S2 subsite consisting of a number of acidic residues (glutamate and/or aspartate) which bind to the C4 hydroxyl of sialic acid. The S3 subsite consists of a hydrophobic pocket that can accommodate the C5 *N*-acetyl methyl group.⁵⁹

The S4 subsite is amphiphilic in nature, containing a mixture of hydrogen bond acceptors to bind to the C8 and C9 alcohol groups of Neu5Ac and a hydrophobic region that can bind to the C7–C9 carbon chain of the triol side chain.⁵⁹ Differences in the amino acids surrounding the active site are believed to be the reason for specificity differences between different substrates (for example sialoglycoproteins versus sialoglycolipids), and the type of linkage (e.g. α -(2,3) versus α -(2,6)).^{61, 62}

Viral Neuraminidase (N1):



Human Neuraminidase (NEU2):



Bacterial Neuraminidase (NanA):

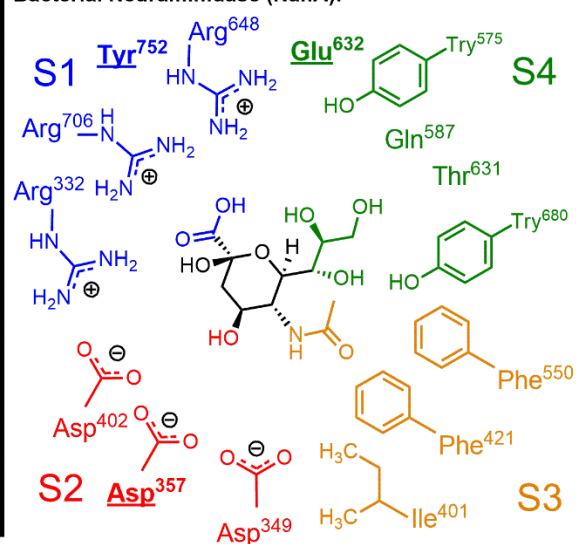


Figure 5. Comparison of active sites of N1 viral (PDB: 2BAT), hNEU2 human (PDB: 2F0Z), and NanA (PDB: 2YA7) bacterial neuraminidase. Putative catalytic residues are underlined.

The mechanism of enzymatic hydrolysis by sialidase has been under extensive study. It was previously hypothesized that the reaction trajectory went through a cationic oxonium intermediate upon departure of the glycoconjugates (Figure 6A).⁶³ However, recent evidence using kinetic isotope effects and the isolation of covalently trapped intermediates indicates the formation of a covalent sialosyl-enzyme entity involving a nucleophilic tyrosine residue (Figure 6B).⁶⁴⁻⁶⁷ Upon binding of sialic acid to neuraminidase, the substrate adopts a boat-like conformation. A tyrosine residue acts as a nucleophile assisted by a general base (Glu),⁶⁸ with the glycoconjugate (“OR”) as the leaving group; a general acid (Asp) assists the departure.⁶⁸ The now covalently bound sialosyl-enzyme intermediate is then cleaved by water releasing Neu5Ac.^{66, 68}

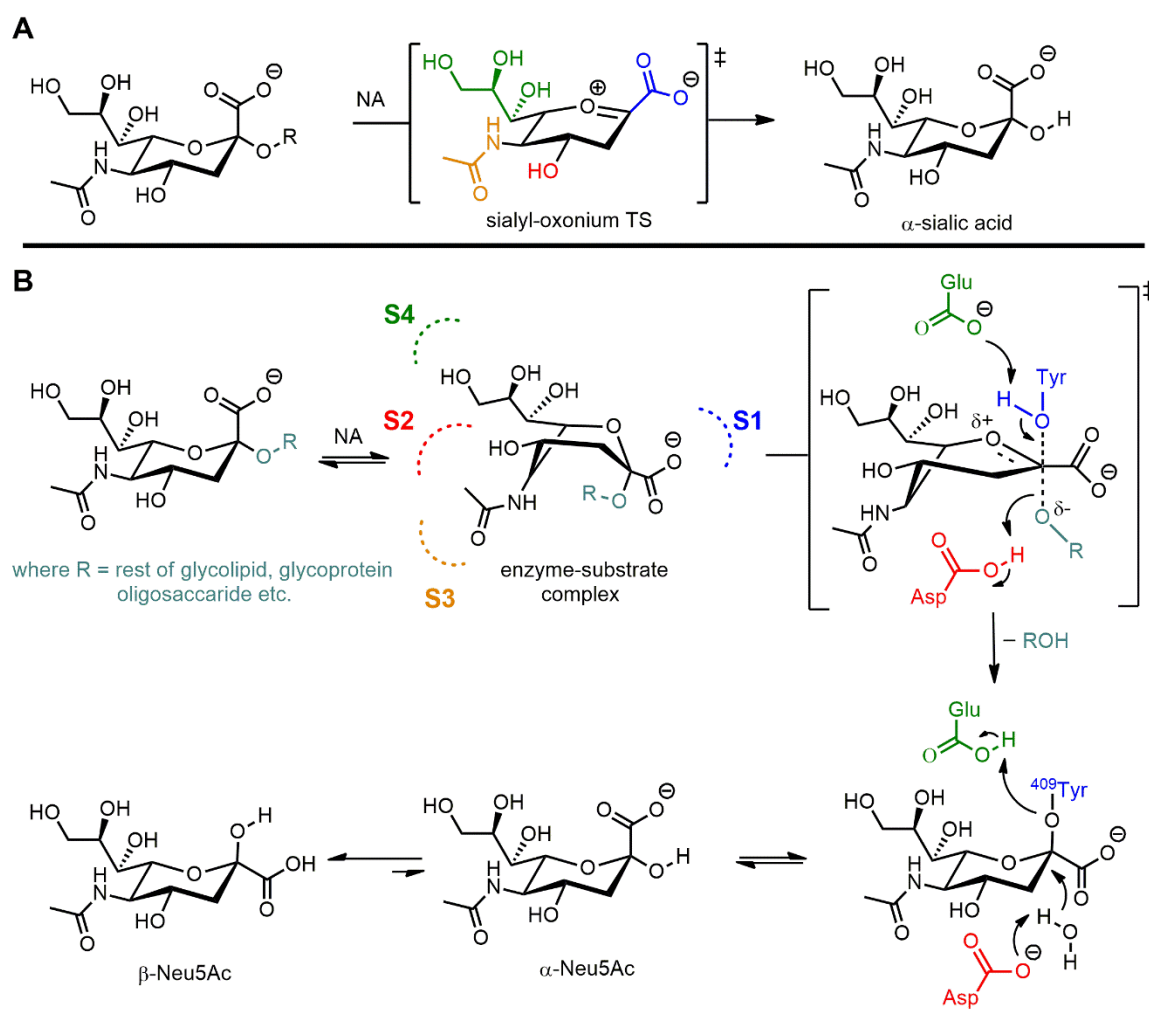


Figure 6. Mechanism of *exo*-sialidase based hydrolysis of Neu5Ac from glycoconjugates.

1.4.0. Viral Neuraminidase and the Generation of Potent Inhibitors

The most well studied of all neuraminidases is influenza A's viral neuraminidase (Figure 7). NA is a 240 kD tetrameric protein, made up of four identical subunits consisting of a catalytic domain anchored by a stem attached to the lipid bilayer envelope of the virus particle with a 6-fold- β -propeller as the distinguishing structural motif.⁶⁹ NA specifically cleaves terminal α -(2,3) and α -(2,6)-Neu5Ac-galactose linkages.⁷⁰

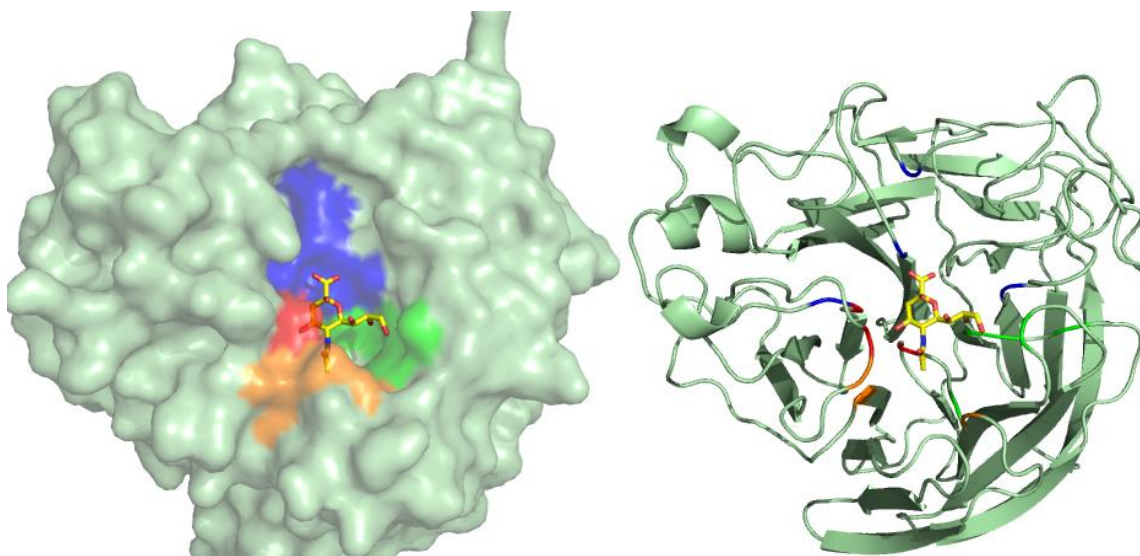


Figure 7. Surface and ribbon view of a N2 neuraminidase complexed with Neu5Ac. (PDB: 2BAT).

The viral neuraminidase active site (Figure 8) is highly conserved amongst group 1 and 2 neuraminidases, even though the amino acid sequence can vary 30-60% between NA subtypes.⁷¹ The S1 sub-site consists of three positively charged arginines (Arg118, Arg292 and Arg371) and the nucleophilic Tyr409. The S2 subsite consists of Glu119, Glu227, Asp151, and a leucine residue (Leu134). The S3 subsite hydrophobic pocket is made up of Trp178 and Ile222, while Arg152 is in proximity to hydrogen bond to the carbonyl portion of the *N*-acetyl group. The S4 subsite is home to two glutamic acid residues Glu276 and Glu277, and a hydrophobic surface consisting of Ala246, Ile222, and the methylene sidechain of Arg224.

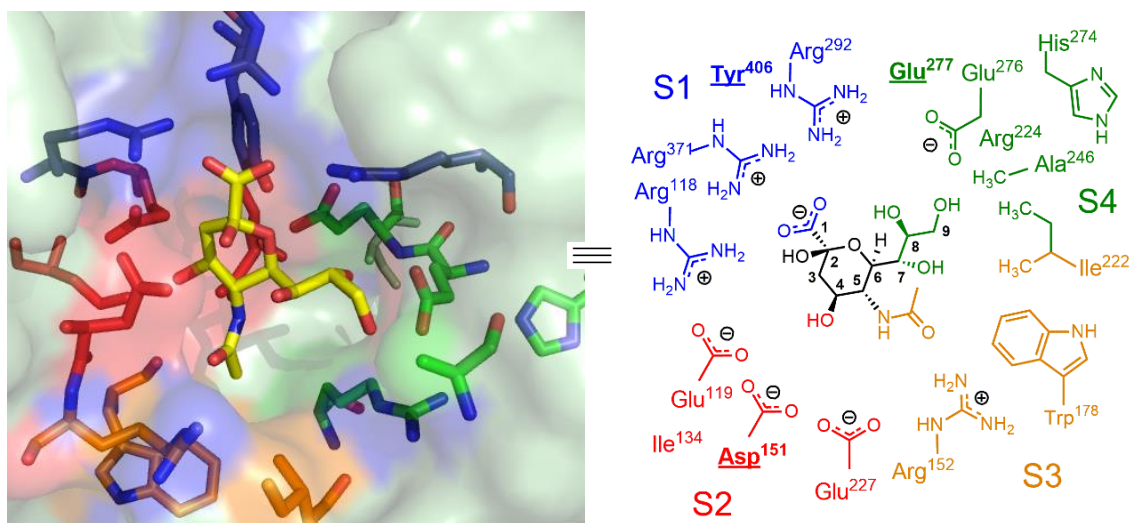


Figure 8. Active site residues and active site map of an N2 viral neuraminidase. (PDB: 2BAT)

In the following subsections, an overview of the key developments in the generation of potent viral neuraminidase inhibitors is presented. The development of inhibitors against neuraminidase was greatly accelerated through the use of X-ray crystallographic analysis of the native enzyme: the first structure determined was of an N2 neuraminidase in 1983.⁶⁹ The utility of a neuraminidase inhibitor as an efficacious therapeutic was initially supported by the observation that neuraminidase-deficient influenza viruses are still infective, but the budding virus particles aggregate or remain bound to the infected cell surface and can be removed through respiratory secretions.^{72, 73}

1.4.1. The Dihydropyran Scaffold: DANA, Zanamivir and Beyond

Neu5Ac2en (DANA, **1-2**), the dehydrated analog of Neu5Ac, was first synthesized in the early 1970's and was shown to be a broad spectrum inhibitor ($K_i = 1\text{-}10\ \mu\text{M}$) of influenza A and B viral neuraminidase, many bacterial neuraminidases, the neuraminidase-hemagglutinin protein of the Newcastle disease virus, and the human neuraminidases NEU1-4.^{74,75} DANA ($K_i = 4\ \mu\text{M}$, $\text{IC}_{50} = 30\ \mu\text{M}$ versus NA)^{75,76} is four orders of magnitude more potent than **1-1**. This is attributed to the ability of **1-2** to mimic the boat-shaped transition state during enzymatic hydrolysis. DANA became the lead structure for further development of more potent and selective inhibitors of viral neuraminidase. The first analogs of DANA studied involved modifications to the S3 binding amide function. The most active of these inhibitors was the trifluoroacetamide analog **1-3** ($K_i = 800\ \text{nM}$).⁷⁵ Despite the respectable *in vitro* activity,⁷⁷ no inhibition of viral replication could be observed *in vivo* due to the fast renal excretion of **1-2** and **1-3**.⁷⁸

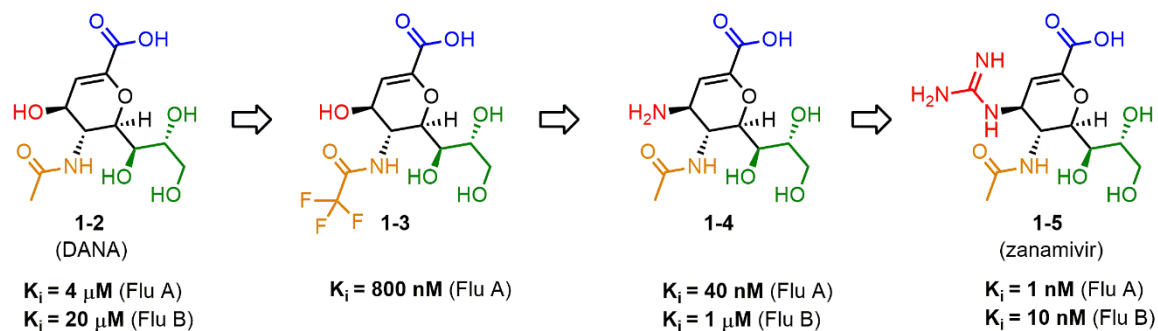


Figure 9. Dihydropyran inhibitors of neuraminidase.

The first inhibitors described with low nanomolar potency against NA were 4-amino-Neu5Ac2en (**1-4**) and 4-guanidino-Neu5Ac2en (zanamivir, **1-5**).^{76,79} Scientists at the Victorian College of Pharmacy in collaboration with Glaxo (now GlaxoSmithKline) performed computational modelling of the recently solved X-ray structure of an N2 neuraminidase bound to DANA. Replacement of the hydroxyl unit of **1-2** with a protonated amine function was modelled to form favorable salt-bridging interactions with residues in the S2 subsite.⁷⁹ Analogs **1-4** and **1-5** were prepared and the inhibition constant (K_i) of

zanamivir was determined to be 1-0.1 nM against N1 and N2 recombinant enzymes. Analysis of the X-ray structure of zanamivir revealed hydrogen bond interactions between the C4-guanidinium function and the carboxylate side chains of Glu119, Glu227 and Asp151 as well as the carbonyl group of Trp178.⁷⁹ More importantly, zanamivir displayed the ability to inhibit viral replication *in vivo*. The drug must be taken by inhalation (oral activity of 2%), 10 mg twice a day (usually for five days) with a bioavailability of 10-20%.⁸⁰ Zanamivir must be taken 1-2 days upon first the onset of symptoms and reduces the symptoms by 24 hours.⁸¹ Many strategies to improve the pharmacological properties of zanamivir have been investigated (Figure 10). Laninamivir (**1-6**) is administered by inhalation as the octanoate pro-drug (CS-8958) and is currently in phase III clinical trials. The pro-drug is slowly hydrolysed in the respiratory tract providing a longer duration of action (a single 20-40 mg dose provides the same benefit as a five day treatment of zanamivir or oseltamivir).⁸² Also in development are a series of multivalent zanamivir analogs tethered together by a hydrophobic linker (**1-7**).⁸³

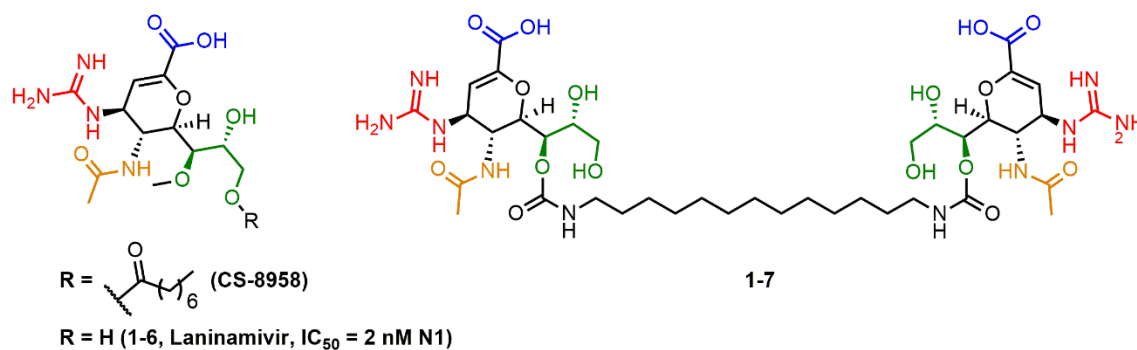


Figure 10. Longer duration of action analogs of zanamivir.

1.4.2. Oseltamivir and the Cyclohexene Scaffold

The idea of utilizing a carbocyclic scaffold for the generation of a neuraminidase inhibitor was first demonstrated in 1992 by Ogawa *et al.* in which a carboxylic analog of Neu5Ac was prepared and found to have minimal neuraminidase inhibitory activity against a few bacterial neuraminidases.⁸⁴ Scientists at Glaxo decided to investigate whether the

dihydropyran ring of zanamivir could be replaced by a more chemically versatile cyclohexene scaffold that could position the functional groups in the same required conformation for binding with NA (Figure 11). Cyclohexene **1-9** was thus prepared and was found to be equipotent when compared with the previously reported dihydropyran derivative (**1-8**).⁸⁵

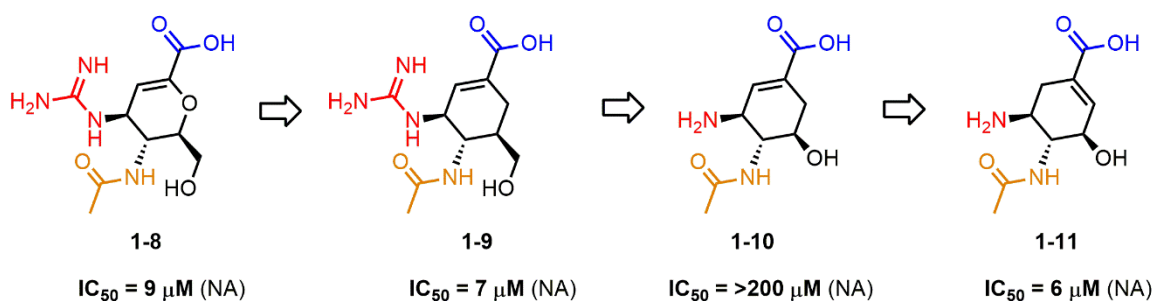


Figure 11. Evolution of the dihydropyran scaffold.

With the primary goal of developing an orally active drug, scientists at the pharmaceutical company Gilead decided to dispense with the polar triol and guanidine functions of zanamivir. The carbocyclic scaffold of **1-9** was simplified by replacing the CH_2OH function with a hydroxyl functional group handle (**1-10**).⁸⁶ The carboxylic analog **1-10** (with the double bond in same position as in zanamivir) was found to be relatively inactive, while the structural isomer **1-11** was found to be a low micromolar inhibitor of NA (Figure 11).⁸⁶ With **1-11** as a lead structure, a series of aliphatic side chains were installed onto the C3-OH moiety of **1-11** to determine the optimum length, geometry and conformational flexibility of the sidechain in order to maximize hydrophobic contacts within the S4 pocket. A series of linear ethers were prepared with increasing length from methyl to butyl; an *n*-propyl substituent was found to be optimum (Figure 12).⁸⁶ Branched alkyl groups were then investigated with the 3-pentyl analog (oseltamivir carboxylate, **1-12**) possessing an IC_{50} of 1 nM.⁸⁶ The accommodation of the 3-pentyl group by the enzyme active site was unexpected due to the presence of the polar Glu276 residue; X-ray crystallography revealed that in order to accommodate the second ethyl branch of the 3-pentyl substituent, Glu276 must rotate out of the active site, forming a salt-bridge interaction with Arg224 (Figure 12).⁸⁶

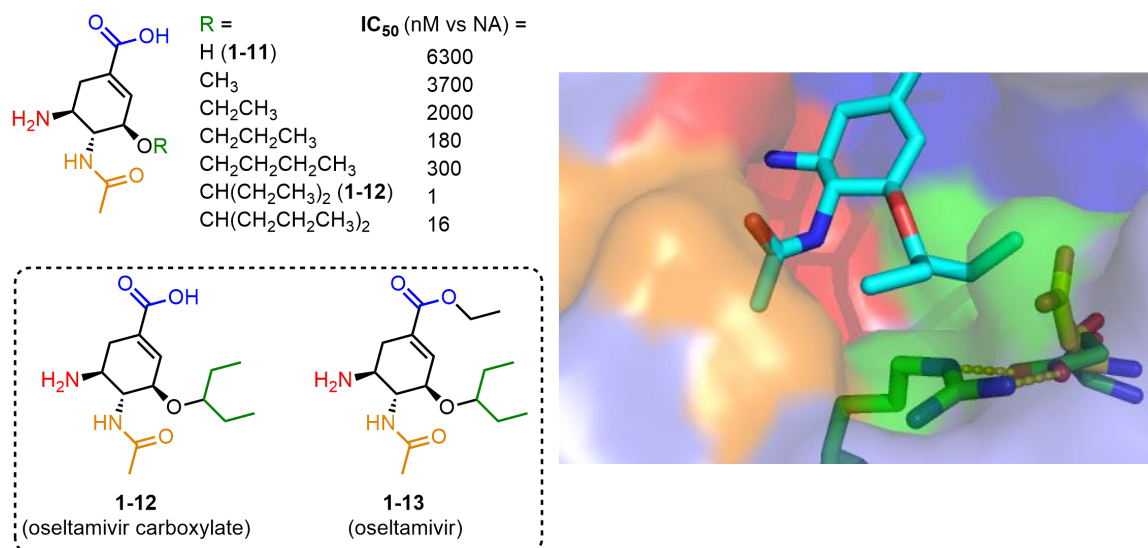


Figure 12. Optimization of the hydrophobic side-chain and conformation change upon binding of oseltamivir. Glu276 (yellow, apo form of the enzyme), Glu276 and Arg224 (green, bound oseltamivir).

Despite the lack of a triol side chain and guanidine function (present in the orally inactive zanamivir), oseltamivir carboxylate was also found to be orally inactive (5% oral bioavailable). Oseltamivir carboxylate was thus formulated and approved by the FDA (mere months after zanamivir) as the ethyl ester prodrug **1-13** with an improved oral bioavailability of 80%.^{87, 88} After permeating the intestines and entering systemic circulation, cleavage of the ethyl ester group by liver esterases releases the active metabolite oseltamivir carboxylate.⁸⁹ Replacement of the amine function of oseltamivir with a guanidine group slightly improved the *in vitro* activity (IC₅₀ = 0.5 nM), however the pro-drug ethyl ester of the latter derivative was found to be orally inactive. The presence of a guanidine function has been established to negatively correlate with intestinal permeability.^{90,91}

1.4.3. Peramivir: The Cyclopentane Scaffold

The main objective of BioCryst pharmaceutical neuraminidase inhibitor program was to improve on the two already existing drugs oseltamivir and zanamivir. The furanose analog of Neu5Ac (**1-14**) was known to inhibit influenza neuraminidase with a similar potency to that of DANA (**1-2**).⁹² Analysis of the X-ray structure revealed that the central ring of the furanose is displaced significantly from the dihydropyran core of DANA, however the projected substituents have the same relative position in order to bind with the active site residues.⁹³ The use of a much simpler cyclopentane scaffold was explored to potentially dispose the required functional groups to target influenza neuraminidase.⁹³ Cyclopentane analog **1-15** was designed to bind to three of the subsites of NA and was found to have similar activity to **1-14**.⁹³ On the basis of the X-ray structure of **1-15**, **1-16** was designed to exploit the S4 subsite using an *n*-butyl group.⁹⁴ X-ray analysis of **1-16** co-crystallized with an N2 neuraminidase identified the active diastereomer in which the carboxylate and guanidinium functions are in a *syn* orientation.⁹⁴ A 3-pentyl group (reminiscent of oseltamivir's sidechain) was installed at the C1' position (to give **1-17**, peramivir) increasing the potency to the low to sub-nanomolar range (Figure 13).⁹⁴

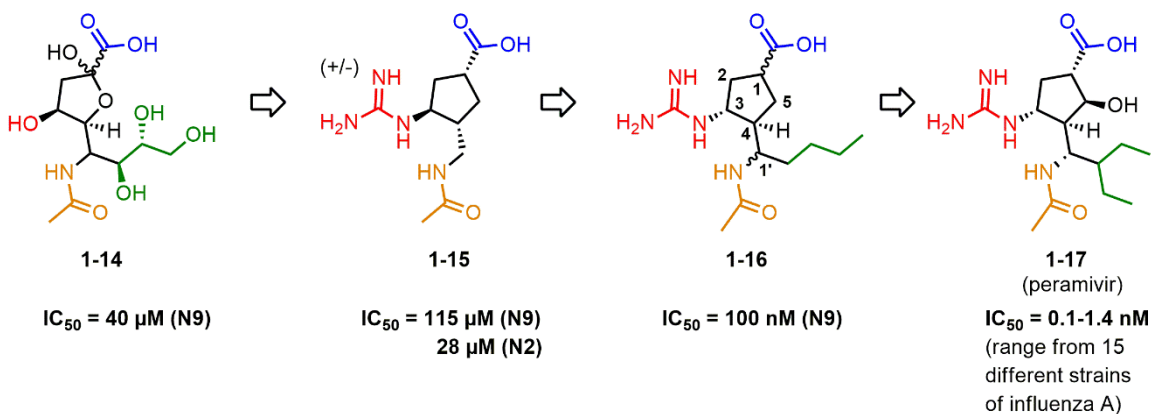


Figure 13. Development of the cyclopentane based scaffold.

The potent activity of peramivir established the theory that the central scaffold serves only to dispose the substituents at suitable vectors to interact efficiently with the four subsites of the NA active site. Peramivir is not orally active even as the ester pro-drug

and was subsequently developed as an injectable.⁹⁵ Peramivir has been approved in Japan (as Rapiatca®) and South Korea (Peramiflu®) since 2010,⁹⁶ and was used in the US on an emergency basis during the 2009 H1N1 swine-flu pandemic.⁹⁷ In 2014, peramivir (Rapivab®) was approved by the FDA, affording it the distinction of being the first influenza antiviral approved since zanamivir (Relenza®) and oseltamivir (Tamiflu®).⁹⁸

1.4.4. The Pyrrolidine Scaffold: A Hydrophobic S2 Subsite

An inhibitor series based on the monocyclic ring structure of pyrrolidine was explored in the late 90's by scientists at Abbott Laboratories. Beginning with the identification of **1-18** as a micromolar inhibitor of NA, hundreds of tetrasubstituted pyrrolidine analogs were prepared using high-throughput solid phase parallel synthesis. Of these **1-19** was one of the more potent derivatives (Figure 14).⁹⁹ Compound **1-19** was predicted to bind in the S1 and S2 subsites with its carboxylate and ammonium groups respectively. However, X-ray crystallographic analysis revealed that the structure was rotated 90° from the predicted binding mode, placing the amine function of **1-19** outside of the S2 binding pocket.⁹⁹ In an effort to coerce the amine group into the S2 subsite, the core was changed to a cyclopentane ring (Figure 14). Serendipitously, **1-20** had an unexpectedly low K_i of 0.7 μM .¹⁰⁰ X-ray crystallography revealed the actual binding mode situated the methyl ester group of **1-20** in the usually highly polar S2 subsite.¹⁰⁰

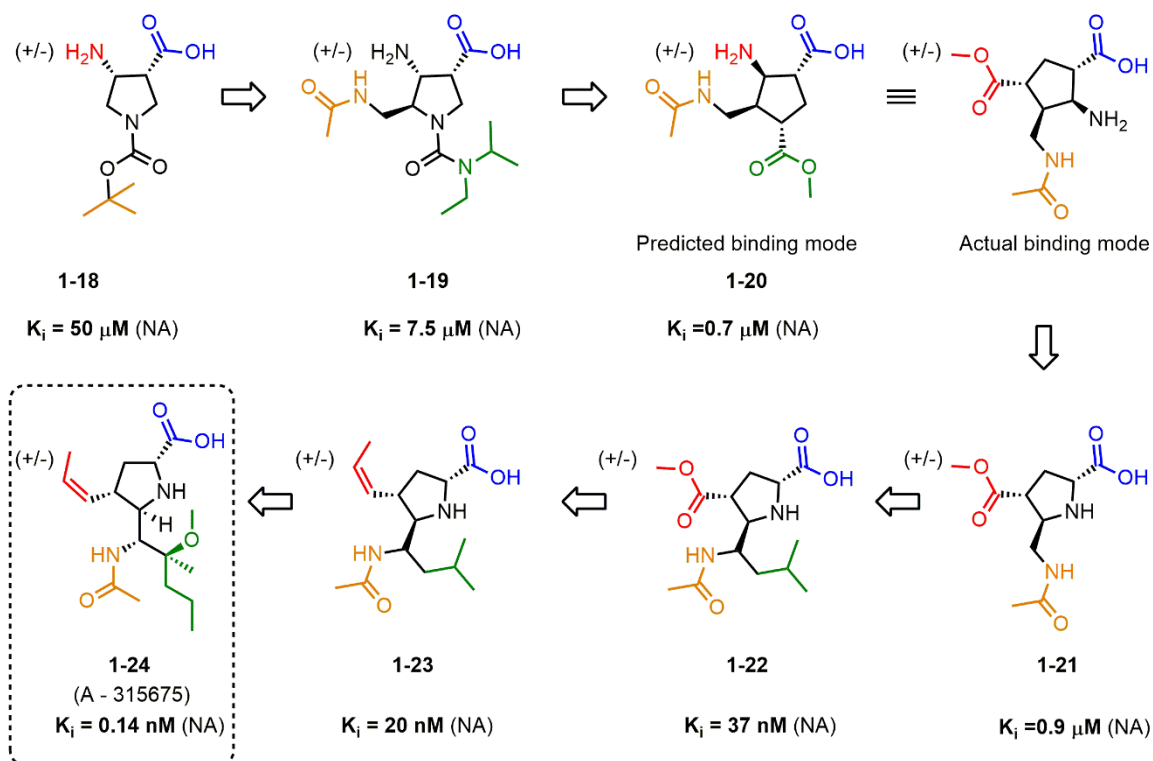


Figure 14. Development of pyrrolidine inhibitor A-315675.

The binding mode of a relatively non-polar function in the S2 binding site was unprecedented. Analysis of the X-ray structure of **1-20** revealed that the methyl ester occupies the same position (in the enzyme active site) as the guanidinium function of zanamivir.¹⁰⁰ The following contributions are believed to explain the binding of the methyl ester in the S2 subsite: two water molecules (conserved during binding of zanamivir, one bound to Glu229 and the other Glu227 and Tyr178) are displaced for an entropic gain, the methyl and ester-oxygen groups engage in van der Waals interactions with Leu134 and the side chain methylene of Asp151.¹⁰⁰ The structure was further optimized to re-introduce the pyrrolidine scaffold by engulfing the amine of **1-20** back into the central ring to form the similarly potent **1-21** (Figure 14). An *iso*-butyl group was added to further increase potency to 37 nM (**1-22**).¹⁰⁰ With a new lead structure in hand an SAR investigation was undertaken to replace the metabolically unstable methyl ester of **1-22**. The C3 methyl ester was replaced by a variety of amides, alkenyl and five-membered ring heterocycles.¹⁰¹ The optimal binding substituent was determined to be a *Z*-propenyl function (Figure 15, **1-**

23).¹⁰¹ After optimization of the S2 pocket, further optimization was performed on the S4 binding *sec*-butyl substituent, eventually arriving at the highly elaborate **1-24** (A-315675).¹⁰² Unfortunately, protonation of the nitrogen atom of the pyrrolidine core causes A-315675 to be zwitterionic under physiological conditions and therefore orally inactive. A prodrug strategy was successful in this case to afford the isopropyl ester prodrug of A-315675 (A-322278).¹⁰³ Comparable efficacy of A-322278 versus oseltamivir was established *in vivo*, however no clinical data in humans has yet been reported.¹⁰³

1.4.5. Aromatic Inhibitors of Neuraminidase

Various attempts to make use of a planar benzene scaffold to target viral neuraminidase have been reported. The simple benzoic acid **1-25** possessing a guanidinium substituent intended to bind in the S2 subsite was designed, however was found to be twisted 180° relative to the expected binding geometry. The guanidinium function was found to make a salt bridge with Glu276 in the S4 subsite.¹⁰⁴ Aromatic analogs of both zanamivir and oseltamivir have been synthesized (Figure 15). The aromatic zanamivir analog **1-26** was found to possess poor activity against NA, likely due to the poor orientation of the triol side chain in the S4 subsite.¹⁰⁵ The aromatic version of guanidino-oseltamivir carboxylate **1-27** was found to be a better inhibitor ($IC_{50} = 1 \mu M$).¹⁰⁶ The most potent aromatic inhibitor reported to date makes use of a branched pyrrolidine; the pendant CH_2OH groups displace a water in the S2 subsite and hydrogen bond to Glu276 in the S4 subsite (Figure 15).¹⁰⁷

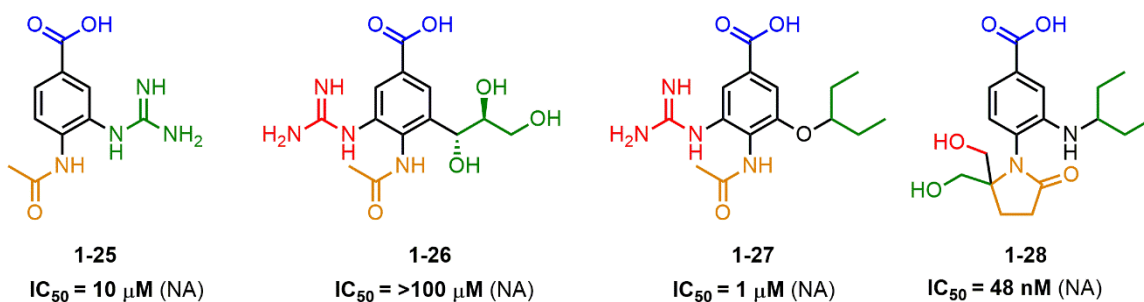


Figure 15. Some aromatic inhibitors of viral neuraminidase.

1.4.6. Mechanism-Based Inhibitors and 150-Cavity Binders

A series of mechanism-inspired inhibitors have been investigated by the Withers group at UBC (Figure 16).⁶⁷ In contrast to zanamivir, oseltamivir, peramivir and A-315675, which bind tightly but reversibly to NA, **1-29** and its amine (**1-30**) and guanidine (**1-31**) analogs act as substrates and bind covalently to the enzyme. This inactivates enzymatic function for a period of time (up to >100 hours).⁶⁷ The highly electronegative fluorine atom at the C3 position slows the hydrolysis step via inductive destabilization of the carbocation-character at the C2 position in the transition state. The C2 fluorine acts as a leaving group allowing the formation of a covalent intermediate.⁶⁷ Analogs **1-30** and **1-31** were selective for viral neuraminidase over human neuraminidase NEU2 by 5-6 orders of magnitude and were shown to reduce viral reproduction *in vivo* with similar efficacy to zanamivir.⁶⁷

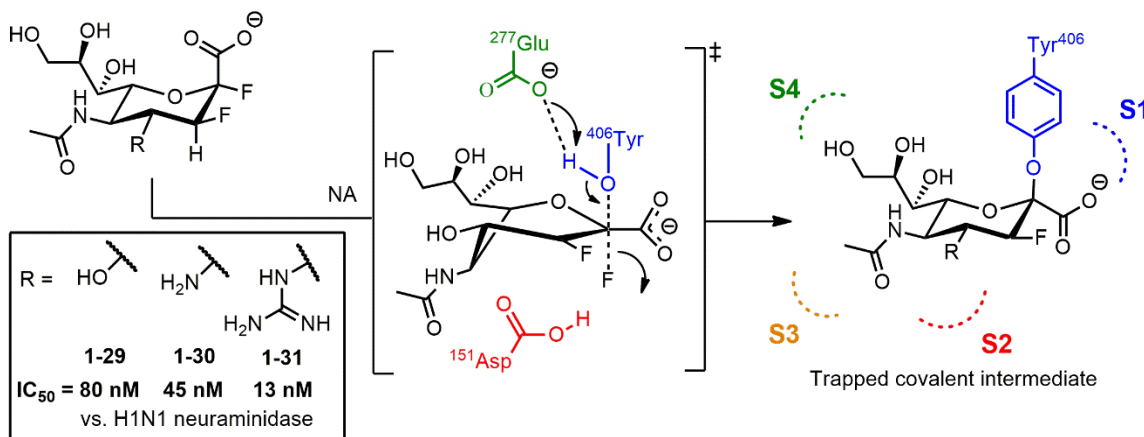


Figure 16. Mechanism-based covalent inhibitors of NA.

A major structural difference between group 1 (N1, N4, N5, N8) and group 2 (N2, N3, N6, N7, N9) neuraminidases is the presence of an adjacent cavity next to the active site: the 150-cavity. In the X-ray structure of N1, N4 and N8 a loop of amino acids (147-152) has been observed to have an open conformation while in group 2 neuraminidases this loop is in a closed conformation (Figure 17). An analog of zanamivir **1-32** was found to be selective for N1 versus N2 by two orders of magnitude (Figure 17). The Pinto group (SFU) has described a “carboxylic zanamivir” analog **1-33** with similar potency to

zanamivir. Using this carboxylic scaffold, **1-34** was designed to breach into the 150 cavity. The selectivity for N1 versus N2 is attributed to the terminal propanol group interacting with the 150 pocket. Analogs of oseltamivir that target the 150 cavity have also been reported which variably occupy the active site or the 150 cavity (but not simultaneously).¹⁰⁸ MD simulations indicate the open and closed states of the 150 loop is dynamic and the opening of the loop may not be exclusive to group 1 NA.¹⁰⁸

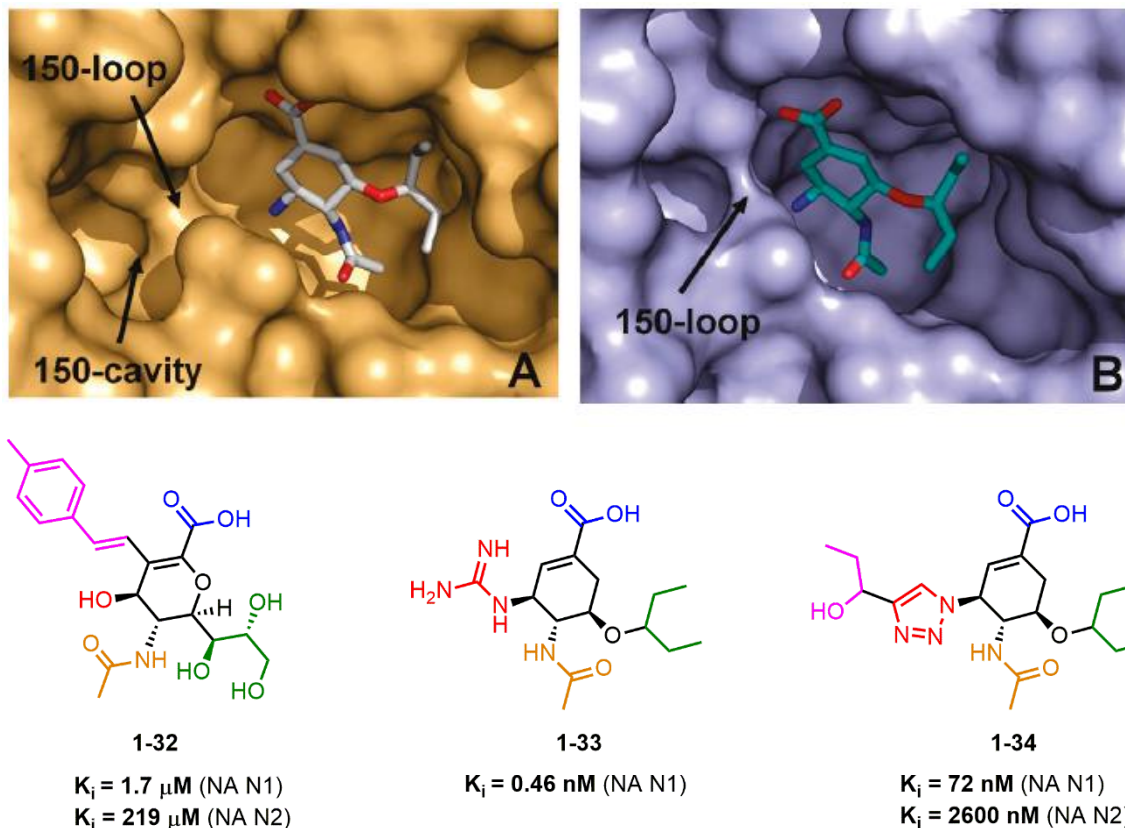


Figure 17. 150-cavity binders and a potent carboxylic-zanamivir analog. A: N1, B: N9. Reprinted with permission from Mohan, S.; McAtamney, S.; Haselhorst, T.; von Itzstein, M.; Pinto, B. M. Carbocycles Related to Oseltamivir as Influenza Virus Group-1-Specific Neuraminidase Inhibitors. Binding to N1 Enzymes in the Context of Virus-like Particles. *Journal of Medicinal Chemistry* 2010, 53, 7377-7391. Copyright (2008) American Chemical Society.

1.5.0. Emergence of Mutation-Induced Resistance

Antivirals zanamivir and oseltamivir were once thought to be immune to mutation-induced resistance with less than 1% of circulating isolates tested conferring resistance between 1999-2007.¹⁰⁹ The most concerning of these antiviral induced-mutations (thus far) is the substitution of a histidine at position 274 for a bulkier tyrosine in the NA active of N1 neuraminidases. In the 2007-2008 flu season, the H274Y point mutation was isolated from 12% of H1N1 viruses tested in the United States. Preliminary testing by the CDC in the 2008-2009 flu season observed the number of H274Y isolates tested increase to 98.5%.^{109, 110} Fortunately, the 2009-2010 H1N1 swine flu pandemic did not contain the H274Y mutation. X-ray crystallographic studies of the H274Y mutant co-crystallized with oseltamivir indicates that the bulkier tyrosine displaces Glu276 two angstroms further into the binding pocket (versus wild-type NA) reducing the size of the induced hydrophobic surface upon binding of the 3-pentyl group of oseltamivir and peramivir (Figure 18). The potency of oseltamivir and peramivir are reduced 754 and 260 fold respectively against the N1 H274Y mutant enzyme (Table 1).¹¹¹ The potency of zanamivir and A-318675 is unaffected by the H274Y mutation since no conformational change of Glu276 is required for binding. N2 neuraminidases have a less bulky residue at the nearby 252 position and can accommodate the H274Y mutation without significant loss in potency.

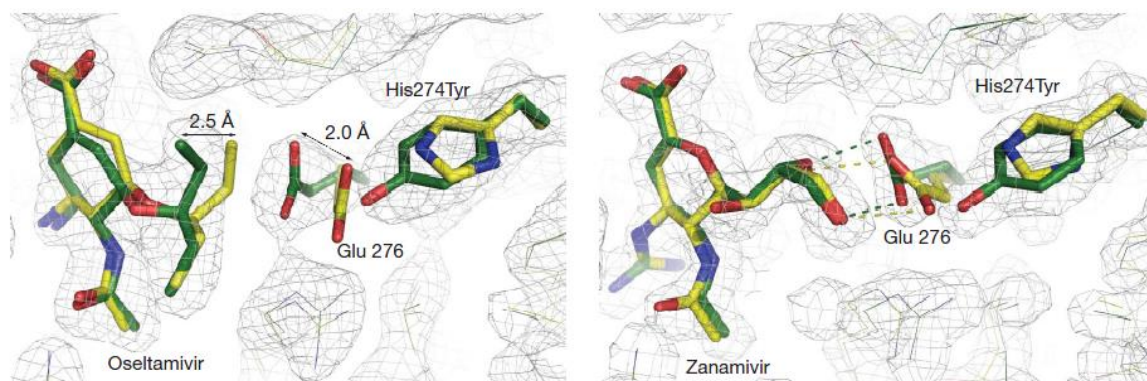


Figure 18. Bound structure of oseltamivir and zanamivir overlaid with the WT and H274Y mutant enzymes.

Reprinted with permission from Macmillan Publishers Ltd: Nature (Collins, P. J.; Haire, L. F.; Lin, Y. P.; Liu, J.; Russell, R. J.; Walker, P. A.; Skehel, J. J.; Martin, S. R.; Hay, A. J.; Gamblin, S. J. Crystal structures of oseltamivir-resistant influenza virus neuraminidase mutants. *Nature* 2008, 453, 1258-1261.), copyright (2008).

A number of other point mutations are known to confer resistance to NA inhibitors (Table 1). Mutants E119V, N294S and R292K mutants have been isolated from oseltamivir treated patients but have not significantly circulated in the population.^{112, 113} Multiple Glu119 mutants have been identified *in vitro* in the presence of zanamivir.^{113, 114} An R152K mutation (in an influenza B strain) has been isolated from patients treated with zanamivir.¹¹⁵ In the case of oseltamivir, the E119V mutation leads to almost complete loss of binding for the amino group.¹¹³ In the E119D mutant, loss of the Glu119 electrostatic interaction with the guanidine results in an appreciable loss of activity for zanamivir.¹¹¹ Since peramivir's guanidine occupies a slightly different position to the guanidine of zanamivir, peramivir retains activity against E119 mutants.¹¹⁶ It is proposed that Glu119 mutations in N2 neuraminidases compromise viral fitness and are not viable *in vivo*.¹¹³ A-315675 has appreciable activity against many of these mutants,¹¹⁷ however the presence of the Z-propenyl function may be liable for mutation-induced resistance.

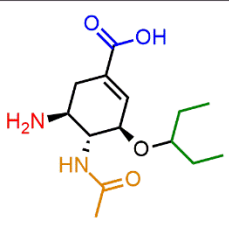
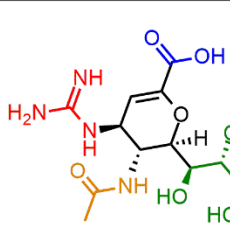
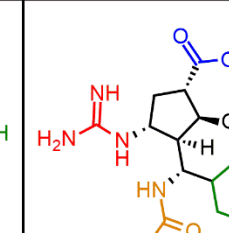
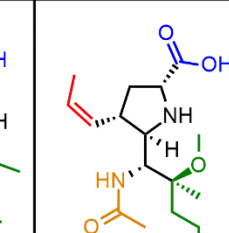
	 oseltamivir carboxylate	 zanamivir	 peramivir	 A-315675
Mutant NA Protein	Fold decrease in IC ₅₀ versus WT	Fold decrease in IC ₅₀ versus WT	Fold decrease in IC ₅₀ versus WT	Fold decrease in IC ₅₀ versus WT
N1 H274Y	754x	1x	260x	2.5x
N2 H274Y	7x	5x	1x	-
N1 N294S	197x	5x	12x	2x
N2 N294S	1879x	8x	0.8x	2x
N2 E119V	1028x	7x	3x	2x
N2 E119D	4.5x	323x	33x	-
N2 R292K	1500x	8x	43x	13x

Table 1. Clinically relevant mutations conferring resistance to NA inhibitors.

1.6.0. Inhibitors of Human and Bacterial Neuraminidases

1.6.1. Human Neuraminidases (NEU1-4)

Four human (or mammalian) sialidases have been discovered to date (NEU1-4). The four isozymes differ by their primary amino acid sequence, sub-cellular position, substrate specificity and optimal pH for activity (Table 2).¹¹⁸ These defining characteristics and the variable expression levels in different cell types, result in different cellular functions for each isozyme. NEU function has been linked to a variety of important cell signaling events including regulation of the immune system and inflammatory response,¹¹⁹ cellular differentiation and proliferation,¹²⁰⁻¹²² and cellular adhesion.¹²³ Furthermore, hNEU function is dysregulated in various diseases such as many cancers,¹²⁴ diabetes,¹²⁵ and obesity.¹²⁶ The fact these isozymes are dysregulated in various regulatory pathways make the hNEU isozymes attractive targets for drug design; however, selectivity between isozymes is likely critical. For example, while NEU3 is overexpressed in many cancers and has been shown to suppress apoptosis^{123, 127} and increase cellular motility,¹²³ the down-regulation of NEU4 has been shown to contribute to the invasiveness of some colon cancers.¹²⁸ Likewise, inhibition of NEU1 may also produce undesired effects: genetic deficiencies of the NEU1 gene result in a terminal illness known as sialidosis.¹²⁹ Interestingly, hNEU inhibition has been shown to prolong the preservation time of blood platelets during storage.¹³⁰

	NEU1	NEU2	NEU3	NEU4
Subcellular location	lysosomal	cytosol	plasma membrane	lysosomes mitochondria ER
Substrate specificity	oligosaccharides glycoproteins	broad	gangliosides	broad
Relative expression levels	10,000	1-10	1000	1000
Primary function	catabolism immune function	cell differentiation	apoptosis adhesion	apoptosis adhesion

Table 2. Some properties of the human neuraminidases.

In part due to the difficulty of purification and lack of structural characterization of the enzymes themselves (X-ray), few potent (<10 nM) inhibitors of hNEU have been reported. Structural analysis for the membrane-associated NEU1, NEU3 and NEU4 isozymes has not yet been achieved; the cytosolic NEU2 structure has been solved both in apo-form and as a co-complex with both DANA and zanamivir.¹³¹ Using the structure of NEU2, homology models have been developed for the other three isozymes.^{132, 133} The putative amino acid residues in the S1 and S2 subsites are similar for NEU1-4, while the S3 and S4 pocket residues of the active site differ substantially.¹³² The conformation of zanamivir is nearly identical when bound to either NEU2 or influenza neuraminidase (Figure 19C). The most significant deviations to the bound inhibitors are slight changes in the orientation of the *N*-acetyl and the C9 hydroxyl (Figure 19C).

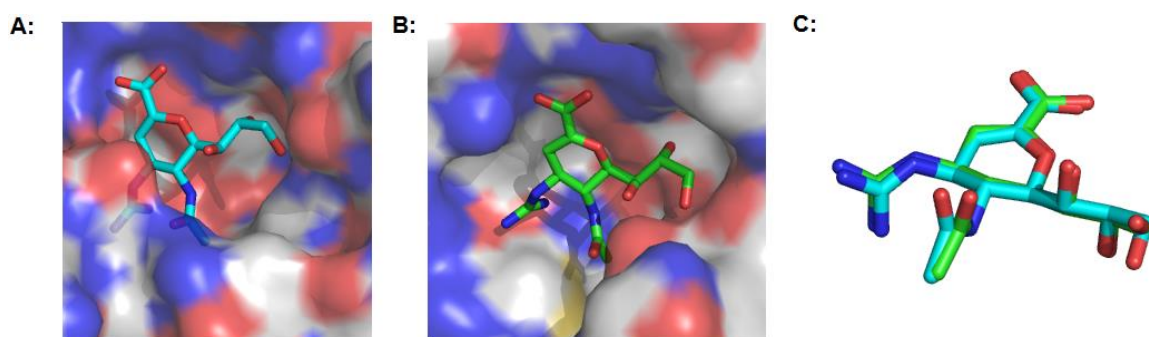


Figure 19. A: Zanamivir complexed with N8 neuraminidase (PDB: 2HTQ). B: Zanamivir complexed with NEU2 (PDB: 2F0Z). C: Overlay of zanamivir co-structures.

In order to deduce the therapeutic potential of NEU1-4 inhibition, selective and potent inhibitors of the isozymes are required. The majority of reports for small molecule inhibition of hNEU utilize the dihydropyran core of DANA; a few analogs of oseltamivir¹³⁴ and a library of benzoic acid derivatives¹³⁵ reporting high micromolar potency for these compounds has been disclosed. DANA itself is a non-specific inhibitor of all four isozymes with low micromolar activity (K_i) against NEU2-4 (Figure 20).¹³⁶ The potent viral neuraminidase inhibitor zanamivir is selective against NEU2-3, suggesting that the S2 subsite for NEU1 and NEU4 cannot effectively accommodate the cationic guanidinium function. The most potent inhibitor of NEU2 is zanamivir, while the most potent inhibitors

of NEU3 are DANA and zanamivir (Figure 20).¹³⁷ The plasma levels of zanamivir are believed to be sufficiently low to not cause significant human neuraminidase inhibition *in vivo*.¹³⁸ Derivatives of DANA with selectivity for NEU2 and NEU3 have been reported (**1-36** and **1-37**).¹³⁶ An analog of DANA with >100 fold selectivity for NEU1 with an IC₅₀ of 10 μM has been reported.¹³⁹ The most potent NEU inhibitor reported to date is **1-38**: an analog of DANA modified at the C6 position with a 500-fold selectivity against the other three isozymes and a K_i of 30 nM against NEU4.¹⁴⁰ Peramivir and oseltamivir are poor inhibitors of NEU1-4, likely due to their hydrophobic 3-pentyl substituents. Ultimately, the therapeutic effect of NEU1-4 inhibition with a small molecule is unknown; the generation of a selective and potent inhibitor for each isozyme would be of great scientific value.⁵¹

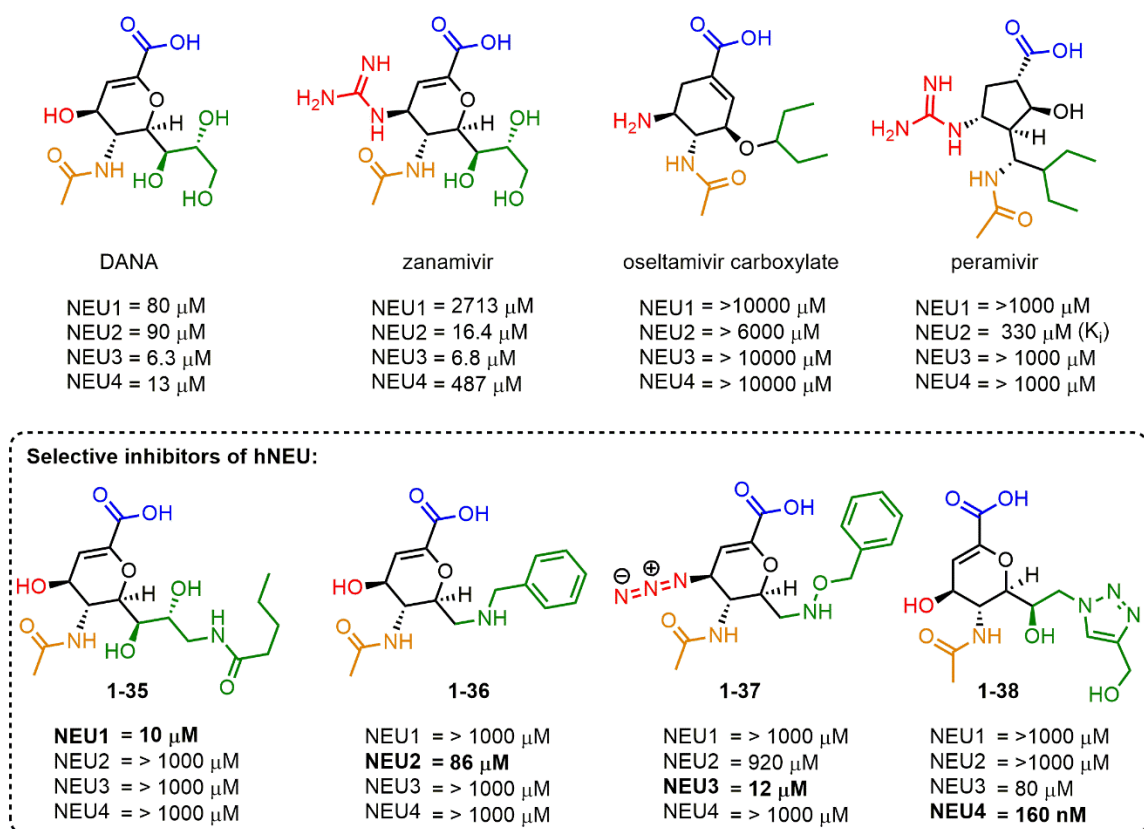


Figure 20. IC₅₀ values of inhibitors designed to target the human neuraminidases (NEU1-4).

1.6.2. Bacterial Neuraminidases

Many bacteria encode their own neuraminidases for a variety of malicious and nutritional purposes, including members of the *Arthrobacter*, *Clostridium*, *Streptococcus*, *Pseudomonas* and *Vibrio* genera.¹⁴¹ The action of many bacterial neuraminidases is known to be important in the pathogenicity of the bacterium. Most commonly, unmasking carbohydrate residues for adherence to the host organism and subsequent colonization and biofilm production.^{142, 143} On the other hand, pathogenic bacteria and many non-pathogenic soil bacteria (*Arthrobacter*) utilize Neu5Ac as a food source since the sugar contains fixed nitrogen.¹⁴⁴ Of the most concern are the pathogenic bacteria *Vibrio cholera* and *Streptococcus pneumoniae*: infections caused by *Vibrio cholera* affect 3-5 million people each year, killing between 100,000-120,000 individuals¹⁴⁵ while secondary bacterial infections (primarily by *Streptococcus pneumoniae*) are estimated to cause between 35-61% of influenza-related deaths.¹⁴⁶ Cleavage of Neu5Ac residues from the epithelial cell surface by viral neuraminidase primes the lungs for infection by bacterial pathogens.¹⁴⁶ *Clostridium perfringens* is responsible for a third of all food poisonings and in advanced stages of infection causes gangrene and tissue necrosis.¹⁴⁷

The X-ray structures of a few bacterial neuraminidases have been successfully solved including *V. cholera*'s VCNA, *S. pneumoniae*'s NanA and *C. perfringens*'s NanI.¹⁴⁸⁻¹⁵⁰ Recently, oseltamivir, DANA and zanamivir have been co-crystallized with NanA.¹⁵¹ Zanamivir is a poor inhibitor due to a steric clash between the guanidine function and Arg332 in the S1 subsite. However, the amine function of oseltamivir makes hydrogen bond contacts with Asp402 and Asp357 in the crystal structure.¹⁵¹ NanA has two cavities in the S4 subsite, which can accommodate either the glycerol side chain of zanamivir, or the 3-pentyl group of oseltamivir.¹⁵¹ Despite much effort, DANA is the most potent inhibitor described for nearly every bacterial sialidase.⁵² DANA is a much poorer inhibitor of *trans*-sialidases NanB and IT-*trans* sialidases NanC (Table 3). 4-Amino-Neu5en (**1-4**) and zanamivir are weaker inhibitors of most bacterial sialidases, suggesting that the S2 subsite of these enzymes cannot effectively accommodate cationic functional groups (Table 3). Drug design against bacterial neuraminidase is still in its early stages, and testing

of the vast libraries of inhibitors of viral neuraminidase would likely lead to the identification of attractive lead structures against specific bacterial enzymes.

	 1-2 (DANA)	 1-4	 1-5 (zanamivir)	 1-12 (oseltamivir carboxylate)
	K_i	K_i	K_i	K_i
Influenza A	4 μ M	40 nM	1 nM	-
<i>Vibrio cholerae</i>	3 μ M	300 μ M	60 μ M	-
<i>Clostridium perfringens</i>	8 μ M (NanI)	300 μ M (NanI)	> 100 μ M (NanI)	-
<i>Streptococcus pneumoniae</i>	2 μ M (NanA) 300 μ M (NanB) 1300 μ M (NanC)	-	720 μ M (NanA)	1.8 μ M (NanA)
<i>Arthrobacter ureafaciens</i>	1 μ M	300 μ M	> 10 mM	

Table 3. Activities of potent influenza neuraminidase inhibitors against bacterial neuraminidases.

1.7.0. Chapter Summary and Thesis Objectives

The function of neuraminidase has been established to be a determinant in the progression of a wide range of disease states including influenza, bacterial infections such as pneumonia, and various cancers. The key discoveries in the development of inhibitors and therapeutics against viral neuraminidase can be summarized as follows:

1. Exploitation of the cationic subpocket of the S2 subsite (zanamivir)
2. The induced hydrophobic pocket in the S4 subsite (oseltamivir)
3. The use of a non-sugar or sugar-mimetic scaffold (peramivir's cyclopropane ring)
4. Hydrophobic nature of the S2 subsite (A-318675's Z-propenyl function)
5. Second generation longer duration of action (single-dose) and covalent mechanism-based inhibitors

Despite several potent drugs targeting influenza neuraminidase, less has been achieved at targeting human and bacterial neuraminidases. Furthermore, the “ideal” drug against viral neuraminidase has not yet been approved. Oseltamivir and peramivir suffer from a high susceptibility to mutation-induced resistance, while zanamivir and peramivir are not orally active. Furthermore, the efficacy and risk-benefit ratio for neuraminidase inhibitors has also been under intense scrutiny: a systematic review of clinical trial data for oseltamivir and zanamivir reveals that both inhibitors do shorten the duration of symptoms of influenza in otherwise healthy adults and children. However there is little statistical evidence that the drugs reduce the number of hospitalizations due to influenza or the development of subsequent complications such as pneumonia and other respiratory syndromes such as bronchitis.^{152, 153}

The vast majority of inhibitors of influenza make use of the highly successful monocyclic dihydropyran, cyclohexene, cyclopropane, aromatic and pyrrolidine scaffolds. Thus far the only competitive inhibitors of bacterial and human neuraminidases have arisen from the dihydropyran and cyclohexene scaffolds. The design of new scaffolds from which

to generate neuraminidase inhibitors may lead to better selectivity profiles against the desired neuraminidase target (isozymes and mutants). Additionally, elements in the core of new scaffold itself may provide additional contacts with the enzyme target which are not present for the peramivir, oseltamivir or zanamivir scaffolds. Our contribution to this field of research will be to explore the ability of a conformationally-restricted **bicyclic** small-molecule to inhibit neuraminidase enzymes. The use of a conformationally restricted scaffold may not only increase the potency and selectivity of an inhibitor against a desired enzyme target, but may also improve the pharmacokinetic properties of an inhibitor by reducing off target binding.

Thesis Objectives:

1. Develop and explore the reactivity between the anion of 3-sulfolene(s) and bis-vinyl ketones in order to synthesize highly-functionalized bicyclic scaffolds (Chapter 2 and 4)
2. Elaborate the scaffold in order to install appropriate groups to target the binding subsites of the neuraminidase active site (Chapter 3)
3. Determine the propensity of the synthesized inhibitor to competitively inhibit influenza A neuraminidase (Chapter 3)
4. Determine the selectivity profile of our “lead” inhibitor against other neuraminidase enzymes (Chapter 3)
5. Further functionalize the bicyclic scaffold and improve potency against viral neuraminidase (Chapter 5)

Chapter 2: Tandem Reactions of Bis-Vinyl Ketones and 3-Sulfolene

The material in Sections 2.2.0-2.4.0 was adapted from: M. G. Brant, C. M. Bromba and J. E. Wulff (2010) Tandem Vinylogous 1,2-Addition/Anionic Oxy-Cope Reaction Leading from Butadiene Sulfone to an Orthogonally Functionalized Bicycle. *Journal of Organic Chemistry*, 75, 6312-6315.¹⁵⁴

All the synthesis, analysis and initial characterization of data was performed by MGB. Dr. Caleb M. Bromba collected NMR data on the 500 MHz instrument for publication purposes. Connor Bohlkin performed the synthesis of **2-9a** and **2-9b** under the supervision of MGB. All X-ray structures were solved by Dr. Allen G. Oliver (University of Notre Dame). Dr. Tyler Trefz and Dr. Ori Granot collected the HRMS data.

2.1.0. Introduction

3-Sulfolene (butadiene sulfone, **2-1a**)¹⁵⁵ is a four carbon building block formed by the cheletropic cycloaddition between 1,3-butadiene and sulfur dioxide (Figure 21).¹⁵⁶ The addition of liquid sulfur dioxide to 1,3-butadiene and various substituted 1,3-dienes (including (*E*)-1,3,5-hexatriene and 1,3,5-cyclooctatriene, Figure 21)^{157, 158} is a facile process at room temperature (often conducted in a sealed vessel)¹⁵⁹⁻¹⁶¹ while the reverse reaction (the extrusion of sulfur dioxide) can be achieved through thermal means (typically temperatures >100 °C).¹⁶¹ Butadiene sulfone is therefore considered a convenient, stable, solid source of 1,3-butadiene (b.p. – 4 °C), and has been utilized in place of 1,3-butadiene for cycloaddition reactions, specifically the (4+2) Diels-Alder reaction.^{162, 163} The liberated sulfur dioxide obtained from the heating of butadiene sulfone has been utilized for the deoxygenation of aromatic *N*-oxides and acid-catalyzed isomerization of olefins.¹⁶⁴ Furthermore, the reversibility of the cycloaddition/retro-cycloaddition process has made the formation of a 3-sulfolene a useful protecting group strategy for oxidation or acid sensitive 1,3-dienes in the total synthesis of natural products.¹⁶⁵⁻¹⁶⁷ The (4+1) cycloaddition between sulfur dioxide and a 1,3-diene was first described in 1914 in which a crystalline mono-adduct of isoprene (2-methyl-1,3-butadiene) and sulfur dioxide was proposed (**2-1b**) and the structure subsequently elucidated using X-ray crystallography.¹⁶⁸

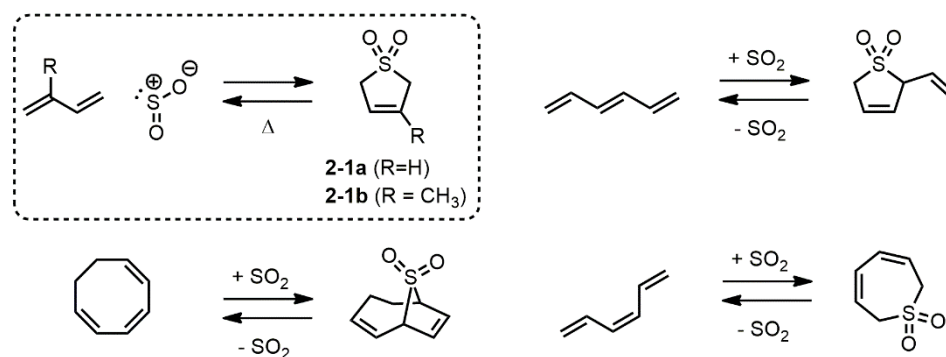


Figure 21. Cycloaddition reactions of sulfur dioxide and some representative dienes.

Consistent with the Woodward-Hoffmann rules governing the stereochemical outcome of pericyclic rearrangements,¹⁶⁹ the thermal cheletropic and extrusion reactions occur through a concerted disrotatory ground state process (Figure 22).^{170, 171} This is well illustrated by the fact that pyrolysis of *cis*-2,5-dimethyl-3-sulfolene results in nearly quantitative conversion to (*E-E*)-2,4-hexadiene, while the *trans*-2,5-dimethyl-3-sulfolene begets the corresponding (*E-Z*)-2,4-hexadiene isomer (Figure 22).¹⁷⁰ Depending on the relative energies of the frontier molecular orbitals of the specific system under study, the cheletropic reaction can occur between the highest occupied molecular orbital (HOMO) of the sulfur dioxide interacting with the lowest unoccupied molecular orbital (LUMO) of the 1,3-diene or the LUMO of the sulfur dioxide can interact with the HOMO of the 1,3-diene. In comparison to the above, the reaction of sulfur dioxide with (*Z*)-1,3,5-hexatriene has been shown to produce the corresponding “chubby” sulfolene (Figure 21) through a conrotatory (6+1) cheletropic process.^{171, 172}

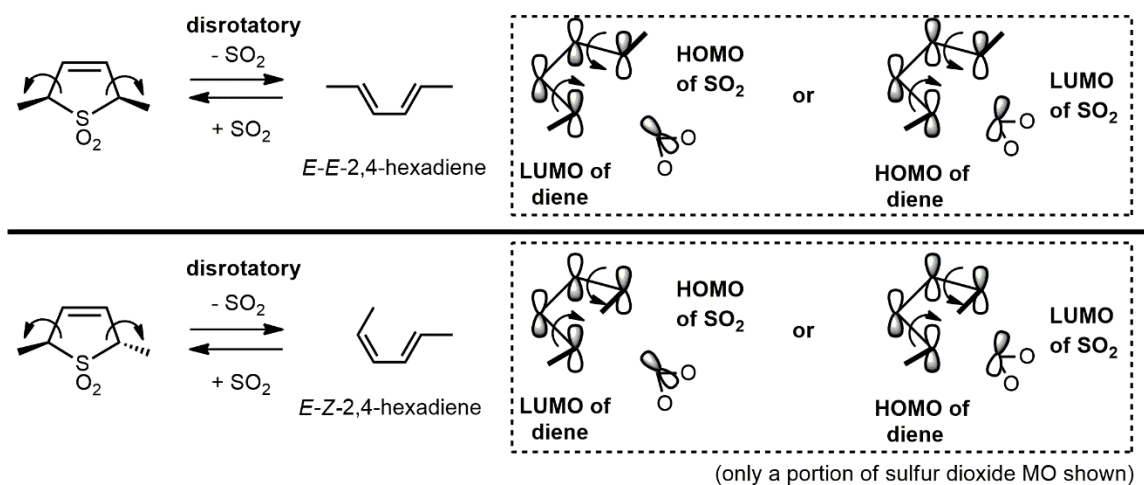


Figure 22. Origin of stereospecificity in the (4+1) cheletropic ring closure and retro-(4+1) ring opening of *cis*-2,5-dimethyl-3-sulfolene and *trans*-2,5-dimethyl-3-sulfolene.

2.1.1. The Anion of 3-Sulfolene

The electron withdrawing sulfone function within the 3-sulfolene framework greatly decreases the acidity of the protons at the 2-position (α -protons, pK_a approximately 18-20). Significant synthetic interest has been focused on the generation of the nucleophilic anion of 3-sulfolene (also called 3-sulfenylate) and subsequent alkylation using an electrophile to provide substituted 3-sulfolenes; cheletropic removal of sulfur dioxide from the resulting substituted-3-sulfolenes provides the corresponding substituted 1,3-diene in a stereospecific fashion (Figure 23). Substituted 1,3-dienes are synthetically valuable molecules as the functional group itself is found in a large number of natural products such as insect pheromones,¹⁷³⁻¹⁷⁵ retinoids,^{176, 177} terpenes and terpenoids.¹⁷⁸⁻¹⁸⁰ Substituted 1,3-dienes are also valuable intermediates in total synthesis sequences for cycloaddition reactions (for example in Diels-Alder reactions).^{181, 182} The key challenges in the alkylation of 3-sulfolene (and subsequent elaboration to the substituted 1,3-dienes) as well as the methods developed to overcome these challenges will be highlighted in this following section (2.1.1). This topic has been previously reviewed by Chou and Bhat.^{168, 183}

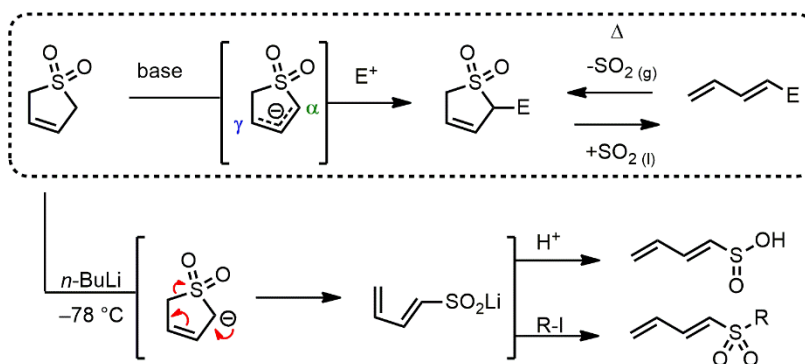


Figure 23. Cheletropic removal of sulfur dioxide from the alkylated butadiene sulfone anion and ring-opening of the butadiene sulfone anion at $-78^\circ C$.

Early attempts at functionalizing the α -position of butadiene sulfone through deprotonation with *n*-butyllithium (*n*-BuLi) followed by addition of an electrophile was plagued with complications due to the fact the 3-sulfolene anion is unstable even at $-78\text{ }^{\circ}\text{C}$ with decomposition occurring through ring opening to the linear sulfinic acid (Figure 23).¹⁸⁴ Similar ring-opening behavior is also observed with the bases potassium *tert*-butoxide and Grignard reagents (PhMgBr).¹⁸⁵ The corresponding lithium (or potassium or magnesium bromide) salt of the sulfinic acid can be alkylated *in situ* through treatment with an alkyl halide to provide the disubstituted linear sulfone (Figure 23).^{184, 185} To circumvent this ring-opening conundrum, a useful synthesis of substituted 1,3-dienes using a cyclopentadiene-masked 3-sulfolene strategy in order to “protect” the basic-labile alkene function has been accomplished (Figure 24).¹⁸⁶ The Diels-Alder adduct of 3-sulfolene and cyclopentadiene was deprotonated with *n*-BuLi then treated with an alkyl halide to furnish the corresponding mono-substituted product in 60-65% yield (Figure 24). Heating of the adduct at $650\text{ }^{\circ}\text{C}$ was required to induce the thermal retro-Diels-Alder reaction and the cheletropic removal of sulfur dioxide (of the presumable 2-substituted-3-sulfolene intermediate). The corresponding substituted (*E*)-1,3-diene in yields of 80-90% were obtained. This method was extended to the synthesis of substituted-(*E,E*)-1,3-dienes including two pheromone natural products (Figure 24).¹⁷⁴

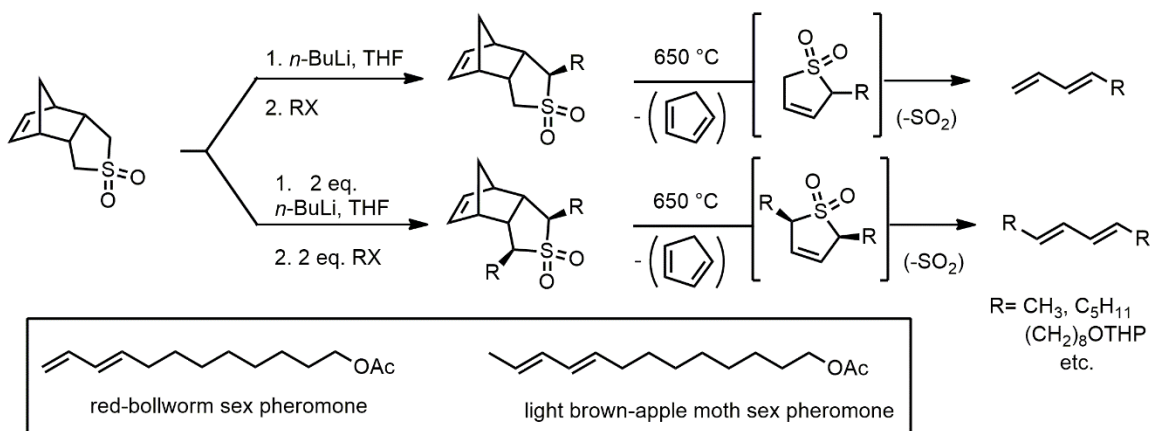


Figure 24. Alkylation of cyclopentadiene-masked 3-sulfolene with *n*-BuLi where X = halogen.

One of the first successful α -alkylations (with an alkyl halide) of a 3-sulfolene adduct was achieved by Takayama and co-workers (Figure 25).¹⁶⁵ Takayama was interested in using sulfur dioxide as a protecting group for the *s-cis*-diene moiety of vitamin D. The THP-protected sulfolene adduct was treated with sodium hydride (NaH) and methyl iodide, resulting in regioselective methylation at the 6-position as a mixture of diastereomers (Figure 25).¹⁶⁵ Using a sterically bulkier base lithium tetramethylpiperidide (LiTMP) with methyl iodide present during deprotonation resulted in methylation at the 19-position (also as a mixture of diastereomers). The presence of the electrophilic species during the deprotonation event was found to be essential to the success of the methylation, since alkylation must occur before the anion-induced ring-opening can occur.¹⁶⁵ Pyrolysis of the methylated products was achieved to produce the corresponding methylated vitamin D derivatives.¹⁶⁵

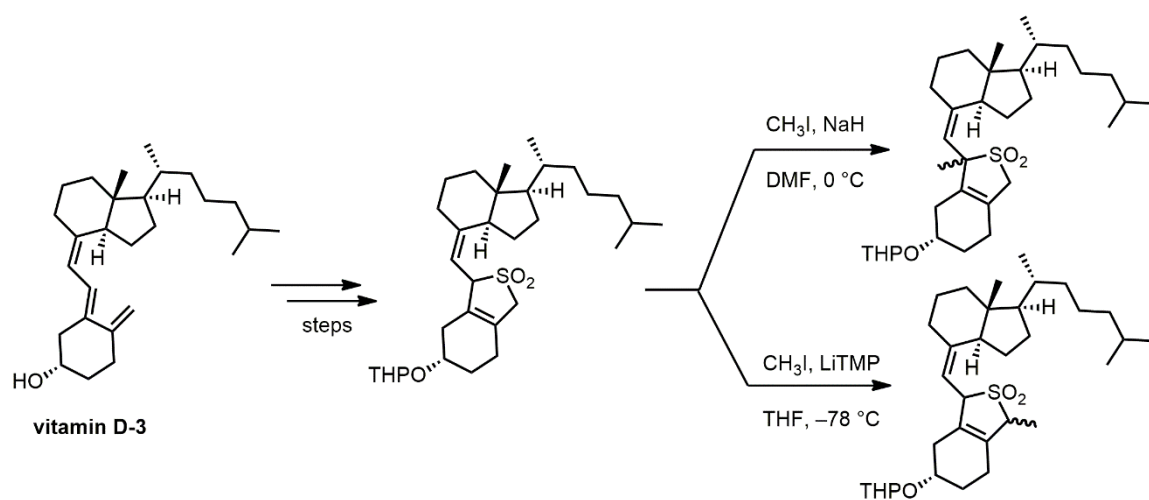


Figure 25. Alkylation of vitamin D-3 derivative with methyl iodide.

Takayama and co-workers extended this methodology, achieving mono- and bis-alkylation of 3-sulfolene itself (to provide 2-substituted-3-sulfolenes and *trans*-2,5-disubstituted-3-sulfolenes) with a variety of primary alkyl iodides using the optimized conditions of lithium bis(trimethylsilyl)amide (LiHMDS) in a mixture of tetrahydrofuran (THF) and hexamethylphosphoramide (HMPA) at $-78\text{ }^\circ\text{C}$ (Figure 26).¹⁸⁷ If the alkyl halide was added after the deprotonation event only traces of product were obtained.¹⁸⁷ Switching the base to potassium hydride (KH) resulted in no conversion, while sodium

is not unexpected under certain basic conditions; upon treatment of 3-sulfolene in aqueous base (NaOH or KOH in water), an almost equimolar equilibrium mixture of 2-sulfolene and 3-sulfolene is known to be established.^{189, 190} Complete conversion and the ring-opening side product could be avoided by simply changing the solvent to the more polar dimethyl formamide (DMF), providing the desired product 2-methyl-3-sulfolene in 69% yield along with 20% of base-isomerized 2-methyl-2-sulfolene (Figure 27). Treatment of the purified 2-substituted-3-sulfolene products with additional NaH resulted in complete conversion to the more stable 2-substituted-2-sulfolene products (Figure 27). More recently it has been shown that substituted 2-sulfolene can be converted to the corresponding substituted diene through isomerization to the substituted 3-sulfolene followed by sulfur dioxide removal in refluxing 1,8-diazabicyclo[5.4.0]undec-7-ene (DBU).¹⁹¹

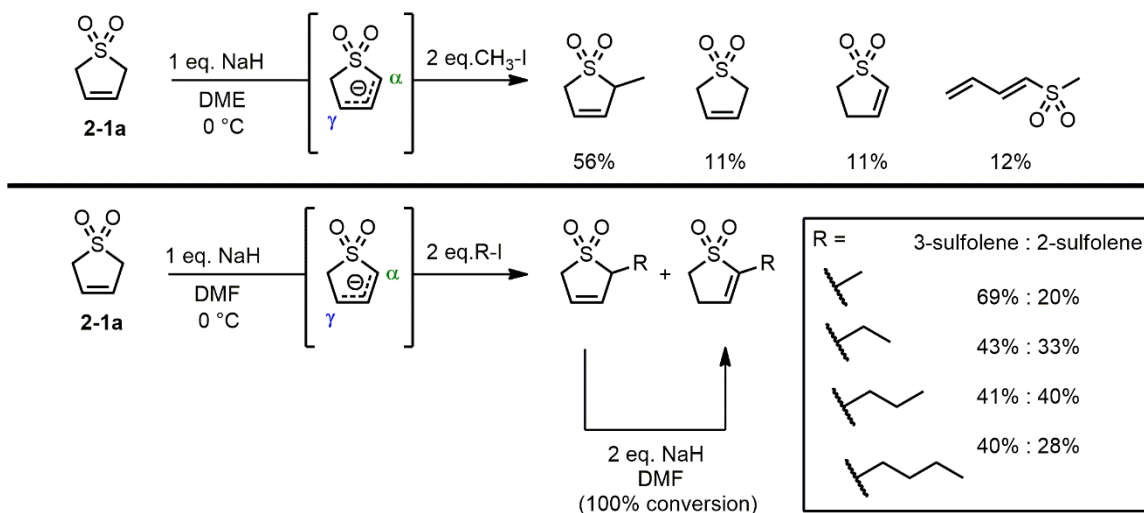


Figure 27. Alkylation of 3-sulfolene using alkyl halides and NaH.

A second study by Chou revealed that the 3-sulfolene anion (generated using *n*-BuLi in THF/HMPA) was stable for up to 15 minutes at -105 °C in the absence of an electrophile.¹⁹² The addition of methyl iodide to this mixture afforded 2-methyl-3-sulfolene in high yield (81%). This change in reaction conditions allowed the addition of electrophiles with acidic protons to be added after the initial deprotonation event. Chou exploited this fact in order to study the acylation of 3-sulfolenes (Figure 28).¹⁹² After the

addition one equivalent of acyl chloride, the proton at the 2-position is now so acidic that formation of the enolate is preferred and a second acylation event occurs at the acetyl oxygen (Figure 28). To circumvent *O*-acylation, methyl iodide was added to react with the enolate before *O*-acylation could take place furnishing 2,2-methyl-acetyl-3-sulfolene products (Figure 28).

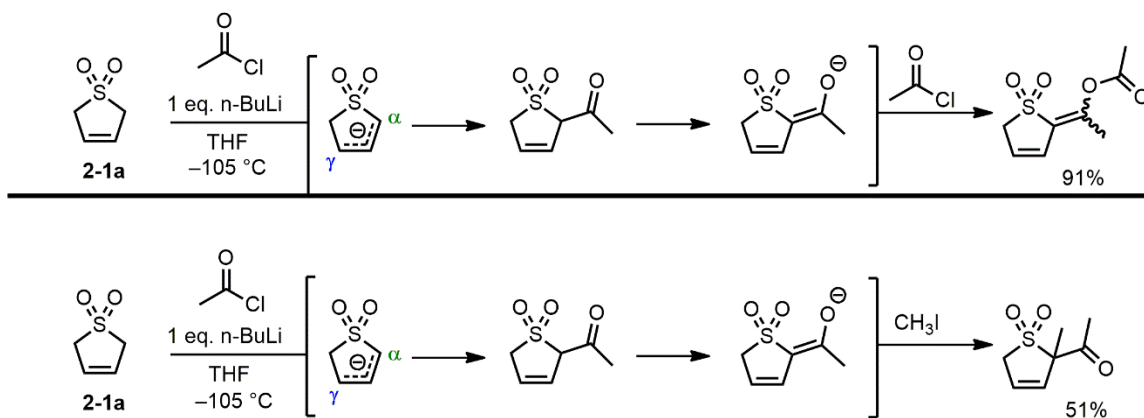
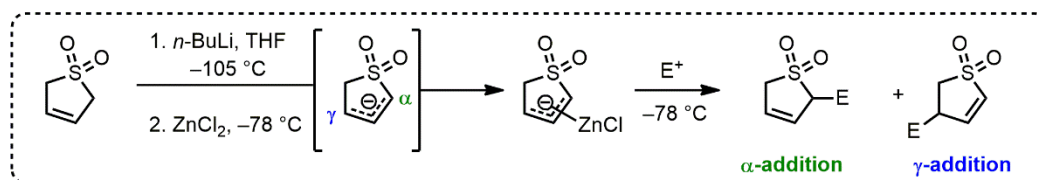


Figure 28. Acylation of 3-sulfolenes with *n*-BuLi.

A strategy developed to stabilize the decomposition-prone 3-sulfolene anion was to exchange the lithium counterion with a softer metal, in order to produce a more covalent species.¹⁹³ Chou investigated the addition of zinc chloride to the pre-formed lithium sulfenylate at $-105\text{ }^{\circ}\text{C}$ which resulted in transmetalation of the lithium cation to zinc(II) (Table 4). The zinc species was found to be stable for multiple days when stored at $0\text{ }^{\circ}\text{C}$. Hard electrophiles such as deuterium oxide (D_2O) and trimethylsilyl chloride (TMSCl) resulted in exclusive alkylation at the α -position, while reaction with the softer diatomic bromine (Br_2) or mono-vinyl carbonyl species resulted in alkylation at the γ -position (Table 4, entry 1-3, 6-7). The reaction of the zinc sulfenylate with cyclohexanone (Table 4, entry 8) when compared with acetone (Table 4, entry 5) indicates a greater amount of γ -addition with greater steric bulk at the electrophilic center. In a second communication, Chou attempted to exchange the zinc sulfenylate back to the lithium sulfenylate by adding lithium chloride.¹⁹⁴ In the case of entry 4 and 8; the addition of eight equivalents of lithium chloride resulted in selectivity for α -addition for entry 4 and a slight selectivity switch for entry 8, a 6:5 ratio of α -: γ -products.¹⁹⁴ From this set of data it appears that the softer nucleophile

(the zinc sulfenylate) prefers to react with soft electrophiles (bromine, vinyl carbonyls) from the γ -position of the 3-sulfolenone anion, while the harder sulfenylate (the lithium sulfenylate) prefers to react from the α -position regardless of the hard/soft nature of the electrophile.¹⁹⁴



	Electrophile (E ⁺)	Product(s)	Yield (%)		Electrophile (E ⁺)	Product(s)	Yield (%)
1 2 3	D ₂ O TMSCl Br ₂	or	99 (α) 72 (α) 92 (γ)	6			95
4		+	86 (1:13)	7			91
5		+	92 (10:1)	8		+	90 (2:3)

Table 4. Reaction of zinc-sulfenylate with a variety of electrophilic partners.

2.1.2. Applications of 3-Sulfolenes to Natural Product Synthesis

The strategy of deprotonation, alkylation and cheletropic removal of sulfur dioxide from substituted-3-sulfolenes has been applied in the total synthesis of a variety of terpene, terpenoids and alkaloid-based natural products.^{168, 175, 178-180, 195, 196} Linear terpene and terpenoid natural products lend themselves well to this aforementioned methodology due to the presence of the 1,3-diene moiety inherent in the core. The mono-terpene *trans*- β -ocimene and sesquiterpene α -farnesene were synthesised by Chou using isoprene sulfone (**2-1b**) via a deprotonation, alkylation and cheletropic removal of sulfur dioxide (Figure 30).¹⁶⁸ Cyclic terpenes α -selinene, α -eudemol natural products were synthesized by utilizing an intramolecular Diels-Alder from a 1,3-diene generated from a 3-sulfolene (Figure 30).¹⁷⁸ The skeleton of the aspidosperma alkaloids was synthesized using an intermolecular Diels Alder from a 3-sulfolene precursor (Figure 30).¹⁹⁵

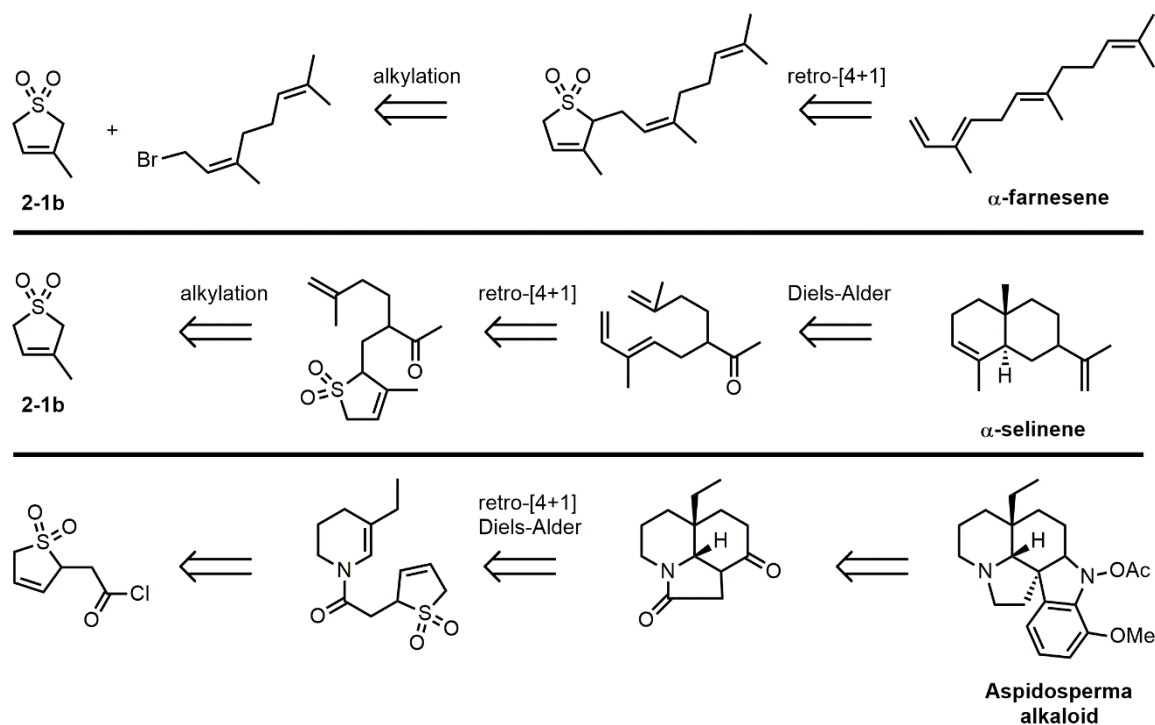


Figure 29. Use of 3-sulfolenes in the total synthesis of a few representative natural products.

2.2.0. Reaction of 3-Sulfolene with Bis-Electrophiles

Tandem reactions between 3-sulfolene with bis-electrophilic alkyl halides have been shown to produce unique [3.3.0] and [3.2.1] sulfone-containing bicyclic frameworks. In order to describe the reactivity between 3-sulfolene(s) and bis-electrophiles, a labeling system has been employed throughout this dissertation (Figure 30). The labeling system can be understood as follows:

1. The 3-sulfolene (**2-1**) is numbered to give the R group the lowest possible designation.
2. Upon first treatment with base, an alpha, beta, gamma, or delta symbol is used to describe the possible positions of the anion on the 3-sulfolene.
3. After mono-alkylation, the mono-alkylated intermediate is numbered to give the newly formed C-C bond the lowest priority.
4. Upon the second treatment with base, an alpha, beta, gamma or delta symbol is again used to describe the position of the anion.
5. In cases where the bis-electrophile is a vinyl carbonyl function, the addition reaction is further classified as occurring in a 1,2 or 1,4 manner.

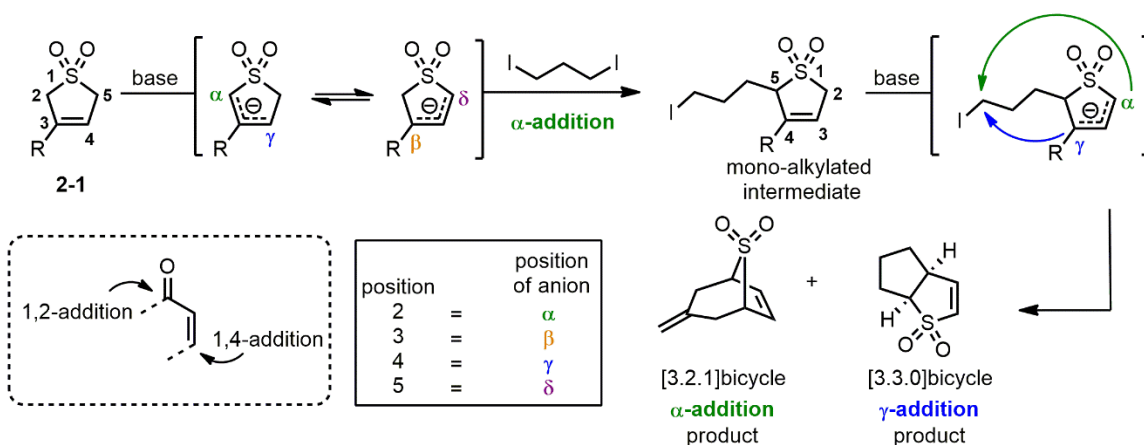


Figure 30. Numbering system employed for describing the reaction between bis-electrophiles and 3-sulfolenes.

The reaction of the 3-sulfolene anion with 1,1-bis(iodomethyl)ethene was shown to produce the corresponding [3.2.1]bicycle (Figure 31).¹⁹⁷ Reductive removal of sulfur dioxide was then achieved with LiAlH_4 to produce the corresponding cycloheptadiene. The formation of the [3.2.1]bicycle can be imagined forming through the addition from the α -position of the 3-sulfolene anion, followed by a second α -addition to form the [3.2.1]bicycle. Reaction of the 3-sulfolene anion with bis-electrophiles 1,3-diopropane and 1,2-bis(bromomethyl)benzene did not produce the expected bridged [3.2.1]bicycles, however instead produced the fused [3.3.0]bicycles (Figure 31).^{198, 199} The mechanism proposed involves the same initial α -addition, however the second nucleophilic addition is now favored from the γ -position after the second deprotonation event. The mechanistic rationale presented for the preference of bridged species (obtained with 1,1-bis(iodomethyl)ethene versus fused species (1,2-bis(bromomethyl)benzene and 1,3-diiodopropane) was that the fused species are favored due to the bulky sulfone group preventing nucleophilic attack from the alpha position, while the bridged species is preferred for 1,1-bis(iodomethyl)ethene due to favorable overlap alignment between the $\text{C}=\text{C}$ π -orbital and the $\text{S}=\text{O}$ π -orbital.¹⁹⁷

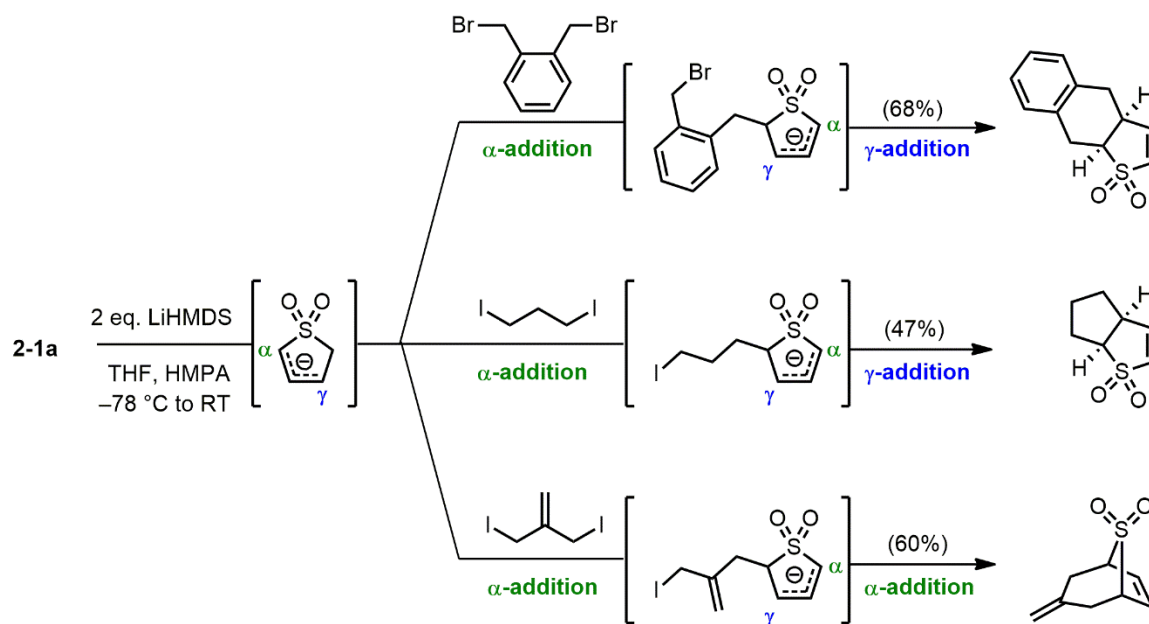


Figure 31. Formation of [3.3.0] and [3.2.1] ring systems from 3-sulfolene and bis-alkyl halides.

Intrigued by the tandem reactivity observed for the dialkylative coupling reactions performed by Chou (Figure 31), the initial direction of this research effort was to utilize 3-sulfolene and bis-vinyl ketone **2-2a** in the synthesis of *meso*-cyclononenone **2-4**. Compound **2-4** is a desired intermediate in our group's proposed synthesis of the spiroketal moiety of the natural product didemnaketal A (Figure 32). The reaction of the **2-1a** with carbonyl and mono-vinyl-carbonyl compounds was briefly studied by Takayama and co-workers.²⁰⁰ The reaction of the butadiene sulfone anion with methyl vinyl ketone was shown to produce the α -1,2-addition product (through nucleophilic attack from the α -position of the butadiene sulfone anion directly to the carbonyl function) and the α -1,4-addition product (proposed to occur through attack of the α -anion to the softer 4-position of the vinyl carbonyl function) in a 1:5 ratio (Figure 32).²⁰⁰ Based on this observation, we were interested in whether the use of a bis-vinyl ketone (**2-2a**) may allow for two α -1,4-additions to occur in either a tandem or sequential fashion to provide the bridged bicyclo[5.2.1]decane structure **2-3**, ideally as the desired *syn*-diastereomer (Figure 32). Elaboration of the bridged sulfur dioxide species to the *meso*-**2-4** could likely be accomplished via a thermally induced retro-(4+1) cycloaddition followed by reduction of the resultant diene to a *cis*-alkene function.

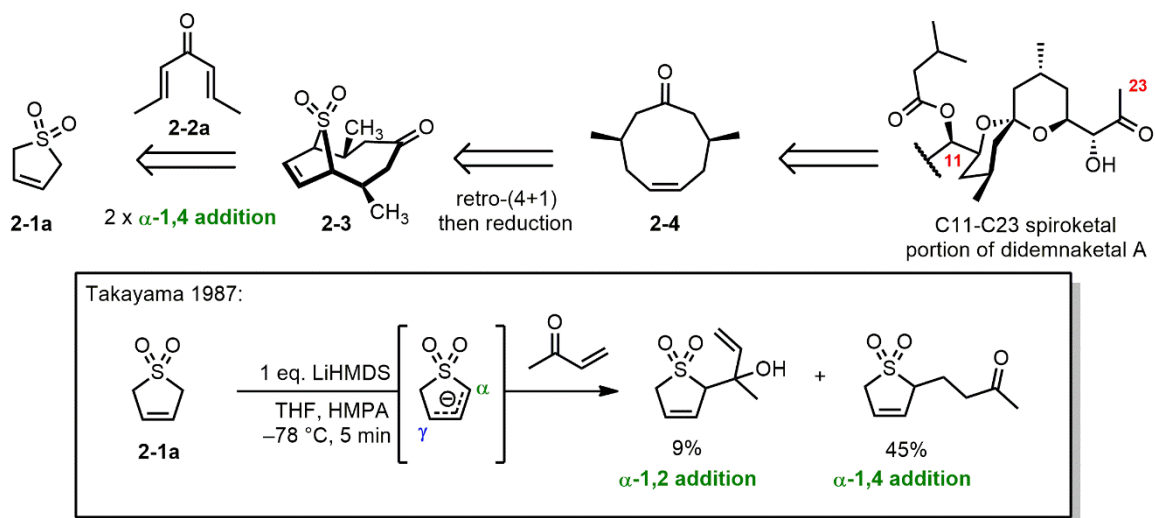
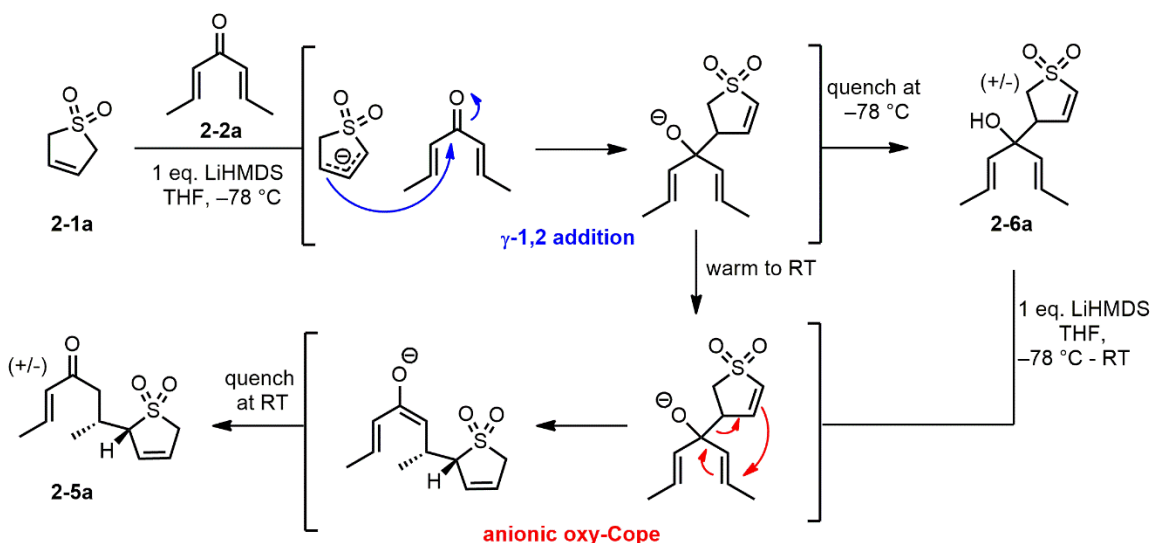


Figure 32. Proposed retrosynthesis of the cyclononenone precursor (**2-3**) and known reactions of the butadiene sulfone anion with methyl vinyl ketone.

In the event, an equimolar mixture of 3-sulfolene and bis-vinyl ketone **2-2a** was treated with LiHMDS at $-78\text{ }^{\circ}\text{C}$, the reaction was stirred for an hour and was allowed to warm to room temperature before quenching with aqueous ammonium chloride to provide the desired net mono- α -1,4 addition product **2-5a**, interestingly as a single diastereomer (Scheme 1). The high diastereoselectivity was surprising as one would expect a close to equimolar distribution of diastereomers through a α -1,4 addition mechanism. In an attempt to explain this anomalous diastereoselectivity, the reaction mixture was quenched at $-78\text{ }^{\circ}\text{C}$ through the addition of acetic acid. In this case, **2-6a** was the major product isolated, originating from attack from the γ -position of the 3-sulfolene anion to the harder 1,2-position of the bis-vinyl ketone (Scheme 1). Upon treatment of intermediate **2-6a** with LiHMDS, smooth conversion to the **2-5a** was observed. The net conversion of **2-1a** to the desired net α -1,4 addition product was therefore most likely obtained through a tandem γ -1,2 addition followed by a diastereoselective [3,3] sigmatropic rearrangement (anionic oxy-Cope).



Scheme 1. Reaction of bis-vinyl ketone **2-2a** with the 3-sulfolene anion to form **2-5a** through a tandem γ -1,2 addition/anionic oxy-Cope.

The 3-sulfolene anion is known to be nucleophilic from the α -position when reacted with alkyl halides and most other electrophiles (see Section 2.1.1), with γ -addition observed in the reaction of the much softer zinc sulfenylate prepared by Chou.^{193, 194} For this reason, the γ -position of the 3-sulfolene anion is often referred to as the soft anion, while the α -position is referred to as the hard anion.²⁰¹ A report by Bhat reports that butanen-1-ol and the butadiene sulfone anion (without HMPA as a co-solvent) produces the α -1,2 addition product but also the γ -1,2 addition product (Figure 33). Under the conditions used by Bhat, no α -1,4 addition product was observed for the reaction of the 3-methyl-3-sulfolene anion and methyl vinyl ketone.²⁰² Exclusive formation of the γ -1,2 addition product was also observed for a severely hindered ketone (Figure 33).²⁰² Upon inspection, it appears possible that the α -1,4 addition product obtained by Takayama,²⁰⁰ may have been formed through a γ -1,2 addition followed by anionic oxy-Cope reaction, similar to the reactivity we observed between **2-1a** and **2-2a**. This is purely speculative, since α -1,4 additions have been previously observed between 3-sulfolene and acrylonitrile (a vinyl nitrile).²⁰³ The preference for γ -addition in our system could be that the sterically hindered ketone leads to the (presumable) thermodynamic 1,2 addition product.

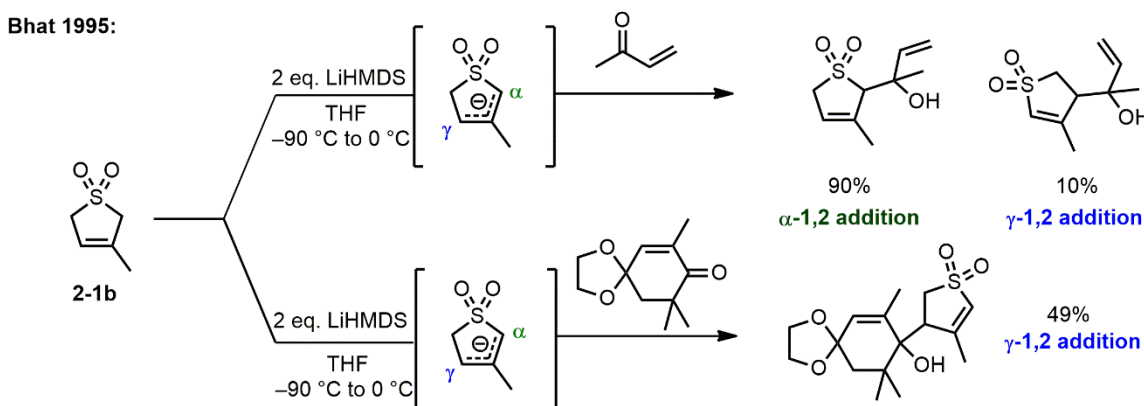
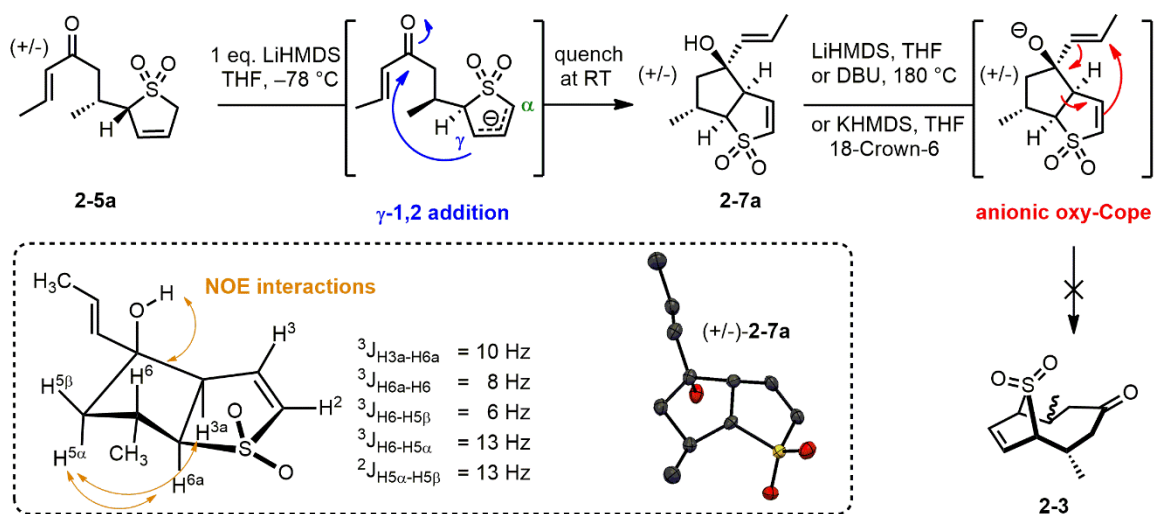


Figure 33. Reaction of 3-methyl-3-sulfolene with mono-vinyl ketones.

With **2-5a** in hand, conversion to the desired bridged [5.2.1]bicycle **2-3** could be envisioned to occur through a second tandem γ -1,2 addition/anionic oxy-Cope event or perhaps through an α -1,4 addition. Post anionic oxy-Cope, prolonged stirring of the enolate

of **2-5a** at room temperature did not induce any further useful reactivity and thus we concluded that the intermediate enolate **2-5a** is not able to deprotonate the α -position of the sulfolene function (Scheme 1). A further treatment of **2-5a** with an equivalent of LiHMDS was required to induce a second γ -1,2-addition to form exclusively the vinyl sulfone **2-7a** as a single diastereomer (Scheme 2). The structure of **2-7a** was elucidated through analysis of 1D and 2D NMR spectroscopy, specifically analysis of the ^1H coupling constant data and nOe interactions (Scheme 2). The 10 Hz coupling constant between bridge head hydrogens H3a and H6a of **2-7a** was indicative of a *cis*-fused ring junction. The relative stereochemistry of the C4 hydroxyl and C6 methyl centers were deduced using an NOESY NMR experiment; correlations were observed between the hydroxyl proton and H6, indicating the C4 hydroxyl and H6 are *syn* with respect to one another. The spectroscopic structural elucidation was later confirmed through X-ray diffraction of a single crystal of **2-7a** (Scheme 2). The large vicinal couplings (13 Hz between H5 α and H6) in the ^1H NMR indicate that the average solution conformation is close to the conformation found in the X-ray structure with the C4 vinyl and C6 methyl groups in *pseudo-equatorial* environments.



Scheme 2. Formation of the [3.3.0] bicyclic sulfone **2-7a** through a γ -1,2 addition.

Unfortunately, no anionic oxy-Cope product **2-3** was observed upon prolonged stirring of the reaction mixture at room temperature (Scheme 2). Further attempts at the synthesis of **2-3** through treatment of **2-7a** with KOtBu and 18-crown-6 or microwave irradiation with DBU were unsuccessful, leading only to recovered starting material or a complex mixtures of products (decomposition). These latter results are unsurprising since it has been well established that the two participating alkenes must be in close proximity to each other for a sigmatropic rearrangement to take place.^{204, 205}

2.3.0. Origin of Diastereoselectivity of **2-5a** and **2-7a**

In order to rationalize the diastereoselective control observed in the tandem γ -1,2 addition/anionic oxy-Cope reaction that led to the formation of **2-5a** we propose that the anionic oxy-Cope arises from a boat shaped transition state (Figure 34).¹⁵⁴ One enantiomeric set of these transition states is shown in Figure 34, with the two chair conformations leading to the unobserved epimer of **2-5a** and the two boat transition states leading to the observed diastereomer. While chair-shaped transition states usually predominate for acyclic substrates since they are usually at a lower energy, conformational restrictions in cyclic systems have been shown to help favour boat-conformations.^{204, 206} In the absence of computational methods, this qualitative analysis does not allow the differentiation between which boat shaped transition state may be preferred; however, it should be noted that the presence of a chelated lithium counter-ion seems essential from the observation that **2-1a** and **2-2a** fail to react cleanly to give **2-5a** in the presence of NaHMDS, KHMDS, or LiHMDS with 18-crown-6 (sequesters lithium). TS-IV may be preferred since it is best oriented to benefit from stabilization through chelation (via the alkoxide and one of the sulfone oxygen atoms) to the lithium counter-ion.

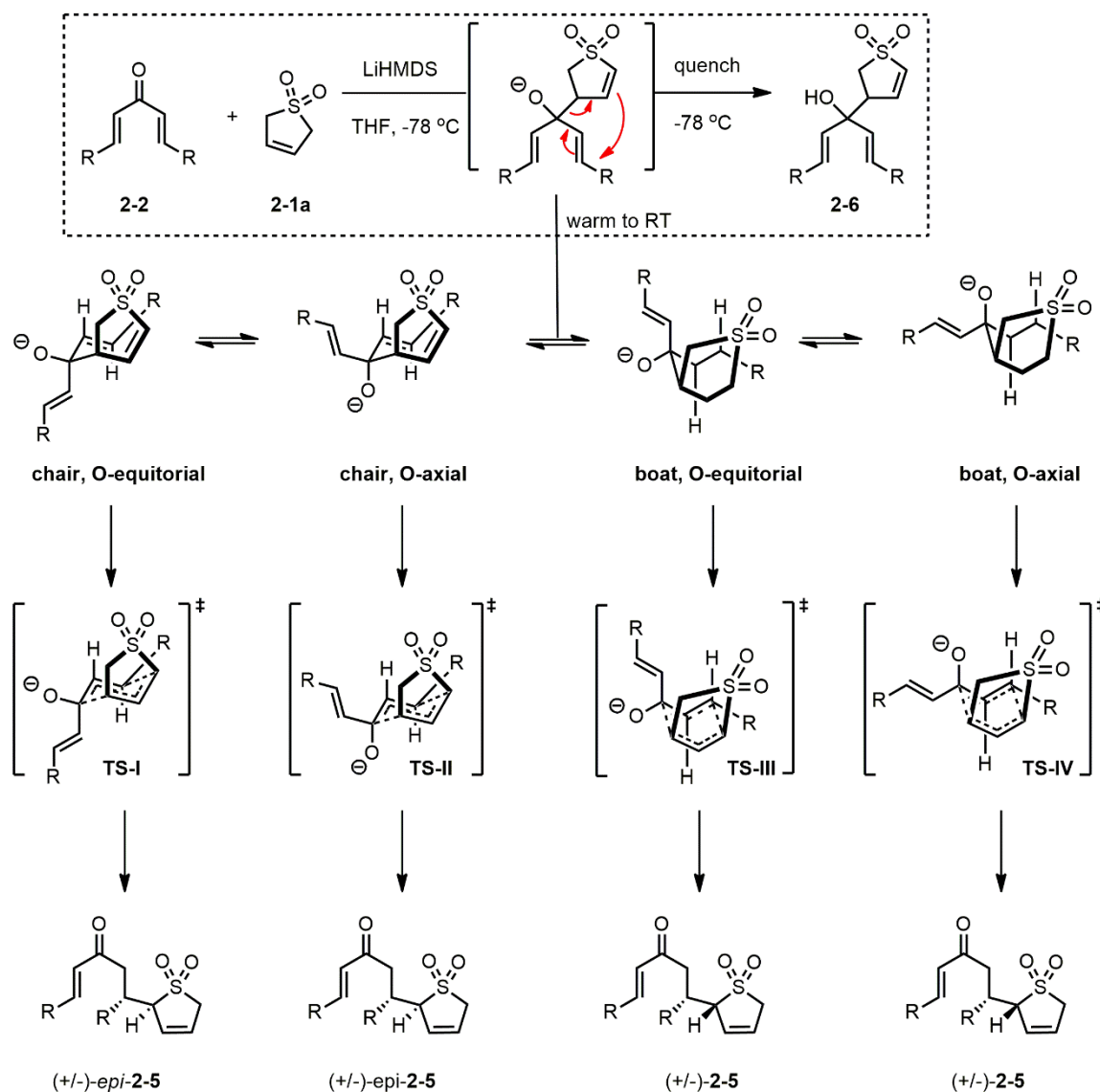


Figure 34. Possible transition states leading to anionic oxy-Cope product **2-5**.

The high level of diastereoselectivity observed during the conversion of **2-5a** into **2-7a** is also of interest. In the most probable reaction pathway leading to the observed diastereomer **2-7a**, we propose that the preferential selection of one diastereotopic face of the ketone is likely due to steric factors. The 3-sulfenylate anion can easily approach the carbonyl group (Figure 35). By contrast, in the most likely pathway leading to the other possible diastereomer of the observed product (*epi-2-7a*) the β -position of the sulfone would suffer an unfavorable steric interaction with the alkene function. Chelation of the

lithium counter-ion by the ketone and sulfone oxygen in the reaction trajectory leading to the observed diastereomer of **2-7** may also be an important factor.

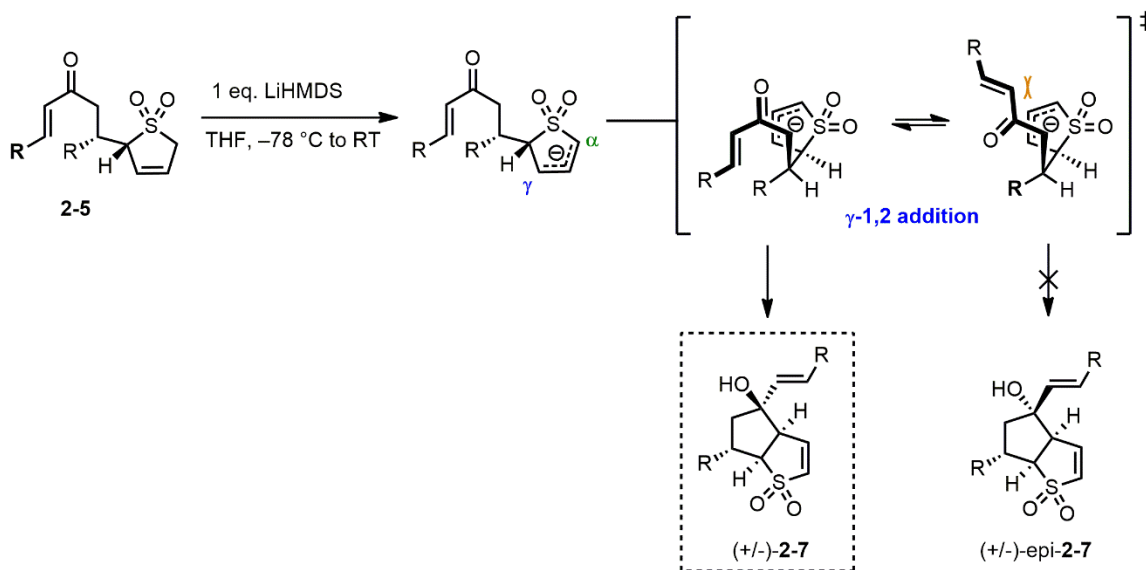
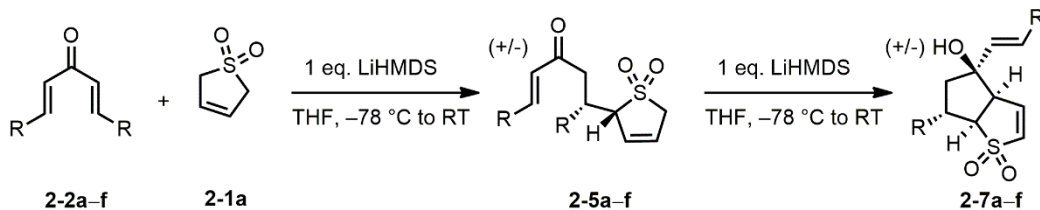


Figure 35. Possible transition state leading to γ -1,2-addition product **2-7**. The orange bracket indicates an unfavorable steric interaction.

2.4.0 Variation of the Bis-Vinyl Ketone Coupling Partner

With the structure of **2-7a** elucidated and a plausible mechanism for its formation rationalized, we next wanted to investigate the scope of our new methodology by varying the substituents on the bis-vinyl ketone (Table 5). Ketone **2-2b** possessing a sterically bulky *iso*-propyl substituent was found to be a competent substrate giving the resultant bicycle **2-7b** over two steps in a 48% yield. Ketones **2-2c–e** were easily synthesized using a double aldol-condensation between acetone and the corresponding bis-aromatic or bis-vinyl aldehydes. Pleasingly, bis-vinyl ketones possessing either a styryl, tolyl, or *p*-methoxyphenyl group in the R position were also good substrates for our two-step procedure, affording the resultant bicycles **2-7c–e** in similar overall yields (Table 5). Reaction of **2-2f** (with an electron withdrawing carboxymethyl group in the R position)

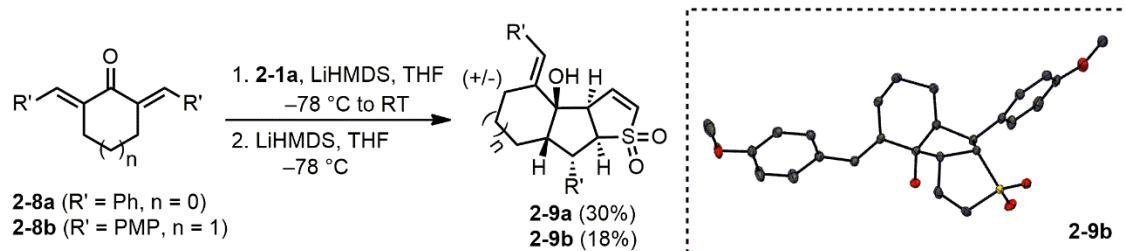
with 3-sulfolene did not yield any identifiable product corresponding to **2-7f**, and only a mixture of isomerized 2-sulfolene and unreacted 3-sulfolene were obtained.



Entry	5a	5b	5c	5d	5e	5f
R =						
Yield from 2-1a (%)	23%	48%	38%	42%	45%	not observed

Table 5. Scope of the tandem γ -1,2 addition/anionic oxy-Cope, followed by a γ -1,2 addition.

With a variety of acyclic bis-vinyl ketones tested, we wondered whether cyclic bis-vinyl ketones **2-8a** and **2-8b** would be capable electrophilic partners (Scheme 3). In the event, the tricyclic products **2-9a** and **2-9b** were obtained in 30% and 18% yield respectively over two steps, each containing five contiguous stereocenters and isolated as single diastereomers. The low yield of **2-9b** can be partially attributed to the lack of solubility of **2-8b** in THF at $-78\text{ }^\circ\text{C}$. The additional fused ring of **2-9a** and **2-9b** was determined to possess a *cis*-geometry about the bicyclic core by ^1H NMR and by single crystal X-ray diffraction (obtained for **2-9b**).



Scheme 3. Formation of tricyclic sulfones using cyclic bis-vinyl ketones.

Although the isolated yields of **2-7a–e** after purification are relatively modest over two steps, the percent conversion of starting material to product for each step is >90% by NMR, indicating the majority of product loss is due to column chromatography. Various methods of purification were investigated: chromatography over different types of silica (pore size, grain size) and alumina (neutral, basic, acidic), as well as recrystallization. Similar yields were obtained using different types of silica and neutral alumina in different solvent systems. Recrystallization of the crude products was possible, however only found to be reliable (high percent recovery and purity) after prior purification by chromatography. The reactions are amenable to scale-up, with batches up to 20 grams of **2-7c** and **2-7e** isolated readily.

2.5.0. Application of the 2-7 Core Towards Neuraminidase Inhibition

Shortly after the synthesis and structure elucidation of **2-7a** was completed, it was identified that the C4 and C6 substituents of bicycle **2-7** are presented in similar *pseudo*-equatorial orientations as the C1-carboxylate and C4-guanidinium groups in the enzyme bound conformation of the viral neuraminidase inhibitor peramivir (**1-17**, Figure 36). Upon closer inspection of the overlaid solid state structure of **2-7a** with the enzyme bound conformation of peramivir, the sulfone moiety overlays well with the carbonyl function of the *N*-acetyl group of peramivir (which binds in the S3 sub-site), while functionality projected from the C2 and C3 positions of **2-7a** would overlay well with the position of the 3-pentyl moiety of peramivir. Using detailed ¹H NMR analysis of the coupling constants and computational modelling studies we have shown unequivocally that the bound state of peramivir differs significantly from both the solution and solid (unbound) phases.²⁰⁷ This conformational flexibility of peramivir in solution means that for efficient binding to the influenza neuraminidase active site, energy (4.5 kJ/mol, MD simulations)²⁰⁷ must be consumed to reach the ideal conformation before binding to the enzyme. The apparent rigidity of **2-7a** in solution (¹H NMR) and close to ideal overlay with peramivir (bound peramivir versus unbound solid state **2-7a**) suggests that the [3.3.0]bicyclic core of **2-7** could be a useful scaffold for the generation of conformationally restricted inhibitors of

neuraminidase enzymes. The benefits of a conformationally-restricted platform for generation of an inhibitor against an enzyme will be discussed in the following thesis chapter.

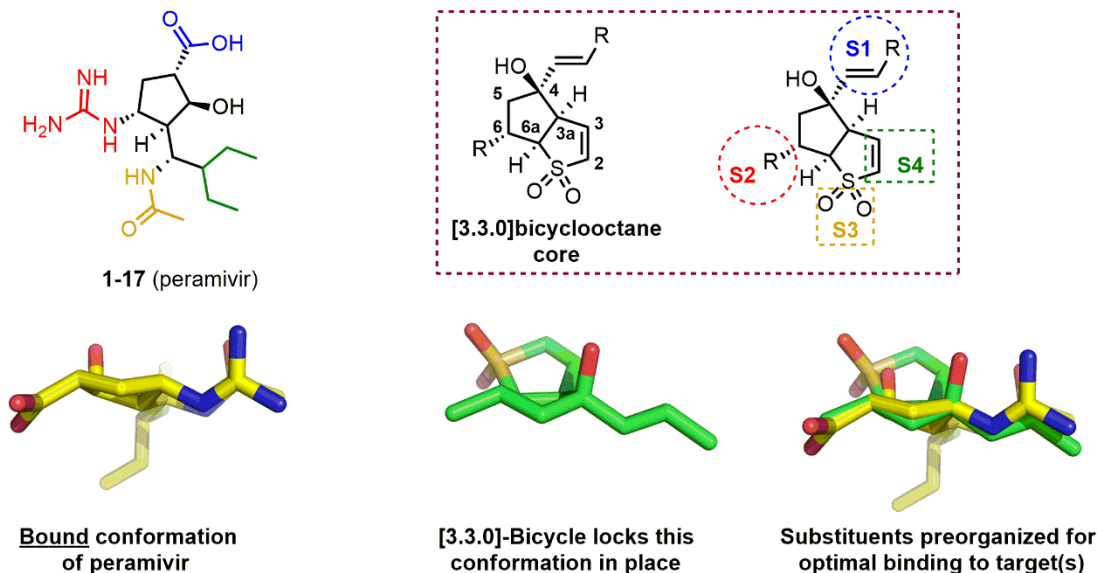


Figure 36. Overlay of **2-7a** (solid phase) and peramivir (enzyme bound).

2.6.0. Chapter Summary

Exploration of the chemistry between bis-vinyl ketones **2-2** and butadiene sulfone **2-1a** was studied and a previously undescribed reactivity profile for **2-1a** was unveiled. The two step tandem γ -1,2 addition/anionic oxy-Cope, followed by a second γ -1,2 addition to form bicycles **2-7a-e** as a single diastereomers was successfully accomplished and a plausible reaction trajectory rationalizing the diastereoselectivity was developed. Although the formation of [3.3.0]bicyclic products has been reported for the reaction of **2-1a** and bis-electrophilic alkyl halides, the products reported here are more highly functionalized, formed through a previously unreported tandem reaction (γ -1,2 addition/anionic oxy-Cope) and were obtained as single diastereomers. Perhaps more importantly, the similarity of the conformation of **2-7a** and the viral neuraminidase inhibitor peramivir was realized. A rigid

bicyclic inhibitor of neuraminidase inspired by the cyclopentane core of peramivir in which the substituents are pre-organized for optimal binding to the S1-4 subsites of the enzyme active site could prove to be a useful strategy for inhibiting neuraminidases. Further rationale as well as the synthesis and characterization of such bicyclic inhibitors based on the **2-7** [3.3.0]bicyclic archetype will be the subject of Chapter 3.

Chapter 3. Bicyclic Inhibitors of Neuraminidase

The material in sections 3.1.0-3.5.0 was adapted from: M. G. Brant and J. E. Wulff (2012) A Rigid Bicyclic Platform for the Generation of Conformationally Locked Neuraminidase Inhibitors. *Organic Letters*, 14, 5876-5879.²⁰⁸

All the synthesis, analysis and characterization of data was performed by MGB. All X-ray structures were solved by Dr. Allen G. Oliver (University of Notre Dame). Dr. Tyler Trefz and Dr. Ori Granot (University of Victoria) collected the HRMS data. NP-40 inactivated virus was provided by Dr. Martin Petric and co-worker Tracy Chan (BC CDC). Jeremy Mason and Dr. Martin Boulanger (University of Victoria) provided recombinant H1N1 neuraminidase (used in preliminary assays) and helpful discussions. Dr. Amgad Albohy and Dr. Christopher W. Cairo (University of Alberta) conducted all enzymatic assays using human neuraminidases NEU1-4. All enzymatic assays using viral or bacterial neuraminidases were performed by MGB with guidance from Dr. Jeremy E. Wulff.

3.1.0. Introduction

The rigidification of a conformationally flexible ligand can be an atom-economical approach to improve the pharmacological properties of a ligand for the purpose of small-molecule drug design/optimization.²⁰⁹ When a flexible molecule binds to a target, energy is required for the ligand to adopt a favorable binding conformation with its host. Entropically, this “freezing” of a bound ligand is inherently unfavorable. Limiting the conformational flexibility of a ligand through ring formation, or through the introduction of a sterically large functional groups which hinder bond rotation, can help to pre-form a favorable binding conformation (Figure 37).²⁰⁹ This pre-organization of the ligand can increase binding affinity to the target by reducing the entropic conformational-change penalties.²⁰⁹ Perhaps more importantly, reducing the number of conformers in solution can improve the pharmacokinetic properties of a drug by improving selectivity against different iso-forms of the target and by reducing off-target binding (*e.g.* some conformers may be more easily degraded by metabolic enzymes).²⁰⁹ Furthermore, it has been well established by Verber *et al.* that there is a correlation between higher oral bioavailability (in an animal model) of small-molecule drug candidates that contain fewer than 10 rotatable bonds.²¹⁰ Despite the benefits of rigidification, care must be taken as this approach can be detrimental when a biological target is prone to mutation-induced resistance: a more rigid molecule may no longer be able to adopt a favorable binding conformation to bind to the mutant.

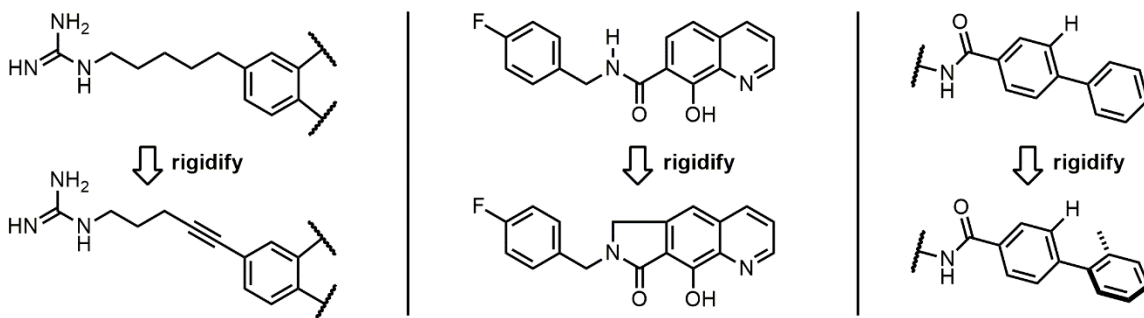


Figure 37. Examples of some rigidification strategies.

As introduced briefly in Section 2.5.0, we have identified that the [3.3.0]bicyclic archetype **2-7** presents its C4 and C6 substituents in *pseudo*-equatorial orientations, reminiscent of the orientation of the C1-carboxylate and C4-guanidinium functions found in the conformation of peramivir when bound to influenza neuraminidase (Figure 38E). The cyclopentane ring of peramivir differs significantly from the six-membered ring scaffolds upon which zanamivir (dihydropyran) and oseltamivir (cyclohexene) are based; yet all three inhibitors present their side chains in similar orientations to bind with influenza neuraminidase.²⁰⁷ Comparison of the solid phase (unbound)²¹¹ and the neuraminidase-bound X-ray structure of peramivir reveals a conformational discrepancy (Figure 38A/B). Therefore, in order to bind to neuraminidase peramivir must undergo a significant conformational change. To formalize and quantify this observation, in collaboration with the Dr. Christopher W. Cairo group (University of Alberta), Dr. Michele R. Richards (University of Alberta) used a number of computational methods (DFT and MD) to arrive at an average solution structure for peramivir which best matches the experimentally observed coupling constants in the ¹H NMR spectrum (recorded in D₂O at 500 MHz and later by Richards at 700 MHz).²⁰⁷ The computationally determined average solution structure overlays well with solid phase (unbound)²¹¹ peramivir with similar angles of projection of the C1-carboxylate and C4-guanidinium substituents with an energy difference between the conformers determined by DFT calculations to be 1.1 kJ/mol (Figure 38). In comparison, the average solution structure has substantially different angles of projection compared to the enzyme-bound structure of peramivir (Figure 38D). DFT calculations revealed the enzyme-bound conformation of peramivir is 4.5 kJ/mol higher in energy than the average solution conformation. The large 10-13 Hz coupling constants and NOE interactions observed in the ¹H NMR spectra for **2-7a** (Scheme 2) indicates that the average solution structure and the solid structure are of similar conformations (*i.e.* the C4-olefin and C6-methyl substituents are in pronounced equatorial positions).²¹² Analysis of the bond angles of the solid state structure of **2-7a** indicates the all carbon ring of **2-7a** presents its C4 and C6 substituents at similar angles of projection as the enzyme-bound conformation of peramivir (Figure 38E). Although the calculated energy difference between the enzyme bound and solution conformation of peramivir is relatively small (4.5 kJ/mol), rigidified scaffolds (such as the [3.3.0]bicyclic core of **2-7a**) could prove useful

for generating selective inhibitors of neuraminidases in which isoform specificity is desired (e.g. human and bacterial neuraminidases). The therapeutic effect of human and bacterial neuraminidase inhibition *in vivo* with a small molecule has yet to be determined. Selective inhibitors of any human or bacterial neuraminidase could prove to be useful tools for studying both structure and function of these enzymes.

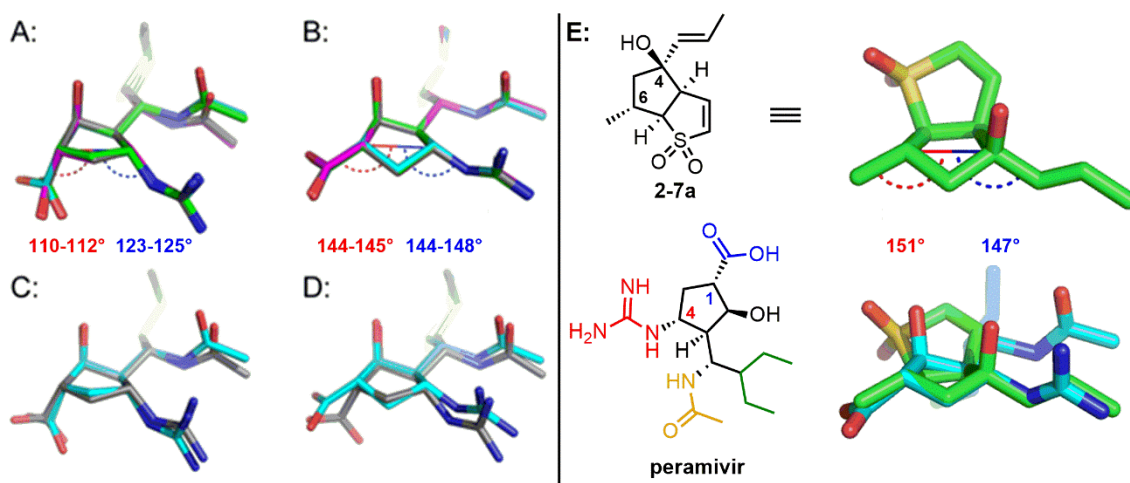


Figure 38. (A): The four conformations of peramivir found in the solid-state X-ray structure of the unbound molecule. (B): Enzyme-bound structure of peramivir in the active site of four influenza A neuraminidases, PDB 2HTU (grey), 1L7F (cyan), 1L7G (green), and 1L7H (magenta); (C): Overlay of computationally determined solution structure of peramivir (grey) overlaid with unbound peramivir (cyan). (D): Overlay of computationally determined solution structure of peramivir (grey) with enzyme-bound peramivir (1L7F, cyan) (E): Crystal structure of 2-7a (green) and overlay of crystal structure of 2-7a with enzyme bound peramivir (cyan, PDB 2HTU).

There are a few reports of bicyclic inhibitors in the influenza neuraminidase literature (Figure 39). Bicyclic analogs of the highly potent Abbott Laboratories pyrrolidine inhibitor A-315675 ($K_i = 0.21 \text{ nM}$)¹⁰² have been disclosed in a patent; no specific inhibition activities were reported, however the patent does note that “preferred compounds of this invention inhibit influenza A neuraminidase and influenza B neuraminidase with K_i values between about 0.1 nanomolar and 3.5 micromolar”.²¹³ Two bicyclic analogs of oseltamivir have been reported (Figure 39). The [3.2.1]bicyclic oseltamivir analog (with a hydroxyl group at the C5 position) displayed activity of $80 \mu\text{M}$.²¹⁴ The activity of the C5-hydroxyl

analog of oseltamivir has not been published for direct comparison with the bicyclic analog; it is known that the activity of the C3-amino analog of zanamivir (320 nM)²¹⁵ differs from that of the C3-hydroxyl analog DANA (6 μ M)²¹⁵ by about twenty fold. It can therefore be roughly concluded that the [3.2.1] bicyclic property in this case is likely detrimental to activity. Similarly, the [2.2.2]bicyclo-hydroxyl analog of *O*-propyl-oseltamivir was found to be almost inactive against the neuraminidase strain tested: 12% inhibition was observed at a concentration of 660 μ M compound.²¹⁶

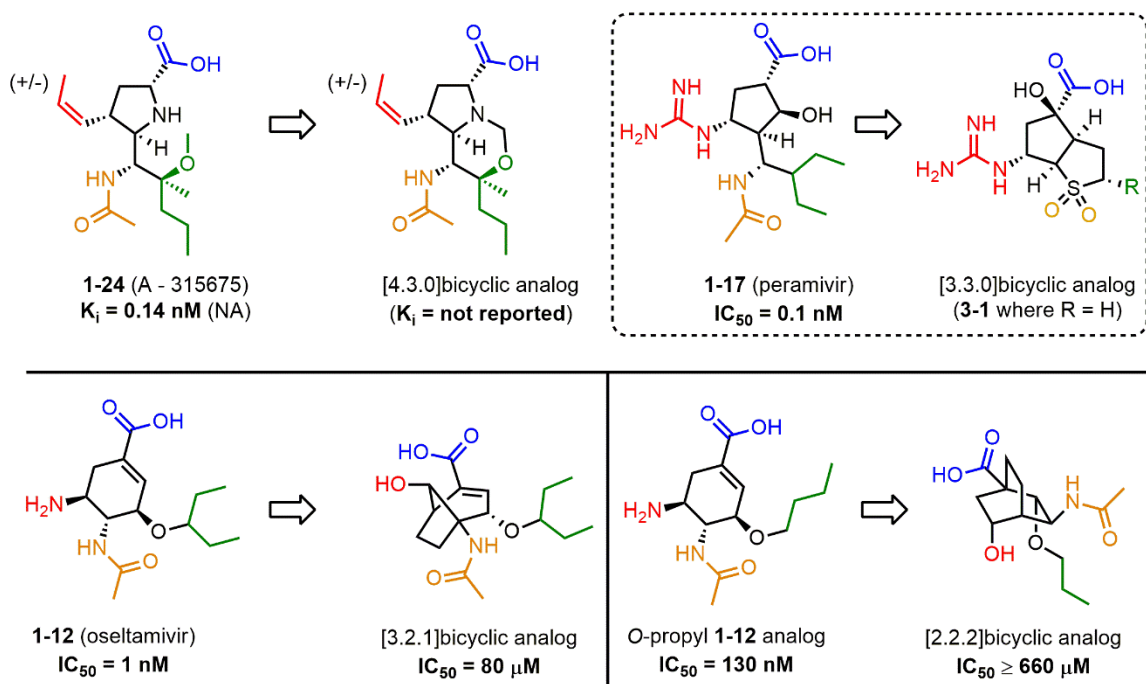


Figure 39. Known bicyclic inhibitors of influenza neuraminidase.

The objective of this thesis chapter is to investigate whether a rigid scaffold based on the [3.3.0]bicyclic archetype of **2-7** can adapt itself to project its substituents in effective positions to bind to a neuraminidase active site. As a proof of principle, we decided to target the S1-S2 subsite binder guanidino-acid **3-1**. Competitive inhibition of neuraminidase using **3-1** would give us valuable evidence that the [3.3.0]bicyclic scaffold is able to project the C4-carboxylate and C6-guanidinium functions into the S1 and S2 subsites, respectively. The X-ray structure of **2-7a** was used to create a model (in MOLOC)²¹⁷ of **3-1** by hydrogenating the vinyl sulfone function and replacing the C4 and

C6 substituents with a carboxylate and a guanidinium group respectively. This model was then energy minimized (in the absence of the enzyme), and overlaid on top of the peramivir bound in the active site of a H5N1 neuraminidase (PDB: 2HTU) using the pair-fitting function in Pymol (Figure 40). The C4-carboxylate and C6-guanidinium groups of the modelled **3-1** overlay well with the corresponding C1-carboxylate and C4-guanidinium functions of peramivir. Of additional interest, one of the sulfone oxygen atoms appears to be well situated to form a hydrogen bond with Arg152 in the S3 subsite (Figure 40), while substituents projected from the C2 position of **3-1** appear to extend towards the S4 subsite.

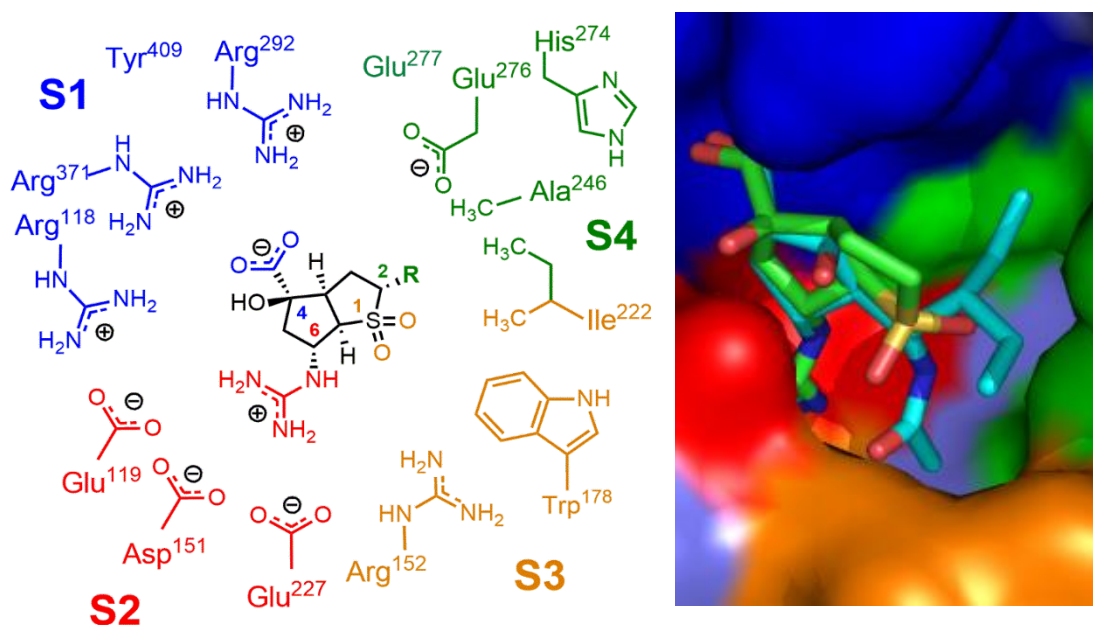


Figure 40. Sulfone 3-1 (R=H) in the neuraminidase active site. Overlay of sulfone 3-1 (green) with peramivir (cyan) docked in the neuraminidase active site.

The proposed synthesis of guanidino-acid **3-1** began with vinyl sulfone **2-7c** (Figure 41). Installation of the S1 probing carboxylic acid function was envisioned through the oxidative degradation of the C4-diene; the C6-nitrogen functionality of **3-1** (to bind in the S2 sub-pocket) could presumably be accessed via a Curtius rearrangement of a carboxylic acid group located at the C6 position. The Curtius rearrangement involves the concerted thermal decomposition of an acyl-azide into an isocyanate through a putative nitrene

intermediate (Figure 41).²¹⁸ Upon *in situ* addition of an alcohol, amine, or water to the isocyanate, the resulting carbamate, urea or free amine can be accessed respectively.

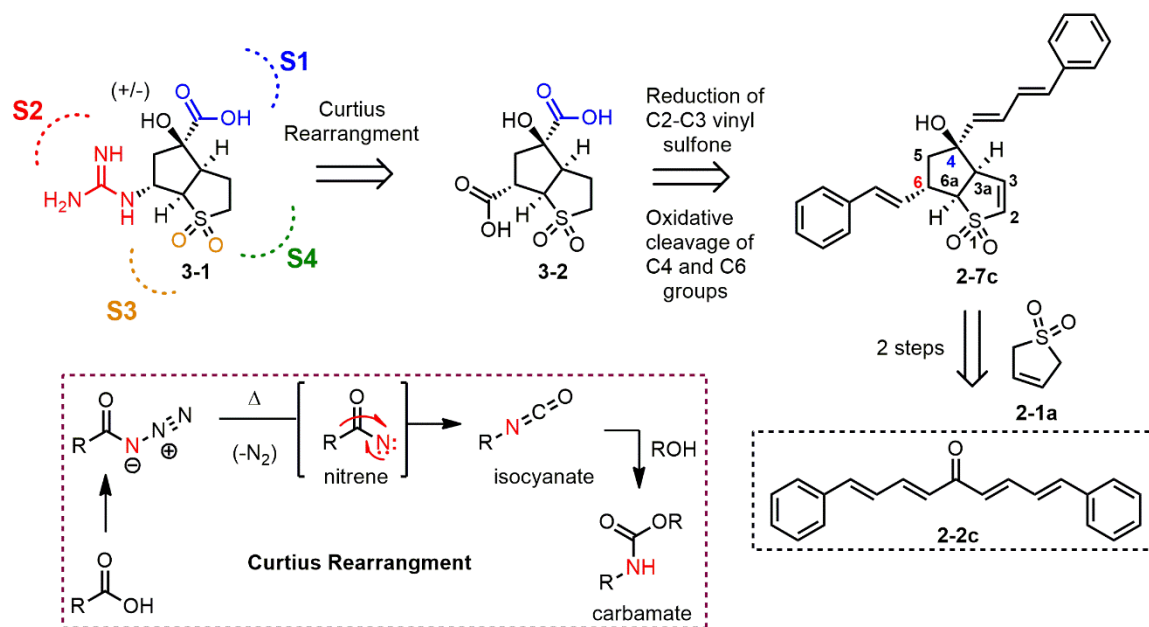
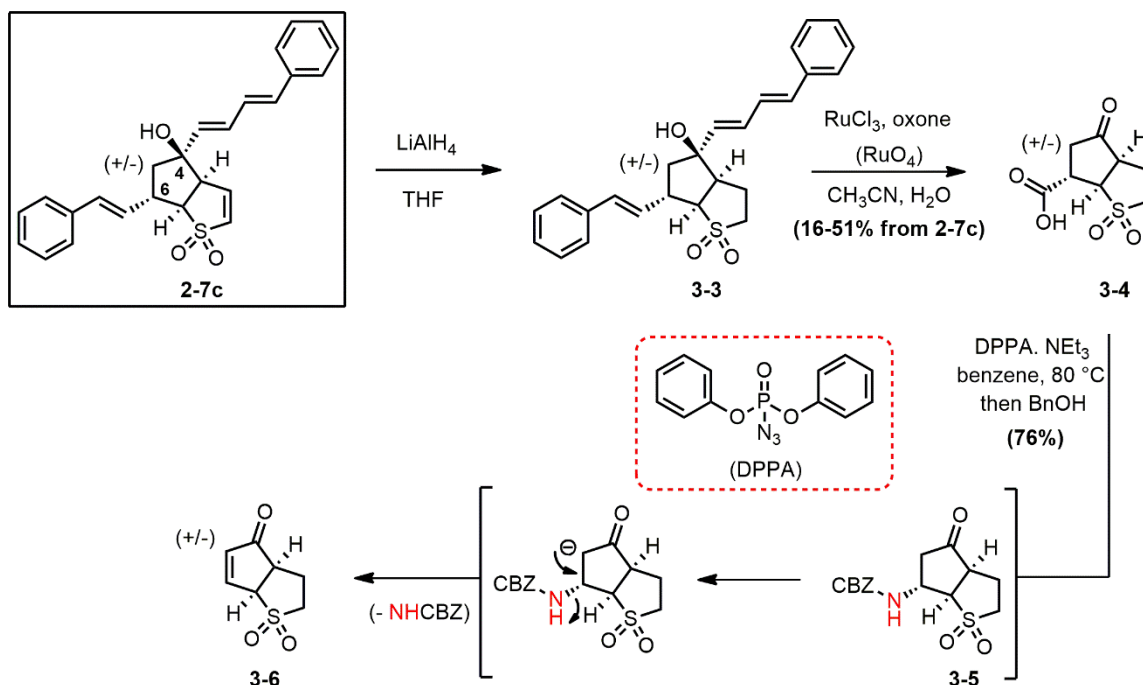


Figure 41. Retrosynthesis of guanidino-acid 3-1 from vinyl sulfone 2-7c via a Curtius rearrangement.

3.2.0. Synthesis of a Bicyclic S1, S2 Viral Neuraminidase Subsite Binder

To begin, the vinyl sulfone function of **2-7c** was reduced with lithium aluminum hydride (LiAlH₄). With the vinyl sulfone function reduced, a number of oxidative conditions were evaluated for their ability to cleave off the extraneous C4-diene and C6-olefin functions of **3-3**. Ozonolysis with reductive work-up (O₃, -78 °C followed by dimethyl sulfide or triphenyl phosphine) in a variety of solvents (methanol, dichloromethane, ethyl acetate) failed to deliver any identifiable product. Treatment of **3-3** with ruthenium tetroxide (RuO₄, generated *in situ* from RuCl₃ and potassium peroxymonosulfate, KHSO₅) in a biphasic acetonitrile/water/carbon tetrachloride solvent system provided cleavage of the C4-diene function to a ketone (Scheme 4). In the event the C6-olefin was also cleaved to a carboxylic acid providing keto-acid **3-4** in one pot. The

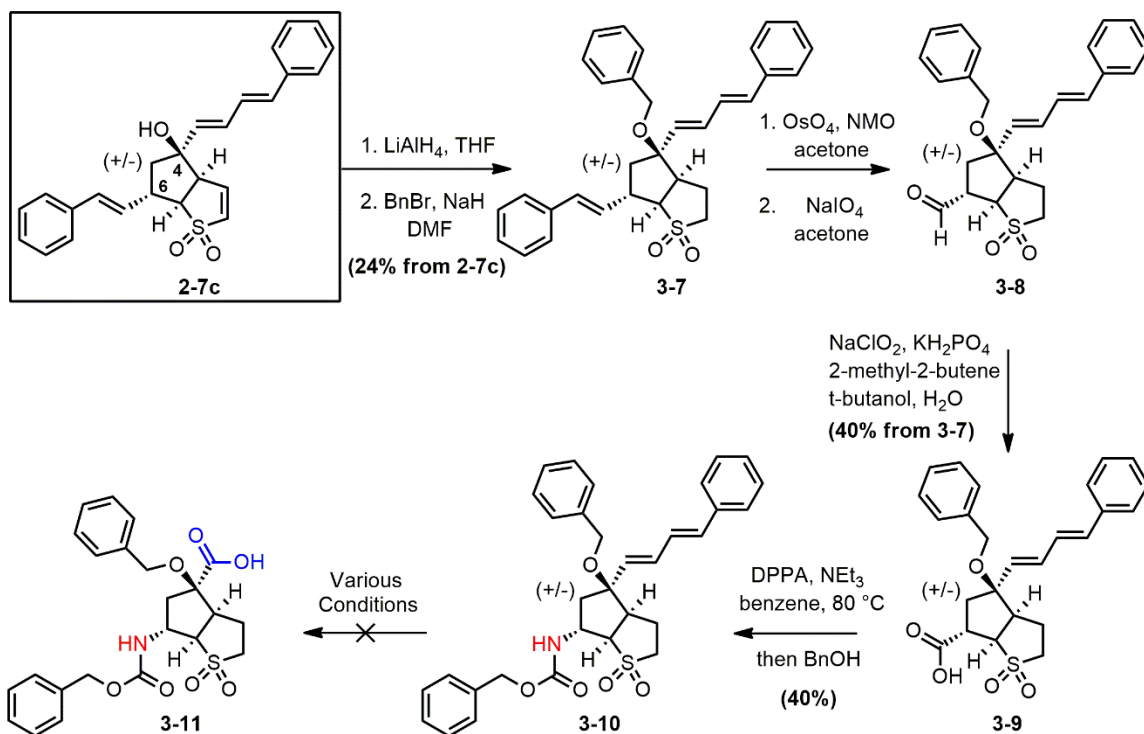
yield for this transformation was highly variable (16-51%) due to the presumable water solubility of **3-4** and the “messy” aqueous extraction required to remove the ruthenium catalyst. With the C6-carboxylic acid in place, Curtius rearrangement using diphenylphosphoryl azide (DPPA) failed to generate the desired CBZ-protected amine **3-5**. Instead α - β -unsaturated ketone **3-6** was isolated in a 76% yield (Scheme 4). It can be imagined that in the presence of base elimination of the carbamate function of **3-5** could occur to generate ketone **3-6**.



Scheme 4. Synthesis of α - β -unsaturated ketone **3-6** from vinyl sulfone **2-7c**.

Since the presumed carbamate intermediate **3-5** was prone to elimination due to the presence of a ketone at the C4 position, it was deemed necessary to protect the C4-alcohol group as a benzyl ether to circumvent formation of the ketone function during the oxidation of vinyl sulfone **3-3** (Scheme 5). Treatment of *O*-benzyl-protected **3-7** with catalytic RuCl_3 and oxone (or catalytic osmium tetroxide (OsO_4) and NaIO_4) provided no identifiable material by ^1H NMR after extraction of the reaction mixtures with ethyl acetate. Similarly, treatment of **3-7** under ozonolysis conditions (O_3 , followed by Ph_3P or Me_2S) produced a

complex mixture of products. Gratifying, with catalytic amounts of OsO₄ and a single equivalent of *N*-methylmorpholine *N*-oxide (NMO) as the stoichiometric oxidant, the C6-olefin function could be selectively dihydroxylated (Scheme 5). Exposure of the crude mixture of diastereomers to NaIO₄ furnished the C6-aldehyde **3-8**. A Pinnick oxidation (sodium chlorite, NaClO₂) was used to convert the C6-aldehyde to the carboxylic acid **3-9** in a 69% yield from **3-7**. Satisfyingly, a Curtius rearrangement on carboxylic acid **3-9** provided the desired *N*-protected product **3-10** in a 40% yield (Scheme 5). However (and discouragingly) cleavage of the C4-diene of **3-10** proved problematic: a number of oxidative conditions were performed (RuCl₃/oxone, RuCl₃/NaIO₄, O₃/Me₂S, and OsO₄/NMO followed by NaIO₄) without success.



Scheme 5. Synthesis of carbamate **3-10** from vinyl sulfone **2-7c**.

Unable to convert the C4-diene of sulfone **3-10** to a carboxyl group we re-directed our synthetic approach to guanidine acid sulfone **3-1** in order to avoid the troublesome oxidative cleavage of a diene function. The new approach would make use of a deliberate step-wise oxidation strategy to first convert the C4-olefin of **2-7e** to a protected carboxylic acid, then convert the *para*-methoxyphenyl ring at the C6-position directly to a carboxylic acid for subsequent use in a Curtius rearrangement (Figure 42).

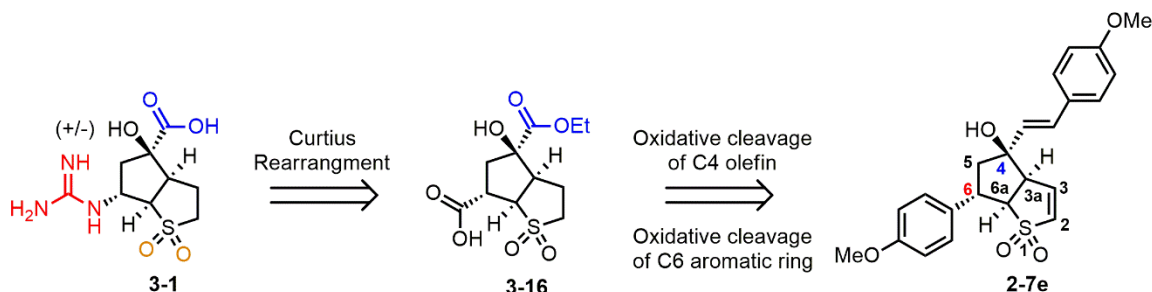
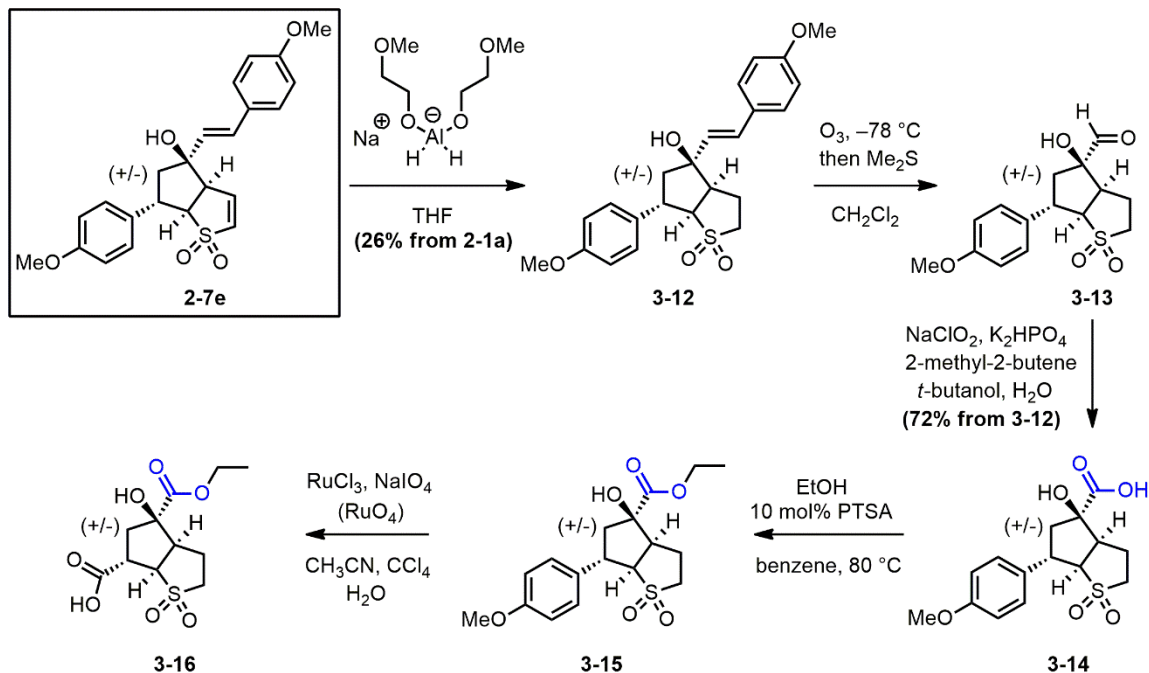


Figure 42. Retrosynthesis of guanidino-acid 3-1 from vinyl sulfone 2-7e.

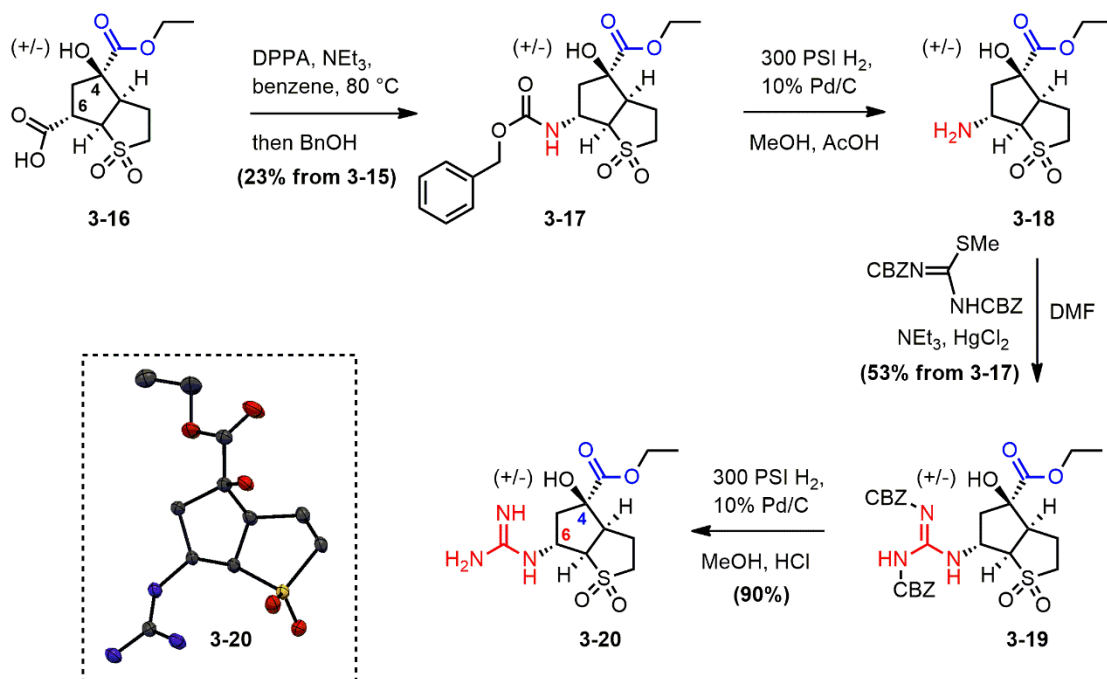
Starting with sulfone **2-7e**, the vinyl sulfone function was reduced using sodium bis-(2-methoxyethoxy)aluminumhydride (Red-Al). These conditions proved superior to reduction with LiAlH_4 , due to the better separation of the desired sulfone from the aluminum salts that were generated during the reaction and subsequent quench. An ozonolysis reaction followed by Pinnick oxidation on sulfone **3-12** provided C4-carboxylic acid **3-14**. Protection of the resulting C4-carboxylic acid was achieved using ethanol and catalytic *para*-toluenesulfonic acid (Scheme 6). Quantitative conversion of **3-14** to ester **3-15** was assisted by the sequestration of water through azeotropic distillation with benzene using a Dean-Stark apparatus. The key synthetic transformation, the aromatic oxidative cleavage of the C6-*p*-methoxyphenyl group with ruthenium chloride and 15 equivalents of NaIO_4 afforded the desired C6 acid **3-16** (Scheme 6). In order to achieve complete conversion, additional aliquots of catalyst were required over the course of reaction due to catalyst escape!



Scheme 6. Conversion of vinyl sulfone 2-7e to carboxylic acid 3-16.

With C6-acid **3-16** in the flask, a Curtius rearrangement provided CBZ protected amine **3-17** in a 23% yield over 2 steps from ester **3-15** (Scheme 7). In order to save a synthetic step (*i.e.* avoid removing the CBZ protecting group) the use of water instead of benzyl alcohol was attempted to provide free amine **3-18** directly; this was not successful in our system likely due to isolation issues. The CBZ group of **3-17** was removed through a hydrogenolysis reaction resulting in the desired C6-amine **3-18** (Scheme 7). Conversion of amine **3-18** to the CBZ-protected guanidine **3-19** was achieved using the same conditions used in the literature synthesis of peramivir.²¹⁹ Treatment of the C6-amine in DMF with triethylamine (NEt₃), and mercury (II) chloride (HgCl₂) with the guanidinylation reagent *N,N'*-bis(dicarboxybenzyl)-*S*-methylisothiourea afforded the CBZ-protected guanidine **3-19** (Scheme 7). The purification of the product was often problematic due to the formation of insoluble mercury salts contributing to a poor overall yield. Hydrogenolysis of the CBZ groups from the protected guanidine **3-19** was accomplished using Pd/C in a pressurized Parr reactor. A suitable single crystal of free guanidine **3-20** for X-ray analysis was obtained through slow evaporation of the guanidino-

ester from a mixture of methanol and ethyl acetate. The relative stereochemistry of **3-20** was thus confirmed (Scheme 7).



Scheme 7. Synthesis of guanidino-ester **3-20** from carboxylic acid **3-16**.

With the synthesis of **3-20** successfully completed, it was time to test the inhibition activity of the free carboxylate **3-1** against viral neuraminidase. The ethyl ester was cleaved from guanidine **3-20** using 10% aqueous sodium hydroxide, and the solution neutralized to provide the guanidino-acid **3-1** in quantitative conversion (Figure 43). The removal of the ethyl ester was confirmed using mass spectrometry and ¹H NMR. In order to determine the activity of **3-1** against influenza neuraminidase we made use of a standard literature protocol involving the enzymatic cleavage reaction of 2'-4-(methylumbelliferyl)-Neu5Ac. NP40-inactivated influenza A/Brisbane/59/2007 (H1N1) was provided by virologist Dr. Martin Petric (BC CDC) and colleague Tracy Chan (BC CDC). The neuraminidase on the surface of these detergent-inactivated virions cleave 2'-4-(methylumbelliferyl)-Neu5Ac and release the fluorescent 4-methylumbelliferyl anion (Figure 43).

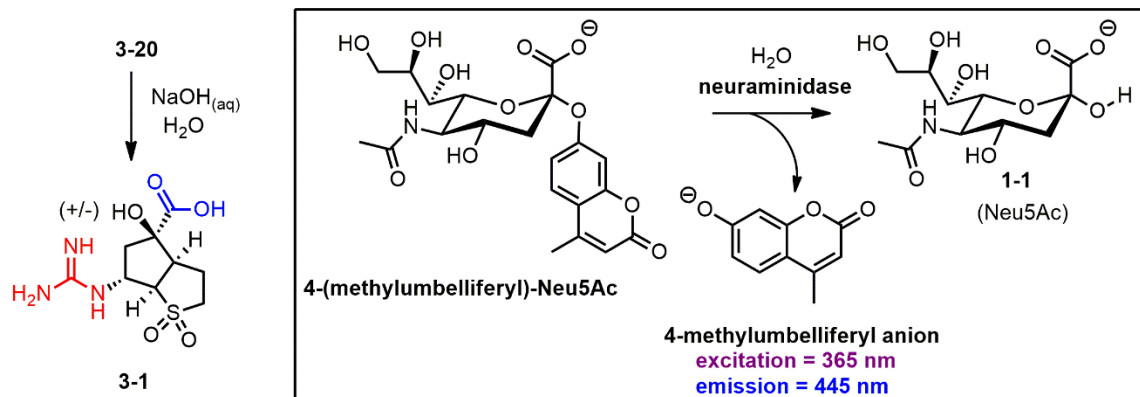


Figure 43. Synthesis of guanidino-acid **3-1** from guanidino-ester **3-20**. Action of neuraminidase on the fluorescent substrate.

By monitoring the rate of emission of the cleavage product over time with varying concentrations of inhibitor present (Figure 44, top), the percent inhibition at each specific concentration of inhibitor was determined by dividing the rate (slope, measured in fluorescence units per second) by the uninhibited reaction. The IC_{50} (half maximal inhibitory concentration) of **3-1** against the neuraminidase was determined through fitting the triplicate measurements of percent inhibition versus the concentration of the inhibitor to a sigmoidal model (Figure 44, bottom). The IC_{50} of **3-1** was determined to be $3770 \pm 70 \mu\text{M}$. The error reported is the standard error of “goodness of fit” determined by the graphing software XLfit.

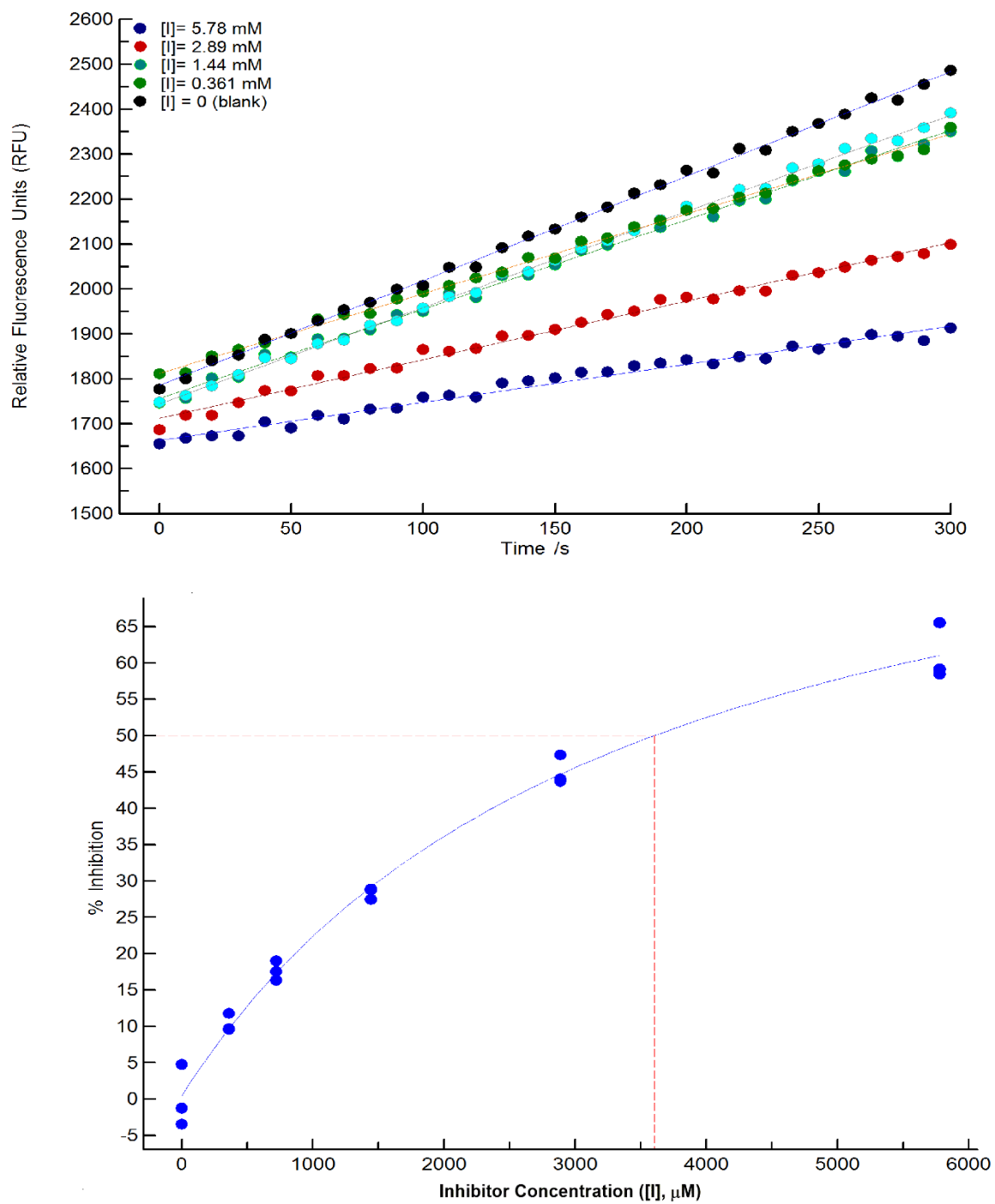


Figure 44. Raw fluorescence data for guanidino-acid 3-1 (top) and IC₅₀ curve for 3-1 (bottom).

Through comparison of the IC_{50} of the bicyclic **3-1** with the simple monocyclic cyclopentane peramivir analog **3-21** (synthesized by Dr. Caleb M. Bromba)²²⁰ it is clear that neither the increased rigidity nor the sulfone moiety (designed to hydrogen bond with Arg152 in the S3 subsite) of **3-1** are significantly increasing the binding affinity (Figure 45). The IC_{50} of the free amino-acid **3-23** was determined to be essentially inactive, with an inhibition of 40% at 10.5 mM.

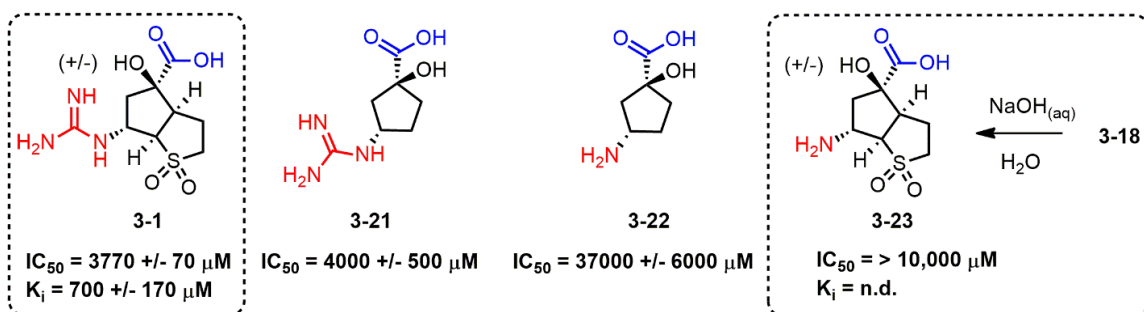


Figure 45. Comparison of monocyclic and bicyclic S1, S2 neuraminidase subsite binders.

In order to deduce the mode of inhibition of **3-1**, a more detailed kinetic analysis was undertaken by varying both the inhibitor concentration and the substrate concentration during the enzymatic assay. The Michaelis-Menten equation (equation 1, Figure 46) describes the rate of product formation for the binding of a single substrate under the assumption that the concentration of substrate is much higher than the concentration of catalytically active enzyme. The mode of inhibition for a reversible inhibitor can be deduced based on how the apparent K_m ($^{App}K_m$, substrate concentration required for half maximal V_{max}) and V_{max} (maximum rate of substrate cleavage) change with differing concentrations of substrate at fixed inhibitor concentrations. The V_{max} of the enzyme during competitive inhibition remains unchanged (since the substrate and inhibitor compete for the same binding site and therefore the observed inhibition can be overcome by increasing the concentration of substrate) while $^{App}K_m$ appears to increase during competitive inhibition, as more substrate is required to achieve a half-maximal V_{max} .

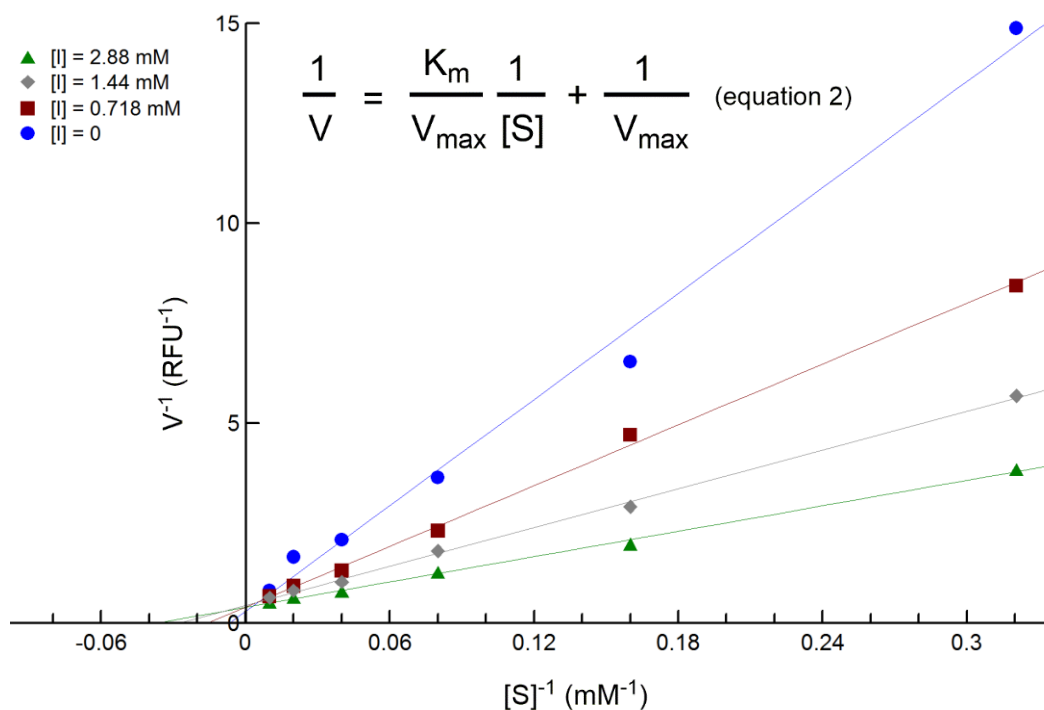
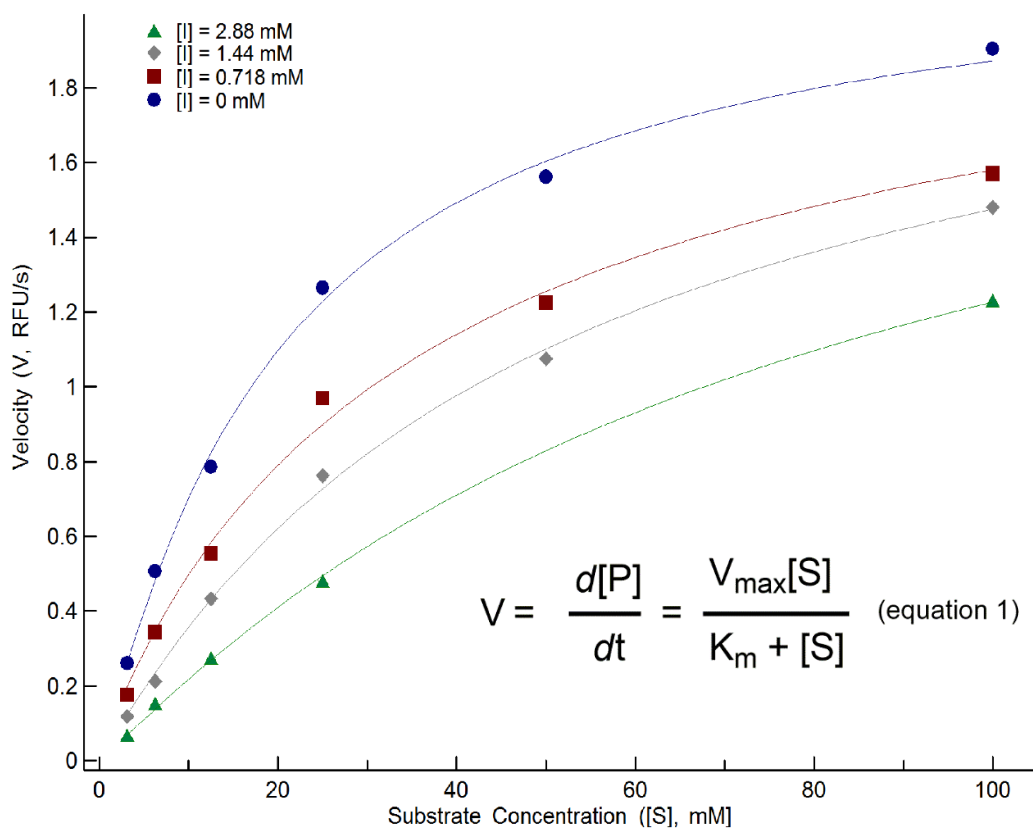


Figure 46. Michaelis-Menten plot (top) and Lineweaver-Burk plot (bottom) for guanidino-acid 3-1 against NP-40 inactivated H1N1 virus.

Using XLfit curve fitting software, the Michaelis-Menten plot for **3-1** indicates a constant V_{\max} and an increasing $^{App}K_m$ over increasing inhibitor concentrations, thereby confirming a competitive mechanism of inhibition (Figure 46). The data can be more easily visualized using a double reciprocal plot (Lineweaver-Burk plot)²²¹ of the observed reaction rates (V) versus substrate concentration. All lines cross at the same point on the y-axis: V_{\max} is the same at all inhibitor concentrations, while the x-intercept ($^{App}K_m^{-1}$) increases linearly as $[I]$ increases.

An alternate method for quantifying inhibition is the inhibition constant (K_i). The K_i of an inhibitor is defined as dissociation constant of the inhibitor from the inhibitor bound-enzyme complex ($K_i = [I][E]/[E-I] = k_{off}/k_{on}$). K_i is a preferred method to report inhibition since it is independent of substrate concentration and thus is more comparable between different assays/experiments. The inhibition constant (K_i) for guanidino-acid **3-1** was determined to be $700 \pm 170 \mu\text{M}$ (Figure 47). The value was obtained through curve fitting of equation 3 by plotting the average $^{App}K_m$ (values obtained from non-linear regression analysis of the Michaelis-Menten plots measured in triplicate) versus the concentration of inhibitor **3-1** (Figure 47).

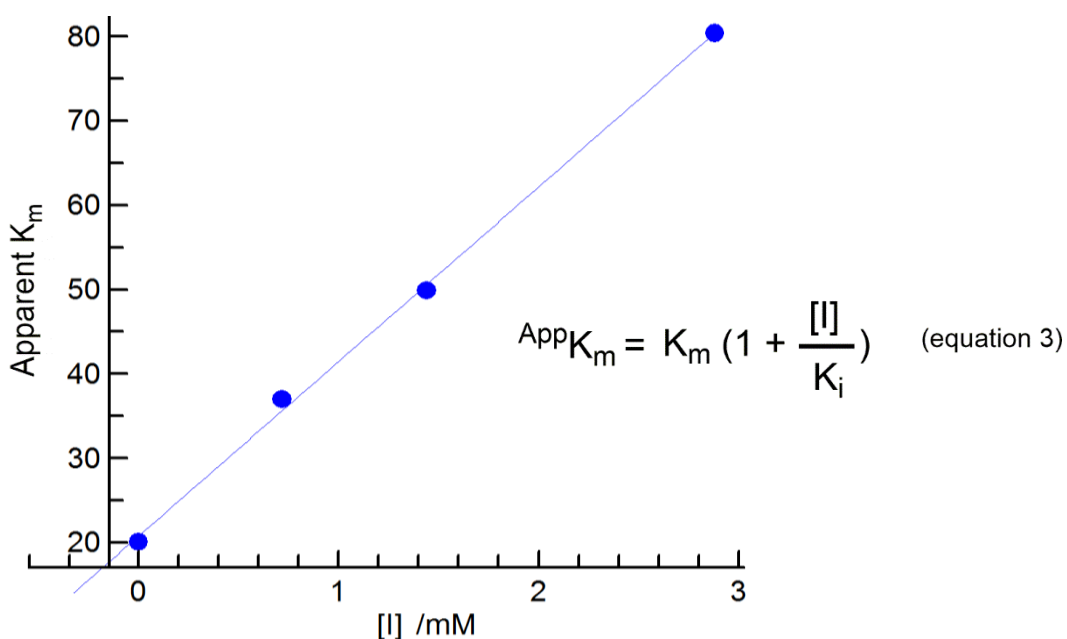


Figure 47. Determination of K_i for guanidino-acid 3-1 against NP-40 inactivated H1N1 virus.

3.3.0. Synthesis of a Bicyclic S1, S2, S3 Viral Neuraminidase Subsite Binder

The fact that the sulfone and bicyclic portions of **3-1** were not increasing the binding affinity (when compared with monocyclic **3-21**) in any significant manner was an unfortunate reality. It was deemed necessary to re-design the **3-1** scaffold in order to target the S3 binding pocket more effectively. The choice of targeting the S3 pocket as the next subsite was decided when a more in-depth literature structure activity relationship (SAR) survey of the neuraminidase inhibitor library was performed, which revealed the importance of the *N*-acetyl group (Figure 48). Specifically, the zanamivir analog **3-24** lacking the *N*-acetyl group at the C4 position of the dihydropyran skeleton was found to be less active by 6 orders of magnitude when compared with zanamivir itself (Figure 48). Upon additional analysis of the neuraminidase inhibition activity of other three subsite binding analogs of zanamivir, peramivir and oseltamivir, a trend emerges in which effective binding of three subsites results in activity in the low-mid micromolar range (1–100 μM). As demonstrated by equipotent zanamivir analogs **3-24** and **3-25**, binding to the S3 and S4 subsites are of equal importance in achieving nanomolar potency. The oseltamivir analog **1-11** lacking the 3-pentyl group displayed an IC_{50} of 6 μM , while the more active nor-amino oseltamivir analog **3-27** showed a more modest loss in activity. Less is known about the structure activity relationships of peramivir; the activity of side chain deleted analog lacking the 3-pentyl substituent (**1-15**) has been reported to be 28–115 μM ; upon close inspection, the relative stereochemistry of the carboxylic acid is inverted in **1-15** versus peramivir.

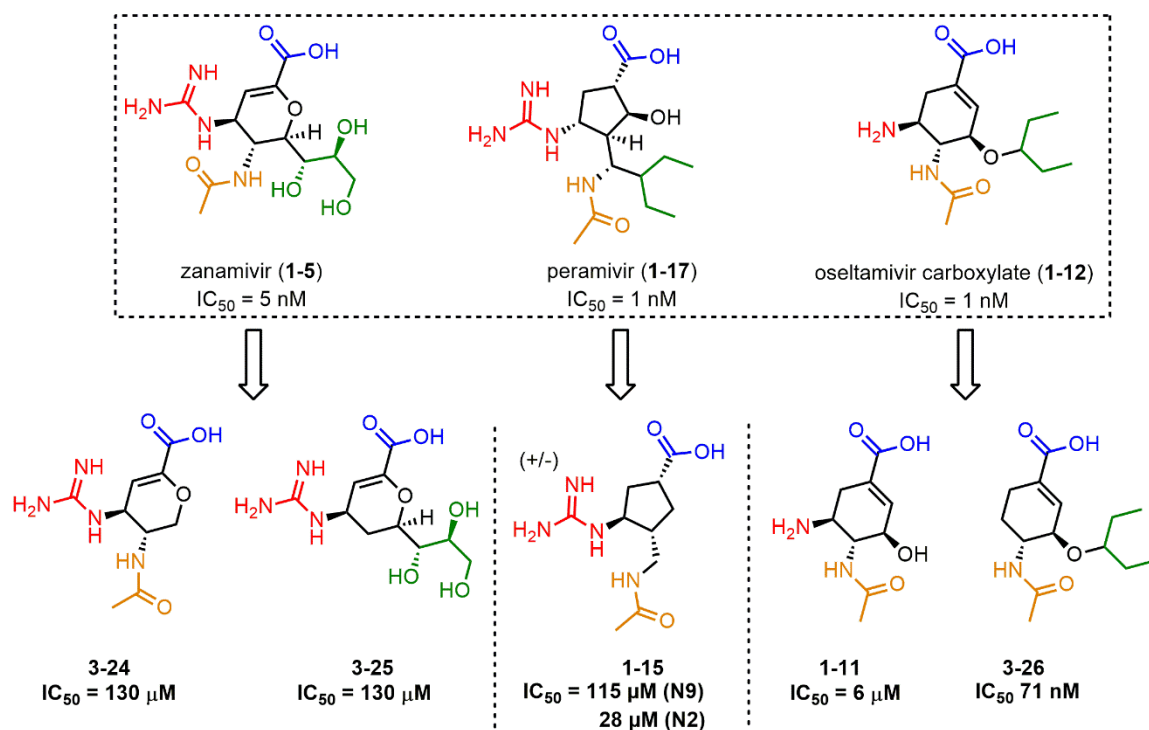


Figure 48. Three subsite binding analogs of zanamivir, oseltamivir and peramivir.

A number of possible strategies were envisioned to install an *N*-acetyl group on the **3-1** scaffold in order to effectively bind to the S3 subsite. One approach considered involved conversion of one of the sulfone oxygens to an *N*-acetyl-sulfonimide function ($S=N\text{Ac}$). This could situate the methyl of the acetyl function in the S3 pocket to form hydrophobic contacts within the subsite. A perhaps more elegant approach became evident when it was established that nitrogen-functionality could be installed at the C3 position of the vinyl sulfone function of **2-7e** through a conjugate addition reaction (Figure 49). If we consider the installation of an *N*-acetyl group to the C3 position of **3-1** (to give **3-1b**, Figure 49), it would mean that if the *N*-acetyl group was bound in the S3 subsite, the C4-carboxylic acid and C6-guanidine groups would be mismatched to their home S1 and S2 binding pockets (Figure 49). By performing a “regiochemical switch” (*i.e.* switching the position of the carboxyl group from C4 to C6 and the guanidine from C6 to C4, relative to the sulfone) the appropriate groups in **3-27** would be situated in the desired S1 and S2 pockets of the enzyme active site and allow for the newly installed *N*-acetyl group to be situated in the S3 binding pocket (Figure 49). The active isomer of **3-27** depicted in Figure 49 would

derive from one enantiomer of **2-7e**, while the depicted isomer of **3-1** would derive from the other enantiomer of **2-7e**. The hypothetical S1, S2, S3 subsite binder **3-27** became the next target for synthesis.

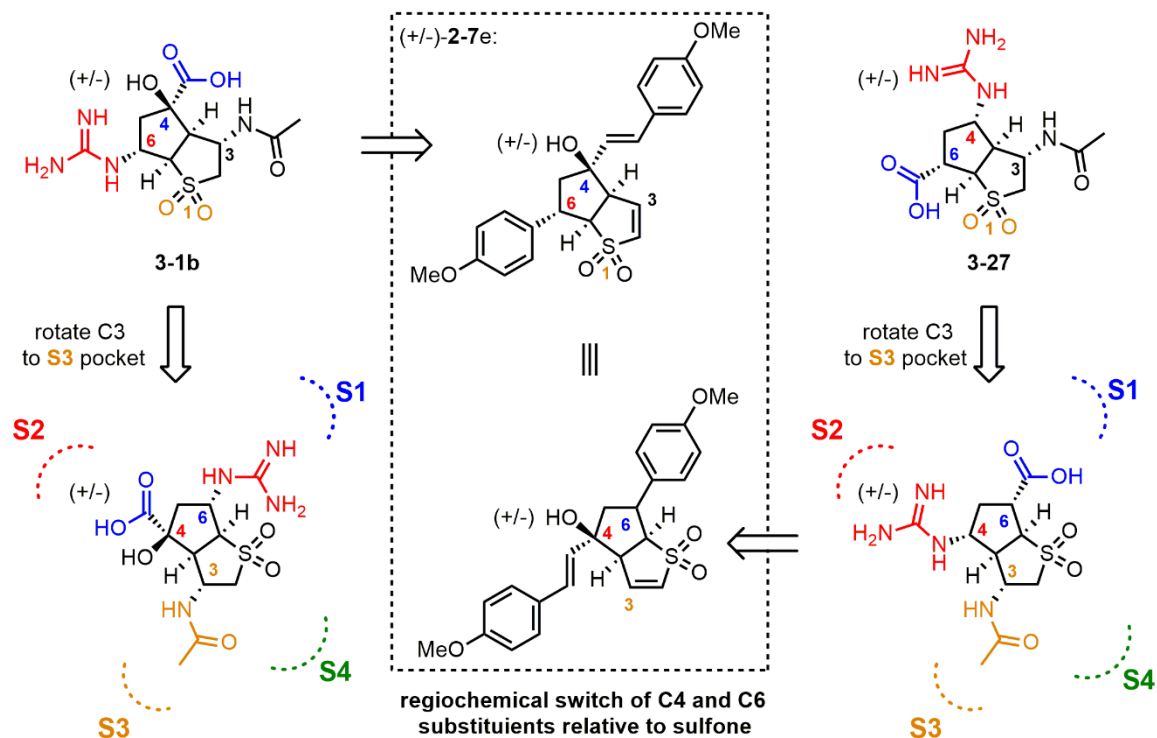
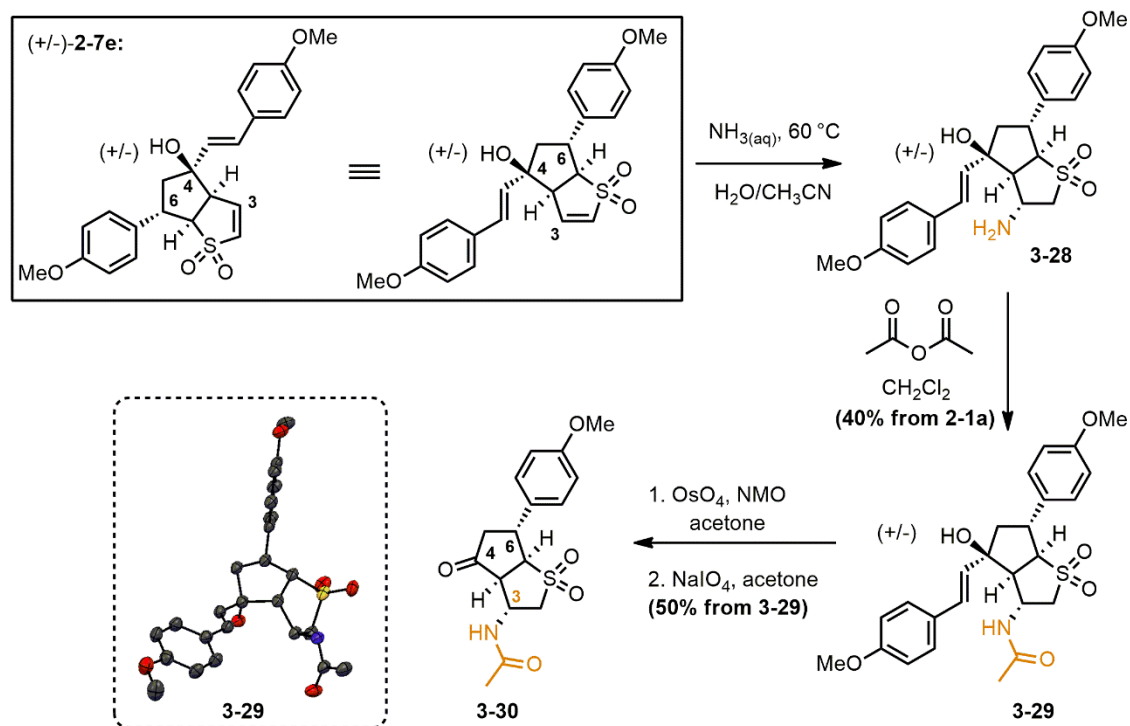


Figure 49. A regiochemical switch of guanidinium and carboxylate functions to achieve a three subsite binder derived from common precursor **(+/-)-2-7e**.

The pursuit of **3-27** began with heating of sulfone **2-7e** in a sealed round-bottom flask with aqueous ammonia in acetonitrile to afford C3-amine **3-28** as a single observable diastereomer by ^1H NMR (Scheme 8). Installation of the *N*-acetyl function was accomplished with acetic anhydride and the nucleophilic catalyst dimethylaminopyridine (DMAP). The relative stereochemistry of the C3-stereogenic center was determined using X-ray crystallography, and is consistent with approach of the ammonia nucleophile to the least hindered face of the bicyclic core. Cleavage of the C4-allylic-alcohol function was accomplished using a dihydroxylation followed by cleavage with NaIO_4 to provide C4-ketone **3-30** (Scheme 8). These conditions were found to be superior to the one step

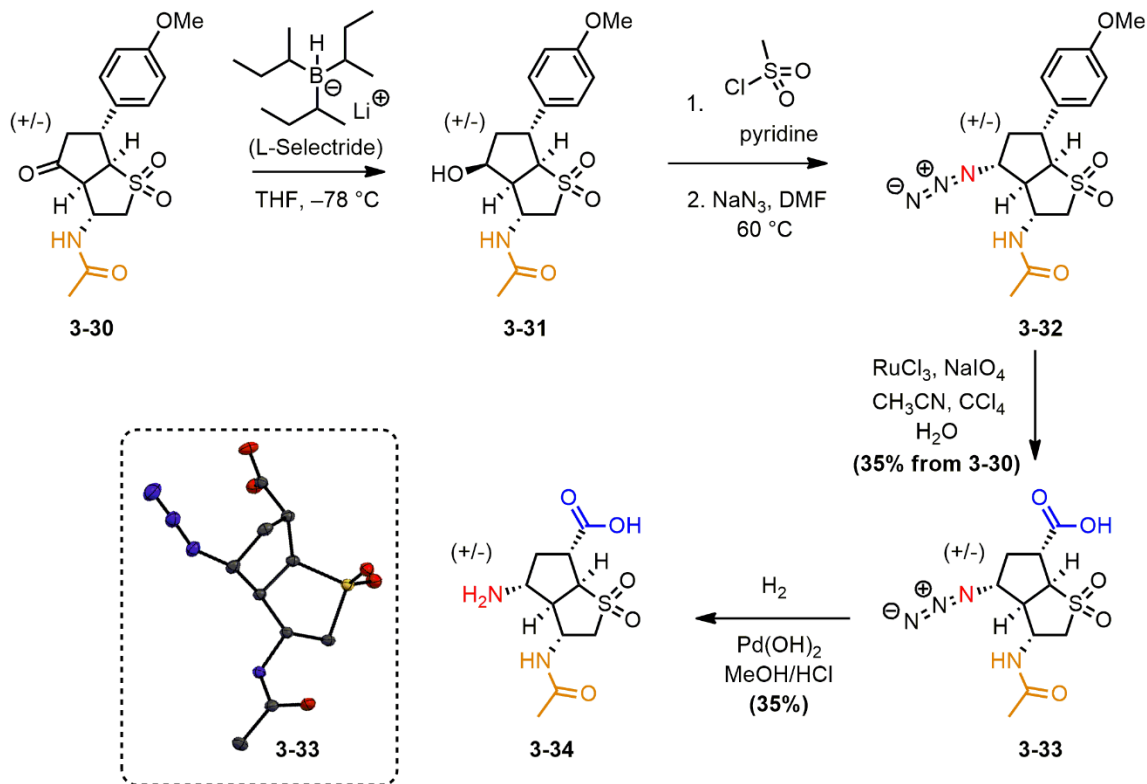
$\text{RuCl}_3/\text{oxone}$ reaction; the latter had a messier work-up and generated a more variable yield of product.



Scheme 8. Conversion of vinyl sulfone **2-7e** to ketone **3-30**; installation of the S3 probing N-acetyl function.

With C4-ketone **3-30** in hand, installation of the amine function at the C4-position became the next synthetic task. Attempts were made at direct conversion of the C4-ketone function to an amine through reductive amination (benzylamine, followed by reduction with sodium cyanoborohydride, NaBH_3CN) however no useful product was obtained. A longer step-wise sequence was undertaken involving the $\text{S}_{\text{N}}2$ nucleophilic displacement of a mesylate with the nucleophilic azide anion (Scheme 9). Reduction of the ketone of **3-30** to an alcohol was accomplished using the sterically bulky reducing agent L-Selectride, which delivered the hydride to the less hindered face of the carbonyl function; the non-bulky reducing agent NaBH_4 gave a mixture of diastereomers which could not be readily separated by chromatography. After reduction of the ketone, the alcohol was made into better leaving group upon treatment with methanesulfonyl chloride (mesyl chloride).

Through addition of sodium azide in a polar aprotic solvent, the mesylate was displaced by the azide anion with inversion of the relative stereochemistry to generate **3-32** as a single stereoisomer (Scheme 9).



Scheme 9. Synthesis of S1, S2, S3 binder **3-34** from ketone **3-30**.

The next synthetic challenge was whether the oxidative cleavage of the C6 *para*-methoxyphenyl group could be accomplished in the presence of the C4-azide group. Upon stirring of **3-32** with our familiar oxidant RuO_4 , the aromatic function was smoothly degraded to a carboxylic acid using 15 equivalents of sodium periodate (Scheme 9). X-ray analysis of the product confirmed that the C4-azide function was installed with the desired relative stereochemistry (Scheme 9). Treatment of the azido-acid **3-33** with Pearlman's catalyst ($\text{Pd}(\text{OH})_2/\text{C}$) under an atmosphere of hydrogen gas afforded the desired amine as the hydrochloride salt. The activity of the amine **3-34** was tested in the fluorescent neuraminidase assay (under the same protocol and treatment of data performed for **3-1**) and was determined to be a competitive inhibitor of viral neuraminidase with an IC_{50} of

118 ± 9 μM and a K_i of 19 ± 1 μM against NP40-inactivated influenza A H1N1 (Figure 50). The IC₅₀ and K_i reported for **3-34** were determined through the amalgamation of inhibition data from three separately synthesized batches of material (starting from **2-1a**), with each assay separately performed in triplicate. A later batch of **3-34** was further tested against H1N1 California/2009 recombinant enzyme and the H1N1 H274Y mutant (purchased from Sino Biologics) which both gave similar activities (Figure 50). The retention of activity of **3-34** against the H274Y mutant would be expected since **3-34** likely does not bind in the S4 subsite. Amino-acid **3-34** was also tested against bacterial neuraminidases from *Vibrio cholerae* and *Clostridium perfringens* (purchased from Sigma-Aldrich) and found to have low millimolar activity (Figure 50). The activity of **3-34** against the human neuraminidases (NEU1-4) was performed by Dr. Amgad Albohy and Dr. Christopher Cairo (University of Alberta); the IC₅₀ values were found to be >1000 μM against all four isozymes. The fact that amino-acid **3-34** is selective for influenza NA versus hNEU would be desirable if targeting an antiviral lead compound.

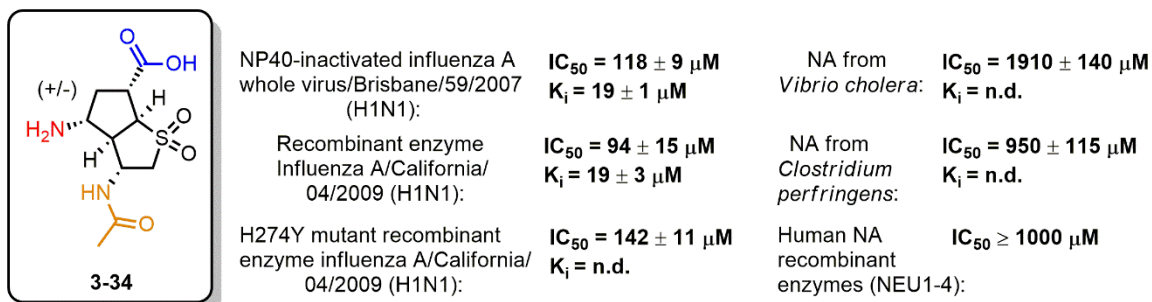
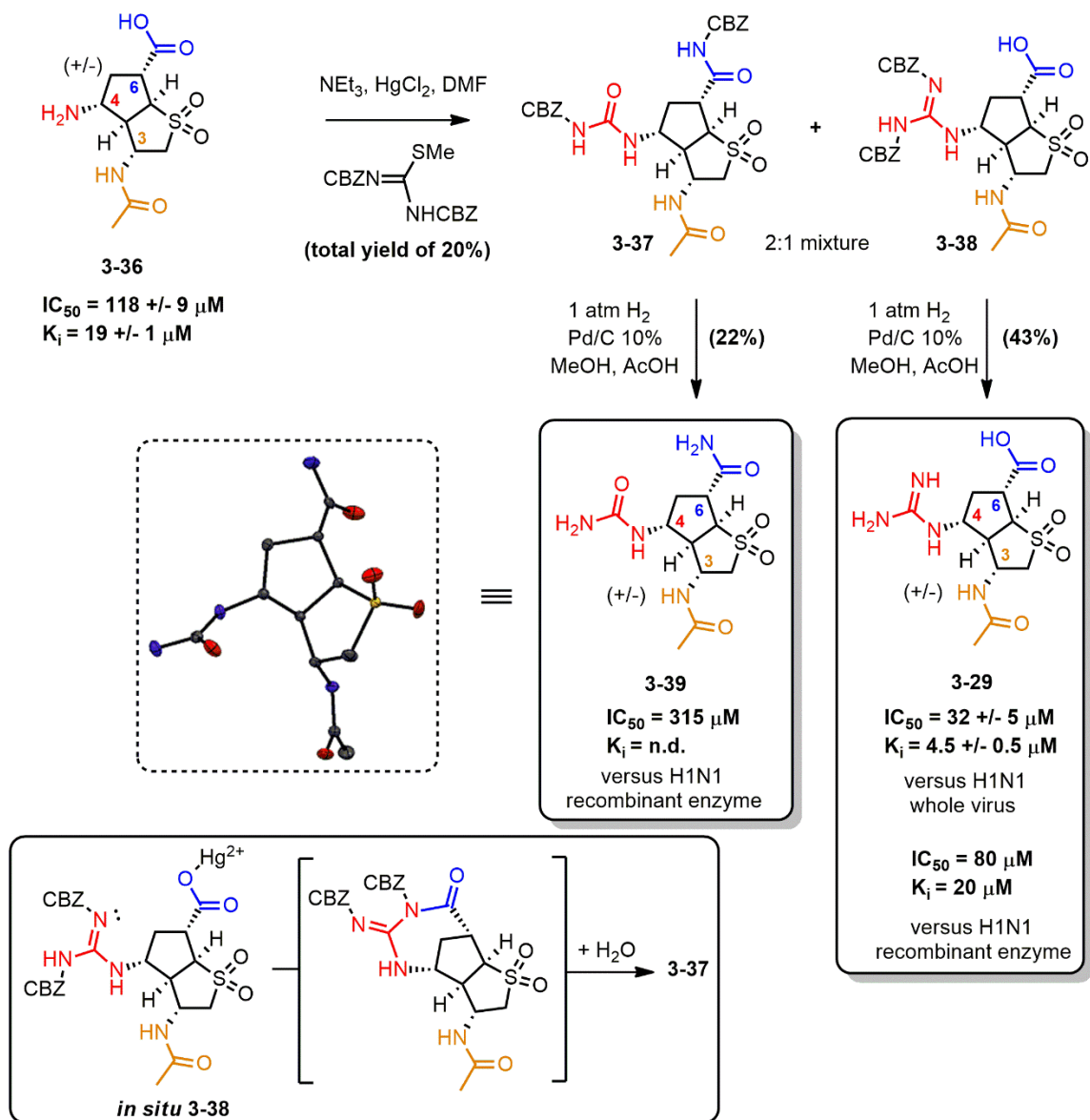


Figure 50. Activity of amino-acid **3-34** against H1N1 whole virus, recombinant N1 neuraminidase, an N1 H274Y mutant, bacterial neuraminidases *V. cholerae* and *C. perfringens* and human neuraminidases NEU1, NEU2, NEU3 and NEU4.

Using the same guanidinylation protocol used for the synthesis of **3-1**, elaboration of amine **3-34** to guanidine **3-27** was unexpectedly challenging (Scheme 10). Once synthesized, guanidine **3-27** was measured to have an activity of $4.5 \pm 0.5 \mu\text{M}$ (K_i) and an IC_{50} of $32 \pm 5 \mu\text{M}$ (average of two independently prepared batches of material, each assayed in triplicate). Guanidine **3-27** was found to have no activity against bacterial neuraminidases from *V. cholerae* and *C. perfringens*. Subsequent batches of guanidine **3-27** were found to have highly variable activity in the high micromolar range ($>100 \mu\text{M}$) against the NP-40 inactivated virus. Similarly, against the human neuraminidases NEU2-3, different batches of **3-27** also had variable activity (IC_{50}) ranging between 11-600 μM (NEU2), and 41-510 μM (NEU3). The IC_{50} of **3-27** against NEU1 and NEU4 was consistently $>1000 \mu\text{M}$. An X-ray quality crystal was grown from one of these latter less active batches of “**3-27**” which revealed the existence of an unexpected side-product, the insidious carbamido-amide **3-37**. It was eventually determined that upon careful purification of the initial guanidinylation reaction, two distinct CBZ protected products **3-35** and **3-36** with differing retention factors (R_f) could be isolated. A possible mechanism for this transformation is the mercury chloride facilitated intramolecular cyclization of **3-36** to form a cyclic 3-imino-2,4-diazabicyclo[4.2.1] intermediate; a subsequent hydrolysis would then form the CBZ-protected carbamido-amide **3-35**. Once the CBZ-protected guanidine **3-36** and CBZ-protected urea **3-35** products were separated, hydrogenolysis provided carbamido-amide **3-37** and guanidino-acid **3-27**. The IC_{50} of carbamido-amide **3-37** was measured to be 315 μM while the IC_{50} of the new batch of **3-27** was determined to be 80 μM with a K_i of 20 μM against H1N1 California/2009 recombinant enzyme. The high micromolar activity of **3-37** is not unexpected due to the presence of a hydrogen bond donor group (C4-carbamide function) which could bind in the S2 subsite; the C6-primary amide function contains a hydrogen bond acceptor (*i.e.* the carbonyl group) that may bind in the S1 subsite.



Scheme 10. Synthesis of guanidino-acid 3-27 and carbamido-amide 3-37.

The activity of guanidino-acid **3-27** against H1N1 NP-40 inactivated virus versus N1-recombinant enzyme differs by a factor of four. Although it is not overly surprising for an inhibitor to differ in activity when using neuraminidases from a difference source, the overall yield from amine **3-34** to guanidine **3-27** is consistently low and **3-27** is very challenging to purify. Since the difference in activity of amine **3-34** versus guanidine **3-27** against recombinant H1N1 enzyme is statistically negligible, installation of the guanidine is likely not a worthwhile investment of material or time for developing inhibitors of viral

or bacterial neuraminidases based on the bicyclic **2-7** archetype. Furthermore, it has been well established that there is a negative correlation between oral bioavailability and the presence of a guanidinium function *in vivo*.²²² Sometimes the juice just isn't worth the squeeze.

3.4.0. Chapter Summary

The structure-activity relationships established for guanidino-acid **3-1**, amino-acid **3-34**, guanidino-acid **3-27** and carbamido-amide **3-37** against influenza neuraminidase are strong evidence that the [3.3.0]bicyclic-archetype can adapt itself to project its substituents in effective positions to bind to a neuraminidase active site. The inhibitory activity of racemic amine **3-34** against H1N1 influenza neuraminidase is in the same range as the analogous S1, S2 and S3 subsite binding analogs of the commercialized drugs peramivir and zanamivir (Figure 51). When compared to the oseltamivir analog **1-11**, amine **3-34** is less potent, however it is approximately two orders of magnitude more potent than the aromatic **BANA108** (Figure 51).²²³ The similar activity of amine **3-34** to the S4 side-chain deleted analogs of oseltamivir, peramivir and zanamivir in addition to a competitive mode of inhibition is convincing evidence that **3-34** is accessing the viral neuraminidase active site as designed. Analogous of amine **3-34** possessing a substituent to probe the S4 subsite could be valuable inhibitors of influenza neuraminidase, with similar potency to the commercialized drugs. Additionally, the measureable activity of **3-34** against bacterial neuraminidases *Vibrio cholerae* and *Clostridium perfringens* is promising. Amino-acid **3-34** could prove useful as a starting point for the development of inhibitors against bacterial neuraminidases. Initial activity results of guanidino-acid **3-27** against human neuraminidases NEU2 and NEU3 is also encouraging; studies are currently underway pin down the reason for variable activity results of **3-27** against these targets.

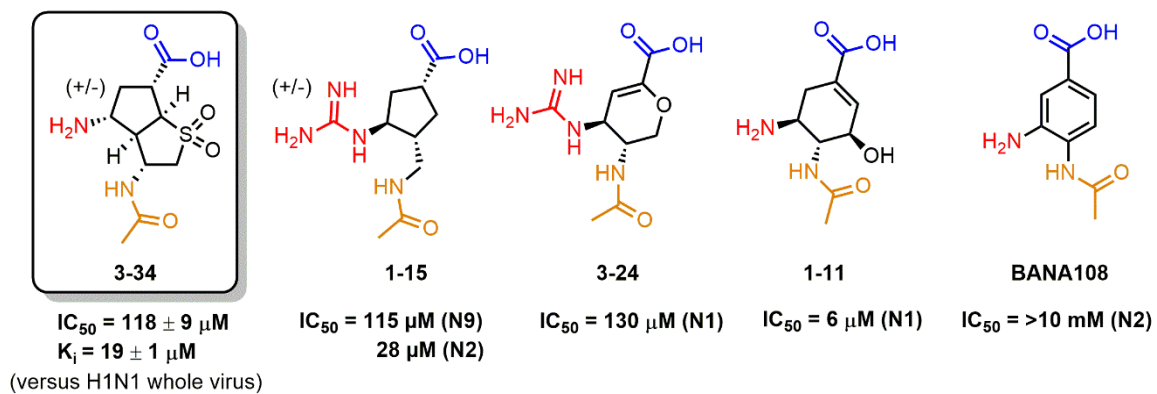


Figure 51. Comparison of activities of S1, S2 and S3 subsite binders constructed from the [3.3.0]bicyclic (3-34), cyclopentane (1-15), dihydropyran (3-24), cyclohexene (1-11) and aromatic (BANA108) templates.

Chapter 4. Tandem Reactions of Bis-Vinyl Ketones and 3-Substituted-3-Sulfolenes

The material in Sections 4.1.0–4.4.0 was adapted from: M. G. Brant, J. N. Friedmann, C. G. Bolhken, A. G. Oliver and J. E. Wulff (2015) Diastereoselective Tandem Reactions of Substituted 3-Sulfolenes with Bis-Vinyl Ketones Leading to Highly Functionalized Bicyclic and Tricyclic Frameworks. *Organic and Biomolecular Chemistry* 13, 4581-4588.²²⁴

All the synthesis, analysis and characterization of data was performed by MGB with the exception of compounds deriving from sulfones **2-1e** and **4-8** which were performed by Jordan N. Friedmann. All X-ray structures were solved by Dr. Allen G. Oliver (University of Notre Dame). Dr. Ori Granot collected the HRMS data.

4.1.0. Rationale and Literature Review:

Inspired by the one-pot dialkylation reactions between the anion of 3-sulfolene (**2-1a**) and bis-alkyl halides (Figure 31),^{198, 199} we made use of a number of acyclic and cyclic bis-vinyl ketones and the anion of **2-1a** to provide a small library of [3.3.0]bicyclic and tricyclic vinyl sulfones (Chapter 2). The [3.3.0]bicyclic archetype was established to be a suitable scaffold for the generation of inhibitors of the neuraminidase enzymes (Chapter 3). We next became interested in expanding the scope of our tandem γ -1,2 addition/anionic oxy-Cope/ γ -1,2 addition methodology. By making use of 3-sulfolenes (**2-1**) with a variable substituents present at the 3-position, we hoped to potentially access other bicyclic systems which could prove useful as inhibitor scaffolds (Figure 52).

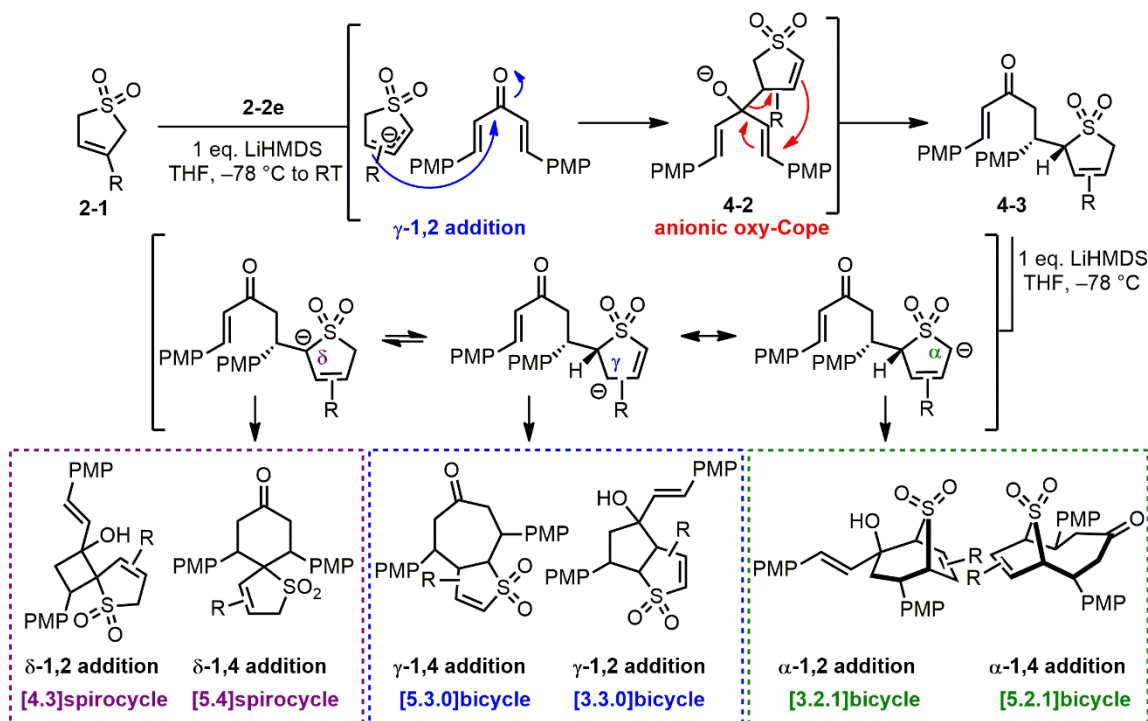


Figure 52. Use of 3-substituted-3-sulfolenes to access up to six bicyclic archetypes.

The presence of a functional group at the 3- or 4-position of **4-3** should allow the predictable (and possibly selective) access of up to six unique bicyclic archetypes via the nucleophilic 1,2 or 1,4 addition of an anion stabilized at the α , γ , or δ position to the electrophilic vinyl carbonyl function (Figure 52). Attack of the anion from the α -position could afford two bridged bicyclic products (*i.e.* a [3.2.1]bicycle or a [5.2.1]bicycle), while attack from the γ -position could proceed to form two possible fused bicycles (*i.e.* a [3.3.0]bicycle or a [5.3.0]bicycle). Attack from the δ -position to the 1,2 or 1,4 vinyl carbonyl function would afford spirocyclic products (Figure 52).

The ability of a substituent to stabilize the position of an anion in 3-sulfonylate systems has been previously explored through the deprotonation of 3-substituted-3-sulfolenes **2-1b-k** followed by the addition of methyl iodide (Figure 53).²²⁵ Substituents that donate electron density through induction or resonance (e.g. methyl and chlorine) result in the formation of α -substituted products.²²⁵ Electron-withdrawing substituents (e.g. carboxymethyl, nitrile and phenylsulfonyl) promote alkylation at the β -position,²²⁶ while 3-sulfolenes possessing a functional group that imposes a significant steric barrier or can stabilize an anion through resonance (e.g. thiophenyl, phenyl and trimethylsilyl) react to form δ -alkylated products.²²⁵

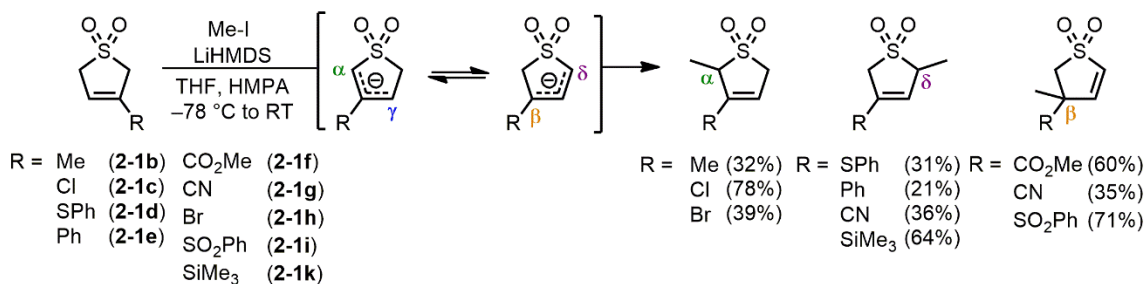


Figure 53. Regiochemical methylation of 3-substituted-3-sulfolenes.

The reactions of 3-substituted-3-sulfolenes **2-1b–c** with the bis-electrophiles 1,3-diiiodopropane, 1,2-bis(bromomethyl)benzene and 1,2-bis(iodomethyl)ethene has been previously reported by Chou.^{197, 199} In the absence of a substituent at the 3-position, the reaction between the **2-1a** anion and 1,3-diiiodopropane or 1,2-bis(bromomethyl)benzene provides exclusively the γ -1,2 addition product. In comparison, the presence of an electron donating methyl group at the 3-position of the mono-alkylated intermediates leads to a preference for the α -addition product. In the case of the similarly sized but more electronegative chlorine substituent, γ -addition was preferred. (Figure 54). The chain length and rigidity of the bis-alkyl halides were also found to be important factors in the outcome of the dialkylative cyclizations. Exclusive formation of the [3.2.1]bicyclic ring system was achieved in the dialkylative cyclization of **2-1a–c** (and **2-1d**) using the more rigid 1,1-bis(iodomethyl)ethene (Figure 54).¹⁹⁷

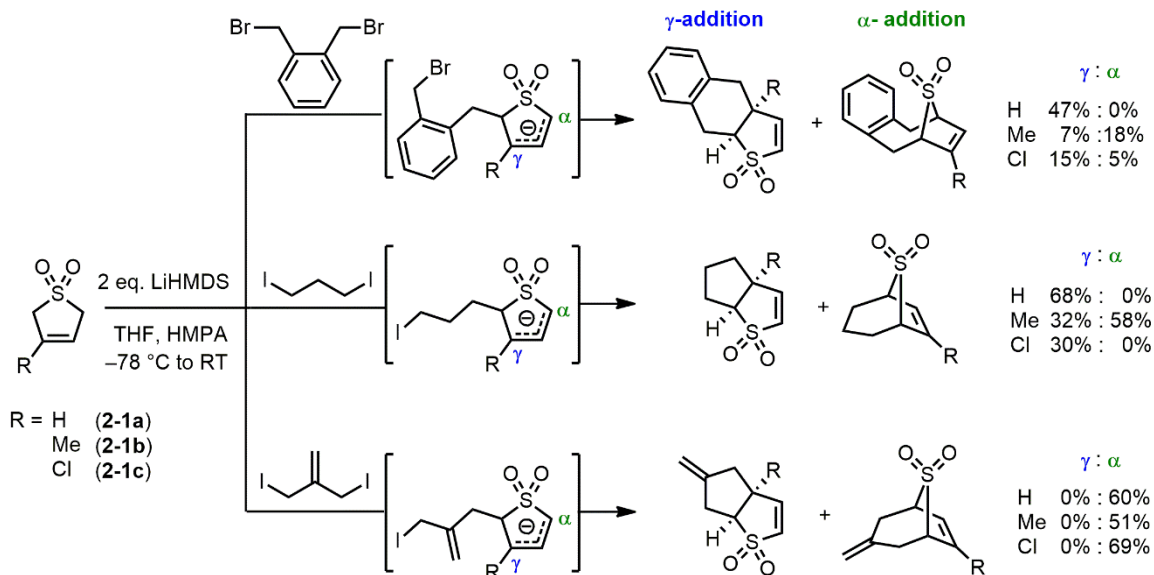


Figure 54 Dialkylative couplings of 3-sulfolene (**2-1a**), 3-methyl-3-sulfolene (**2-1b**) and 3-chloro-3-sulfolene (**2-1c**) with bis-alkyl halides.

In the case of 3-thiophenyl-3-sulfolene (**2-1d**), the dialkylative coupling was found to be highly dependent on the chain-length of the bis-alkyl halide (Figure 55). Exclusive formation of the γ -addition product was observed with 1,3-diiodopropane,²²⁷ while the use of the longer chain 1,3-diiodobutane or 1,3-diiodopentane afforded the corresponding [5.4]spirocycles through δ -alkylation.²²⁸

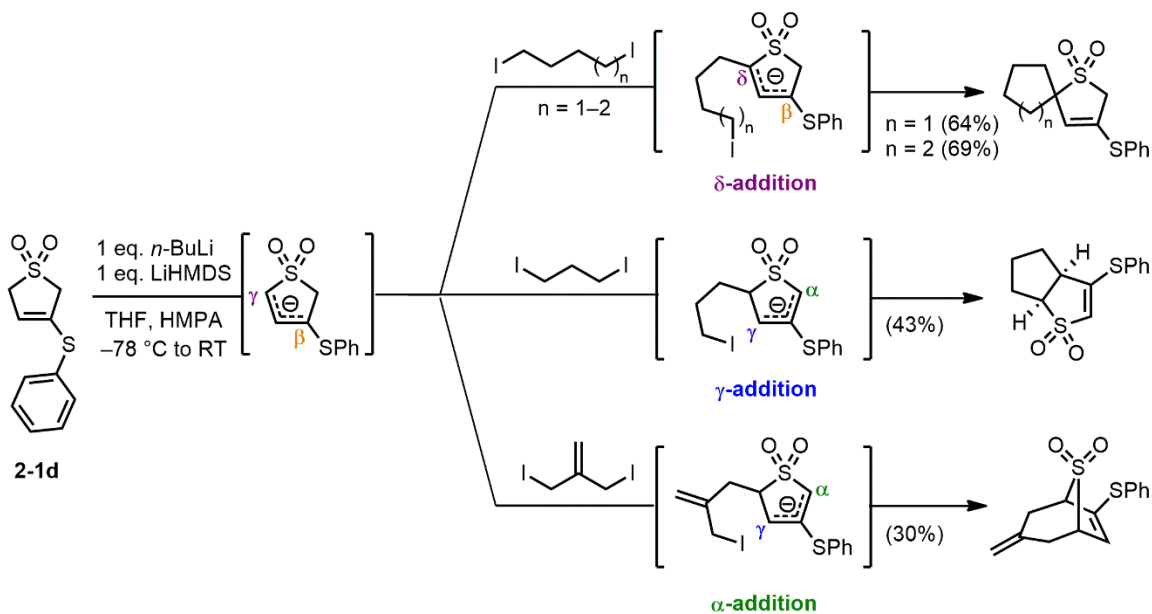
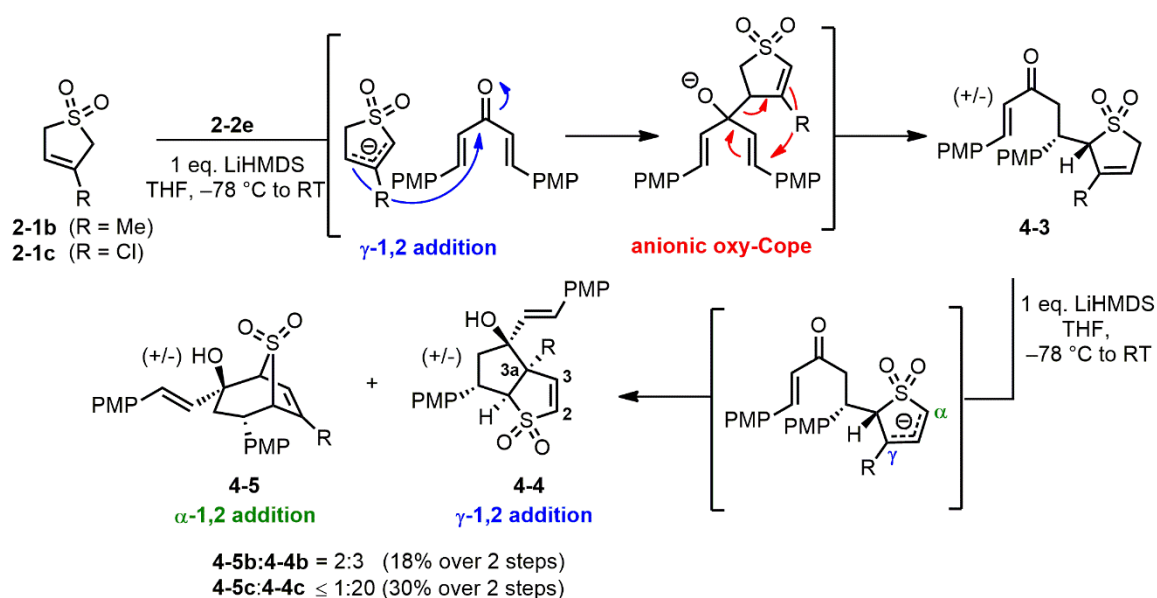


Figure 55. Dialkylative coupling of 3-thiophenyl-3-sulfolene with bis-alkyl halides.

4.2.0. Reactivity of 3-Substituted-3-Sulfolenes with Bis-Vinyl Ketones

To begin our investigation we attempted the tandem γ -1,2 addition/anionic oxy-Cope reaction using the commercially available 3-methyl-3-sulfolene (**2-1b**) and 3-chloro-3-sulfolene (**2-1c**). The initial deprotonation of these 3-sulfolenes occurred at the α -position providing **4-3b** and **4-3c** as the major regioisomers after γ -1,2 addition/anionic oxy-Cope (Scheme 11). Cyclization of crude **4-3b** provided two identifiable products in a 3:2 ratio: γ -1,2 addition product **4-4b** and direct α -1,2 addition product **4-5b** (possessing a [3.2.1]bicyclic framework), both isolated as a single diastereomers. In contrast, the cyclization of **4-3c** with LiHMDS produced exclusively γ -1,2 addition product **4-4c** (by ^1H NMR), with a chlorine atom present at the C3a-quaternary bridge head carbon. Unexpectedly, electron density attributed to the chlorine atom was observed at the C3 position in the X-ray structure of **4-4c**, indicating the presence of **4-4c'** as a minor product (see Scheme 13). While the methyl and chlorine are approximately the same size sterically, the chlorine atom is able to donate electron density through resonance to the α -position (thus destabilizing the anion) and simultaneously withdraw electron density through induction at the γ -position (thus stabilizing the anion): γ -1,2 addition is hence preferred.



Scheme 11. Reaction of 3-methyl-3-sulfolene and 3-chloro-3-sulfolene with 2-2e.

To rationalize the high level of diastereoselectivity in the formation of bridged [3.2.1]bicycle **4-5b** we propose that the reaction trajectory involves a chair-shaped transition state (Figure 56). In the likely chair conformation leading to **4-5b**, the α -anion approaches the carbonyl function (situated in the axial position) while the larger vinyl-PMP group occupies the equatorial position. The transition state leading to **4-5b** may also be favored due to chelation of the lithium counter-ion by both the carbonyl and sulfone functions. In the proposed pathway leading to *epi*-**4-5b** the large vinyl-PMP group would experience significant 1,3-diaxial repulsion. The relative stereochemistry of [3.2.1]bicycle **4-5b** was confirmed using single crystal X-ray diffraction. Unfortunately, compound **4-5b** was found to be particularly unstable at room temperature both in solution and in the solid state, with decomposition occurring within a matter of days. The instability of **4-5b** may be due to the facile extrusion of sulfur dioxide (to form a 1,3-heptadiene structure) followed by decomposition/polymerization. The solid state structure of **4-5b** reveals C–S bond lengths of 1.7964(17) Å and 1.8004(18) Å and a C–SO₂–C angle of 90°. Compared with the parent **2-1b** (C–S bond lengths 1.809(6) Å and 1.816(4) Å; C–SO₂–C angle of 97°),²²⁹ the smaller angle indicates **4-5b** is a more strained system which may explain its inherent instability.

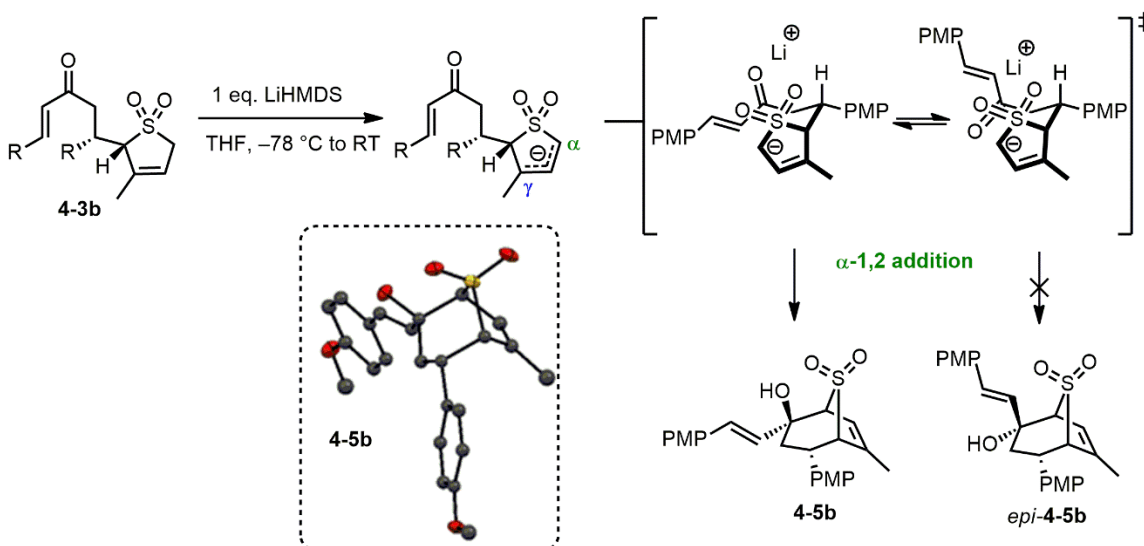
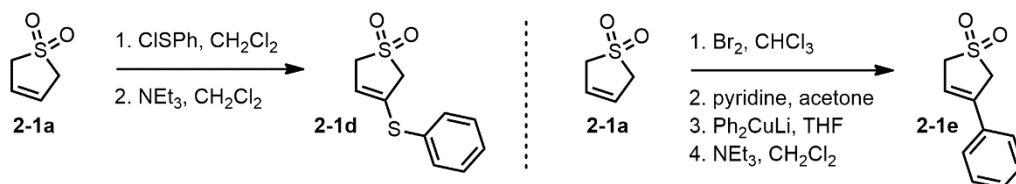


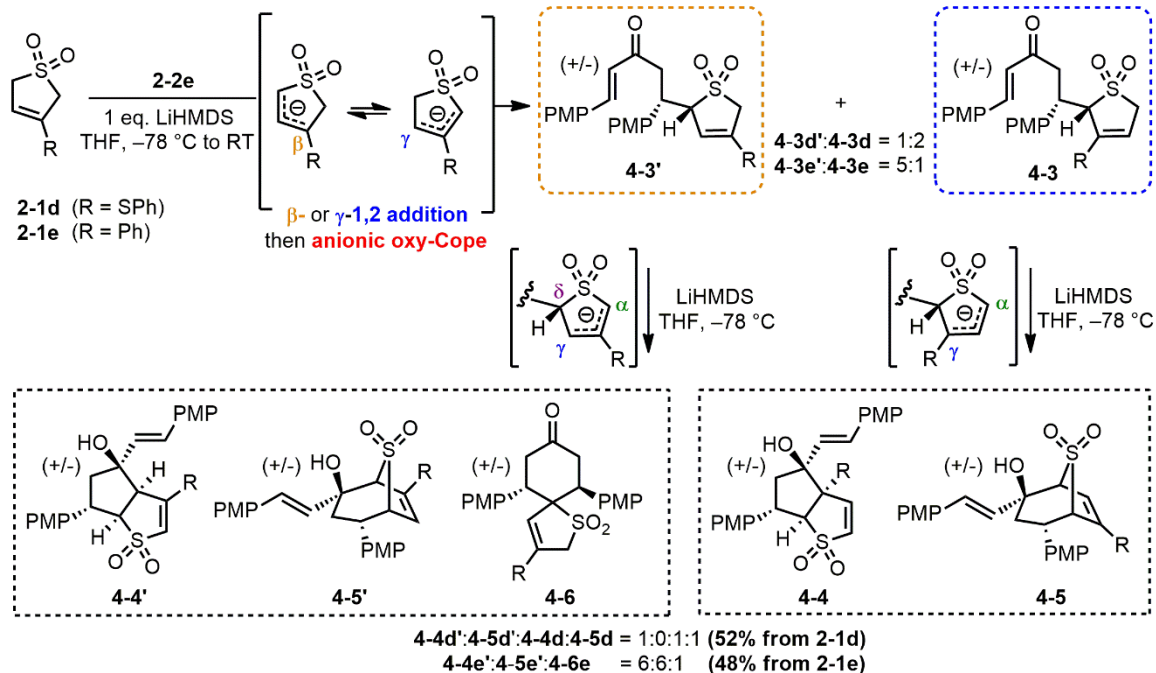
Figure 56. Origin of diastereoselectivity during α -1,2 addition.

The isolation of the [3.2.1]bicycle **4-5b** (albeit with low selectivity) suggested that substituents present on the 3-sulfolene ring of **4-3** could in fact bias the reaction trajectory to provide other bicyclic ring systems in a diastereoselective manner. Since very few 3-substituted-3-sulfolenes are commercially available, 3-thiophenyl-3-sulfolene (**2-1d**)²³⁰ and 3-phenyl-3-sulfolene (**2-1e**)²³¹ were both synthesized from the parent unsubstituted 3-sulfolene **2-1a** through literature protocols (Scheme 12).



Scheme 12. Synthesis of 3-substituted-3-sulfolenes 2-1d and 2-1e.

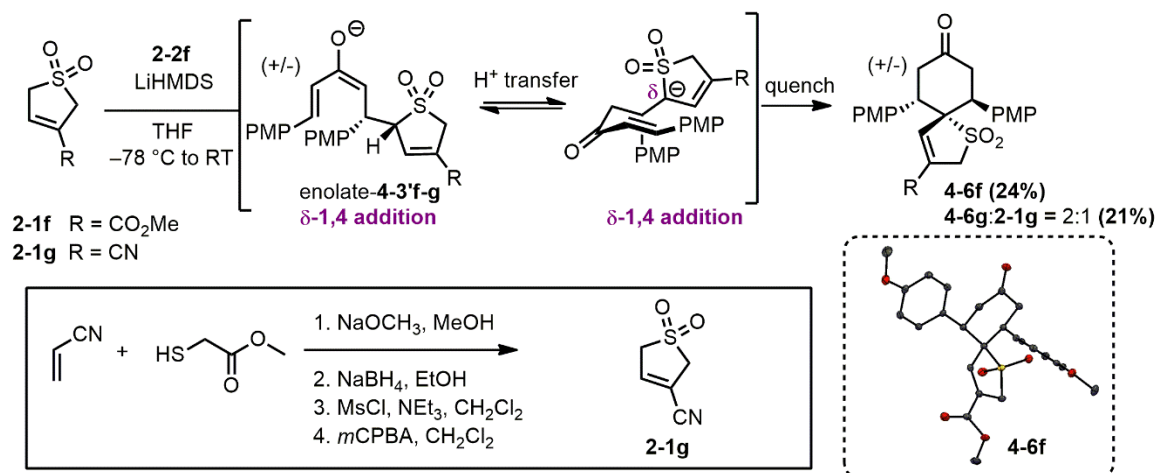
The reaction of 3-thiophenyl-3-sulfolene (**2-1d**) with vinyl ketone **2-2e** provided regioisomers **4-3d** (formed through a γ -1,2 addition followed by an anionic oxy-Cope) and **4-3d'** (formed through a β -1,2 addition followed by an anionic oxy-Cope) in a 2:1 ratio (Scheme 13). The formation of **4-3d'** may be rationalized since the sterically large, anion-stabilizing thiophenyl group of **4-1d** can direct deprotonation at the δ -position, facilitating the nucleophilic 1,2-addition from the β -position. Upon subjection of the crude mixture to LiHMDS, the major regioisomer **4-3d** cyclized to produce a 1:1 mixture of γ -1,2 addition product **4-4d** and α -1,2 addition product **4-5d** (Scheme 13). The increase in ratio of α -1,2-addition to γ -1,2-addition products (when compared with **4-3b**) was expected, due to the larger steric size of the thiophenyl group in **4-3d** versus methyl substituent in **4-3b**. Regioisomer **4-3d'** cyclized to form **4-4d'**, with no α -1,2 addition product **4-5d'** observed.



Scheme 13. Reaction of 3-thiophenyl-3-sulfolene and 3-phenyl-3-sulfolene with 2-2e.

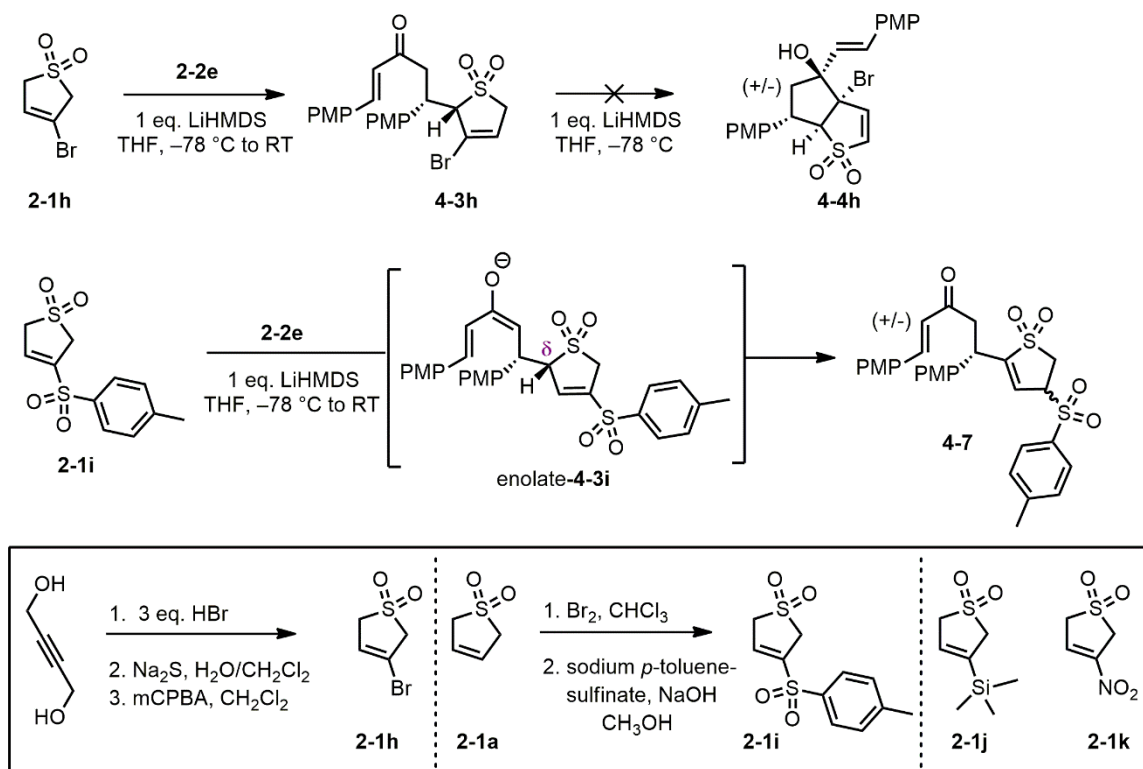
Reaction of 3-phenyl-3-sulfolene (**2-1e**) with **2-2e** resulted in a 1:5 mixture of **4-3e** and **4-3e'** regioisomers (Scheme 13). The formation of the **4-3e'** as the major regioisomer is now preferable since the 3-phenyl group is able to directly stabilize the anion at the δ/β -position of **2-1e** anion via resonance delocalization. Upon cyclization of the crude mixture of **4-3e** and **4-3e'** an equimolar mixture of **4-4e'** and **4-5e'** was isolated, along with a relatively minor third product determined to be [5.4]spirocycle **4-6e**. The formation of [3.2.1]bicycle **4-5e'** may be the result of the 3-phenyl group imposing a significant steric effect on the neighboring γ -position. Evidently, the 3-phenyl group of **4-3e'** also facilitates the formation of **4-6e** via stabilization of the δ -anion through resonance delocalization. The product distribution varied slightly upon additional replicates, giving between a 6:6:1 and 6:9:2 distribution of **4-4e'**:**4-5e'**:**4-6e**, upon slow or fast addition of the base respectively. No products originating from the minor regioisomer **4-3e** were identified before or after column chromatography.

The 3-phenyl substituent of **4-3e'** was able to direct deprotonation at the δ -position, facilitating the formation of the [5.4]spirocyclic compound **4-6e** as a minor product. We reasoned that it should be possible to increase the selectivity towards this third isolated structural archetype by use of an electron-withdrawing function which can more effectively stabilize an anion at the δ -position of **4-3'**. Commercially available 3-carboxymethyl-3-sulfolene (**2-1f**) and synthetically prepared 3-cyano-3-sulfolene (**2-1g**)²³² were found to react smoothly with **2-2e** to produce exclusively the [5.4]spirocycles **4-6f-g** upon a single treatment of one equivalent of LiHMDS (Scheme 14). The high level of selectivity for the [5.4]spirocycles **4-6f-g** can be attributed to the fact that the anion is now highly stabilized in the δ -position through conjugation with the electron-withdrawing group. This leads to a softening of the anion, and selective attack onto the 4-position of the vinyl carbonyl function. When the reaction mixtures were quenched at $-78\text{ }^\circ\text{C}$, no β -1,2 addition product, or anionic oxy-Cope product **4-3f'** was isolated. This may indicate that the expected β -1,2 addition does not occur at $-78\text{ }^\circ\text{C}$, or perhaps the formation of the intermediate enolate of **4-3f'** occurs through a 1,4 addition of the δ -anion of **2-1f**. The enolate function of **4-3f'** is evidently able to deprotonate the δ -position of the sulfone and a second δ -1,4 addition occurs *in situ* to form **4-6f** (or **4-6g**). The relative stereochemistry of the [5.4]spirocycle was determined using ^1H and NOESY NMR experiments which indicated that the two PMP groups were *trans* with respect to one another; the structure was later confirmed using single crystal X-ray diffraction (Scheme 14).



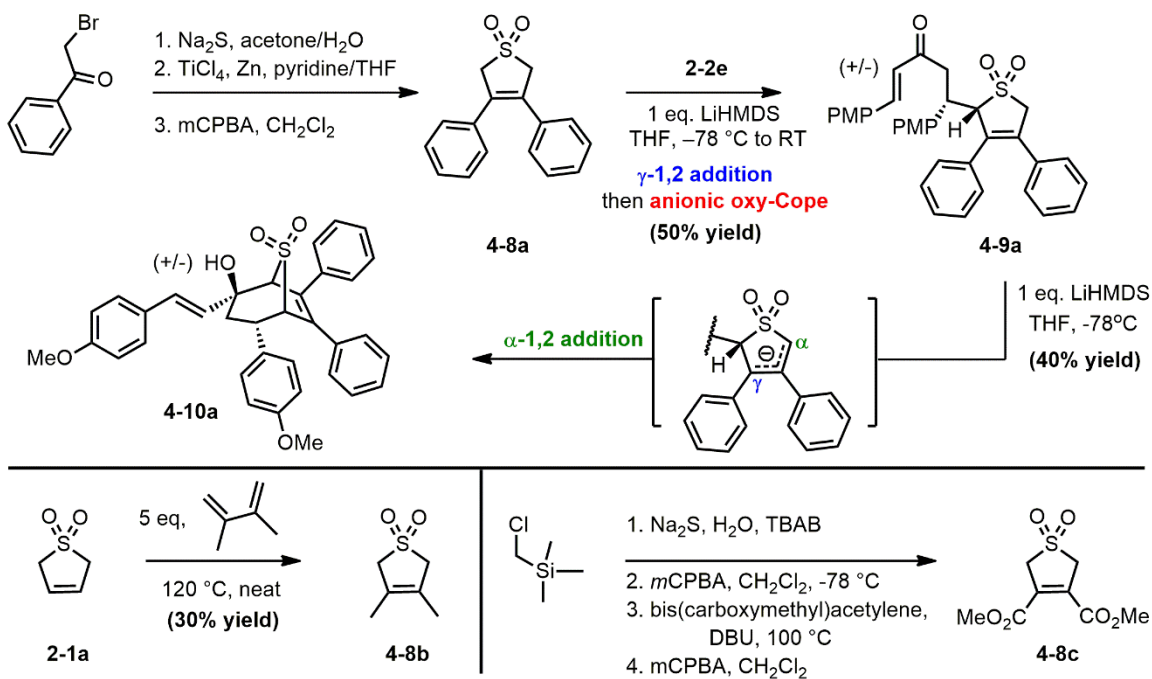
Scheme 14. Reaction of 3-carboxymethyl-3-sulfolene and 3-cyano-3-sulfolene with **2-2e**.

Other 3-substituted-3-sulfolenes that were prepared in our investigations included 3-bromo-3-sulfolene (**2-1h**) and 3-sulfonyltolyl-3-sulfolene (**2-1i**), prepared through literature protocols from 1,4-butynediol and **2-1a** respectively (Scheme 15).^{233, 234} Reaction of **2-1h** afforded the expected **4-3h** regioisomer, however upon attempted cyclization with LiHMDS no identifiable products were observed in the crude ¹H NMR. Subjection of 3-sulfonyltolyl-3-sulfolene **2-1i** to the usual protocol produced **4-7** as an equimolar mixture of diastereomers. It seems probable that the expected β -1,2-addition/anionic oxy-Cope to give enolate **4-3i** did occur (analogous to the reactivity seen with phenyl sulfolene **2-1e**) however an *in situ* proton transfer occurred from the δ -position to the enolate; upon quenching the reaction protonation occurred at the 3-position giving rise to a mixture of diastereomers which were not readily separable (Scheme 15). 3-Trimethylsilyl-3-sulfolene (**2-1j**) and 3-nitro-3-sulfolene (**2-1k**) were also targeted as substrates, but could not be synthesized using the reported literature procedures.^{235, 236}



Scheme 15. Reaction of 3-bromo-3-sulfolene and 3-sulfonyltolyl-3-sulfolene with **2-2e**.

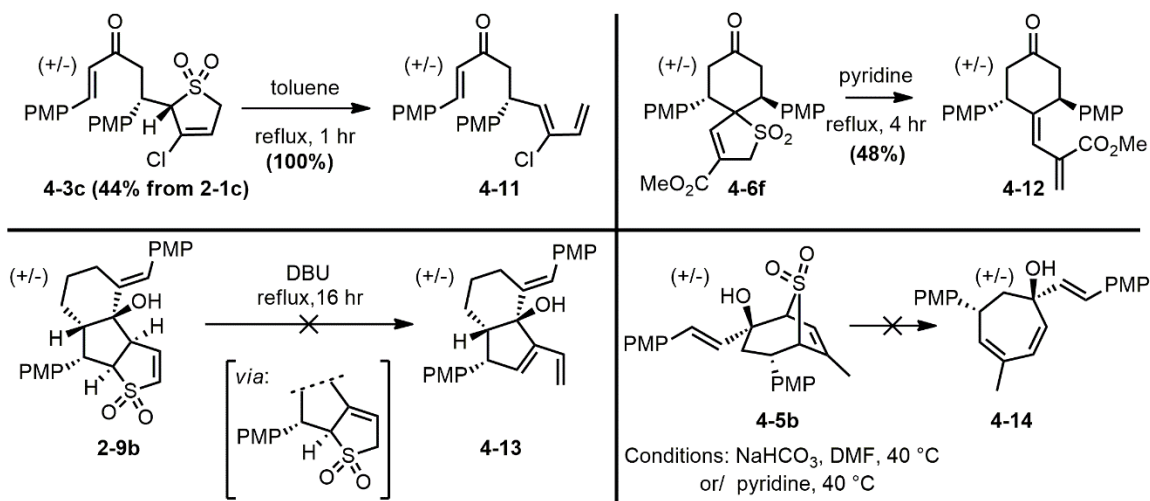
With examples of selective γ -1,2 addition and δ -1,2 addition leading to [3.3.0]bicycles and [5.4]spirocycles respectively, we desired to selectively access the [3.2.1]bicyclic ring system formed through α -1,2 addition. In order to selectively obtain the [3.2.1]bicycle ring system we turned our attention to the 3,4-disubstituted-3-sulfolene **4-8** (Scheme 16). The sterically large phenyl groups in **4-9a** should disfavor the formation of the γ -1,2 addition product. In the event, the reaction of **4-8a** with **2-2e** resulted in the formation of 3-sulfolene **4-9a** in a 50% yield. The purified 3-sulfolene **4-9** was cyclized with LiHMDS to provide exclusively the desired [3.2.1]bicycle **4-10** as a single diastereomer in a 40% yield (20% from **4-8a**). Two additional 3,4-disubstituted-3-sulfolenes were prepared: 3,4-dimethyl-3-sulfolene (**4-8b**) and 3,4-dicarboxymethyl-3-sulfolene (**4-8c**). While no identifiable products formed in the reaction of **4-8c** with **2-2e**, the dimethylsulfones **4-9b** and **4-10b** were isolated however could not be obtained in sufficiently pure form after column chromatography. Of potential interest is the previously unreported “sulfur dioxide transfer reaction” between 3-sulfolene and a 1,3-butadiene (in this case 3,4-dimethyl-butadiene) used to prepare sulfolene **4-8b** in an un-optimized 30% yield after recrystallization.



Scheme 16. Reaction of 3,4-diphenyl-3-sulfolene with **2-2e**.

4.3.0. 1,3-Diene Formation from the Bicyclic Sulfone Archetypes

The cheletropic removal of sulfur dioxide from substituted 3-sulfolenes is a convenient method for generating otherwise difficult to prepare 1,3-dienes. Out of interest, we explored the extrusion of sulfur dioxide from a few representative 3-sulfolene substrates isolated over the course of this methodology study. Upon heating of 3-sulfolene **4-3c** in refluxing toluene, quantitative conversion to the expected 1,3-butadiene **4-11** was observed (Scheme 17). When the spirocyclic 3-sulfolene **4-6f** was subjected to heating in pyridine, the expected diene **4-12** was obtained in a 48% yield after column chromatography. The low yield of **4-12** is evidently due to the formation of undesired isomers of **4-12**, observed in the ^1H NMR spectrum of the crude reaction mixture. Attempted isomerization of 2-sulfolene **2-9b** to the 3-sulfolene isomer (and tandem cheletropic removal of sulfur dioxide) in refluxing 1,8-diazabicyclo[5.4.0]undec-7-ene (DBU) was unsuccessful likely due to the inherent ring strain in the 3-sulfolene intermediate. Deliberate removal of sulfur dioxide from the bridged 3-sulfolene **4-5b** was not possible even under relatively mild conditions: decomposition occurred readily to provide an intractable red tar.



Scheme 17. Cheletropic removal of sulfur dioxide from 3-sulfolenes and 2-sulfolenes.

4.4.0. Chapter Summary:

In summary we were able to expand the tandem-reactivity observed with the unsubstituted 3-sulfolene **2-1a** to selectively access two additional ring systems (*i.e.* [5.4]spirocycles and [3.2.1]bicycles) along with C3- and C3a- functionalized [3.3.0]bicycles through use of 3-substituted-3-sulfolenes and 3,4-disubstituted-3-sulfolenes. Although mixtures of regioisomers were obtained in some cases, selective formation of three bicyclic archetypes was achieved; small molecule X-ray characterization of each of these archetype was also obtained (Figure 57). The elaboration of [3.3.0]bicycle **2-7e** into inhibitors of neuraminidase suggests that some of these other rigid bicyclic sulfones may be similarly useful for generating medicinally active compounds.

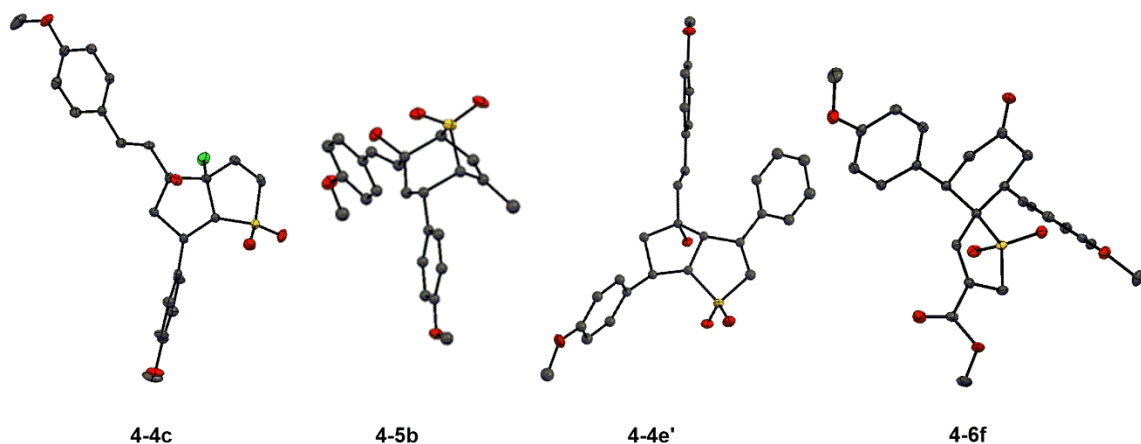


Figure 57. Summary of X-ray structures of each structural archetype prepared.

Chapter 5. Targeting the S4 Subsite of Viral Neuraminidase

The material in Section 5.3.0 was adapted from: S. S. Y. Wong, M. G. Brant, C. Barr, A. G. Oliver and J. E. Wulff (2013) Dipolar Addition to Cyclic Vinyl Sulfones Leading to Dual Conformation Tricycles. *Beilstein Journal of Organic Chemistry*, 9, 1419-1425.²³⁷

All the synthesis, analysis and characterization of data was performed by MGB with exception of compounds **5-12**, **5-14a-c**, **5-15a-c** and **5-17** which were prepared by Steven S. Y. Wong. All X-ray structures were solved by Dr. Allen G. Oliver (University of Notre Dame). Dr. Ori Granot collected the HRMS data.

5.1.0. Introduction

The synthetic sequence to elaborate the [3.3.0]bicyclic sulfone **2-7e** into a micromolar inhibitor of viral neuraminidase (**3-34**) was presented in Chapter 3. In order to increase the potency of our bicyclic structure against the neuraminidase enzymes, installation of a substituent to probe the S4 binding pocket of these enzymes is required. Using MOLOC, amino-acid **3-34** analog **5-1a** (possessing a 3-pentyl group at the C2-position) was modelled and overlaid with peramivir bound in an N2 neuraminidase active site (Figure 58). Once sulfone **5-1a** was dragged on top of peramivir in the active site, **5-1a** was allowed to energy minimize (with the enzyme remaining static) to maximize van der Waals, electrostatic, and hydrogen bonding interactions with the enzyme. The energy-minimized model of **5-1a** overlays well with peramivir except for the 3-pentyl group of **5-1a** which is displaced deeper into the S4 subsite (Figure 58). The SAR investigation undertaken during the optimization of oseltamivir indicates that nearly any hydrophobic function should increase the inhibitory activity of our bicyclic structures against influenza A neuraminidase. We thus desired to develop a synthetic method with which to install substituents at the C2 position of **3-34** (to arrive at structures such as **5-1a**).

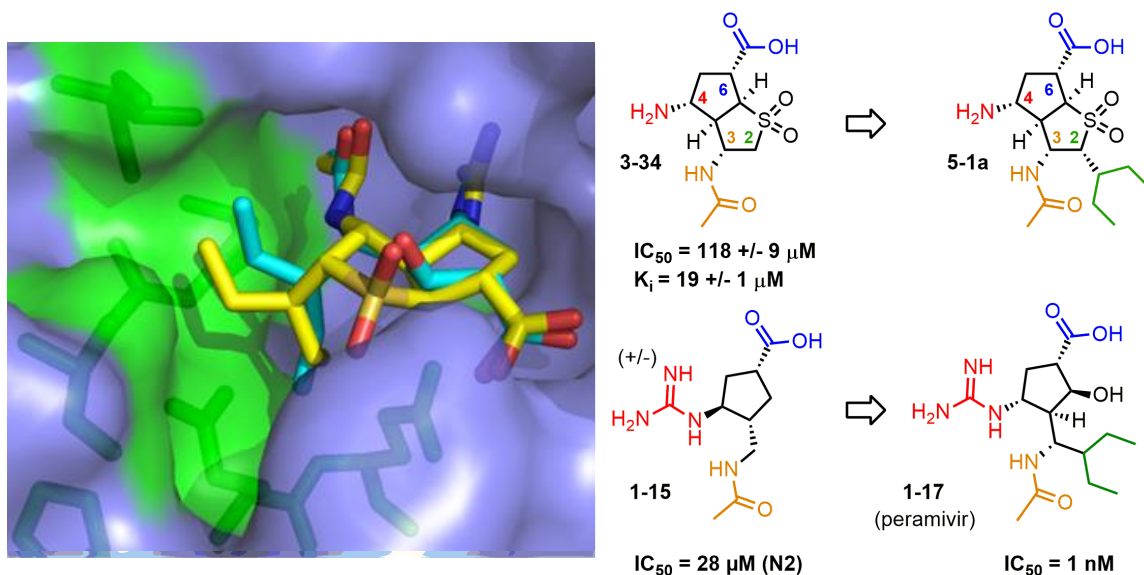


Figure 58. Targeting the S4 subsite (shaded green) of viral neuraminidase. 5-1a (yellow) peramivir (cyan).

In order to install an S4 probing substituent onto the C2-position, two initial strategies were devised: C2-alkylation and 1,3-dipolar cycloaddition. The first strategy explored involved exploiting the electron-withdrawing sulfone function to direct deprotonation and subsequent alkylation at the C2 position of the [3.3.0]bicyclic core. The second method involved exploring the possibility of a 1,3-dipolar cycloaddition between the C2-C3 vinyl sulfone function (a dipolarophile) and a suitable 1,3-dipole in order to simultaneously install the desired C3-nitrogen functionality and a functional group at the C2-position. A third approach making use of 3-sulfolenes pre-functionalized at the C2 position (as a way to access **5-2**) was also explored. The successes and shortcomings of these three approaches will be the subject of discussion in the following chapter subsections. Once synthesized, elaboration of **5-2** to the corresponding amino-acid **5-1** should be readily achievable using the synthetic sequence outlined in Chapter 3.

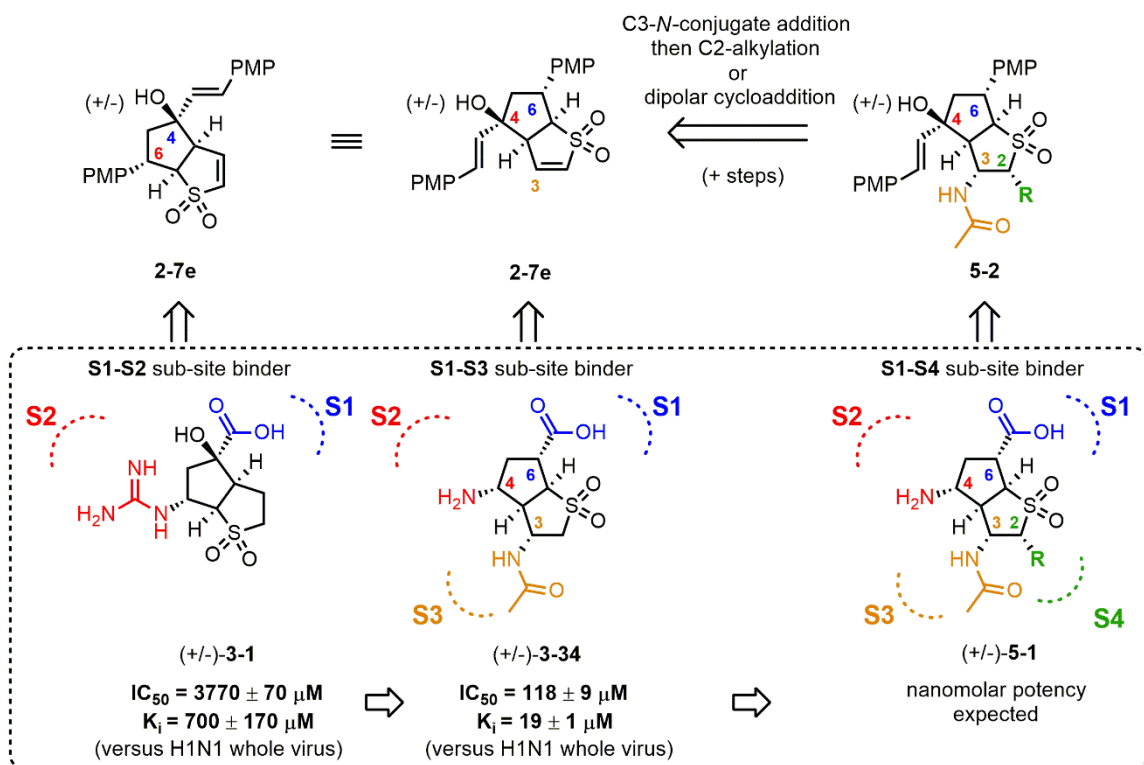
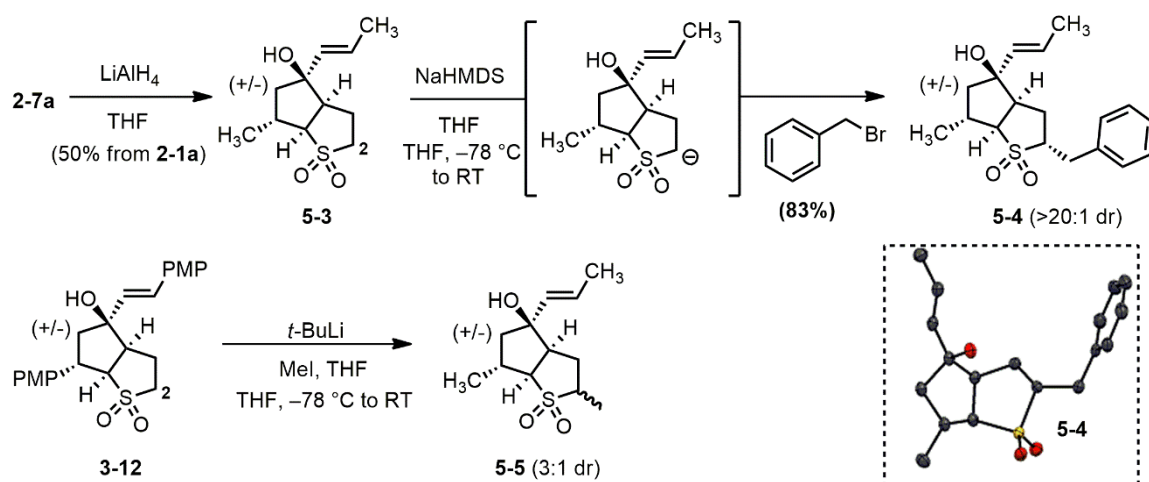


Figure 59. Summary of approaches to arrive at C2 functionalized analogs of 3-34.

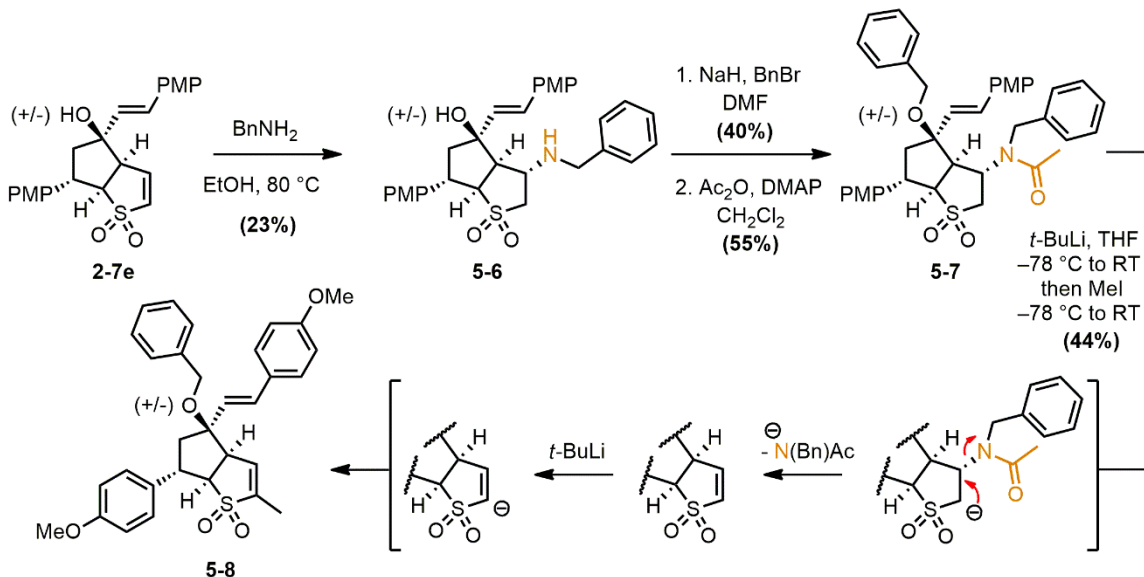
5.2.0. C2 Alkylation

We began investigating the conditions required to alkylate the assembled bicyclic sulfone at the C2-position using a simple model system lacking nitrogen-functionality at the C3-position. Reduced vinyl-sulfone **5-3** was prepared from vinyl sulfone **2-7a** using LiAlH_4 . The electron-withdrawing sulfone function of **5-3** reduces the acidity of the protons at the C2 position ($\text{pK}_a \sim 30\text{-}32$); treatment of **5-3** with a suitably strong base and an alkyl halide should afford the corresponding C2-functionalized product. One of the first C2-alkylation reactions attempted was the most successful. Treatment of **5-3** with sodium bis(trimethylsilyl)amide (NaHMDS) and benzyl bromide provided the desired C2-benzylated sulfone **5-4** in a 83% yield (as a single diastereomer). The observed diastereomer (confirmed using X-ray crystallography) is consistent with the electrophile approaching from the less hindered face of the [3.3.0]bicyclic core. Unfortunately, attempts to switch the benzyl bromide to other less electrophilic alkyl halides (methyl iodide, allyl bromide) failed to deliver any C2-alkylation product. After several dozen attempts at optimizing the deprotonation conditions, success was eventually achieved using **3-12** and the more basic *tert*-butyl lithium (*t*-BuLi) with methyl iodide and THF as the solvent. The product distribution was determined (by ^1H NMR) to be a 3:1 mixture of diastereomers; the diastereomers were not readily separable by column chromatography.



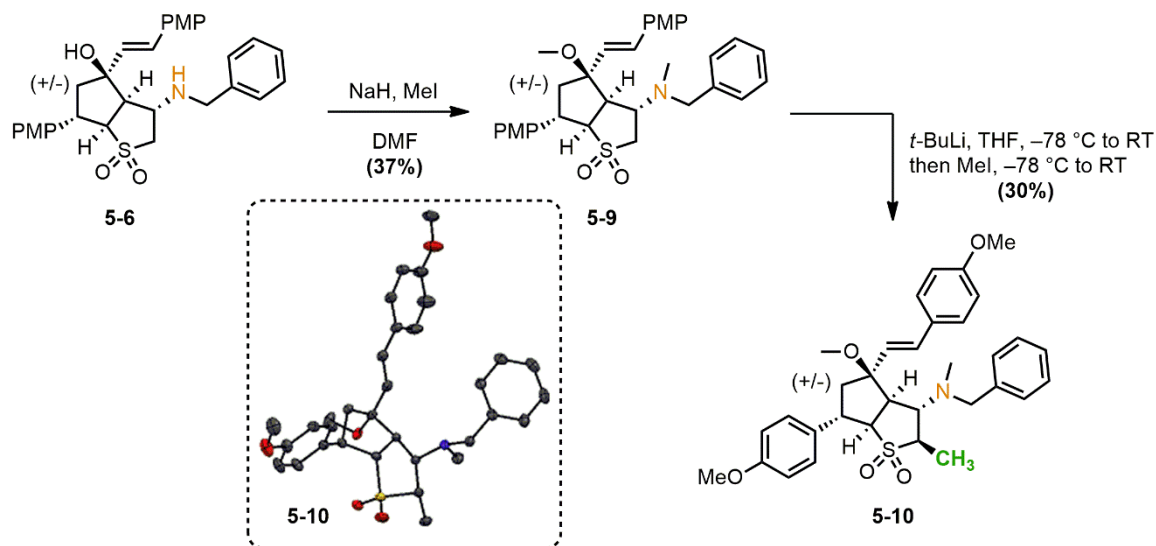
Scheme 18. Successful C2-alkylation studies performed on reduced vinyl sulfones **5-3** and **3-12**.

The results of the alkylation studies on the model system **5-3** and **3-12** were encouraging, however direct installation of nitrogen functionality (to eventually become the *N*-acetyl group) at the C3 position of **5-4** or **5-5** is likely not feasible. Therefore it was deemed necessary to install the C3-nitrogen functionality prior to C2-alkylation. Conjugate addition of benzylamine to the C3-position of the vinyl sulfone function of **2-7e** was achieved by mild heating of the substrates in ethanol (Scheme 19). An *N*-acetyl and *O*-benzyl group were then installed to provide the heavily fortified bis-*N*-protected **5-7**. Upon treatment of **5-7** with *t*-BuLi at $-78\text{ }^{\circ}\text{C}$, followed by the addition of methyl iodide, a mixture of starting material and methylated vinyl-sulfone **5-8** were isolated (Scheme 19). The presence of the C2-vinylic methyl group could have arisen through two pathways: sp^3 -C2-methylation followed by elimination of the *N*-benzyl acetamide anion, or elimination followed by sp^2 -C2-methylation. If methylation occurred first, the subsequent deprotonation of the sterically hindered C2 center may be unlikely. The latter pathway is probably more likely as the methylation of a C2 vinyl-sulfone sp^2 -center has been previously observed by Chou *et al.*¹⁹⁸



Scheme 19. Alkylation study of **5-7** using previously optimized *t*-BuLi and THF.

In order to circumvent the elimination of the C3-amine function, more electron-rich amine protecting groups were explored. Benzyl amine **5-6** was treated with excess methyl iodide and NaH in DMF to afford the “globally” methylated product **5-9** (Scheme 20). The methylbenzylamine moiety of **5-9** should be less prone to elimination since the methylbenzylamine anion leaving group is more basic than the *N*-benzylacetamide anion leaving group of **5-7**. In fact, treatment of **5-9** with *t*-BuLi, THF and methyl iodide provided the desired α -methylated product **5-10** as a single diastereomer. From X-ray crystallography the relative stereochemistry of the newly installed methyl center was found to be *anti* relative to the C3-amine function (Scheme 20). The difference in diastereoselectivity versus that observed with C2-benzylated **5-4** is likely due to the large amine function blocking the *syn*-face of the anion. Despite achieving C2-alkylation in the presence a C3 *N*-function, this route towards an analog of **5-2** was not explored further. The removal of the methyl ether and methyl amine protecting groups of **5-10** is likely not a trivial exercise. Furthermore, the synthetic route was getting a bit long and atom uneconomical for our purposes.



Scheme 20. Successful C2-methylation of globally protected sulfone 5-10.

5.3.0. 1,3-Dipolar Cycloaddition of Vinyl Sulfones and Azomethine Imines

A second approach envisioned to access sulfone **5-2** was use of a 1,3-dipolar cycloaddition to simultaneously deliver both the C3 *N*-functionality and a functional group at the C2-position (Figure 60). Using vinyl sulfone **2-7e** as the dipolarophile, the selection of a suitable 1,3-dipole must satisfy three requirements: the *N*-portion of the 1,3-dipole must be nucleophilic (to react with the electrophilic C3 position of **2-7e**), the bond between the *N*-function of the 1,3-dipole and the central atom must be easily cleavable, and the 3-position of the 1,3 dipole must provide a useful functional group handle to elaborate into a suitable S4 subsite binding substituent. Of the many 1,3-dipoles considered the most likely to accomplish our desired transformation was an azomethine imine (Figure 60).

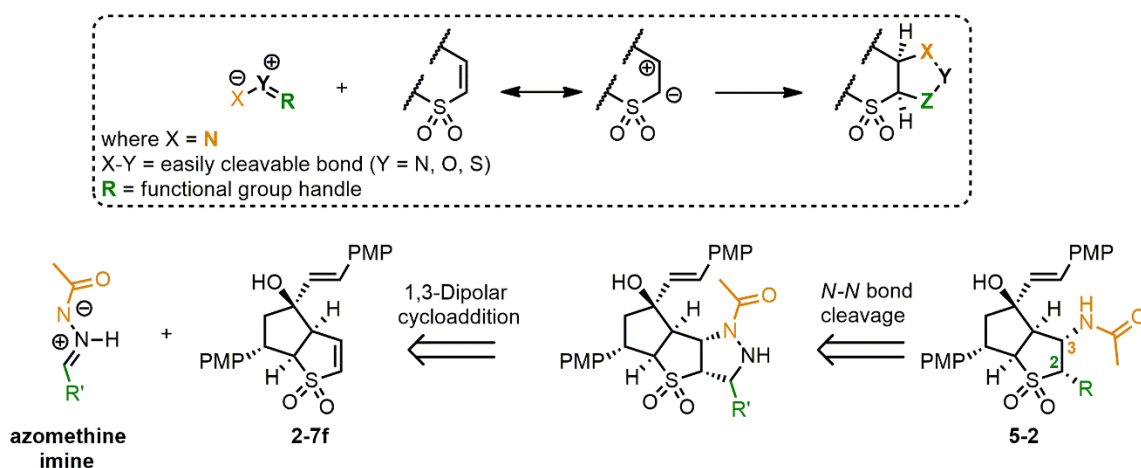
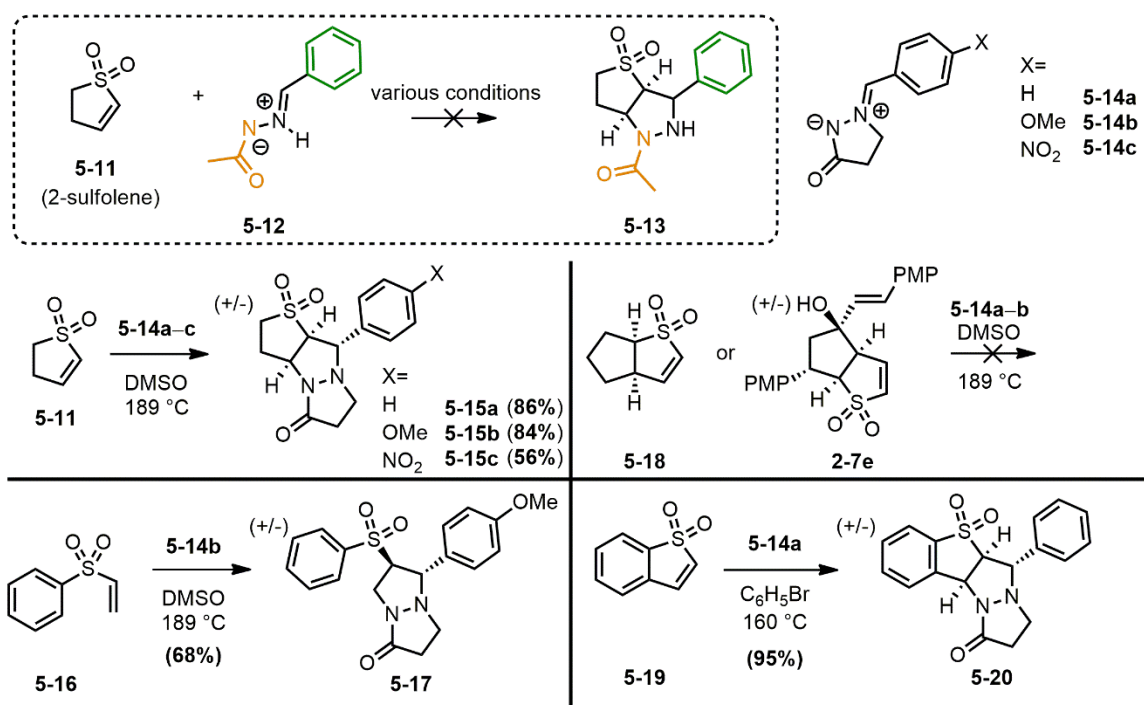


Figure 60. Dipolar cycloaddition using an azomethine imine in order to access **5-2**.

The 1,3-dipolar cycloaddition of azomethine imines has been previously described with α,β -unsaturated carbonyls,²³⁸⁻²⁴⁰ propargyl esters,²⁴¹ and *N*-vinyl-pyrroles.²⁴² The dipolar cycloaddition of azomethine imines with cyclic vinyl sulfones has not been previously reported. Undergraduate researcher Steven Wong was tasked with investigating the reaction between azomethine imine **5-12** with monocyclic 2-sulfolene **5-11** (envisioned here as an initial model system for **2-7e**). Unfortunately, under a variety of conditions involving Lewis acids and bases, elevated temperatures and different solvents no 1,3-dipolar cycloaddition product was observed with the linear azomethine imine. After much

discussion, Mr. Wong decided to try the 1,3-dipolar cycloaddition using cyclic azomethine imines **5-14a–c**. Using elevated temperatures (refluxing dimethylsulfoxide or bromobenzene) the corresponding 1,3-dipolar cycloaddition products could be successfully isolated from 2-sulfolene, phenyl vinyl sulfone (**5-16**) and bicyclic sulfone **5-19** to afford bicyclic, tricyclic or tetracyclic products in yields ranging from 56-95% (Scheme 21). Unfortunately, no 1,3-dipolar cycloaddition products were produced from [3.3.0]bicyclooctane sulfones **5-18** or **2-7e**. The lack of reactivity was rationalized due to the steric hindrance of these latter substrates. Although the desired 1,3-dipolar cycloaddition was unsuccessful with vinyl sulfone **2-7e**, the polycyclic products highlighted in Scheme 21 nonetheless represent new chemical entities. We should note that we cannot rule out the possibility that the apparent dipolar cycloaddition shown here may occur through a step wise process (*i.e.* a Michael addition followed by an intramolecular addition to the imminium).



Scheme 21. Dipolar cycloaddition of cyclic azomethine imines with a variety of monocyclic and bicyclic vinyl sulfones.

5.4.0. Tandem Reactivity of 2-Substituted 3-Sulfolenes and Bis-vinyl Ketones

With the C2-alkylation and 1,3-dipolar cycloaddition chemistry unfruitful at generating our desired intermediate **5-2**, we decided to (yet again) re-visit the methodology used to generate our bicyclic sulfone scaffolds. We wondered whether a 1,2 addition/anionic oxy-Cope followed by a subsequent γ -1,2 addition would tolerate the presence of a substituent at the 2-position of 3-sulfolene (Figure 61). Elaboration of **5-23** to the desired intermediate **5-2** could be envisioned occurring through a conjugate addition of a nitrogen nucleophile such as ammonia, followed by amide formation.

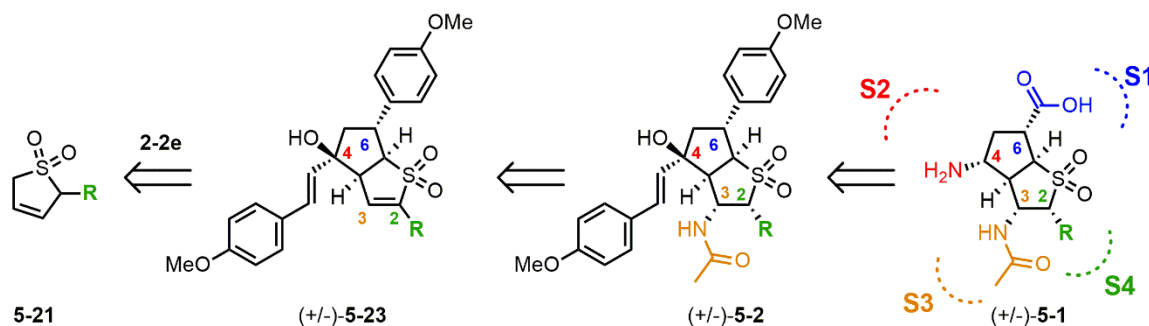
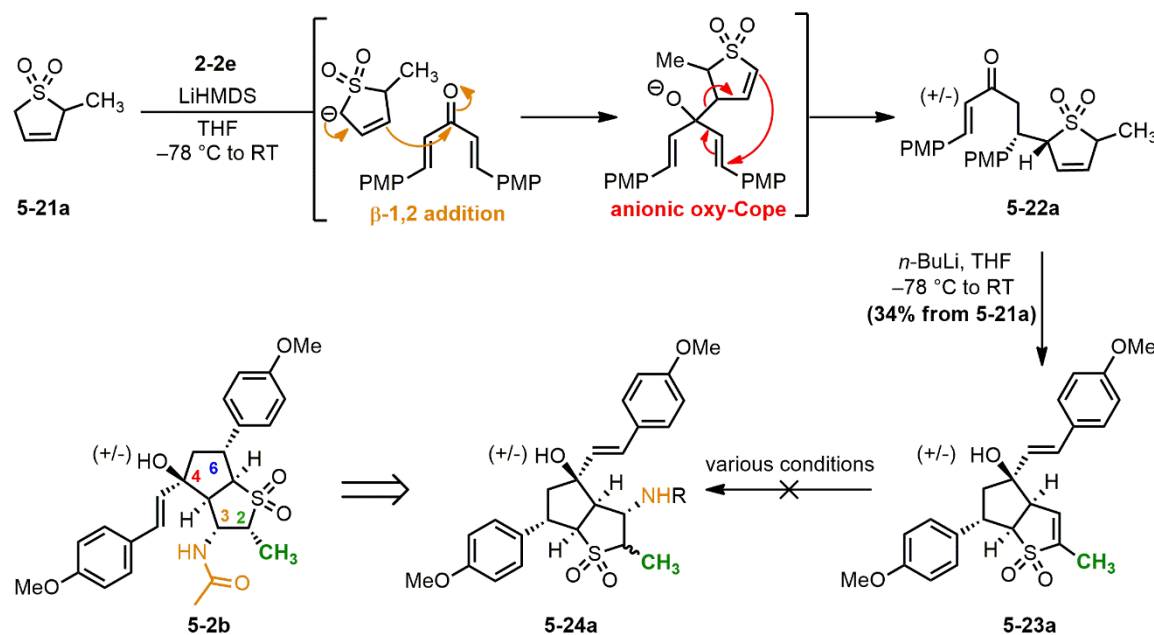


Figure 61. Use of 2-substituted-3-sulfolenes as a way to access key intermediate **5-2**.

In order to judge the feasibility of this approach we decided to start with the simplest 2-substituted-3-sulfolene, 2-methyl-3-sulfolene (**5-21a**). In the event, deprotonation of **5-21a** with LiHMDS exclusively occurred at the unhindered δ -position resulting in a single regioisomer of ketone **5-22a** after the anionic oxy-Cope. NMR analysis suggests that **5-22a** was formed as a single diastereomer (Scheme 22). Treatment of **5-22a** with LiHMDS did not result in conversion to the expected vinyl-sulfone bicycle **5-23a** likely due to the reduced acidity and greater steric bulk at the α -position of **5-22a**. Treatment with the less sterically hindered and more basic *n*-BuLi was required to induce a γ -1,2 addition, leading to the desired C2-methyl substituted bicycle **5-23a** in 34% yield over two steps (Scheme 22). Displeasingly, the conjugate addition of a variety of nitrogen nucleophiles (ammonia, benzyl amine, methylamine, allylamine and the azide anion) in a variety of solvents at elevated temperatures (methanol, bromobenzene, acetonitrile, *etc.*)

failed to deliver any conjugate addition product **5-24a**: unreacted starting material was recovered in nearly every instance.



Scheme 22. Tandem reactivity of 2-substituted-3-sulfolenes and bis-vinyl ketone **2-2e**.

5.5.0. Future Work

In conclusion, we were ultimately unable to elaborate our lead structure amino-acid **3-34** (through the installation of a group at the C2 position to probe the S4 subsite) to what would likely be a nanomolar inhibitor of viral neuraminidase. However the primary hypothesis of this thesis research was confirmed: a conformationally-restricted scaffold based on a [3.3.0]bicyclic archetype can appropriately orient its substituents to effectively bind to the active site of neuraminidase. Without an efficient way to install functionality at the C2 position, it seems unlikely sulfone **3-34** would make a good lead compound for the further design and synthesis of an inhibitor library against viral neuraminidase or other bacterial or human neuraminidase enzymes. At the same time, the low micromolar activity of the amino-acid **3-34** suggests that other bicyclic archetypes could also possess promising

activity against neuraminidase enzymes (Figure 62). One of these inspired scaffolds is the nor-sulfone analog of **3-34** targeted by Jeremy M. Mason. Comparison of compound **5-25** with sulfone **3-34** would be a valuable data point for determining the contribution of the sulfones activity against viral neuraminidase. The sulfone function of **3-34** may or may not be contributing to the binding affinity, and the removal of this functional group would be advantageous due to its high polarity. Jun Chen (Wulff group) is currently investigating the synthesis of a variety of bridged bicyclic systems as potential scaffolds for neuraminidase inhibition (*e.g.* amino-acid **5-26**). It is hoped that one of these bicyclic archetypes will prove to be an ideal scaffold for the generation of potent and selective inhibitors of a variety of neuraminidase enzymes.

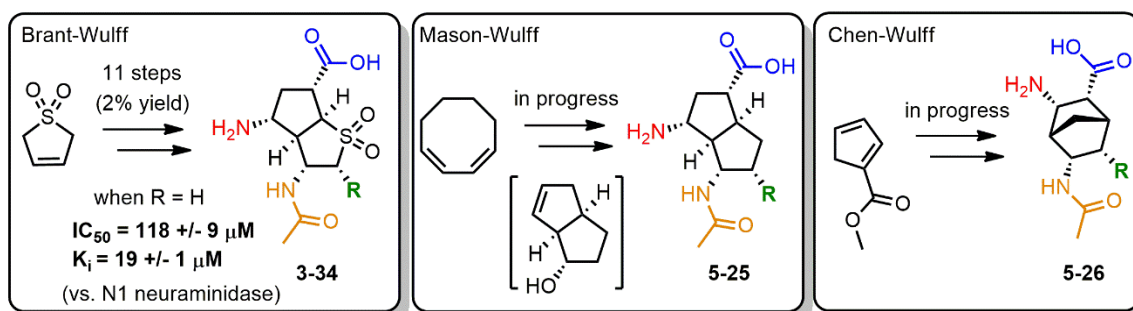


Figure 62. Bicyclic templates for the generation of conformationally-restricted enzyme inhibitors of neuraminidase.

Chapter 6. Experimental

6.1.0. General Remarks

General Experimental Procedures: All reactions were performed in single-neck, flame-dried, round-bottom flasks fitted with rubber septa under a positive pressure of argon, unless otherwise noted. Liquid reagents were transferred via glass syringe. Solvents were transferred via syringe with a stainless steel needle. Organic solutions were concentrated at 30 °C by rotary evaporation under vacuum. Analytical thin-layer chromatography (TLC) was performed using aluminum plates pre-coated with silica gel (0.20 mm, 60 Å pore-size, 230-400 mesh, Macherey-Nagel) impregnated with a fluorescent indicator (254 nm). TLC plates were visualized by exposure to ultraviolet light. Flash column chromatography was carried out over silica gel (60 Å, 63-200 µM, Caledon). Unless otherwise noted, all compounds isolated by chromatography were sufficiently pure (>95 % by NMR) for use in subsequent preparative reactions.

General Materials: Commercial solvents and reagents were used as received with the following exceptions. Tetrahydrofuran was dried by distillation over sodium and benzophenone. Dichloromethane and tetrahydrofuran (when > 50 mL of solvent was used in the reaction) were dried by passage through alumina in a commercial solvent purification system (SPS).

Instrumentation: Proton nuclear magnetic resonance spectra (¹H NMR) were recorded at 300 MHz or 500 MHz at 23 °C. Proton chemical shifts are expressed in parts per million (ppm, δ scale) downfield from tetramethylsilane, and are referenced to residual protium in the NMR solvent (CD₃C(O)CD₃, δ 2.05; CDCl₃, δ 7.26; CD₃OD, 3.31; CD₃S(O)CD₃ 2.50; D₂O 4.79). Data are represented as follows: chemical shift, multiplicity (s = singlet, d = doublet, t = triplet, q = quartet, sext = sextet, m = multiplet and/or multiple resonances, br = broad, app = apparent), coupling constant (two digits) in Hertz, and relative integration. Carbon nuclear magnetic resonance spectra (¹³C NMR) were recorded at 75 MHz or 125

MHz at 23 °C. Carbon chemical shifts are reported in parts per million downfield from tetramethylsilane and are referenced to the carbon resonance of the solvent ($\text{CD}_3\text{C}(\text{O})\text{CD}_3$, δ 29.85; CDCl_3 , δ 77.22; CD_3OD , 49.00; $\text{CD}_3\text{S}(\text{O})\text{CD}_3$, 39.52). Carbon assignments (e.g. CH_2) were inferred using a DEPT spectrum. Infrared (IR) spectra were obtained using a Perkin Elmer 1000 FT-IR spectrometer referenced to a polystyrene standard with an air background. Diagnostic peaks are represented as follows: frequency of absorption (cm^{-1}). High-resolution mass spectra were obtained at the UVic Genome BC Proteomics Centre using an Orbitrap system.

6.1.1. Enzyme Assay Protocol

All enzyme assays were conducted on a SpectraMax M5 plate reader using standard sensitivity settings. The following solutions were prepared for the enzyme assays:

1. Assay Buffer: 50 mM tris(hydroxymethyl)aminomethane, 5 mM CaCl_2 , 200 mM NaCl, pH 7.5.

2. Protein Stock Solution: inactivated virus suspension (or purchased enzyme) was diluted in Assay Buffer at 4 °C to obtain a concentration which, when used in the assays described below, gave a slope of approximately 2 (fluorescence units versus time in seconds) in the absence of inhibitors.

3. Substrate Stock Solution: 2'-4(Methylumbelliferyl)- α -D-N-acetylneuraminic acid was dissolved in DMSO to a concentration of 10 mM (working stock).

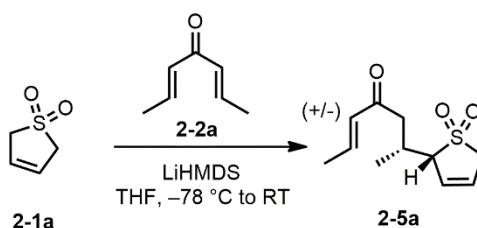
4. Substrate Working Solution: 20 μL of the substrate stock solution was diluted to 1000 μL with assay buffer, with a final concentration of 200 μM (2% DMSO).

5. Inhibitor Solutions: Inhibitors were diluted in assay buffer to provide a range of working concentrations. Peramivir, oseltamivir and zanamivir were used as positive controls.

Sample wells of a black 96-well plate (Nunc, optical bottom) were charged with 40 μL of protein stock solution, followed by 10 μL of inhibitor solution. The samples were incubated at room temperature for two hours, after which 50 μL of substrate working solution was added (i.e. final substrate concentration = 100 μM). The samples were mixed briefly by pipetting, and fluorescence was monitored over 5 minutes ($\lambda_{\text{exc}} = 365 \text{ nm}$; $\lambda_{\text{em}} = 445 \text{ nm}$). For kinetic data, the working substrate solution was subjected to serial dilution to obtain a range of substrate concentrations. Progress of the reaction was measured over 10 minutes at various concentrations of substrate and inhibitor. Control experiments (substrate buffer only) showed no significant background reaction. IC_{50} values were obtained by plotting percent inhibition against inhibitor concentration using XLfit (IDBS software) and identifying the concentration required to achieve 50% inhibition of enzymatic activity. K_m values at a range of inhibitor concentrations were obtained by fitting the kinetic data to Michaelis-Menten curves in XLfit, and K_i values were obtained by plotting $^{\text{APP}}K_m$ against inhibitor concentration. K_i was determined by dividing the y-intercept value by the slope as determined by XLfit. Estimates of error for IC_{50} values were obtained by plotting the data from three separate experiments (each of which was done in triplicate) and determining the “goodness of fit” to a sigmoidal function. Error values reported for K_i results correspond to the standard deviation for two separate determinations of K_i (each of which was run in duplicate).

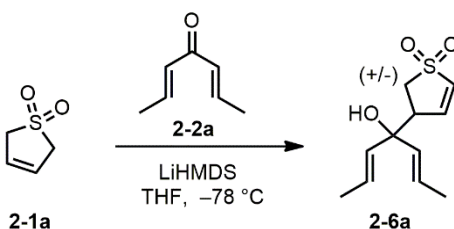
6.2.0. Chapter 2 Experimental

Chapter Specific Materials: Ketone **2-2a** was prepared from 4-heptanone by the method of H. Krabbenhoft.²⁴³ Ketone **2-2b** was prepared from 2,8-dimethyl-5-nonanone following an analogous procedure. Ketones **2-2c–e** were prepared using a double aldol condensation between acetone and the pleasant smelling *p*-tolualdehyde, cinnamaldehyde or *p*-anisaldehyde, respectively, following the general procedure provided by Conrad and Dolliver.²⁴⁴ Ketones **2-8a–b** were prepared from the corresponding cyclic ketones (cyclopentanone or cyclohexanone) and benzaldehyde or *p*-anisaldehyde, respectively, in a similar manor.



Hexamethyldisilazane (8.80 mL, 42.2 mmol) was dissolved in tetrahydrofuran (60 mL). The solution was cooled to $-78\text{ }^{\circ}\text{C}$, and *n*-butyllithium (17.8 mL, 2.20 M in hexanes, 39.2 mmol) was slowly added. The solution was stirred at $-78\text{ }^{\circ}\text{C}$ for 15 min, then warmed to room temperature for 45 min. 3-Sulfolene (**2-1a**) (4.20 g, 35.6 mmol) and ketone **2-2a** (4.80 g, 43.6 mmol) were dissolved in tetrahydrofuran (300 mL), and the solution was cooled to $-78\text{ }^{\circ}\text{C}$. The prepared solution of LiHMDS was added via cannula. The reaction mixture was stirred for 30 min at $-78\text{ }^{\circ}\text{C}$, then removed from the cooling bath and stirred 1 h at room temperature. The reaction was quenched by the addition of 10% aqueous HCl (50 mL), and the mixture was partially concentrated in vacuo. The resulting yellow solution was partitioned between 10% aqueous HCl and chloroform. The organic fraction was washed with brine and dried with Na_2SO_4 then concentrated in vacuo to provide 7.80 g of sulfone **2-5a**. The crude product was carried to the next step with no further purification.

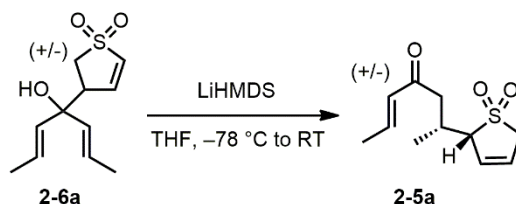
2-5a: yellow oil; $R_f = 0.5$ (hexanes:ethyl acetate, 1:1); IR (film) 1694, 1303, 1133, 971 cm^{-1} ; ^1H NMR (CDCl_3 500 MHz) δ 6.89 (dq, $J = 16, 6.8$ Hz, 1 H), 6.12 (dq, $J = 16, 1.6$ Hz, 1 H) 6.11-6.00 (m, 2 H), 3.78-3.63 (m, 3 H), 2.92 (dd, $J = 16, 5.0$ Hz, 1 H), 2.74-2.65 (m, 1 H), 2.55 (dd, $J = 16, 8.1$ Hz, 1 H), 1.89 (dd, $J = 7.0, 1.8$ Hz, 3 H), 1.14 (d, $J = 7.0$ Hz, 3 H); ^{13}C NMR (125 MHz) δ 198.6 (C), 144.0 (CH), 132.1 (CH), 129.1 (CH), 124.2 (CH), 69.1 (CH), 56.6 (CH_2), 43.1 (CH_2), 29.9 (CH), 18.5 (CH_3), 16.8 (CH_3); MS (ES⁺) m/z 251 (100); HRMS calcd for $\text{C}_{11}\text{H}_{16}\text{O}_3\text{S}$ ($\text{M}+\text{Na}$): 251.0718. Found: 251.0715.



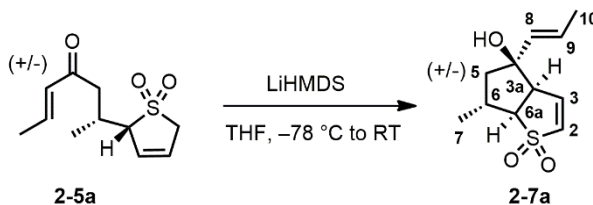
Hexamethyldisilazane (2.10 mL, 10.2 mmol) was dissolved in tetrahydrofuran (10 mL). The solution was cooled to -78 °C and *n*-BuLi (4.50 mL, 2.06 M in hexanes, 9.35 mmol) was slowly added. The solution was stirred for 15 min, then warmed to room temperature for 45 min. 3-Sulfolene (**2-1a**) (1.00 g, 8.5 mmol) and ketone **2-2a** (1.20 g, 10.9 mmol) were dissolved in tetrahydrofuran (60 mL), and the solution was cooled to -78 °C. The prepared solution of LiHMDS was added via cannula. The mixture was stirred for 10 min at -78 °C, then acetic acid (2 mL) was added. The reaction mixture was diluted with 10% aqueous HCl (50 mL), then partially concentrated in vacuo. The resulting yellow solution was partitioned between 10% HCl and chloroform, and the organic fraction was dried with Na_2SO_4 and concentrated in vacuo to provide a crude mixture of sulfone **2-5a** and intermediate **2-6a**. Extensive flash column chromatography (1:1 hexanes:ethyl acetate) afforded 131 mg of **2-6a**.

2-6a: thick colorless oil; $R_f = 0.6$ (hexanes:ethyl acetate, 1:1); IR (film) 3479 (br), 1289, 1135, 973 cm^{-1} ; ^1H NMR (CDCl_3 500 MHz) δ 6.67 (dd, $J = 6.8, 2.4$ Hz, 1 H), 6.67 (dd, $J = 6.8, 2.4$ Hz, 1 H), 5.75 (dq, $J = 15, 6.5$ Hz, 1 H), 5.72 (dq, $J = 15, 6.5$ Hz, 1 H), 5.47 (dq, $J = 15, 1.5$ Hz, 1 H), 5.44 (dq, $J = 15, 1.5$ Hz, 1 H), 3.27-3.19 (m, 1 H), 3.18-3.05 (m, 2

H), 2.13 (s, 1 H), 1.71 (dd, $J = 6.6, 1.5$ Hz, 3 H), 1.67 (dd, $J = 6.6, 1.5$ Hz, 3 H); ^{13}C NMR (CDCl_3 125 MHz) δ 140.2 (CH), 133.1 (CH), 132.0 (CH), 127.5 (CH), 127.3 (CH), 75.4 (C), 50.0 (CH_2), 49.2 (CH), 17.7 (CH_3); MS (ES^+) m/z 251 (100); HRMS calcd for $\text{C}_{11}\text{H}_{16}\text{O}_3\text{S}$ ($\text{M}+\text{Na}$): 251.0718. Found: 251.0712.



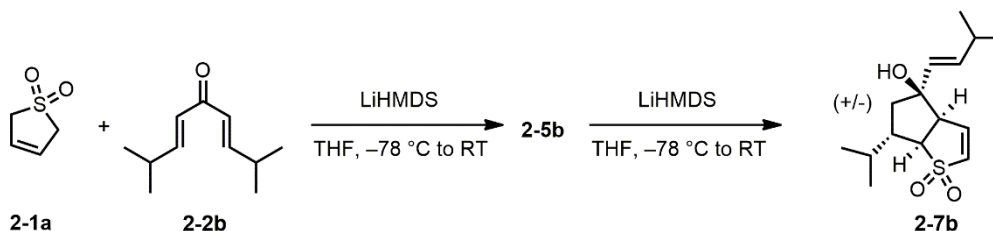
Compound **2-6a** (68 mg, 0.30 mmol) was dissolved in tetrahydrofuran (5 mL). LiHMDS (1.65 mL, 0.20 M, 0.33 mmol) was added via cannula at $-78\text{ }^\circ\text{C}$. The pink reaction mixture was stirred for 10 min at $-78\text{ }^\circ\text{C}$ and allowed to warm to room temperature for 1 h. The reaction mixture was partitioned between saturated NH_4Cl and ethyl acetate, washed with brine, and the organic fraction was dried with Na_2SO_4 then concentrated in vacuo to provide 56 mg of crude sulfone **2-5a**.



Hexamethyldisilazane (8.54 mL, 41.0 mmol) was dissolved in tetrahydrofuran (60 mL). The solution was cooled to $-78\text{ }^\circ\text{C}$, and $n\text{-BuLi}$ (15.1 mL, 2.50 M, 37.6 mmol) was slowly added. The solution was stirred at $-78\text{ }^\circ\text{C}$ for 15 min then warmed to room temperature for 45 min. Compound **2-5a** (crude, 7.80 g, 34.2 mmol) was dissolved in tetrahydrofuran (400 mL), and the solution was cooled to $-78\text{ }^\circ\text{C}$. The prepared solution of LiHMDS was added via cannula. The reaction mixture was stirred for 30 min at $-78\text{ }^\circ\text{C}$ then removed from the cooling bath and stirred 5 h at room temperature. The reaction was quenched by the addition of 10% aqueous HCl (100 mL), and the mixture was partially concentrated in vacuo. The resulting red solution was partitioned between 10% aqueous HCl and

chloroform. The organic fraction was washed with brine, dried with Na₂SO₄ and concentrated in vacuo. Flash column chromatography (25:1 dichloromethane:ethyl acetate) afforded 2.18 g (23% from **2-1a**) of vinyl sulfone **2-7a**. A single crystal suitable for X-ray crystallographic analysis was obtained via slow evaporation of **2-7a** dissolved in a mixture of dichloromethane and ethyl acetate.

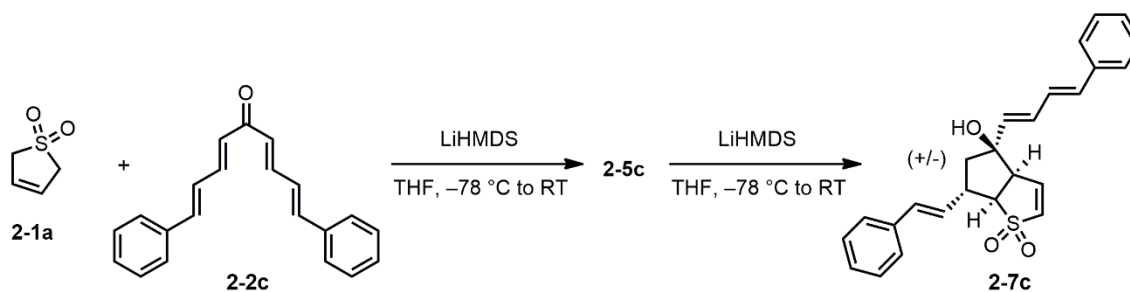
2-7a: yellow oil; R_f = 0.3 (dichloromethane:ethyl acetate, 10:1); Mp 107-110 °C; IR (film) 3485 (br), 1282, 1132 cm⁻¹; ¹H NMR (CDCl₃ 500 MHz) δ 6.52 (dd, *J* = 6.8, 1.7 Hz, 1 H, H2), 6.49 (dd, *J* = 6.7, 3.1 Hz, 1 H, H3), 5.79 (dq, *J* = 15, 6.5 Hz, 1 H, H9), 5.58 (dq, *J* = 15, 1.6 Hz, 1 H, H8), 3.53 (ddd, *J* = 9.4, 3.1, 1.8 Hz, 1 H, H3a), 3.19 (dd, *J* = 9.5, 8.2 Hz, 1 H, H6a), 2.97-2.85 (m, 1 H, H6), 2.02 (dd, *J* = 13, 6.2 Hz, 1 H, H5_{eq}), 1.71 (dd, *J* = 6.6, 1.5 Hz, 3 H, H10), 1.70 (t, *J* = 13 Hz, 1 H, H5_{ax}), 1.24 (d, *J* = 6.9 Hz, 3 H, H7); ¹³C NMR (CDCl₃ 125 MHz) δ 137.1 (CH), 133.7 (CH), 132.7 (CH), 125.9 (CH), 80.6 (C), 67.8 (CH), 57.8 (CH), 51.6 (CH₂), 33.6 (CH), 19.6 (CH₃), 17.8 (CH₃); MS (ES⁺) *m/z* 251 (100); HRMS calcd for C₁₁H₁₆O₃S (M+Na): 251.0718. Found: 251.0715.



Hexamethyldisilazane (350 μL, 1.68 mmol) was dissolved in tetrahydrofuran (5 mL). The solution was cooled to -78 °C, and *n*-BuLi (780 μL, 1.98 M in hexanes, 1.55 mmol) was slowly added. The solution was stirred at -78 °C for 15 min, then warmed to room temperature for 45 min. 3-Sulfolene (**2-1a**) (152 mg, 1.29 mmol) and ketone **2-2b** (215 mg, 1.29 mmol) were dissolved in tetrahydrofuran (20 mL), and the solution was cooled to -78 °C. The prepared solution of LiHMDS was added via cannula. The reaction mixture was stirred for 40 min at -78 °C, then removed from the cooling bath and stirred 1 h at room temperature. The reaction was quenched by the addition of 10% aqueous HCl (10 mL), and the mixture was partially concentrated in vacuo. The resulting yellow solution was

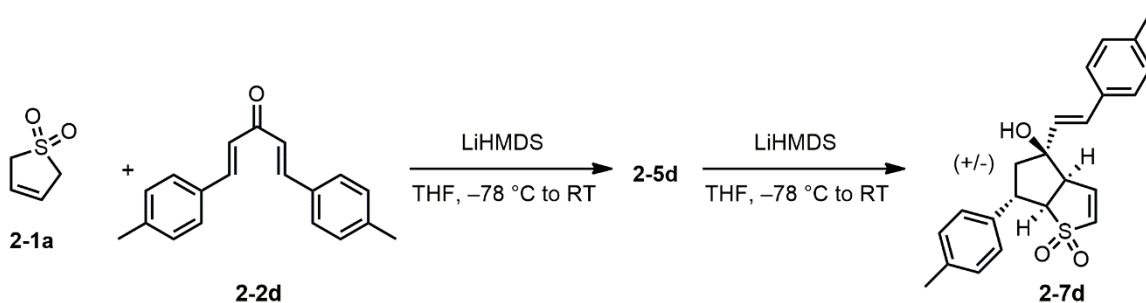
partitioned between 10% aqueous HCl and dichloromethane. The organic fraction was washed with brine and dried with Na₂SO₄ then concentrated in vacuo to provide 398 mg of **2-5b** as a yellow oil. The crude product was carried to the next step with no further purification. Hexamethyldisilazane (217 μ L, 0.803 mmol) was dissolved in tetrahydrofuran (10 mL). The solution was cooled to -78 $^{\circ}$ C, and *n*-BuLi (487 μ L, 1.98 M in hexanes, 0.964 mmol) was slowly added. The solution was stirred at -78 $^{\circ}$ C for 15 min then warmed to room temperature for 45 min. The crude keto-sulfone (228 mg, 0.739 mmol) was dissolved in tetrahydrofuran (20 mL), and the solution was cooled to -78 $^{\circ}$ C. The prepared solution of LiHMDS was added via cannula. The reaction mixture was stirred for 30 min at -78 $^{\circ}$ C then removed from the cooling bath and stirred 5 h at room temperature. The reaction was quenched by the addition of 10% aqueous HCl (10 mL), and the mixture was partially concentrated in vacuo. The resulting yellow solution was partitioned between 10% aqueous HCl and dichloromethane. The organic fraction was washed with brine, dried with Na₂SO₄ and concentrated in vacuo. Flash column chromatography (25:1 dichloromethane:ethyl acetate) afforded 102 mg (48% from **2-1a**) of vinyl sulfone **2-7b**.

2-7b: yellow oil; R_f = 0.3 (dichloromethane:ethyl acetate, 25:1); IR (film) 3486 (br), 1282, 1135 cm^{-1} ; ¹H NMR (CDCl₃ 500 MHz) δ 6.58 (dd, J = 6.8, 1.8 Hz, 1 H), 6.46 (dd, J = 6.8, 3.7 Hz, 1 H), 5.75 (dd, J = 16, 6.6 Hz, 1 H), 5.46 (dd, J = 16, 1.4 Hz, 1 H), 3.47 (ddd, J = 9.7, 3.7, 1.8 Hz, 1 H), 3.31 (dd, J = 9.7, 7.4 Hz, 1 H), 2.60 (dtd, J = 13, 6.8, 6.5 Hz, 1 H), 2.29 (od, J = 6.6, 1.4 Hz, 1 H), 2.08 (dd, J = 13, 6.5 Hz, 1 H), 1.70 (t, J = 13 Hz, 1 H), 1.65-1.52 (m, 1 H), 1.05 (d, J = 6.6 Hz, 3 H) 0.97 (d, J = 6.8 Hz, 6 H), 0.94 (d, J = 6.6 Hz, 3 H); ¹³C NMR (CDCl₃ 125 MHz) δ 138.2 (CH), 136.5 (CH), 133.3 (CH), 128.9 (CH), 80.4 (C), 65.4 (CH), 58.1 (CH), 48.7 (CH₂), 45.5 (CH), 33.0 (CH), 30.8 (CH), 22.5 (CH₃), 22.5 (CH₃), 22.6 (CH₃), 21.1 (CH₃); MS (ES⁺) m/z 307 (100); HRMS calcd for C₁₅H₂₄O₃S (M+Na): 307.1344. Found: 307.1325.



Hexamethyldisilazane (432 μL , 2.08 mmol) was dissolved in tetrahydrofuran (5 mL). The solution was cooled to $-78\text{ }^{\circ}\text{C}$, and *n*-BuLi (1.25 mL, 1.54 M in hexanes, 1.92 mmol) was slowly added. The solution was stirred at $-78\text{ }^{\circ}\text{C}$ for 15 min, then warmed to room temperature for 45 min. 3-Sulfolene (**2-1a**) (188 mg, 1.60 mmol) and ketone **2-2c** (458 mg, 1.60 mmol) were dissolved in tetrahydrofuran (20 mL), and the solution was cooled to $-78\text{ }^{\circ}\text{C}$. The prepared solution of LiHMDS was added via cannula. The reaction mixture was stirred for 40 min at $-78\text{ }^{\circ}\text{C}$, then removed from the cooling bath and stirred 1 h at room temperature. The reaction was quenched by the addition of 10% aqueous HCl (10 mL), and the mixture was partially concentrated in vacuo. The resulting yellow solution was partitioned between 10% aqueous HCl and dichloromethane. The organic fraction was washed with brine and dried with Na_2SO_4 then concentrated in vacuo at $30\text{ }^{\circ}\text{C}$ to provide 701 mg of crude keto-sulfone as a red oil. The crude product was carried to the next step with no further purification. Hexamethyldisilazane (362 μL , 1.74 mmol) was dissolved in tetrahydrofuran (10 mL). The solution was cooled to $-78\text{ }^{\circ}\text{C}$, and *n*-BuLi (1.06 mL, 1.54 M in hexanes, 1.59 mmol) was slowly added. The solution was stirred at $-78\text{ }^{\circ}\text{C}$ for 15 min then warmed to room temperature for 45 min. The crude keto-sulfone (573 mg, 1.31 mmol) was dissolved in tetrahydrofuran (20 mL), and the solution was cooled to $-78\text{ }^{\circ}\text{C}$. The prepared solution of LiHMDS was added via cannula. The reaction mixture was stirred for 30 min at $-78\text{ }^{\circ}\text{C}$ then removed from the cooling bath and stirred 5 h at room temperature. The reaction was quenched by the addition of 10% aqueous HCl (10 mL), and the mixture was partially concentrated in vacuo. The resulting yellow solution was partitioned between 10% aqueous HCl and dichloromethane. The organic fraction was washed with brine, dried with Na_2SO_4 and concentrated in vacuo. Flash column chromatography (25:1 dichloromethane:ethyl acetate) afforded 201 mg (38% from **2-1a**) of vinyl sulfone **2-7c**.

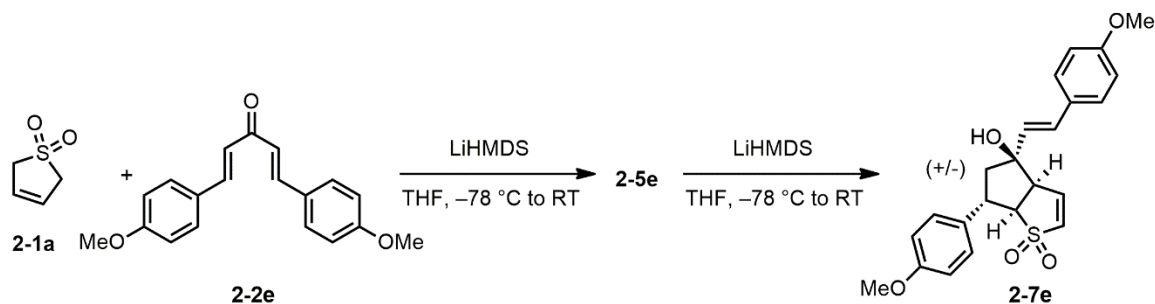
2-7c: yellow oil; $R_f = 0.3$ (dichloromethane:ethyl acetate, 50:1); IR (film) 3479 (br), 1284, 1132 cm^{-1} ; ^1H NMR (CDCl_3 500 MHz) δ 7.50-7.16 (m, 10 H, Ph), 6.78 (dd, $J = 16, 10$ Hz), 6.64-6.53 (m, 5 H), 6.23 (dd, $J = 16, 7.2$ Hz, 1 H), 5.91 (d, $J = 16$ Hz, 1 H), 3.78 (ddt, $J = 13, 7.6, 6.8$ Hz, 1 H), 3.65 (ddd, 9.7, 3.2, 2.2 Hz, 1 H), 3.57 (dd, $J = 9.6, 8.1$ Hz, 1 H), 2.23 (dd, $J = 13, 6.4$ Hz, 1 H), 2.11 (t, $J = 13$ Hz, 1 H); ^{13}C NMR (CDCl_3 125 MHz) δ 137.0 (C), 136.7 (C), 136.4 (CH), 135.0 (CH), 134.3 (CH), 133.4 (CH), 132.2 (CH), 130.7 (CH), 129.0 (CH), 128.9 (CH), 128.8 (CH), 128.2 (CH), 127.9 (CH), 127.4 (CH), 126.7 (CH), 126.6 (CH), 80.6 (C), 66.0 (CH), 57.8 (CH), 50.0 (CH_2), 41.8 (CH); MS (ES⁺) m/z 429 (4), 427 (100); HRMS calcd for $\text{C}_{25}\text{H}_{24}\text{O}_3\text{S}$ (M+Na): 427.1344. Found: 427.1350.



3-Sulfolene (**2-1a**) (262 mg, 2.22 mmol) and ketone **2-2d** (583 mg, 2.22 mmol) were dissolved in tetrahydrofuran (30 mL), and the solution was cooled to $-78\text{ }^\circ\text{C}$. LiHMDS (2.44 mL, 1M in THF, 2.44 mmol) was added in one portion. The reaction mixture was stirred for 1 h at $-78\text{ }^\circ\text{C}$, then removed from the cooling bath and stirred 1 h at room temperature. The reaction was quenched by the addition of 10% aqueous HCl (10 mL), and the mixture was partially concentrated in vacuo at $30\text{ }^\circ\text{C}$. The resulting yellow solution was partitioned between 10% aqueous HCl and dichloromethane. The organic fraction was washed with brine and dried with Na_2SO_4 then concentrated in vacuo to provide 875 mg of crude keto-sulfone **2-5d** as a yellow oil. The crude intermediate **2-5d** (651 mg, 1.71 mmol) was dissolved in tetrahydrofuran (30 mL), and the solution was cooled to $-78\text{ }^\circ\text{C}$. LiHMDS (1.88 mL, 1M in THF, 1.88 mmol) was added in one portion. The reaction mixture was stirred for 30 min at $-78\text{ }^\circ\text{C}$ then removed from the cooling bath and stirred 2 h at room temperature. The reaction was quenched by the addition of 10% aqueous HCl

(10 mL), and the mixture was partially concentrated in vacuo. The resulting red solution was partitioned between 10% aqueous HCl and dichloromethane. The organic fraction was washed with brine, dried with Na₂SO₄ and concentrated in vacuo. Flash column chromatography (25:1 to 10:1 dichloromethane:ethyl acetate gradient) afforded 261 mg (42% from **2-1a**) of vinyl sulfone **2-7d**.

2-7d: yellow oil; $R_f = 0.2$ (dichloromethane:ethyl acetate, 25:1); IR (film) 3413 (br), 1280, 1133 cm^{-1} ; ¹H NMR (CD₃S(O)CD₃ 500 MHz) δ 7.35 (d, $J = 8.1$ Hz, 2 H), 7.28 (d, $J = 8.0$ Hz, 2 H), 7.17 (d, $J = 7.6$ Hz, 2 H), 7.16 (d, $J = 7.6$ Hz, 2 H), 6.88 (dd, $J = 6.7, 2.1$ Hz, 1 H), 6.68 (d, $J = 16$ Hz, 1 H), 6.66 (dd, $J = 6.8, 3.2$ Hz, 1 H), 6.51 (d, $J = 16$ Hz, 1 H), 3.97-3.88 (m, 2 H), 3.73 (t, $J = 9.2$ Hz, 1 H), 2.34 (t, $J = 13$ Hz, 1 H), 2.29 (s, 6 H), 2.22 (dd, $J = 13, 6.0$ Hz, 1 H); ¹³C NMR (CD₃S(O)CD₃ 125 MHz) δ 138.6 (C), 138.5 (CH), 136.7 (C), 135.8 (C), 133.7 (C), 132.9 (CH), 131.7 (CH), 129.2 (CH), 129.2 (CH), 127.8 (CH), 127.3 (CH), 126.3 (CH), 79.5 (C), 67.1 (CH), 57.5 (CH), 49.6 (CH₂), 43.2 (CH), 20.8 (CH₃), 20.6 (CH₃); MS (ES+) m/z 405 (4), 403 (100); HRMS calcd for C₂₃H₂₄O₃S (M+Na): 403.1344. Found: 403.1328.



3-Sulfolene (**2-1a**) (4.15 g, 35.2 mmol) and ketone **2-2e** (10.3 g, 35.2 mmol) were dissolved in tetrahydrofuran (200 mL), and the solution was cooled to -78 °C. LiHMDS (42.3 mL, 1 M in tetrahydrofuran, 42.3 mmol) was added in one portion. The reaction mixture was stirred for 1 h at -78 °C, then removed from the cooling bath and stirred 1 h at room temperature. The reaction was quenched by the addition of 10% aqueous HCl (50 mL), and the mixture was partially concentrated in vacuo. The resulting orange solution was

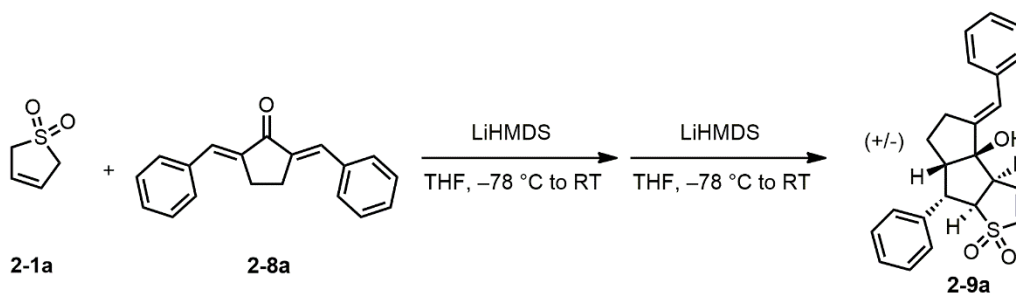
partitioned between 10% aqueous HCl and dichloromethane. The organic fraction was washed with brine and dried with Na₂SO₄ then concentrated in vacuo to provide 14.5 g of crude keto-sulfone **2-5e**. The crude product was carried to the next step with no further purification.

2-5e: light orange foam; IR (film) 1683, 1305, 1173 cm⁻¹; ¹H NMR (CDCl₃ 300 MHz) δ 7.51 (d, *J* = 16 Hz, 1 H), 7.47 (d, *J* = 8.7 Hz, 2 H), 7.27 (d, *J* = 8.7 Hz, 2 H), 6.90 (d, *J* = 8.7 Hz, 2 H), 6.83 (d, *J* = 8.7 Hz, 2 H), 6.56 (d, 16 Hz, 1 H), 6.20-6.06 (m, 2 H), 4.11-4.05 (m, 1 H), 4.00-3.91 (m, 1 H), 3.83 (s, 3 H), 3.76 (s, 3 H), 3.72-3.64 (m, 1 H), 3.52 (ddd, *J* = 16, 4.5, 2.3 Hz, 1 H), 3.33 (dd, *J* = 16, 5.2 Hz, 1 H), 3.14 (dd, *J* = 16, 9.2 Hz, 1 H); ¹³C NMR (CDCl₃ 75 MHz) δ 197.9 (C), 161.8 (C), 158.8 (C), 143.2 (CH), 131.3 (C), 130.2 (CH), 129.5 (CH), 128.6 (CH), 127.0 (C), 124.6 (CH), 123.6 (CH), 114.5 (CH), 114.0 (CH), 69.1 (CH), 56.0 (CH₂), 55.4 (CH₃), 55.2 (CH₃), 42.4 (CH₂), 40.0 (CH); MS (ES+) *m/z* 435 (100); HRMS calcd for C₂₃H₂₄O₅S (M+H): 413.1423. Found: 413.1423.

Compound **2-5e** (crude, 14.5 g, 35.2 mmol) was dissolved in tetrahydrofuran (400 mL), and the solution was cooled to -78 °C. LiHMDS (42.3 mL, 1 M in tetrahydrofuran, 42.3 mmol) was added in one portion. The reaction mixture was stirred for 30 min at -78 °C then removed from the cooling bath and stirred 2.5 h at room temperature. The reaction was quenched by the addition of saturated aqueous NH₄Cl and the mixture was partially concentrated in vacuo. The resulting red solution was partitioned between saturated aqueous NH₄Cl and dichloromethane. The organic fraction was washed with brine, dried with Na₂SO₄ and concentrated in vacuo to provide 14.5 g of crude vinyl sulfone **2-7e** as a brick red solid. Flash column chromatography (50:1 to 10:1 dichloromethane:ethyl acetate gradient) afforded 6.53 g (45% from **2-1a**) of vinyl sulfone **2-7e**.

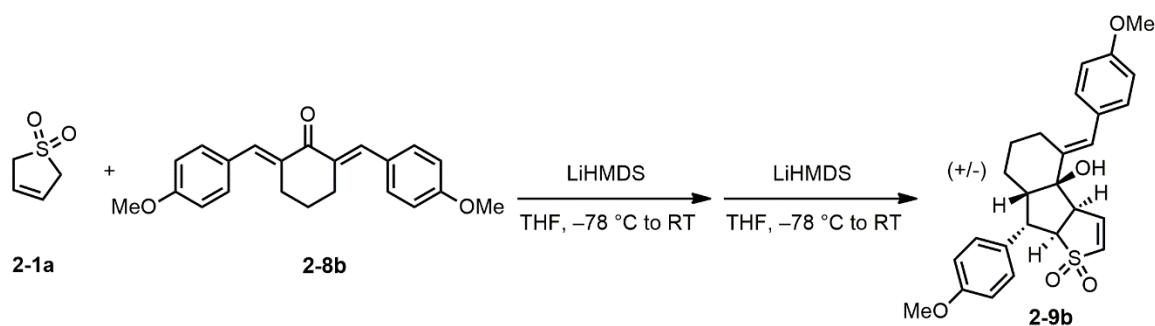
2-7e: light yellow solid; R_f = 0.2 (dichloromethane:ethyl acetate, 25:1); IR (film) 3479 (br), 1250, 1132 cm⁻¹; ¹H NMR (CDCl₃ 300 MHz) δ 7.35 (d, *J* = 8.6 Hz, 2 H), 7.28 (d, *J* = 8.6 Hz, 2 H), 6.89 (d, *J* = 8.8 Hz, 2 H), 6.88 (d, *J* = 8.8 Hz, 2 H), 6.74 (d, *J* = 16 Hz, 1 H), 6.66 (dd, *J* = 6.8, 1.5 Hz, 1 H), 6.59 (dd, *J* = 6.8, 3.1 Hz, 1 H), 6.23 (d, *J* = 16 Hz, 1 H), 4.25-4.13 (m, 1 H), 3.82 (s, 3 H), 3.80 (s, 3 H), 3.77 (ddd, *J* = 9.7, 3.1, 2.5 Hz, 1 H), 3.72 (dd, *J*

= 9.7, 7.4 Hz, 1 H), 2.42 (d, $J = 9.8$ Hz, 2 H); ^{13}C NMR (CDCl_3 75 MHz) δ 159.8 (C), 158.8 (C), 136.3 (CH), 133.3 (CH), 132.7 (C), 129.6 (CH), 128.8 (CH), 128.6 (C), 128.4 (CH), 128.0 (CH), 114.4 (CH), 114.3 (CH), 80.7 (C), 67.9 (CH), 58.0 (CH), 55.5 (CH_3), 55.5 (CH_3), 50.6 (CH_2), 42.6 (CH); MS (ES^+) m/z 435 (100); HRMS calcd for $\text{C}_{23}\text{H}_{24}\text{O}_5\text{S}$ ($\text{M}+\text{Na}$): 435.1242. Found: 435.1239.



3-Sulfolene (**2-1a**) (107 mg, 0.904 mmol) and ketone **2-8a** (234 mg, 0.903 mmol) were dissolved in tetrahydrofuran (20 mL), and the solution was cooled to $-78\text{ }^\circ\text{C}$. LiHMDS (1.1 mL, 1 M in THF, 1.10 mmol) was added dropwise. The reaction mixture was stirred for 1 h at $-78\text{ }^\circ\text{C}$, then removed from the cooling bath and stirred 1 h at room temperature. The reaction was quenched by the addition of saturated aqueous NH_4Cl (10 mL), and the resulting solution was extracted twice with ethyl acetate. The organic fraction was dried with Na_2SO_4 then concentrated in vacuo to provide the anionic oxy-Cope sulfone product as a light orange foam. Flash column chromatography (100:0 to 25:1 dichloromethane:ethyl acetate gradient) afforded 177 mg of the 3-sulfolene intermediate. The purified 3-sulfolene intermediate (177 mg, 0.468 mmol) was dissolved in tetrahydrofuran (10 mL), and the solution was cooled to $-78\text{ }^\circ\text{C}$. LiHMDS (0.562 mL, 1 M in THF, 0.562 mmol) was added dropwise. The reaction mixture was stirred for 1 h at $-78\text{ }^\circ\text{C}$. The reaction was quenched by the addition of saturated aqueous NH_4Cl (10 mL), and the resulting solution was warmed to room temperature then extracted twice with ethyl acetate. The combined organic extracts were dried over Na_2SO_4 , filtered, concentrated in vacuo. Flash column chromatography (25:1 to 10:1 dichloromethane:ethyl acetate gradient) afforded 103 mg (30% from **2-1a**) of vinyl-sulfone **2-9a**.

2-9a: white solid; $R_f = 0.3$ (dichloromethane:ethyl acetate, 50:1); IR (film) 3470, 1603, 1285, 1131 cm^{-1} ; ^1H NMR (CDCl_3 300 MHz) δ 7.41-7.21 (m, 10 H), 6.78 (dd, $J = 6.7, 3.4$ Hz, 1 H), 6.63-6.59 (m, 2 H), 4.30 (dd, $J = 9.1, 6.2$ Hz, 1 H), 4.08 (t, $J = 9.3$ Hz, 1 H), 3.84 (dd, $J = 9.5, 2.7$ Hz, 1 H), 2.94-2.70 (m, 3 H), 1.94-1.80 (m, 1 H), 1.50-1.32 (m, 1 H); ^{13}C NMR (CDCl_3 75 MHz) δ 147.0 (C), 138.7 (C), 137.2 (CH), 136.9 (C), 132.0 (CH), 130.6 (CH), 128.9 (CH), 128.7 (CH), 128.6 (CH), 127.8 (CH), 127.3 (CH), 127.0 (CH), 89.7 (C), 64.5 (CH), 62.0 (CH), 60.1 (CH), 56.4 (CH), 46.2 (CH), 28.8 (CH_2), 24.8 (CH_2); HRMS calcd for $\text{C}_{23}\text{H}_{22}\text{O}_3\text{S}$ (M+Na): 401.1182. Found: 401.1180.

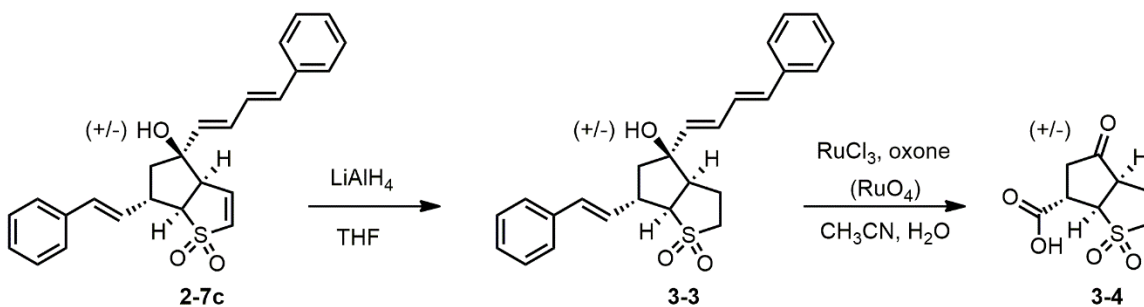


3-Sulfolene (**2-1a**) (1.16 g, 9.83 mmol) and ketone **2-8b** (2.76 g, 10.1 mmol) were dissolved in tetrahydrofuran (150 mL), and the solution was cooled to $-78\text{ }^\circ\text{C}$. LiHMDS (10.8 mL, 1 M in THF, 10.8 mmol) was added dropwise. The reaction mixture was stirred for 1 h at $-78\text{ }^\circ\text{C}$, then removed from the cooling bath and stirred 1 h at room temperature. The reaction was quenched by the addition of saturated aqueous NH_4Cl (10 mL), and the resulting solution was extracted twice with ethyl acetate. The organic fraction was dried with Na_2SO_4 then concentrated in vacuo to provide the anionic oxy-Cope sulfone product as a light orange foam. The crude 3-sulfolene intermediate (3.0 g, 6.6 mmol) was dissolved in tetrahydrofuran (100 mL), and the solution was cooled to $-78\text{ }^\circ\text{C}$. LiHMDS (7.3 mL, 1 M in THF, 7.3 mmol) was added dropwise. The reaction mixture was stirred for 1 h at $-78\text{ }^\circ\text{C}$. The reaction was quenched by the addition of saturated aqueous NH_4Cl and the mixture was partially concentrated in vacuo. The residue was partitioned between saturated aqueous NH_4Cl then extracted twice with ethyl acetate. The combined organic fractions were washed with brine, dried with Na_2SO_4 and concentrated in vacuo. Flash column chromatography (25:1 to 10:1 dichloromethane:ethyl acetate gradient) afforded 701 mg

(18% from **2-1a**) of vinyl-sulfone **2-9b**. A single crystal suitable for X-ray crystallographic analysis was obtained via slow evaporation of **2-9b** dissolved in a mixture of dichloromethane and ethyl acetate.

2-9b: white solid; $R_f = 0.5$ (dichloromethane:ethyl acetate, 25:1); IR (film) 3480, 1278, 1129 cm^{-1} ; ^1H NMR (CDCl_3 300 MHz) δ 7.21 (d, $J = 8.7$ Hz, 2 H), 7.16 (d, $J = 8.7$ Hz, 2 H), 6.92-6.86 (m, 4 H), 6.84-6.79 (m, 1 H), 6.62 (dd, $J = 6.9, 1.2$ Hz, 1 H), 6.58 (dd, $J = 6.8, 2.6$ Hz, 1 H), 4.45 (dd, $J = 9.4, 6.1$ Hz, 1 H), 4.10 (t, $J = 9.6$ Hz, 1 H), 4.02-3.96 (m, 1 H), 3.82 (s, 3 H), 3.80 (s, 3 H), 3.08 (d, 16 Hz, 1 H), 2.39 (td, $J = 12, 5.9$ Hz, 1 H), 2.08-1.92 (m, 1 H), 1.83-1.45 (m, 2 H), 1.28-0.97 (m, 2 H); ^{13}C NMR (CDCl_3 75 MHz) δ 158.7 (C), 158.7 (C), 139.8 (C), 136.8 (CH), 133.0 (CH), 130.5 (CH), 129.6 (C), 129.5 (C), 129.0 (CH), 123.9 (CH), 114.3 (CH), 113.9 (CH), 82.5 (C), 62.7 (CH), 59.3 (CH), 55.4 (CH_3), 55.4 (CH_3), 54.3 (CH), 47.2 (CH), 27.3 (CH_2), 26.5 (CH_2), 25.4 (CH_2); HRMS calcd for $\text{C}_{26}\text{H}_{28}\text{O}_5\text{S}$ (M+Na): 475.1549. Found: 475.1550.

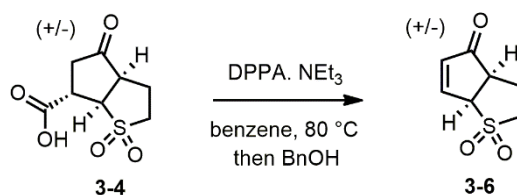
6.3.0. Chapter 3 Experimental:



Compound **2-7c** (1.20 g, 3.03 mmol) was dissolved in tetrahydrofuran (80 mL). The solution was cooled to 0 °C and LiAlH_4 (143 mg, 3.60 mmol) was added in three small portions over 5 min. The solution was stirred at 0 °C for 30 min. Wet Na_2SO_4 was added in small portions over 5 min until gas evolution desisted. The reaction mixture was filtered then washed with ethyl acetate. The organic fraction was dried with Na_2SO_4 and concentrated in vacuo. The crude product was carried on to the next step with no further purification. Compound **3-3** (crude, 150 mg, 0.38 mmol) was dissolved in acetonitrile (15

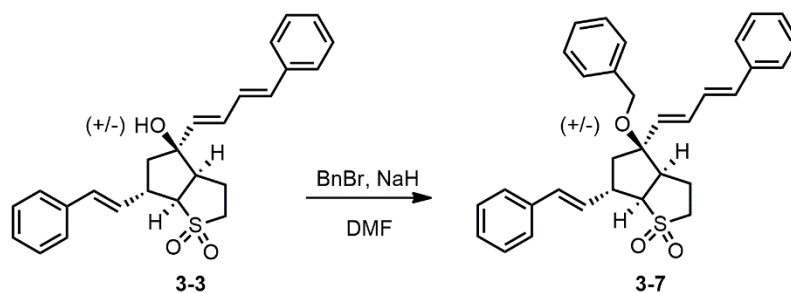
mL) and water (9 mL). RuCl_3 (8 mg, 0.038 mmol) was added. NaHCO_3 (319 mg, 3.8 mmol) was added, followed by oxone (1.40 g, 2.28 mmol) in three portions over 5 min. The reaction mixture was stirred for 45 min. Due to the volatility of RuO_4 additional aliquots of RuCl_3 (18 mg, 0.019 mmol) were added as necessary. The reaction mixture was partitioned between saturated aqueous $\text{Na}_2\text{S}_2\text{O}_3$ and dichloromethane. The organic fraction was dried with Na_2SO_4 then concentrated in vacuo. Flash column chromatography (100:5:1 dichloromethane:methanol:acetic acid) afforded 28 mg (33% from **2-7c**) of **3-4** as a white solid (yield varied upon additional replicates, 16-51%).

3-4: white solid; $R_f = 0.2$ (dichloromethane:methanol, 90:10); ^1H NMR (CDCl_3 300 MHz) δ 4.07 (dd, $J = 10, 2.9$ Hz, 1 H), 3.73 (ddd, $J = 9.1, 5.6, 3.1$ Hz, 1 H), 3.27 (ddd, $J = 10, 8.2, 3.2$ Hz, 1 H), 3.17 (ddd, $J = 13, 7.6, 5.3$, 1 H), 2.82-2.66 (m, 3 H), 2.51-2.30 (m, 2 H); ^{13}C NMR (CDCl_3 75 MHz) δ 212.8 (C), 176.2 (C), 62.2 (CH), 49.9 (CH_2), 48.1 (CH), 40.1 (CH_2), 39.3 (CH), 21.9 (CH_2).



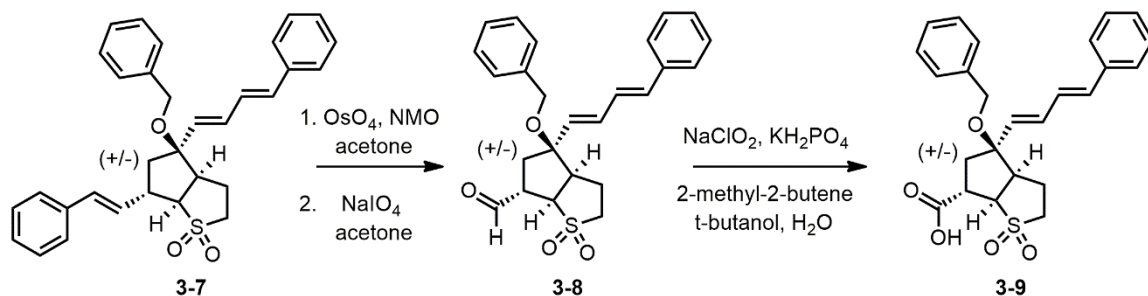
Compound **3-4** (30 mg, 0.14 mmol) was dissolved in d_6 -benzene (5 mL). Triethylamine (19 μL , 0.14 mmol) was added, followed by diphenylphosphoryl azide (30 μL , 0.14 mmol). The reaction mixture was stirred at 80 $^\circ\text{C}$ for 1.5 h. Benzyl alcohol (15 μL , 0.14 mmol) was added and the reaction mixture was stirred at 80 $^\circ\text{C}$ for 16 h. The reaction mixture was quenched with saturated aqueous NH_4Cl then partitioned between saturated aqueous NH_4Cl and dichloromethane. The organic fraction was dried with Na_2SO_4 and then concentrated in vacuo. Flash column chromatography (10:1 dichloromethane:ethyl acetate) afforded 18 mg (76% from **3-4**) of **3-6**.

3-6: light brown solid; $R_f = 0.4$ (dichloromethane:ethyl acetate; 10:1); IR (film) 1713, 1306, 1118 cm^{-1} ; ^1H NMR (CDCl_3 300 MHz) δ 7.74 (dd, $J = 5.6, 2.9$ Hz, 1 H), 6.51 (dd, $J = 5.8, 1.8$ Hz, 1 H), 4.28 (ddt, $J = 6.5, 3.3, 1.6$ Hz, 1 H), 3.23-3.16 (m, 1 H), 3.02-2.93 (m, 1 H), 2.82-2.57 (m, 1 H), 2.50-2.41 (m, 2 H); ^{13}C NMR (CDCl_3 75 MHz) δ 206.6 (C), 157.1 (CH), 137.9 (CH), 64.2 (CH), 46.4 (CH_2), 45.2 (CH), 22.6 (CH_2).



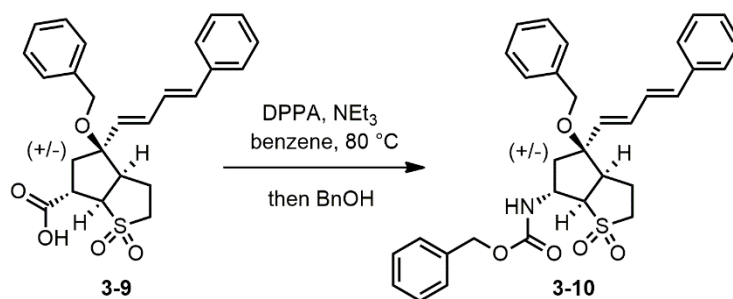
Compound **3-3** (crude, 1.31 g, 3.22 mmol) was dissolved in dimethylformamide (25 mL). The solution was cooled to 0 °C. NaH (516 mg, 60% in mineral oil, 12.9 mmol) was added in one portion. The solution was stirred at room temperature for 30 min. Benzyl bromide (570 μL , 4.83 mmol) was added. The solution was then stirred for 16 h. The reaction mixture was quenched with 10% HCl then extracted with dichloromethane. The organic layer was washed with 10% HCl, and the organic fraction was dried with Na_2SO_4 and concentrated in vacuo. Flash column chromatography (3:1 chloroform:hexanes) afforded 380 mg (23% from **2-7c**) of *O*-benzylated product **3-7**.

3-7: yellow solid; $R_f = 0.2$ (chloroform:hexanes, 3:1); ^1H NMR (CDCl_3 300 MHz) δ 7.52-7.12 (m, 15 H), 6.82 (dd, $J = 15, 10$ Hz, 1 H), 6.62 (d, $J = 16$ Hz, 1 H), 6.61 (d, $J = 16$ Hz, 1 H), 6.49 (dd, $J = 15, 10$ Hz, 1 H), 6.28 (dd, $J = 16, 7.2$ Hz, 1 H), 5.84 (d, $J = 16$ Hz, 1 H), 4.46 (d, $J = 11$ Hz, 1 H), 4.35 (d, $J = 11$ Hz, 1 H), 3.63-3.50 (m, 1 H), 3.41-3.30 (m, 2 H), 3.00 (dd, $J = 10, 8.0$ Hz, 1 H), 2.94 (dd, $J = 12, 7.2$ Hz, 1 H), 2.58 (dd, $J = 13, 6.0$ Hz, 1 H), 2.38 (dd, $J = 14, 7.6$ Hz, 1 H), 2.18-2.03 (m, 1 H), 1.85 (t, $J = 13$ Hz, 1 H).



Compound **3-7** (54 mg, 0.109 mmol) was dissolved in 10 mL acetone. *N*-Methylmorpholine *N*-oxide (20 mg, 0.171 mmol) was added, followed by OsO₄ (40 μL, 4% in water, 0.0063 mmol). The reaction mixture was stirred at 0 °C for 30 min, then warmed to room temperature and stirred for 1 h. The reaction mixture was partitioned between 0.5 M aqueous sodium thiosulfate and ethyl acetate then stirred 1 h at room temperature. The aqueous layer was washed with dichloromethane, and the combined organic extracts were dried with Na₂SO₄ and concentrated in vacuo. The crude triol was dissolved in 6 mL acetone and 1 mL water. NaIO₄ (28 mg, 0.131 mmol) was added, and the reaction mixture was stirred for 48 h. The reaction mixture was partitioned between saturated brine and dichloromethane. The combined organic extracts were dried with Na₂SO₄ and concentrated in vacuo. The crude product was applied to a short plug of silica and eluted with dichloromethane (to remove the *p*-anisaldehyde by-product) then 1:1 dichloromethane:ethyl acetate. Concentration of the latter fraction afforded 25 mg of **3-8**. Compound **3-8** (25 mg, 0.059 mmol) was dissolved in *t*-butanol (3 mL), tetrahydrofuran (3 mL) and water (1 mL). KH₂PO₄ (38 mg, 0.279 mmol) was added, followed by 2-methyl-2-butene (0.3 mL, 0.6 mmol). The reaction mixture was stirred for 5 min, then sodium chlorite (8.5 mg, 0.094 mmol) in water (0.5 mL) was added dropwise. The reaction mixture was stirred for a further 2 h at room temperature then partitioned between ethyl acetate and 10% aqueous HCl. The aqueous layer was washed with ethyl acetate, and the combined organic fractions were dried with Na₂SO₄ and concentrated in vacuo. Flash column chromatography (40:10:1 dichloromethane:ethyl acetate:acetic acid) afforded 18 mg (40% from **3-7**) of **3-9**.

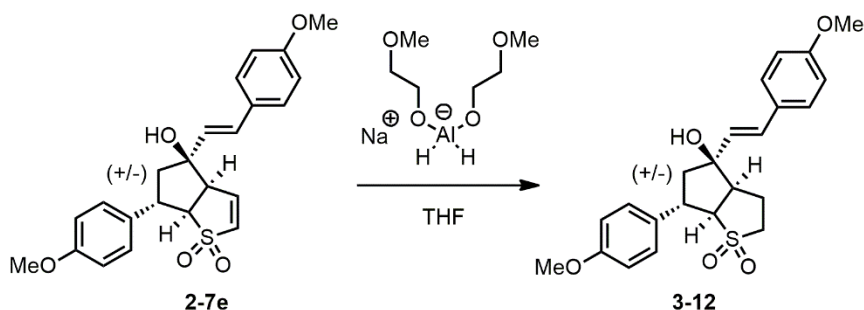
3-9: white solid; $R_f = 0.5$ (dichloromethane:ethyl acetate, 4:1); IR (film) 3300 (br), 1732, 1289, 1111 cm^{-1} ; ^1H NMR (CDCl_3 300 MHz) δ 7.44-7.24 (m, 10 H), 6.80 (dd, $J = 16, 10$ Hz, 1 H), 6.61 (d, $J = 16$ Hz, 1 H), 6.47 (dd, $J = 16, 10$ Hz, 1 H), 5.79 (d, $J = 16$ Hz, 1 H), 4.44 (d, $J = 11$ Hz, 1 H), 4.33 (d, $J = 11$ Hz, 1 H), 3.90 (d, $J = 10, 7.6$ Hz, 1 H), 3.65 (dt, $J = 12, 7.1, 7.1$ Hz, 1 H), 3.29 (dt, $J = 13, 7.6, 7.6$ Hz, 1 H), 3.05-2.92 (m, 2 H), 2.75 (dd, $J = 13, 6.4$ Hz, 1 H), 2.36 (dd, $J = 13, 7.2$ Hz, 1 H), 2.23-2.11 (m, 1 H), 2.07 (t, $J = 13$ Hz, 1 H); ^{13}C NMR (CDCl_3 75 MHz) 177.2 (C), 138.0 (C), 136.9 (C), 134.8 (CH), 133.0 (CH), 130.8 (CH), 129.0 (CH), 128.9 (CH), 128.4 (CH), 128.1 (CH), 127.9 (CH), 127.5 (CH), 126.8 (CH), 87.8 (C), 65.7 (CH_2), 64.4 (CH), 52.4 (CH), 52.1 (CH_2), 44.9 (CH), 37.3 (CH_2), 29.9 (CH_2).



Compound **3-9** (18 mg, 0.041 mmol) was dissolved in freshly distilled benzene (3 mL). Triethylamine (11 μL , 0.082 mmol) was added, followed by diphenylphosphoryl azide (18 μL , 0.082 mmol). The reaction mixture was stirred at 80 °C for 2 h. Benzyl alcohol (7 μL , 0.062 mmol) was added and the reaction mixture was stirred at 80 °C for 16 h. The reaction mixture was concentrated in vacuo. Flash column chromatography (10:1 dichloromethane:ethyl acetate) afforded 9 mg (40% from **3-9**) of **3-10**.

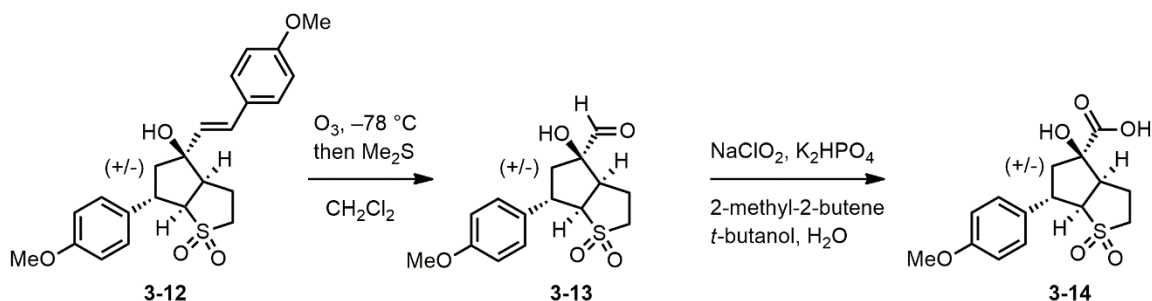
3-10: light brown solid; $R_f = 0.4$ (dichloromethane:ethyl acetate, 25:1); IR (film) 3351, 1716, 1290, 1109 cm^{-1} ; ^1H NMR (CDCl_3 300 MHz) δ 7.50-7.20 (m, 15 H), 6.78 (dd, $J = 15, 10$ Hz, 1 H), 6.59 (d, $J = 16$ Hz, 1 H), 6.44 (dd, $J = 16, 10$ Hz, 1 H), 5.78 (d, $J = 16$ Hz, 1 H), 5.27 (br s, 1 H), 5.11 (s, 2 H), 4.41 (d, $J = 11$ Hz, 1 H), 4.30 (d, $J = 11$ Hz, 1 H), 4.32-4.18 (m, 1 H), 3.89-3.73 (m, 1 H), 3.31 (dt, $J = 13, 7.9, 7.9$ Hz, 1 H), 3.17-3.02 (m, 1 H),

2.92 (dd, $J = 12, 7.5$ Hz, 1 H), 2.60-2.41 (m, 2H), 2.33 (dd, $J = 14, 7.9$ Hz, 1 H), 2.18-1.99 (m, 1 H); HRMS calcd for $C_{32}H_{33}NO_5$ (M+Na): 566.1972. Found: 566.1977.



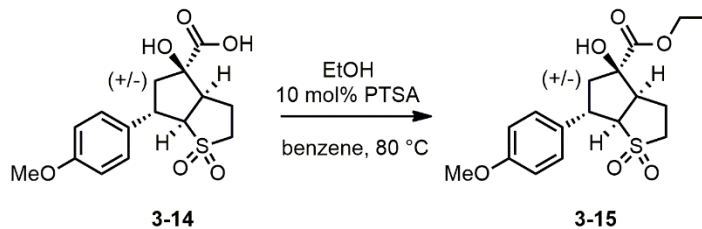
Compound **2-7e** (crude, 5.01 g, 12.5 mmol) was dissolved in tetrahydrofuran (200 mL). The solution was cooled to 0 °C and Red-Al (5.7 mL, 65% in toluene, 18.5 mmol) was added in one portion. The solution was stirred at 0 °C for 45 min. An aqueous 10% solution of Rochelle's salt was added in small portions over 5 minutes until gas evolution desisted. The reaction mixture was partitioned between ethyl acetate and water. The organic fraction was dried with Na_2SO_4 and concentrated in vacuo. Flash column chromatography (25:1 dichloromethane:ethyl acetate) afforded 1.33 g (26% from **2-1a**) of sulfone **3-12**.

3-12: yellow solid; $R_f = 0.3$ (dichloromethane:ethyl acetate, 25:1); IR (film) 3477 (br), 1250, 1108 cm^{-1} ; ^1H NMR (CDCl_3 300 MHz) δ 7.22 (d, $J = 8.8$ Hz, 2 H), 7.14 (d, $J = 8.8$ Hz, 2 H), 6.76 (d, $J = 8.8$ Hz, 2 H), 6.74 (d, $J = 8.8$ Hz, 2 H), 6.56 (d, $J = 16$ Hz, 1 H), 6.01 (d, $J = 16$ Hz, 1 H), 4.00-3.89 (m, 1 H), 3.70 (s, 3 H), 3.66 (s, 3 H), 3.44-3.30 (m, 2 H), 2.98-2.80 (m, 2 H), 2.20-1.87 (m, 4 H); ^{13}C NMR (CDCl_3 75 MHz) δ 159.5 (C), 158.6 (C), 133.4 (C), 129.6 (CH), 129.0 (CH), 128.9 (C), 128.5 (CH), 127.8 (CH), 114.2 (CH), 114.2 (CH), 82.4 (C), 70.0 (CH), 55.4 (CH_3), 55.4 (CH_3), 51.3 (CH_2), 51.0 (CH), 49.0 (CH_2), 44.8 (CH), 19.3 (CH_2); MS (ES+) m/z 437 (100); HRMS calcd for $C_{23}H_{26}O_5\text{S}$ (M+Na): 437.1399. Found: 437.1393.



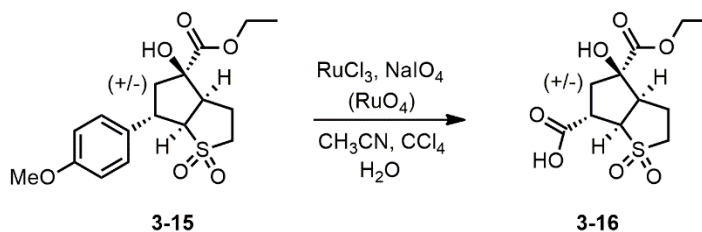
Compound **3-12** (1.33 g, 3.21 mmol) was dissolved in dichloromethane (80 mL). The solution was cooled to -78°C , then ozone was bubbled through until a light blue color persisted. The solution was purged with argon for 10 min, then dimethylsulfide (3.21 mL) was added at -78°C . The reaction mixture was warmed to room temperature and stirred for 16 h. The reaction mixture was concentrated in vacuo, and the crude aldehyde **3-13** was carried on to the next step with no further purification. Aldehyde **3-13** was dissolved in *t*-butanol (16 mL), tetrahydrofuran (8 mL) and water (8 mL). KH_2PO_4 (2.2 g, 16 mmol) was added, followed by 2-methyl-2-butene (1.7 mL, 16 mmol). The reaction mixture was stirred for 5 min, then sodium chlorite (725 mg, 8.03 mmol) in water (2 mL) was added dropwise. The reaction mixture was stirred for a further 60 min at room temperature then partitioned between ethyl acetate and 10% aqueous HCl. The aqueous layer was washed with ethyl acetate, and the combined organic fractions were dried with Na_2SO_4 and concentrated in vacuo. Flash column chromatography (100:1:1 to 100:5:2 dichloromethane:methanol:acetic acid gradient) afforded 752 mg (72% from **3-12**) of **3-14**.

3-14: white solid; $R_f = 0.2$ (dichloromethane:ethyl acetate, 3:2); IR (film) 3460 (br), 1732, 1251, 1113 cm^{-1} ; ^1H NMR ($\text{CD}_3\text{C}(\text{O})\text{CD}_3$ 300 MHz) δ 7.35 (d, $J = 8.6$ Hz, 2 H), 6.90 (d, $J = 8.6$ Hz, 2 H), 4.02-3.89 (m, 1 H), 3.78 (s, 3 H), 3.71 (dd, $J = 10, 9.2$ Hz, 1 H), 3.55 (dd, $J = 10, 9.2$ Hz, 1 H), 3.35 (td, $J = 13, 7.6$ Hz, 1 H), 3.00-2.91 (m, 1 H), 2.45 (t, $J = 13$ Hz, 1 H), 2.34-2.22 (m, 2 H), 2.19-2.08 (m, 1 H); ^{13}C NMR ($\text{CD}_3\text{C}(\text{O})\text{CD}_3$ 75 MHz) δ 175.4 (C), 159.5 (C), 134.0 (C), 129.6 (CH), 114.8 (CH), 82.9 (C), 69.9 (CH), 55.4 (CH_3), 51.6 (CH_2), 50.7 (CH), 47.4 (CH_2), 46.6 (CH), 20.9 (CH_2); MS (ES+) m/z 349 (100); HRMS calcd for $\text{C}_{15}\text{H}_{18}\text{O}_6\text{S}$ (M+Na): 349.0722. Found: 349.0717.



Compound **3-14** (752 mg, 0.576 mmol) was dissolved in benzene (60 mL) and ethanol (5 mL). *p*-tolylsulfonic acid (4 mg, 0.023 mmol) was added and the solution was heated at 80 °C using a Dean-Stark apparatus for 16 h. The reaction mixture was cooled to room temperature, then partitioned between water and ethyl acetate. The organic fraction was dried with Na₂SO₄ and concentrated in vacuo to provide 773 mg of crude ethyl ester **3-15**. The crude product was carried to the next step with no further purification.

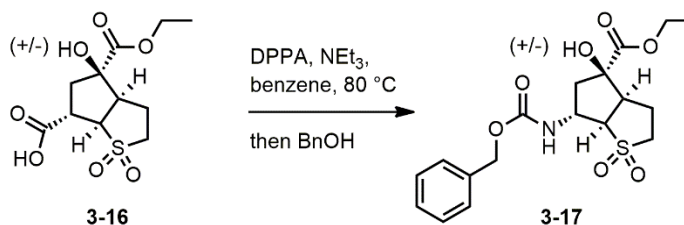
3-15: white solid; IR (film) 3465 (br), 1732, 1252, 1113 cm⁻¹; ¹H NMR (CDCl₃ 300 MHz) δ 7.28 (d, *J* = 8.6 Hz, 2 H), 6.88 (d, *J* = 8.6 Hz, 2 H), 4.32 (m, 2 H), 3.99 (ddd, *J* = 13, 10, 7.3 Hz, 1 H), 3.80 (s, 3 H), 3.67-3.51 (m, 2 H), 3.50-3.34 (m, 1 H), 3.02-2.92 (m, 1 H), 2.36 (t, *J* = 13 Hz, 1 H), 2.24 (dd, *J* = 13, 7.2 Hz, 1 H), 2.19-2.06 (m, 2 H), 1.34 (t, *J* = 7.2 Hz, 3 H); ¹³C NMR (CDCl₃ 75 MHz) δ 174.3 (C), 158.8 (C), 132.3 (C), 128.6 (CH), 114.3 (CH), 82.4 (C), 69.1 (CH), 63.1 (CH₂), 55.4 (CH₃), 50.6 (CH₂), 49.6 (CH), 46.8 (CH₂), 46.0 (CH), 20.5 (CH₂), 14.3 (CH₃); MS (ES⁺) *m/z* 377 (100); HRMS calcd for C₁₇H₂₂O₆S (M+Na): 377.1035. Found: 377.1032.



Compound **3-15** (crude, 640 mg, 1.81 mmol) was dissolved in carbon tetrachloride (5 mL), acetonitrile (5 mL) and water (15 mL). NaHCO₃ (152 mg, 1.81 mmol) was added, followed by NaIO₄ (5.81 g, 27.2 mmol). RuCl₃ (18 mg, 0.091 mmol) was added and the reaction mixture was stirred 16 h. Due to the volatility of RuO₄ additional aliquots of RuCl₃ (18 mg,

0.019 mmol) were added as necessary. The reaction mixture was partitioned between 10% aqueous HCl and ethyl acetate. The organic fraction was dried with Na₂SO₄ then concentrated in vacuo. The crude solid was dissolved in chloroform, filtered through cotton, and then concentrated in vacuo to provide 373 mg of crude acid **3-16**. The crude product was carried to the next step with no further purification.

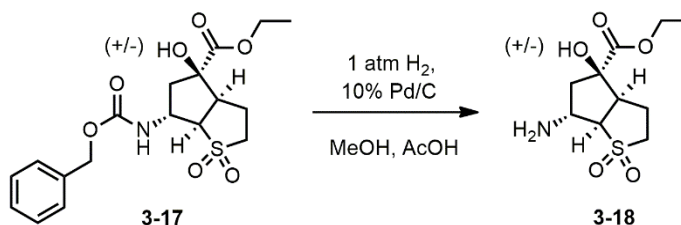
3-16: white solid; IR (film) 3470 (br), 1734, 1265, 1114 cm⁻¹; ¹H NMR (CDCl₃ 300 MHz) δ 4.29 (m, 2 H), 3.99-3.90 (m, 1 H) 3.73 (td, *J* = 10, 8.4 Hz, 1 H), 3.50-3.41 (m, 1 H), 3.41-3.38 (m, 1 H), 3.07-2.96 (m, 1 H), 2.42-2.32 (m, 2 H), 2.25-2.06 (m, 2 H), 1.32 (t, *J* = 7.3 Hz, 3 H); ¹³C NMR (CDCl₃ 75 MHz) δ 177.1 (C), 173.6 (C), 82.4 (C), 63.9 (CH), 63.3 (CH₂), 50.8 (CH₂), 49.1 (CH), 45.6 (CH), 42.6 (CH₂), 20.5 (CH₂), 14.3 (CH₃); MS (ES+) *m/z* 315 (100); HRMS calcd for C₁₁H₁₆O₇S (M+Na): 315.0515. Found: 315.0516.



Compound **3-16** (crude, 373 mg, 1.28 mmol) was dissolved in benzene (30 mL). Triethylamine (271 μL, 1.92 mmol) was added, followed by diphenylphosphoryl azide (277 μL, 1.28 mmol). Benzyl alcohol (200 μL, 1.92 mmol) was added and the reaction mixture was stirred at 80 °C for 16 h. The reaction mixture was quenched with saturated aqueous NH₄Cl then partitioned between saturated aqueous NH₄Cl and ethyl acetate. The organic fraction was dried with Na₂SO₄ and then concentrated in vacuo. Flash column chromatography (20:1 to 2:1 dichloromethane:ethyl acetate gradient) afforded 171 mg (23% from **3-14**) of **3-17**.

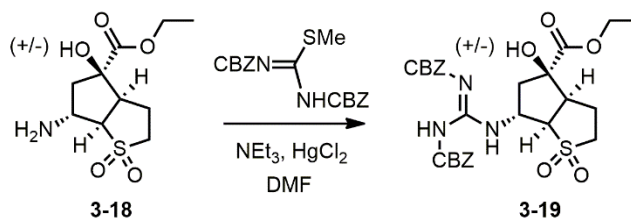
3-17: light brown solid; R_f = 0.4 (dichloromethane:ethyl acetate, 5:1); IR (film) 3349 (br), 1722, 1265, 1113 cm⁻¹; ¹H NMR (CD₃C(O)CD₃ 300 MHz) δ 7.43-7.23 (m, 5 H), 6.83 (s, 1 H), 5.08 (s, 2 H), 4.76-4.63 (m, 1 H), 4.21 (q, *J* = 7.3 Hz, 2 H), 3.69-3.48 (m, 2 H) 3.26 (td, *J* = 10, 8.4 Hz, 1 H), 2.98-2.88 (m, 1 H), 2.80 (d, *J* = 9.2 Hz, 2 H), 2.45-2.13 (m, 3 H),

1.26 (t, $J = 13$ Hz, 3 H); ^{13}C NMR (CD_3COD 75 MHz) δ 174.4 (C), 157.8 (C), 138.1 (C), 129.5 (CH), 129.2 (CH), 129.0 (CH), 82.3 (C), 67.6 (CH), 67.5 (CH_2), 67.3 (CH), 62.9 (CH_2), 55.0 (CH), 52.0 (CH_2), 45.3 (CH_2), 21.3 (CH_2), 14.4 (CH_3); MS (ES+) m/z 420 (100); HRMS calcd for $\text{C}_{18}\text{H}_{23}\text{NO}_7\text{S}$ ($\text{M}+\text{Na}$): 420.1093. Found: 420.1092.



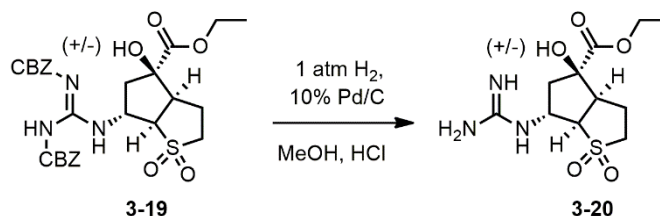
Compound **8** (151 mg, 0.380 mmol) was dissolved in methanol (8 mL). Acetic acid (~ 100 μL) was added, followed by Pd/C 10% (~ 10 mg). The reaction mixture was stirred inside a Parr reactor pressurized to 300 PSI H_2 and was stirred for 16 h. The reaction mixture was filtered through cotton, diluted with cyclohexane (10 mL), and then concentrated in vacuo to provide 111 mg of the acetic acid salt of amine **3-18**. The crude product was carried to the next step with no further purification.

3-18: white solid; IR (film) 3261 (br), 1739, 1262, 1114 cm^{-1} ; ^1H NMR ($\text{CD}_3\text{C}(\text{O})\text{CD}_3$ 300 MHz) δ 4.63 (dt, $J = 11, 6.8$ Hz, 1 H), 4.20 (m, 2 H), 3.66-3.47 (m, 2 H), 3.31-3.17 (m, 1 H), 2.97-2.85 (m, 1 H), 2.33-2.07 (m, 4 H), 1.26 (t, $J = 7.4$ Hz, 3 H); ^{13}C NMR ($\text{CD}_3\text{C}(\text{O})\text{CD}_3$ 75 MHz) δ 173.7 (C), 83.9 (C), 71.0 (CH), 64.1 (CH), 63.4 (CH_2), 52.7 (CH_2), 50.6 (CH), 46.9 (CH_2), 22.3 (CH_2), 15.5 (CH_3); MS (ES+) m/z 264 (100); HRMS calcd for $\text{C}_{10}\text{H}_{17}\text{NO}_5\text{S}$ ($\text{M}+\text{H}$): 264.0906. Found: 264.0901.



Compound **3-18** (crude, 54 mg, 0.167 mmol) was dissolved in DMF (5 mL). Triethylamine (120 μ L, 0.836 mmol) was added, followed by HgCl₂ (45 mg, 0.167 mmol). 1,3-bis(benzyloxycarbonyl)-2-methylisothioureia (**9**, 60 mg, 0.167 mmol) was added and the reaction mixture was stirred 16 h. The reaction mixture was diluted ethyl acetate, filtered through Celite, and then concentrated in vacuo. Flash column chromatography (25:1 to 10:1 dichloromethane:ethyl acetate gradient) afforded 55 mg (53% from **3-17**) of **3-19**.

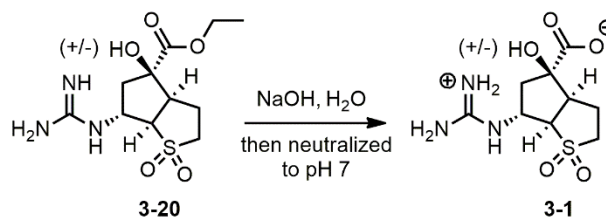
3-19: white solid; R_f = 0.5 (hexanes:ethyl acetate, 1:1); IR (film) 3477 (br), 3288 (br), 1771, 1732, 1622, 1271, 1114 cm^{-1} ; ¹H NMR (CD₃C(O)CD₃ 300 MHz) δ 11.89 (s, 1 H), 8.70 (d, J = 8.0 Hz, 1 H), 7.49-7.29 (m, 10 H), 5.26 (s, 2 H), 5.12 (s, 2 H), 4.21 (q, J = 7.1 Hz, 2 H), 3.88 (dd, J = 10, 8.9 Hz, 1 H), 3.66-3.57 (m, 1 H), 3.35-3.22 (m, 1 H), 3.01-2.90 (m, 1 H), 2.45-2.37 (m, 2 H), 2.28-2.06 (m, 3 H), 1.24 (t, J = 7.1 Hz, 3 H); ¹³C NMR (CD₃C(O)CD₃ 75 MHz) δ 173.7 (C), 164.5 (C), 156.5 (C), 154.2 (C), 138.1 (C), 136.3 (C), 129.5 (CH), 129.4 (CH), 129.4 (CH), 129.2 (CH), 129.1 (CH), 128.7 (CH), 82.3 (C), 68.9 (CH₂), 67.8 (CH₂), 67.3 (CH), 62.4 (CH₂), 54.5 (CH), 51.7 (CH₂), 49.1 (CH), 44.9 (CH₂), 21.2 (CH₂), 14.4 (CH₃); MS (ES⁺) m/z 596 (100); HRMS calcd for C₂₇H₃₁N₃O₉S (M+Na): 596.1678. Found: 596.1674.



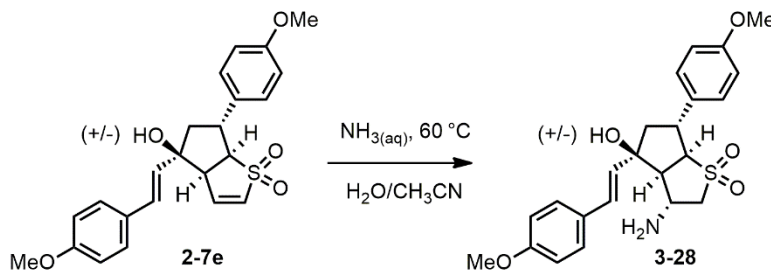
Compound **3-19** (54 mg, 0.094 mmol) was dissolved in methanol (5 mL). Acetic acid (~100 μ L) and 10% aqueous HCl (~50 μ L) was added, followed by Pd/C 10% (~10 mg). The reaction mixture was stirred inside a Parr reactor pressurized to 300 PSI H₂ and was stirred for 16 h. The reaction mixture was filtered through cotton, diluted with cyclohexane (10 mL) then concentrated in vacuo. Prior to biological testing compound **3-20** was purified through recrystallization from methanol and dichloromethane to provide 29 mg (90% from **3-19**) of the hydrochloride salt of guanidine **3-20**. A single crystal suitable for X-ray

crystallographic analysis was obtained from slow evaporation of **3-20** dissolved in a mixture of methanol and ethyl acetate.

3-20: white solid; $R_f = 0.1$ (dichloromethane:methanol, 90:10); Mp: decomposed at 218 °C; IR (film) 3350 (br), 1732, 1667, 1260, 1108 cm^{-1} ; ^1H NMR (CD_3OD 300 MHz) δ 4.61-4.51 (m, 1 H), 4.25 (m, 2 H), 3.59-3.51 (m, 2 H), 3.38 (td, $J = 13, 7.6$ Hz, 1 H), 3.13-3.02 (m, 1 H), 2.26-2.07 (m, 4 H), 1.30 (t, $J = 7.1$ Hz, 3 H); ^{13}C NMR (CD_3OD 75 MHz) δ 173.7 (C), 158.3 (C), 82.0 (C), 69.3 (CH), 63.2 (CH_2), 56.0 (CH), 52.1 (CH_2), 50.1 (CH), 45.3 (CH_2), 21.7 (CH_2), 14.4 (CH_3); MS (ES+) m/z 306(100); HRMS calcd for $\text{C}_{11}\text{H}_{19}\text{N}_3\text{O}_5\text{S}$ (M+H): 306.1124. Found: 306.1117.



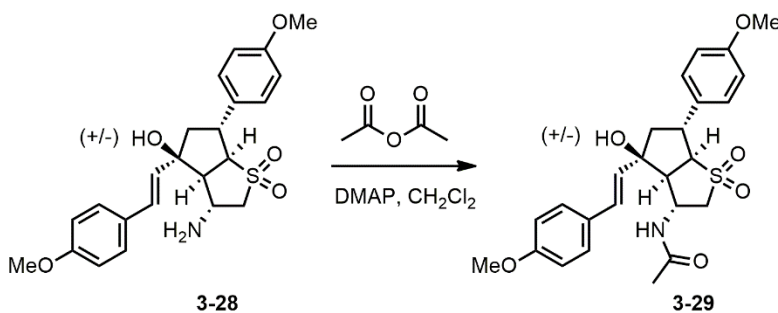
Compound **3-20** (HCl salt, 22.6 mg, 0.0661 mmol) was dissolved in 750 μL of 10% NaOH in H_2O and 100 μL DMSO. The reaction mixture was stirred for 16 h, then neutralized with 12 M HCl to provide a standard solution (61.9 mM) of sulfone **10**. Hydrolysis of the ester function was confirmed through MS (ES+) m/z 276 (100).



Compound **2-7e** (crude, 10.3 g, 25.0 mmol) was dissolved in 50 mL acetonitrile and 50 mL of aqueous ammonia (28% w/w). The reaction mixture was heated at 60 °C for 3 days in a sealed vessel. The reaction mixture was partitioned between ethyl acetate and water. The

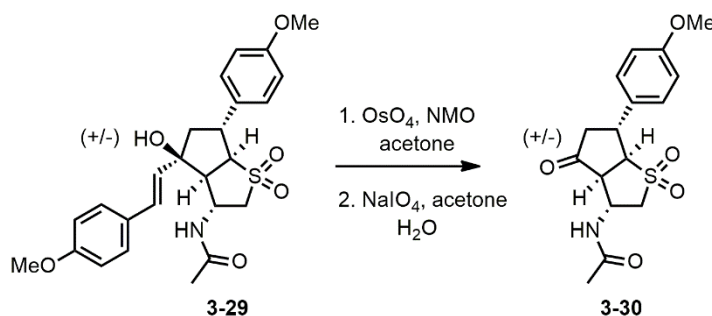
aqueous layer was washed with ethyl acetate, and the combined organic extracts were dried with Na_2SO_4 and concentrated in vacuo to provide 10.5 g of compound **3-28**. The crude product was carried to the next step with no further purification.

3-28: yellow solid; IR (film) 3470 (br), 3348 (br) 1513, 1250, 1112 cm^{-1} ; ^1H NMR (CDCl_3 , 300 MHz) δ 7.34 (d, $J = 8.6$ Hz, 2 H), 7.25 (d, $J = 8.6$ Hz, 2 H), 6.87 (d, $J = 8.6$ Hz, 2 H), 6.87 (d, $J = 8.7$ Hz, 2 H), 6.70 (d, $J = 16$ Hz, 1 H), 6.21 (d, $J = 16$ Hz), 4.15-4.03 (m, 1 H), 3.81 (s, 3 H), 3.79 (s, 3 H), 3.80-3.68 (m, 3 H), 3.04-2.95 (m, 2 H), 2.25-2.17 (m, 2 H); ^{13}C NMR (CDCl_3 , 75 MHz) δ 159.7 (C), 158.7 (C), 133.2 (C), 129.6 (CH), 129.2 (CH), 128.8 (C), 128.5 (C), 128.0 (CH), 114.4 (CH), 114.3 (CH), 81.4 (C), 68.8 (CH), 61.7 (CH), 59.8 (CH_2), 55.4 (CH_3), 55.4 (CH_3), 49.2 (CH_2), 46.3 (CH), 44.6 (CH); MS (ES+) m/z 452 (100); HRMS calcd for $\text{C}_{23}\text{H}_{27}\text{NO}_5\text{S}$ ($\text{M}+\text{Na}$): 452.1502. Found: 452.1496.



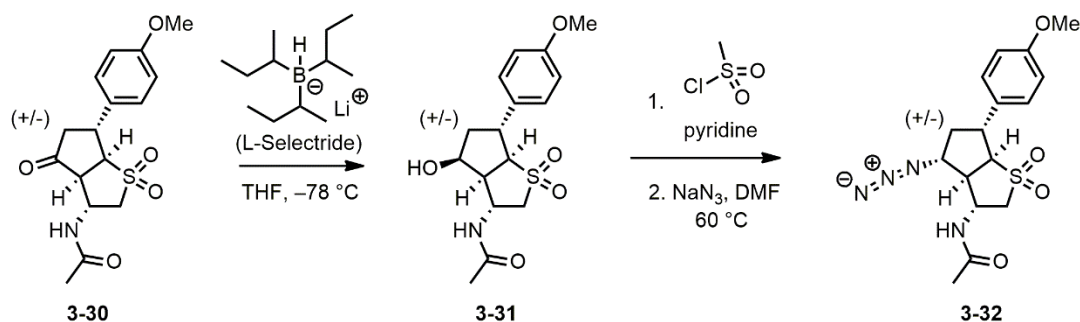
Compound **3-28** (crude, 10.5 g, 24.5 mmol) was dissolved in 200 mL dichloromethane. DMAP (599 mg, 4.9 mmol) followed by acetic anhydride (6.95 mL, 73.5 mmol) was added. The reaction mixture was stirred at room temperature for 16 h. The reaction mixture was partitioned between 10% aqueous NaHCO_3 and dichloromethane. The aqueous layer was washed with dichloromethane, and the combined organic extracts were dried with Na_2SO_4 and concentrated in vacuo. Flash column chromatography (4:1 to 1:1 dichloromethane:ethyl acetate gradient) afforded 4.6 g (40% from **2-1a**) of **3-29**. A single crystal suitable for X-ray crystallographic analysis was obtained from slow evaporation of **3-29** dissolved in a mixture of dichloromethane and ethyl acetate.

3-29: yellow solid; $R_f = 0.3$ (dichloromethane:ethyl acetate, 4:1); IR (film) 3360 (br), 1658, 1250, 1113 cm^{-1} ; ^1H NMR (CDCl_3 300 MHz) δ 7.36 (d, $J = 8.6$ Hz, 2 H), 7.26 (d, $J = 8.6$ Hz, 2 H), 6.88 (d, $J = 8.6$ Hz, 2 H), 6.86 (d, $J = 8.6$ Hz, 2 H), 6.73 (d, $J = 16$ Hz, 1 H), 6.44 (d, $J = 8.7$ Hz, 1 H), 6.36 (d, $J = 16$ Hz, 1 H), 4.91 (dd, $J = 8.5, 7.0$ Hz, 1 H), 4.10-3.99 (m, 1 H), 3.81 (s, 3 H), 3.80 (s, 3 H), 3.79-3.74 (m, 1 H), 3.67-3.58 (m, 1 H), 3.13-3.06 (m, 1 H), 2.97-2.89 (m, 1 H), 2.30-2.15 (m, 2 H) 1.95 (s, 3 H); ^{13}C NMR (CDCl_3 75 MHz) δ 169.9 (C), 159.4 (C), 158.5 (C), 132.7 (C), 129.0 (C), 129.0 (CH), 128.9 (CH), 128.3 (CH), 127.8 (CH), 114.1 (CH), 114.1 (CH), 80.6 (C), 69.5 (CH), 58.9 (CH), 56.1 (CH_2), 55.2 (CH_3), 55.2 (CH_3), 48.1 (CH_2), 45.5 (CH), 44.0 (CH), 23.0 (CH_3); MS (ES+) m/z 494 (100); HRMS calcd for $\text{C}_{25}\text{H}_{29}\text{NO}_6\text{S}$ ($\text{M}+\text{Na}$): 494.1608. Found: 494.1598.



Compound **3-29** (5.90 g, 12.5 mmol) was dissolved in 200 mL acetone. *N*-Methylmorpholine *N*-oxide (2.92 g, 25 mmol) was added, followed by OsO_4 (4.0 mL, 4% in water, 0.625 mmol). The reaction mixture was stirred at 0 °C for 30 min, then warmed to room temperature and stirred for 1 h. The reaction mixture was partitioned between 0.5 M aqueous sodium thiosulfate and ethyl acetate. The aqueous layer was washed with ethyl acetate, and the combined organic extracts were dried with Na_2SO_4 and concentrated in vacuo. The crude triol was dissolved in 160 mL acetone and 40 mL water. NaIO_4 (10.7 g, 50 mmol) was added, and the reaction mixture was stirred for 16 h. The reaction mixture was partitioned between 0.5 M aqueous sodium thiosulfate and ethyl acetate. The aqueous layer was washed with ethyl acetate, and the combined organic extracts were dried with Na_2SO_4 and concentrated in vacuo. Flash column chromatography (20:1 to 5:1 dichloromethane:tetrahydrofuran gradient) afforded 2.2 g (52% from **3-29**) of **3-30**.

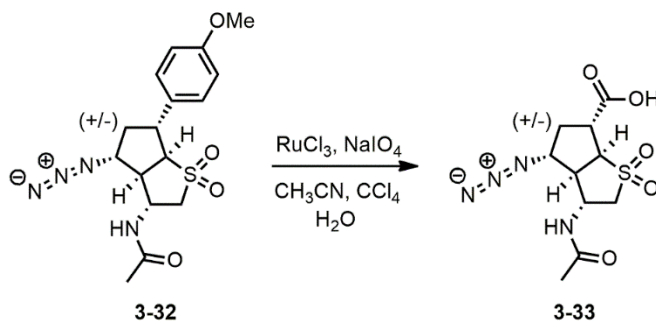
3-30: white solid; $R_f = 0.4$ (dichloromethane:ethyl acetate, 1:1); IR (film) 3335 (br), 1751, 1652, 1255, 1114 cm^{-1} ; ^1H NMR ($\text{CD}_3\text{S(O)CD}_3$ 300 MHz) δ 8.39 (d, $J = 7.2$ Hz, 1 H), 7.32 (d, $J = 8.6$ Hz, 2 H), 6.93 (d, $J = 8.6$ Hz, 2 H), 4.46 (pentet, $J = 6.3$ Hz, 1 H), 4.10 (dd, $J = 9.8, 8.1$ Hz, 1 H), 3.93-3.81 (m, 1 H), 3.74 (s, 3 H), 3.60 (dd, $J = 13, 6.9$ Hz, 1 H), 3.51 (dd, $J = 10, 6.0$ Hz, 1 H), 3.13 (dd, $J = 13, 7.1$ Hz, 1 H), 2.79 (dd, $J = 18, 8.6$ Hz, 1 H), 2.68 (dd, $J = 18, 10$ Hz, 1 H), 1.95 (s, 3 H); ^{13}C NMR ($\text{CD}_3\text{S(O)CD}_3$ 75 MHz) δ 211.3 (C), 169.2 (C), 158.3 (C), 133.6 (C), 128.4 (CH), 114.1 (CH), 67.3 (CH), 55.1 (CH_2), 55.1 (CH_3), 54.2 (CH), 46.0 (CH_2), 45.1 (CH), 33.8 (CH), 22.5 (CH_3); MS (ES+) m/z 360 (100); HRMS calcd for $\text{C}_{16}\text{H}_{19}\text{NO}_5\text{S}$ (M+Na): 360.0876. Found: 360.0870.



Compound **3-20** (2.20 g, 6.53 mmol) was dissolved in 80 mL tetrahydrofuran. The solution was cooled to -78 °C, then L-Selectride (9.80 mL, 1 M in tetrahydrofuran, 9.80 mmol) was added. The solution was stirred at -78 °C for 1 h. The reaction mixture was quenched with methanol at -78 °C, then warmed to room temperature and partitioned between ethyl acetate and 10% NaHCO_3 . The aqueous layer was washed with ethyl acetate, and the combined organic extracts were dried with Na_2SO_4 and concentrated in vacuo to provide 2.21 g of a crude **3-21** as a white solid. Compound **3-21** (crude, 2.21 g, 6.53 mmol) was dissolved in 40 mL pyridine. The solution was cooled to 0 °C, then methanesulfonyl chloride (1.02 mL, 13.06 mmol) was added. The solution was stirred at room temperature for 16 h. The reaction mixture was concentrated in vacuo, then partitioned between dichloromethane and water. The aqueous layer was washed with ethyl acetate, and the combined organic extracts were dried with Na_2SO_4 and concentrated in vacuo. The crude mesylate (2.72 g, 6.53 mmol) was dissolved in 25 mL dimethylformamide. NaN_3 (1.27 g, 19.6 mmol) was added. The reaction mixture was heated at 60 °C for 16 h. The reaction

mixture was partitioned between dichloromethane and water. The aqueous layer was washed with dichloromethane, and the combined organic extracts were dried with Na_2SO_4 and concentrated in vacuo to provide 2.35 g of crude azide **3-32**. The crude product was typically carried to the next step with no further purification. Flash column chromatography of a 776 mg portion of crude azide **3-32** (10:1 to 1:1 dichloromethane:tetrahydrofuran gradient) afforded 383 mg (48% from **3-30**) of **3-32**.

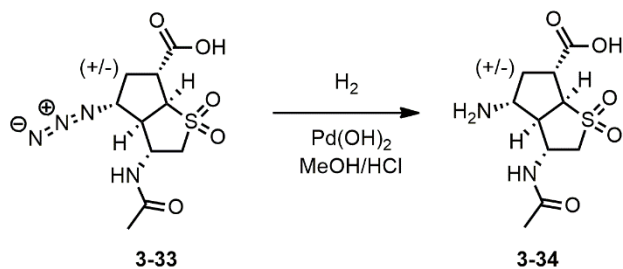
3-32: light yellow solid; $R_f = 0.5$ (dichloromethane:tetrahydrofuran, 3:1); IR (film) 3354 (br), 2103, 1661, 1252, 1119 cm^{-1} ; ^1H NMR (CD_3OD 300 MHz) δ 7.27 (d, $J = 8.7$ Hz, 2 H), 6.89 (d, $J = 8.7$ Hz, 2 H), 4.53 (dt, $J = 8.0, 6.3$ Hz, 1 H), 4.17-4.02 (m, 1 H), 3.89 (dd, $J = 9.8, 8.1$ Hz, 1 H), 3.78 (s, 3 H), 3.79-3.67 (m, 2 H), 3.55 (dd, $J = 13, 6.0$ Hz, 1 H), 3.24 (dd, $J = 13, 8.1$ Hz, 1 H), 3.04-2.94 (m, 1 H), 2.59 (dt, $J = 12, 6.3$ Hz, 1 H), 2.00 (s, 3 H); ^{13}C NMR (CD_3OD 75 MHz) δ 173.2 (C), 160.3 (C), 133.8 (C), 129.4 (CH), 115.2 (CH), 70.5 (CH), 66.3 (CH), 56.5 (CH_2), 56.1 (CH), 55.7 (CH_3), 49.6 (CH), 44.0 (CH), 42.4 (CH_2), 22.5 (CH_3); MS (ES+) m/z 387 (100); HRMS calcd for $\text{C}_{16}\text{H}_{20}\text{N}_4\text{O}_4\text{S}$ (M+Na): 387.1098. Found: 387.1098.



Compound **3-32** (crude, 1.02 g, 2.80 mmol) was dissolved in carbon tetrachloride (5 mL), acetonitrile (5 mL) and water (15 mL). NaIO_4 (7.80 g, 36.4 mmol) was added, followed by RuCl_3 (29 mg, 0.140 mmol). The reaction mixture was stirred 16 h. Due to the volatility of RuO_4 additional aliquots of RuCl_3 (29 mg, 0.140 mmol) were added as necessary. The reaction mixture was partitioned between ethyl acetate and water. The aqueous layer was washed with ethyl acetate, and the combined organic fractions were dried with Na_2SO_4

then concentrated in vacuo. The crude solid was dissolved in ethyl acetate, filtered through cotton, and then concentrated in vacuo to provide 610 mg of crude acid **3-33** as a white solid. Flash column chromatography (100:2:1 to 100:5:1 dichloromethane:methanol:acetic acid gradient) afforded 312 mg (35% from **3-30**) of **3-33**. A single crystal suitable for X-ray crystallographic analysis was obtained from slow evaporation of **3-33** dissolved in a mixture of methanol and ethyl acetate.

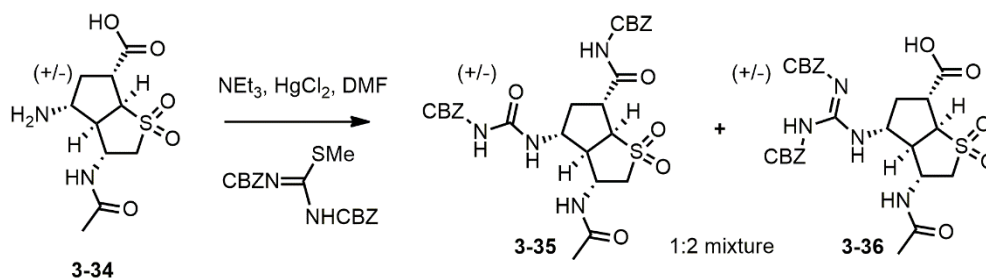
3-33: white solid; IR (film) 3352 (br), 2105, 1731, 1654, 1253, 1121 cm^{-1} ; ^1H NMR ($\text{CD}_3\text{S(O)CD}_3$ 300 MHz) δ 8.34 (d, $J = 7.3$ Hz, 1 H), 4.20-4.05 (m, 2 H), 3.60-3.47 (m, 1 H), 3.41-3.25 (m, 2 H), 3.15 (dd, $J = 13, 9.3$ Hz, 1 H), 2.91-2.80 (m, 1 H), 2.39-2.26 (m, 1 H), 2.16-2.03 (m, 1 H), 1.85 (s, 3 H); ^{13}C NMR ($\text{CD}_3\text{S(O)CD}_3$ 75 MHz) δ 173.0 (C), 170.4 (C), 64.0 (CH), 63.4 (CH), 54.5 (CH_2), 53.9 (CH), 47.0 (CH), 42.5 (CH), 34.6 (CH_2), 22.6 (CH_3); MS (ES+) m/z 325 (100); HRMS calcd for $\text{C}_{10}\text{H}_{14}\text{N}_4\text{O}_5\text{S}$ (M+Na): 325.0577. Found: 325.0579.



Compound **3-33** (236 mg, 0.779 mmol) was dissolved in methanol (5 mL). $\text{Pd(OH)}_2/\text{C}$ 10% (~ 50 mg) and 10% aqueous HCl (~ 50 μL) were added, then H_2 was bubbled through the solution for 5 min. The reaction mixture was stirred under 1 atm H_2 for 16 h. The reaction mixture was filtered through cotton, then concentrated in vacuo to provide 225 mg of crude **3-34**. The crude product was carried to the next step with no further purification. Prior to biological testing, flash column chromatography of a 65 mg portion of crude **3-34** (100:2:1 to 60:40:20 dichloromethane:methanol:acetic acid gradient) afforded 23.0 mg (35% from **3-33**) of the hydrochloride salt of amine **3-34**. Compound **3-34** (HCl salt, 23.0 mg, 0.736

mmol) was dissolved in 500 μL of DMSO to provide a standard solution (147 mM) of amine **3-34**.

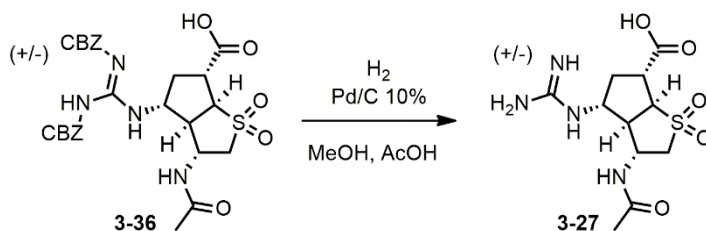
3-34: white solid; $R_f = 0.1$ (dichloromethane:methanol:acetic acid 80:20:1); IR (film) 3351 (br), 3248 (br), 1727, 1653, 1299, 1122 cm^{-1} ; ^1H NMR (D_2O 300 MHz) δ 4.46 (ddd, $J = 7.3, 6.5, 6.5$ Hz, 1 H), 4.30 (dd, $J = 10, 6.6$ Hz, 1 H), 3.83 (ddd, $J = 7.2, 6.7, 6.7$ Hz, 1 H), 3.69 (dd, $J = 14, 6.5$ Hz, 1 H), 3.54-3.45 (m, 2 H), 3.25 (ddd, $J = 10, 6.7, 6.5$ Hz, 1 H), 2.64 (ddd, $J = 13, 7.5, 7.5$ Hz, 1 H), 2.15 (ddd, $J = 13, 8.1, 8.1$ Hz, 1 H), 2.04 (s, 3 H); ^{13}C NMR (D_2O 75 MHz) δ 175.0 (C), 172.2 (C), 63.0 (CH), 52.6 (CH), 51.1 (CH_2), 50.6 (CH), 45.6 (CH), 42.6 (CH), 32.2 (CH_2), 19.6 (CH_3); MS (ES+) m/z 299 (100); HRMS calcd for $\text{C}_{10}\text{H}_{16}\text{N}_2\text{O}_5\text{S}$ (M+Na): 299.0672. Found: 299.0678.



Compound **3-34** (crude, 270 mg, 0.804 mmol) was dissolved in dimethylformamide (10 mL). Triethylamine (560 μL , 4.02 mmol) was added, followed by HgCl_2 (261 mg, 0.964 mmol). 1,3-bis(benzyloxycarbonyl)-2-methylisothiurea (345 mg, 0.964 mmol) was added and the reaction mixture was stirred 16 h. The reaction mixture was concentrated in vacuo. Flash column chromatography (100:1 to 100:10:1 dichloromethane:methanol:acetic acid gradient) afforded 95 mg (impure, 17% from **3-33**) of **3-35** and 180 mg (32% from **3-33**) of **3-36**.

3-36: white solid, $R_f = 0.1$ (dichloromethane:ethyl acetate, 1:1); IR (film) 3313 (br), 1771, 1714, 1651, 1302, 1116 cm^{-1} ; ^1H NMR (CD_3COD 500 MHz) δ 7.43-7.29 (m, 10 H), 5.20 (s, 2 H), 5.17 (s, 1 H), 4.42 (dd, $J = 11, 6.0$ Hz, 1 H), 4.31 (dd, $J = 10, 6.9$ Hz, 1 H), 4.23-

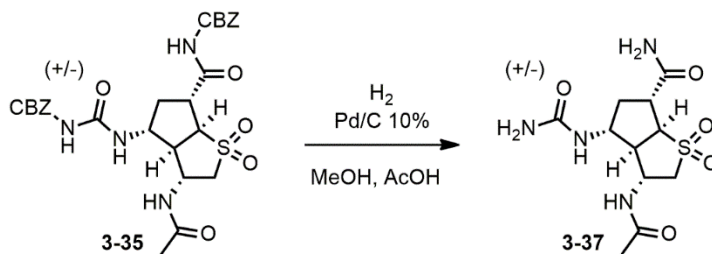
4.17 (m, 1 H), 3.73-3.65 (m, 1 H), 3.51 (dd, $J = 13, 6.5$ Hz, 1 H), 3.22 (dd, $J = 13, 6.0$ Hz, 1 H), 3.04-2.97 (m, 1 H), 2.63-2.54 (m, 1 H), 1.94 (s, 3 H), 1.93-1.89 (m, 1 H); ^{13}C NMR (CD_3COD 125 MHz) δ 173.7 (C), 173.3 (C), 155.9 (C), 155.1 (C), 153.1 (C), 137.0 (C), 136.9 (C), 129.6 (CH), 129.6 (CH), 129.5 (CH), 129.4 (CH), 129.4 (CH), 129.3 (CH), 68.6 (CH₂), 68.5 (CH₂), 64.4 (CH), 55.9 (CH), 55.7 (CH), 55.6 (CH₂), 54.8 (CH), 46.5 (CH), 38.0 (CH₂), 22.5 (CH₃); MS (ES⁺) m/z 609 (100); HRMS calcd for C₂₇H₂₆N₄O₇S (M+Na): 609.1626. Found: 609.1614.



Compound **3-36** (50 mg, 0.085 mmol) was dissolved in methanol (8 mL). Acetic acid (~100 μL) and 10% aqueous HCl (~50 μL) was added, followed by Pd/C 10% (~10 mg). The reaction mixture was stirred under 1 atm H₂ for 16 h. The reaction mixture was filtered through cotton, diluted with cyclohexane (10 mL) then concentrated in vacuo. Prior to biological testing, flash column chromatography (100:2:1 to 60:40:20 dichloromethane:methanol:acetic acid gradient) afforded 14.3 mg (43% from **3-36**) of the acetic acid salt of guanidine **3-27**. Compound **3-27** (AcOH salt, 14.3 mg, 0.0378 mmol) was dissolved in 500 μL of DMSO to provide a standard solution (75.6 mM) of guanidine **3-27**.

3-27: white solid; $R_f = 0.05$ (dichloromethane:methanol, 4:1); IR (film) 3348 (very br), 1667, 1557, 1650, 1317, 1120 cm^{-1} ; ^1H NMR (D_2O 500 MHz) δ 4.47 (ddd, $J = 5.6, 5.6, 5.1$ Hz, 1 H), 4.14 (dd, $J = 11, 8.2$ Hz, 1 H), 4.08-4.00 (m, 1 H), 3.68 (dd, $J = 14, 6.5$ Hz, 1 H), 3.67-3.44 (m, 2 H), 2.97 (ddd, $J = 11, 7.4, 4.6$ Hz, 1 H) 2.49 (ddd, $J = 12, 6.6, 6.6$ Hz, 1 H), 2.00 (s, 3 H), 1.85 (ddd, $J = 12, 11, 11$ Hz, 1 H); ^{13}C NMR (D_2O 125 MHz) δ 176.7 (C), 173.9 (C), 160.7 (C), 63.6 (CH), 54.8 (CH), 54.0 (CH₂), 53.8 (CH), 47.8 (CH),

43.8 (CH), 37.0 (CH₂) 21.9 (CH₃); MS (ES⁺) m/z 341 (100); HRMS calcd for C₁₁H₁₈N₄O₅S (M+Na): 341.0890. Found: 341.0890.



Compound **3-36** (95 mg, 0.162 mmol) was dissolved in methanol (10 mL). Acetic acid (~ 50 μ L) and 10% aqueous HCl (~ 50 μ L) was added, followed by Pd(OH)₂ 10% (~ 10 mg). The reaction mixture was stirred under 1 atm H₂ for 16 h. The reaction mixture was filtered through cotton, diluted with cyclohexane (10 mL) then concentrated in vacuo. Prior to biological testing, flash column chromatography (100:5:5 to 50:50:5 dichloromethane:methanol:acetic acid gradient) afforded 11 mg (21% from **3-35**) of **3-37**. Compound **3-37** (1.5 mg, 0.0040 mmol) was dissolved in 397 μ L of a 2:1 H₂O:DMSO mixture to provide a standard solution (10 mM) of urea **3-37**.

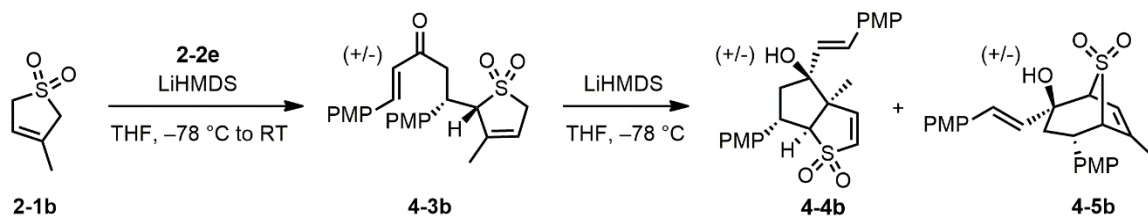
3-37: white solid; R_f = 0.2 (dichloromethane:methanol, 4:1); IR (film) 3338 (br), 3158, 3047, 1661, 1407, 1309, 1119 cm^{-1} ; ¹H NMR (D₂O 500 MHz) δ 4.50 (ddd, J = 6.6, 6.6, 6.5 Hz, 1 H), 4.26 (dd, J = 11, 7.6 Hz, 1 H), 4.03 (ddd, J = 9.2, 6.8, 6.8 Hz, 1 H), 3.70 (dd, J = 14, 6.5 Hz, 1 H), 3.50-3.42 (m, 2 H), 3.11 (ddd, J = 11, 6.7, 5.9 Hz, 1 H), 2.64 (ddd, J = 13, 6.6, 6.6 Hz, 1 H), 2.02 (s, 3 H), 2.02-1.97 (m, 1 H); ¹³C NMR (D₂O 125 MHz) δ 177.9 (C), 175.9(C), 174.1 (C), 64.2 (CH), 56.5 (CH), 54.3 (CH₂), 54.0 (CH), 48.1 (CH), 43.3 (CH), 36.9 (CH₂) 21.8 (CH₃); MS (ES⁺) m/z 318 (100).

6.4.0. Chapter 4 Experimental:

Chapter Specific Materials: **2-1d–e**, **2g–j**, **2-8a** and **2-8c**, were prepared according to literature protocols as indicated in Chapter 4 and were recrystallized from methanol before use.

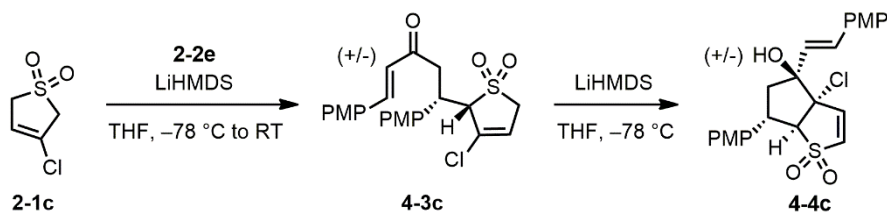
General Procedure for 1,2 addition/anionic oxy-Cope and subsequent 1,2 addition:

The 3-sulfolene (**2-1b–e**, **2h–j**) (1 eq.) and ketone **2-2e** (1 eq.) were dissolved in tetrahydrofuran (10 mL per 1 mmol), and the solution was cooled to $-78\text{ }^{\circ}\text{C}$. LiHMDS (1 M in THF, 1.1 eq.) was added dropwise. The reaction mixture was stirred for 1 h at $-78\text{ }^{\circ}\text{C}$, then removed from the cooling bath and stirred 1 h at room temperature. The reaction was quenched by the addition of saturated aqueous NH_4Cl (10 mL), and the resulting solution was extracted twice with ethyl acetate. The organic fraction was dried with Na_2SO_4 then concentrated in vacuo to provide the anionic oxy-Cope sulfone product as a light orange foam. The crude product was typically carried to the next step with no further purification. 3-Sulfolenes **4-3c** and **4-9a** were obtained by purification by flash column chromatography using a 100:0 to 25:1 dichloromethane:ethyl acetate gradient. The crude 3-sulfolene **4-3** or purified **4-9a** (1 eq.) was dissolved in tetrahydrofuran (20 mL per 1 mmol), and the solution was cooled to $-78\text{ }^{\circ}\text{C}$. LiHMDS (1 M in THF, 1.1 eq.) was added dropwise. The reaction mixture was stirred for 1 h at $-78\text{ }^{\circ}\text{C}$. The reaction was quenched by the addition of saturated aqueous NH_4Cl (10 mL), and the resulting solution was warmed to room temperature then extracted twice with ethyl acetate. The combined organic extracts were dried over Na_2SO_4 , filtered, concentrated in vacuo. Flash column chromatography (100:0 to 25:1 dichloromethane:ethyl acetate gradient) afforded the final bicyclic products. (Note: On scales larger than 500 mg the tetrahydrofuran was removed prior to liquid-liquid extraction). Yields reported are calculated from the initial 3-sulfolene starting material. Single crystals suitable for X-ray crystallographic analysis were obtained from slow evaporation of **4-4c**, **4-5b**, **4-4e'** or **4-6f** dissolved in a mixture of dichloromethane and ethyl acetate.



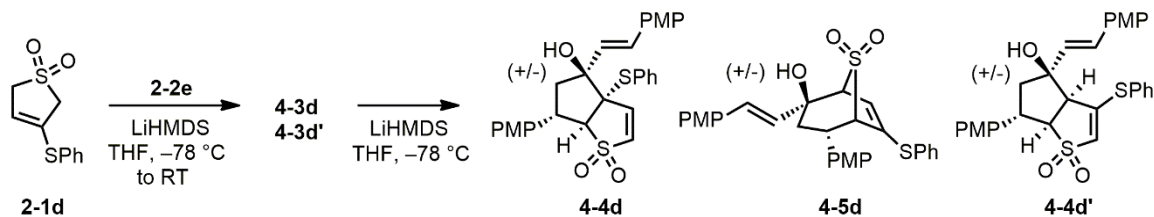
4-4b: white solid (160 mg, 13% yield); $R_f = 0.1$ (dichloromethane:ethyl acetate, 100:1); IR (film) 3479, 1283, 1122, 830 cm^{-1} ; $^1\text{H NMR}$ (CDCl_3 300 MHz) δ 7.36 (d, $J = 8.8$ Hz, 2 H), 7.28 (d, $J = 8.8$ Hz, 2 H), 6.98-6.87 (m, 4 H), 6.71 (d, $J = 16$ Hz, 1 H), 6.53 (d, $J = 6.7$ Hz, 1 H), 6.49 (d, $J = 6.6$ Hz, 1 H), 6.22 (d, $J = 16$ Hz, 1 H), 4.20 (ddd, $J = 13, 8.2, 6.7$ Hz, 1 H), 3.84 (s, 3 H), 3.81 (s, 3 H), 3.34 (d, $J = 8.2$ Hz, 1 H), 2.61 (t, $J = 13$ Hz, 1 H), 2.39 (dd, $J = 13, 6.7$ Hz, 1 H); $^{13}\text{C NMR}$ (75 MHz) δ 159.8 (C), 158.7 (C), 142.3 (CH), 133.2 (C), 130.8 (CH), 130.5 (CH), 128.8 (C), 128.4 (CH), 128.0 (CH), 126.9 (CH), 114.4 (CH), 114.3 (CH), 82.5 (C), 75.8 (CH), 62.6 (C), 55.4 (CH_3), 55.4 (CH_3), 47.8 (CH_2), 41.7 (CH), 25.7 (CH_3); HRMS calcd for $\text{C}_{24}\text{H}_{26}\text{O}_5\text{S}$ ($\text{M}+\text{Na}$): 449.1393. Found: 449.1390.

4-5b: white solid (60 mg, 5% yield); $R_f = 0.5$ (dichloromethane:ethyl acetate, 100:1); IR (film) 3476, 1292, 1106 cm^{-1} ; $^1\text{H NMR}$ (CDCl_3 300 MHz) δ 7.35 (d, $J = 8.7$ Hz, 2 H), 7.15 (d, $J = 8.7$ Hz, 2 H), 6.88 (d, $J = 8.7$ Hz, 2 H), 6.87 (d, $J = 8.8$ Hz, 2 H), 6.81 (d, $J = 16$ Hz, 1 H), 6.29-6.24 (m, 1 H), 5.99 (dd, $J = 16, 1.4$ Hz, 1 H), 5.37 (d, $J = 1.4$ Hz, 1 H), 3.94 (dd, $J = 15, 4.7$ Hz, 1 H), 3.81 (s, 3 H), 3.81 (s, 3 H), 3.59 (d, $J = 4.8$ Hz, 1 H), 3.53 (s, 1 H), 2.26 (dd, $J = 15, 13$ Hz, 1 H), 1.89 (dd, $J = 15, 4.8$ Hz, 1 H), 1.88 (d, $J = 1.5$ Hz, 3 H); $^{13}\text{C NMR}$ (CDCl_3 75 MHz) δ 159.7 (C), 159.2 (C), 140.4 (C), 132.3 (C), 130.7 (CH), 129.4 (CH), 129.1 (C), 128.6 (CH), 128.1 (CH), 124.6 (CH), 114.5 (CH), 114.2 (CH), 73.1 (C), 68.7 (CH), 68.2 (CH), 55.5 (CH_3), 55.5 (CH_3), 38.4 (CH), 37.8 (CH_2), 20.8 (CH_3); HRMS calcd for $\text{C}_{24}\text{H}_{26}\text{O}_5\text{S}$ ($\text{M}+\text{Na}$): 449.1393. Found: 449.1390.



4-3c: white solid (251 mg, 44% yield); $R_f = 0.5$ (dichloromethane:ethyl acetate, 50:1); IR (film) 1683, 1319, 1131, 835 cm^{-1} ; ^1H NMR (CDCl_3 300 MHz) δ 7.60 (d, $J = 16$ Hz, 1 H), 7.51 (d, $J = 8.8$ Hz, 2 H), 7.41 (d, $J = 8.8$ Hz, 2 H), 6.91 (d, $J = 8.8$ Hz, 2 H), 6.81 (d, $J = 8.8$ Hz, 2 H), 6.66 (d, $J = 16$ Hz, 1 H), 5.88 (ddd, 4.4, 2.0, 0.8 Hz, 1 H), 4.15-4.06 (m, 1 H), 4.04-4.00 (m, 1 H), 3.84 (s, 3 H), 3.78 (s, 3 H), 3.69 (dd, $J = 18, 8.0$ Hz, 1 H), 3.48 (dd, $J = 18, 6.6$ Hz, 1 H), 3.45 (dd, $J = 16, 4.4$ Hz, 1 H), 2.85 (dt, $J = 16, 1.8$ Hz, 1 H); ^{13}C NMR (CDCl_3 75 MHz) δ 197.3 (C), 162.0 (C), 159.2 (C), 143.4 (CH), 131.5 (C), 130.9 (CH), 130.4 (CH), 128.6 (C), 127.1 (C), 124.0 (CH), 121.7 (CH), 114.6 (CH), 113.5 (CH), 71.9 (CH), 56.4 (CH_2), 55.5 (CH_3), 55.3 (CH_3), 40.9 (CH_2), 39.1 (CH); HRMS calcd for $\text{C}_{23}\text{H}_{23}^{35}\text{ClO}_5\text{S}$ (M+Na): 469.0847. Found: 469.0846.

4-4c: light yellow solid (95 mg, 30% yield); $R_f = 0.2$ (dichloromethane:ethyl acetate, 50:1); IR (film) 3465, 1290, 1135, 831, 733 cm^{-1} ; ^1H NMR (CDCl_3 300 MHz) δ 7.37 (d, $J = 8.7$ Hz, 2 H), 7.30 (d, $J = 8.7$ Hz, 2 H), 6.90 (d, $J = 8.7$ Hz, 2 H), 6.88 (d, $J = 8.8$ Hz, 2 H), 6.72 (d, $J = 16$ Hz, 1 H), 6.69 (d, $J = 6.6$ Hz, 1 H), 6.58 (d, $J = 6.7$ Hz, 1 H), 6.44 (d, $J = 16$ Hz, 1 H), 4.18 (dt, $J = 12, 6.7$ Hz, 1 H), 4.02 (d, $J = 7.4$ Hz, 1 H), 3.82 (s, 3 H), 3.81 (s, 3 H), 2.89 (dd, $J = 13, 12$ Hz, 1 H), 2.47 (dd, $J = 13, 6.7$ Hz, 1 H); ^{13}C NMR (CDCl_3 75 MHz) δ 160.0 (C), 159.1 (C), 137.0 (CH), 133.7 (CH), 132.3 (C), 132.3 (C), 131.5 (CH), 128.6 (CH), 128.2 (CH), 125.5 (CH), 114.7 (CH), 114.4 (CH), 84.1 (C), 82.1 (C), 78.2 (CH), 55.5 (CH_3), 55.5 (CH_3), 48.4 (CH_2), 41.7 (CH); HRMS calcd for $\text{C}_{23}\text{H}_{23}^{35}\text{ClO}_5\text{S}$ (M+Na): 469.0847. Found: 469.0849.

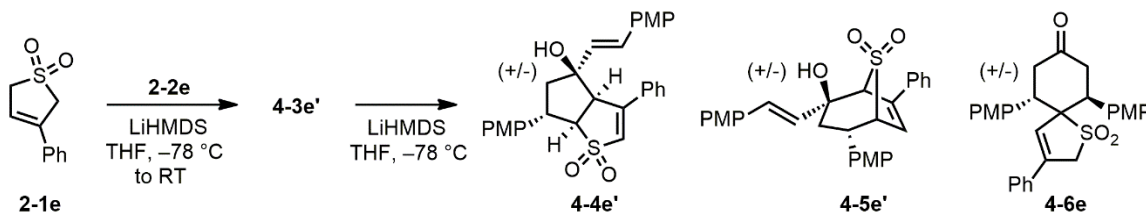


4-4d: light yellow solid (66 mg, 16% yield); $R_f = 0.1$ (dichloromethane:ethyl acetate, 25:1); IR (film) 3468, 1305, 1128, 831, 732, 693 cm^{-1} ; ^1H NMR (CDCl_3 300 MHz) δ 7.51-7.23 (m, 9 H), 6.95-6.82 (m, 4 H), 6.77 (d, $J = 16$ Hz, 1 H), 6.69 (d, $J = 6.7$ Hz, 1 H), 6.43 (d, $J = 6.6$ Hz, 1 H), 6.40 (d, $J = 16$ Hz, 1 H), 4.22 (dt, $J = 13, 6.7$ Hz, 1 H), 3.82 (s, 3 H), 3.81 (s, 3 H), 3.56 (d, $J = 7.5$ Hz, 1 H), 3.10 (t, $J = 13$ Hz, 1 H), 2.49 (dd, $J = 13, 6.7$ Hz, 1 H); ^{13}C NMR (CDCl_3 75 MHz) δ 160.0 (C), 158.9 (C), 139.9 (CH), 137.2 (CH), 133.0 (C), 133.0 (C), 132.2 (CH), 131.8 (CH), 130.5 (C), 129.7 (CH), 129.1 (CH), 128.7 (CH), 128.3 (CH), 125.3 (CH), 114.6 (CH), 114.3 (CH), 83.8 (C), 72.8 (C), 72.8 (CH), 55.5 (CH_3), 55.5 (CH_3), 48.3 (CH_2), 42.2 (CH); HRMS calcd for $\text{C}_{29}\text{H}_{28}\text{O}_5\text{S}_2$ ($\text{M}+\text{Na}$): 543.1270. Found: 543.1276.

4-5d: light yellow solid (44 mg, 12% yield); $R_f = 0.5$ (dichloromethane:ethyl acetate, 100:1); IR (film) 3468, 1293 1110 cm^{-1} ; ^1H NMR (CDCl_3 300 MHz) δ 7.53-7.47 (m, 2 H), 7.42-7.35 (m, 5 H), 7.04 (d, $J = 8.7$ Hz, 2 H), 6.90 (d, $J = 8.7$ Hz, 2 H), 6.84 (d, $J = 8.7$ Hz, 2 H), 6.79 (d, $J = 16$ Hz, 1 H), 6.30 (dd, $J = 16, 1.5$ Hz, 1 H), 6.00 (d, $J = 5$ Hz, 1 H), 5.35 (d, $J = 1.5$ Hz, 1 H), 3.89-3.78 (m, 2 H), 3.83 (s, 3 H), 3.78 (s, 3 H), 3.47 (s, 1 H), 2.14 (dd, $J = 15, 12$ Hz, 1 H), 1.89 (dd, $J = 15, 5.0$ Hz, 1 H); ^{13}C NMR (CDCl_3 75 MHz) δ 159.7 (C), 159.2 (C), 141.2 (C), 134.3 (CH), 133.1 (C), 130.0 (CH), 129.9 (CH), 129.8 (CH), 129.6 (CH), 129.4 (C), 129.3 (C), 128.3 (CH), 128.1 (CH), 121.0 (CH), 114.6 (CH), 114.1 (CH), 72.4 (C), 69.0 (CH), 67.0 (CH), 55.5 (CH_3), 55.5 (CH_3), 40.4 (CH_2), 39.5 (CH); HRMS calcd for $\text{C}_{29}\text{H}_{28}\text{O}_5\text{S}_2$ ($\text{M}+\text{H}$): 521.1450. Found: 521.1453.

4-4d': light yellow solid (98 mg, 24% yield); $R_f = 0.2$ (dichloromethane:ethyl acetate, 50:1); IR (film) 3448, 1604, 1513, 1250, 1120, 1106, 1032 cm^{-1} ; ^1H NMR (CDCl_3 300 MHz) δ 7.55-7.34 (m, 7 H), 7.27 (d, $J = 8.6$ Hz, 2 H), 6.90 (d, $J = 8.8$ Hz, 2 H), 6.89 (d, $J = 8.8$ Hz, 2 H), 6.84 (d, $J = 16$ Hz, 1 H), 6.28 (d, $J = 16$ Hz, 1 H), 5.75 (d, $J = 1.0$ Hz, 1 H),

4.31 (dt, $J = 13$, 7.2 Hz, 1 H), 3.98 (dd, $J = 9.9$, 8.0 Hz, 1 H), 3.87-3.81 (m, 1 H), 3.83 (s, 3 H), 3.80 (s, 3 H), 2.50 (dd, $J = 13$, 6.7 Hz, 1 H) 2.39 (t, $J = 13$ Hz, 1 H); ^{13}C NMR (CDCl_3 75 MHz) δ 159.8 (C), 158.8 (C), 153.2 (C), 135.1 (CH), 132.8 (C), 130.7 (CH), 130.3 (CH), 130.3 (C), 130.2 (C), 129.4 (CH), 129.0 (CH), 128.4 (CH), 128.0 (CH), 122.7 (CH), 114.5 (CH), 114.3 (CH), 81.0 (C), 71.5 (CH), 59.9 (CH), 55.5 (CH_3), 55.5 (CH_3), 50.1 (CH_2), 42.6 (CH); HRMS calcd for $\text{C}_{29}\text{H}_{28}\text{O}_5\text{S}_2$ ($\text{M}+\text{Na}$): 543.1270. Found: 543.1269.

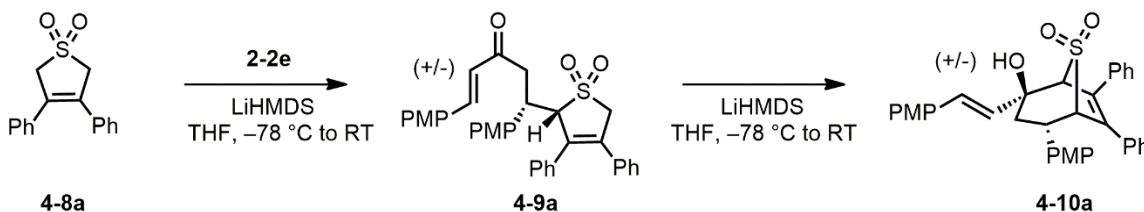


4-4e': white solid (243 mg, 19% yield); $R_f = 0.1$ (dichloromethane:ethyl acetate, 100:1); IR (film); 3438, 1277, 1116 cm^{-1} ; ^1H NMR (CDCl_3 300 MHz) δ 7.44-7.39 (m, 2 H), 7.36-7.29 (m, 5 H), 7.02 (d, $J = 8.8$ Hz, 2 H), 6.91 (d, $J = 8.5$ Hz, 2 H), 6.79 (d, $J = 9.0$ Hz, 2 H), 6.73 (d, $J = 1.1$ Hz, 1 H), 6.18 (d, $J = 16$ Hz, 1 H), 5.88 (d, $J = 16$ Hz, 1 H), 4.38-4.28 (m, 2 H), 4.04 (dd, $J = 9.6$, 7.9 Hz, 1 H), 3.81 (s, 3 H), 3.79 (s, 3 H), 2.50 (t, $J = 13$ Hz, 1 H) 2.42 (dd, $J = 13$, 7 Hz, 1 H); ^{13}C NMR (CDCl_3 75 MHz) δ 159.5 (C), 158.9 (C), 149.6 (C), 133.1 (CH), 132.6 (C), 130.7 (CH), 129.9 (CH), 129.0 (C), 128.9 (C), 128.7 (CH), 128.4 (CH), 127.8 (CH), 127.7 (CH), 127.6 (CH), 114.5 (CH), 114.1 (CH), 81.2 (C), 70.7 (CH), 58.6 (CH), 55.5 (CH_3), 55.4 (CH_3), 50.4 (CH_2), 42.0 (CH); HRMS calcd for $\text{C}_{29}\text{H}_{28}\text{O}_5\text{S}$ ($\text{M}+\text{Na}$): 511.1549. Found: 511.1549.

4-5e': white solid (310 mg, 24% yield); $R_f = 0.7$ (dichloromethane:ethyl acetate, 100:1); IR film) 3479, 1284, 1119 cm^{-1} ; ^1H NMR (CDCl_3 300 MHz) δ 7.61-7.57 (m, 2 H), 7.43-7.40 (m, 3 H), 7.18 (d, $J = 8.7$ Hz, 2 H), 7.00 (d, $J = 8.7$ Hz, 2 H), 6.91 (d, $J = 8.7$ Hz, 2 H), 6.82 (d, $J = 0.9$ Hz, 1 H), 6.82 (d, $J = 16$ Hz, 1 H), 6.74 (d, $J = 8.8$ Hz, 2 H), 5.67 (dd, $J = 16$, 1.6 Hz, 1 H), 5.57 (d, $J = 1.7$ Hz, 1 H), 4.10 (s, 1 H), 4.02-3.93 (m, 2 H), 3.82 (s, 3 H), 3.77 (s, 3 H), 2.16 (dd, $J = 15$, 12 Hz, 1 H), 1.94 (dd, $J = 15$, 5.0 Hz, 1 H); ^{13}C NMR (CDCl_3 75 MHz) δ 159.6 (C), 159.2 (C), 143.9 (C), 133.6 (C), 133.3 (C), 130.7 (CH), 129.7 (CH), 129.7 (C), 129.3 (CH), 129.1 (CH), 128.4 (CH), 127.9 (CH), 126.1 (CH), 120.7

(CH), 114.7 (CH), 114.1 (CH), 72.9 (C), 68.0 (CH), 66.6 (CH), 55.5 (CH₃), 55.4 (CH₃), 40.5 (CH₂), 40.1 (CH); HRMS calcd for C₂₉H₂₈O₅S (M+Na): 511.1549. Found: 511.1548.

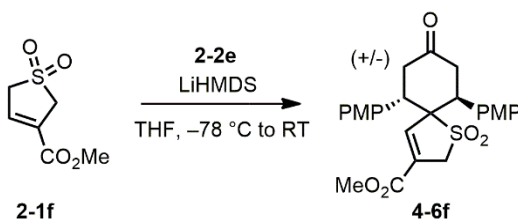
4-6e: white solid (56 mg, 5% yield); R_f = 0.6 (dichloromethane:ethyl acetate, 100:1); IR (film) 1715, 1302, 1128 cm⁻¹; ¹H NMR (CDCl₃ 300 MHz) δ 7.32-7.27 (m, 3 H), 7.17 (d, *J* = 8.9 Hz, 2 H), 7.17 (d, *J* = 8.8 Hz, 2 H), 7.03-7.00 (m, 2 H), 6.94 (d, *J* = 8.8 Hz, 2 H), 6.67 (d, *J* = 8.9 Hz, 2 H), 5.78 (d, *J* = 2.4 Hz, 1 H), 4.32 (dd, *J* = 7.0, 2.1 Hz, 1 H), 4.12 (dd, *J* = 16, 15 Hz, 1 H), 3.85 (s, 3 H), 3.77 (s, 1 H), 3.71 (m, 3 H) 3.67 (s, 1 H), 3.19 (dd, *J* = 16, 7.1 Hz, 1 H), 2.92 (dd, *J* = 15, 2.7 Hz, 1 H), 2.86-2.76 (m, 2 H); ¹³C NMR (CDCl₃ 75 MHz) δ 209.7 (C), 159.4 (C), 159.1 (C), 136.4 (C), 134.2 (C), 131.9 (CH), 131.8 (C), 131.0 (C), 129.3 (C), 129.0 (C), 128.2 (C), 127.3 (CH), 125.5 (CH), 114.4 (CH), 113.0 (CH), 74.4 (C), 57.1 (CH₂), 55.5 (CH₃), 55.4 (CH₃), 44.3 (CH₂), 44.0 (CH), 42.9 (CH), 42.2 (CH₂); HRMS calcd for C₂₉H₂₈O₅S (M+Na): 511.1549. Found: 511.1546.



4-9a: white solid (560 mg, 50% yield); R_f = 0.5 (dichloromethane:ethyl acetate, 100:1); IR (film) 1653, 1309, 1172 cm⁻¹; ¹H NMR (CDCl₃ 300 MHz) δ 7.51 (d, *J* = 16 Hz, 1 H), 7.41 (d, *J* = 8.8 Hz, 2 H), 7.23 (d, *J* = 8.9 Hz, 2 H), 7.21-7.18 (m, 5 H), 7.11-7.03 (m, 3 H), 6.81 (d, *J* = 8.8 Hz, 2 H), 6.75 (d, *J* = 8.7 Hz, 2 H), 6.73-6.70 (m, 2 H), 6.56 (d, *J* = 16 Hz, 1 H), 4.66 (d, *J* = 3.2 Hz, 1 H), 3.82 (dd, *J* = 16, 8.9 Hz, 1 H), 3.73 (s, 3 H), 3.72 (s, 3 H), 3.39 (d, *J* = 16 Hz, 1 H), 3.25 (dd, *J* = 16, 5.0 Hz, 1 H), 3.22 (d, *J* = 16 Hz, 1 H); ¹³C NMR (CDCl₃ 75 MHz) δ 197.9 (C), 161.8 (C), 159.0 (C), 143.1 (CH), 136.1 (C), 135.7 (C), 134.8 (C), 134.0 (C), 132.3 (C), 131.2 (CH), 130.2 (CH), 129.5 (CH), 129.3 (C), 128.7 (CH), 128.5 (CH), 128.2 (CH), 128.1 (CH), 127.1 (CH), 124.0 (CH), 114.5 (CH), 113.1 (CH), 72.6 (CH), 59.5 (CH₂), 55.4 (CH₃), 55.3 (CH₃), 41.4 (CH₂), 39.6 (CH); HRMS calcd for C₃₅H₃₂O₅S (M+Na): 587.1862. Found: 587.1861.

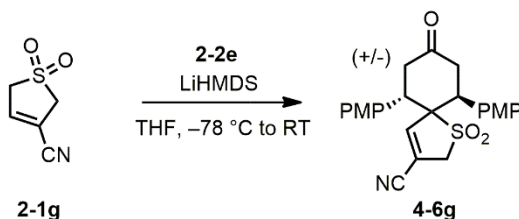
4-10a: white solid (459 mg, 40% yield) $R_f = 0.5$ (dichloromethane:ethyl acetate, 100:1); IR (film) 3481, 1293, 1175 cm^{-1} ; $^1\text{H NMR}$ (CDCl_3 300 MHz) δ 7.31-7.24 (m, 5 H), 7.19 (d, $J = 8.7$ Hz, 2 H), 7.08-7.02 (m, 1 H), 6.95 (t, $J = 7.5$ Hz, 2 H), 6.85 (d, $J = 9.0$ Hz, 2 H), 6.82 (d, $J = 9.5$ Hz, 2 H), 6.73 (d, $J = 16$ Hz, 1 H), 6.66 (d, $J = 8.7$ Hz, 2 H), 5.70 (dd, $J = 16, 1.6$ Hz, 1 H), 5.47 (d, $J = 1.5$ Hz, 1 H), 4.20 (dd, $J = 13, 4.1$ Hz, 1 H), 4.13-4.12 (m, 1 H), 4.02 (d, $J = 2.1$ Hz, 1 H), 3.78 (s, 3 H), 3.72 (s, 3 H), 2.54 (dd, $J = 15, 13$ Hz, 1 H), 2.03 (dd, $J = 15, 4.4$ Hz, 1 H); $^{13}\text{C NMR}$ (CDCl_3 75 MHz) δ 159.5 (C), 159.3 (C), 138.3 (C), 136.3 (C), 135.5 (C), 135.4 (C), 132.1 (C), 130.8 (CH), 129.4 (CH), 129.2 (CH), 129.2 (C), 129.2 (CH), 129.0 (CH), 128.7 (CH), 128.6 (CH), 128.4 (CH), 128.4 (CH) 127.9 (CH), 114.6 (CH), 114.0 (CH), 73.9 (CH), 73.2 (C), 72.3 (CH), 55.6 (CH_3), 55.4 (CH_3), 39.2 (CH), 37.8 (CH_2); HRMS calcd for $\text{C}_{35}\text{H}_{32}\text{O}_5\text{S}$ ($\text{M}+\text{Na}$): 587.1862. Found: 587.1864.

General Procedure for intermolecular δ -1,2-addition followed by intramolecular δ -1,2-addition: The 3-sulfolene (**2-1f** or **2-1g**) (1 eq.) and ketone **2-2e** (1 eq.) were dissolved in tetrahydrofuran (10 mL per 1 mmol), and the solution was cooled to -78 °C. LiHMDS (1 M in THF, 1.1 eq.) was added dropwise. The reaction mixture was stirred for 0.5 h at -78 °C, then removed from the cooling bath and stirred 0.5 h at room temperature. The reaction was quenched by the addition of saturated aqueous NH_4Cl (10 mL), then extracted twice with ethyl acetate. The combined organic extracts were dried over Na_2SO_4 , filtered, concentrated in vacuo. Flash column chromatography (100:0 to 10:1 dichloromethane: ethyl acetate gradient) afforded **4-6f** and **4-6g**.



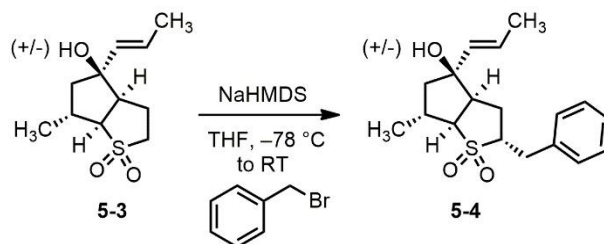
4-6f: white solid (160 mg, 24% yield); $R_f = 0.2$ (dichloromethane:ethyl acetate, 50:1); IR (film) 1720, 1314, 1136 cm^{-1} ; $^1\text{H NMR}$ (CDCl_3 300 MHz) δ 7.12 (d, $J = 8.8$ Hz, 2 H), 7.08 (d, $J = 8.8$ Hz, 2 H), 6.91 (d, $J = 8.8$ Hz, 2 H), 6.72 (d, $J = 8.8$ Hz, 2 H), 6.53 (d, $J = 2.3$ Hz, 1 H), 4.24 (dd, $J = 6.9, 2.0$ Hz, 1 H), 4.03 (dd, $J = 16, 14$ Hz, 1 H), 3.82 (s, 3 H), 3.74

(s, 3 H), 3.76-3.63 (m, 2 H) 3.66 (s, 3 H), 3.11 (dd, $J = 16, 7.2$ Hz, 1 H), 2.83-2.69 (m, 3 H); ^{13}C NMR (CDCl_3 75 MHz) δ 208.8 (C), 162.2 (C), 159.5 (C), 159.3 (C), 142.6 (CH), 131.7 (CH), 130.8 (CH), 129.9 (C), 129.2 (C), 127.3 (C), 114.5 (CH), 113.1 (CH), 75.2 (C), 55.9 (CH_2), 55.4 (CH_3), 55.3 (CH_3), 52.6 (CH_3), 43.7 (CH_2), 43.3 (CH), 42.2 (CH), 41.8 (CH_2); HRMS calcd for $\text{C}_{25}\text{H}_{26}\text{O}_7\text{S}$ ($\text{M}+\text{Na}$): 493.1291. Found: 493.1291.



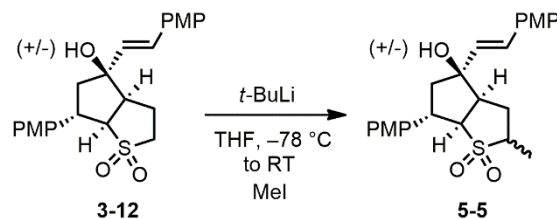
4-6g: pale yellow solid (45 mg, 21% yield, 2:1 contaminated with **2-1g**); $R_f = 0.3$ (dichloromethane:ethyl acetate, 100:1); IR (film) 2229, 1713, 1323, 1130 cm^{-1} ; ^1H NMR (CDCl_3 300 MHz) δ 7.14 (d, $J = 8.8$ Hz, 2 H), 7.09 (d, $J = 8.8$ Hz, 2 H), 6.94 (d, $J = 8.8$ Hz, 2 H), 6.81 (d, $J = 8.9$ Hz, 2 H), 6.37 (d, $J = 2.5$ Hz, 1 H), 4.24 (dd, $J = 6.9, 1.9$ Hz, 1 H), 4.04 (dd, $J = 16, 14$ Hz, 1 H), 3.85 (s, 3 H), 3.80 (s, 3 H), 3.69 (dd, $J = 14, 4.6$ Hz, 1 H) 3.52 (d, $J = 16$ Hz, 1 H), 3.09 (dd, $J = 16, 7.2$ Hz, 1 H), 2.87-2.71 (m, 3 H); ^{13}C NMR (CDCl_3 75 MHz) δ 208.0 (C), 159.8 (C), 159.7 (C), 149.0 (C), 131.7 (CH), 130.8 (CH), 130.2 (C), 126.5 (C), 114.8 (CH), 113.2 (CH), 113.2 (CH), 110.1 (C), 74.2 (C), 55.5 (CH_3), 55.4 (CH_3), 55.2 (CH_2), 43.7 (CH_2), 43.6 (CH), 42.0 (CH), 41.7 (CH_2); HRMS calcd for $\text{C}_{24}\text{H}_{23}\text{NO}_5\text{S}$ ($\text{M}-\text{H}$): 436.1224. Found: 436.1213.

General Procedure for the cheletropic removal of SO_2 : Compound **3c**, **4-5b**, **4-6f** or **2-9b** was dissolved in the indicated solvent and heated in a sealed vessel until all the starting material was consumed (TLC). The solvent was removed in vacuo. Diene **4-12** was purified by flash column chromatography using a 100:0 to 10:1 dichloromethane:ethyl acetate gradient.



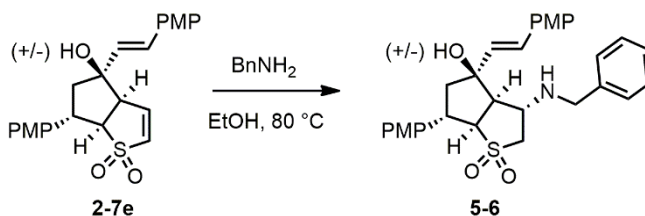
Compound **5-3** (265 mg, 1.2 mmol) was dissolved in tetrahydrofuran (15 mL). The solution was cooled to $-78\text{ }^\circ\text{C}$. NaHMDS (2.65 mL, 1M in THF, 2.65 mmol) was added in one portion. The solution was warmed to room temperature over 30 min. The reaction mixture was cooled to $-78\text{ }^\circ\text{C}$ whereupon benzyl bromide (175 μL , 1.5 mmol) was added. The solution was stirred for 2 h at $-78\text{ }^\circ\text{C}$ then warmed to room temperature and stirred for 16 h. The reaction mixture was partitioned between ethyl acetate and saturated aqueous NH_4Cl . The aqueous layer was washed with ethyl acetate, and the combined organic fractions were washed with brine then dried with Na_2SO_4 and concentrated in vacuo. Flash column chromatography (2:1 hexanes:ethyl acetate) afforded 316 mg (83% from **5-3**) of **5-4**.

5-4: white solid, $R_f = 0.5$ (hexanes:ethyl acetate, 2:1); Mp $129\text{--}132\text{ }^\circ\text{C}$; IR (film) 3502 (br), 1288, 1114, 967 cm^{-1} ; ^1H NMR (CDCl_3 500 MHz) δ 7.27-7.15 (m, 5 H), 5.58 (dq, $J = 15$, 6.6 Hz, 1 H), 5.40 (dq, $J = 15$, 1.8 Hz, 1 H), 3.66 (dddd, $J = 13$, 9.3, 6.6, 5.7 Hz, 1 H), 3.18 (dd, $J = 14$, 5.4 Hz, 1 H), 2.99 (dd, $J = 11$, 8.8 Hz, 1 H), 2.83-2.73 (m, 1 H), 2.71 (dd, $J = 14$, 9.2 Hz, 1 H), 2.65 (dd, $J = 10$, 9.3 Hz, 1 H), 2.02 (dd, $J = 13$, 6.7 Hz, 1 H), 1.80 (d, $J = 1.5$ Hz, 1 H), 1.78 (dd, $J = 13$, 6.1 Hz, 1 H), 1.66 (ddd, $J = 13$, 13, 6.8 Hz, 1 H), 1.62 (dd, $J = 6.6$, 1.6 Hz, 3 H), 1.42 (t, $J = 13$ Hz, 1 H), 1.17 (d, $J = 6.6$ Hz, 3 H); ^{13}C NMR (CDCl_3 125 MHz) δ 137.6 (C), 134.3 (CH), 129.0 (CH), 128.7 (CH), 126.7 (CH), 124.8 (CH), 81.8 (C), 69.8 (CH), 60.4 (CH), 49.3 (CH_2), 47.7 (CH), 36.1 (CH), 32.4 (CH_2), 26.0 (CH_2), 19.2 (CH_3), 17.7 (CH_3); MS (ES+) m/z 343 (100); HRMS calcd for $\text{C}_{18}\text{H}_{24}\text{O}_3\text{S}$ (M+Na): 343.1344. Found: 343.1342.



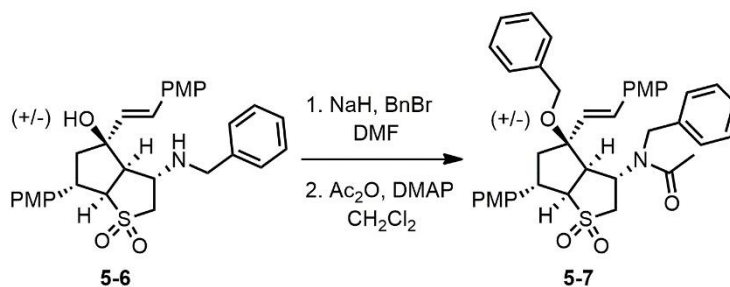
Compound **3-12** (62 mg, 0.15 mmol) was dissolved in tetrahydrofuran (10 mL). The solution was cooled to $-78\text{ }^\circ\text{C}$. *t*-BuLi (0.22 mL, 1.5 M in pentane, 0.330 mmol) was added in one portion and stirred for 5 min at $-78\text{ }^\circ\text{C}$. The solution was warmed to room temperature over 20 min. The reaction mixture was cooled to $-78\text{ }^\circ\text{C}$ whereupon methyl iodide (11 μL , 0.18 mmol) was added. The solution was stirred for 10 min at $-78\text{ }^\circ\text{C}$ then warmed to room temperature and stirred for 16 h. The reaction mixture was partitioned between ethyl acetate and saturated aqueous NH_4Cl . The aqueous layer was washed with ethyl acetate, and the combined organic fractions were washed with brine then dried with Na_2SO_4 and concentrated in vacuo. Flash column chromatography (50:1 dichloromethane: ethyl acetate) afforded **5-5** as a 3:1 mixture of diastereomers.

5-5 (major diastereomer): white solid; $R_f = 0.2$ (dichloromethane:ethyl acetate, 50:1); ^1H NMR (CDCl_3 300 MHz) δ 7.34 (d, $J = 8.8$ Hz, 2 H), 7.30 (d, $J = 8.8$ Hz, 2 H), 6.88 (d, $J = 8.8$ Hz, 4 H), 6.69 (d, $J = 16$ Hz, 1 H), 6.16 (d, $J = 16$ Hz, 1 H), 4.06 (dt, $J = 11, 8.4$ Hz, 1 H), 3.83 (s, 3 H), 3.81 (s, 3 H), 3.65 (dt, $J = 13, 6.5$ Hz, 1 H), 3.65 (dd, $J = 11, 8.5$ Hz, 1 H), 3.51-3.47 (m, 1 H), 3.00-2.91 (m, 1 H), 2.29 (dd, $J = 14, 7.0$ Hz, 1 H), 2.20-2.18 (m, 1 H), 1.76-1.69 (m, 1 H), 1.35 (d, $J = 6.7$ Hz, 3 H); ^{13}C NMR (CDCl_3 75 MHz) δ 159.6 (C), 158.6 (C), 133.2 (C), 129.8 (CH), 128.9 (CH), 128.7 (C), 128.5 (CH), 127.7 (CH), 114.2 (CH), 114.2(CH), 82.2 (C), 69.5 (CH), 55.3 (CH_3), 55.3 (CH_3), 55.0 (CH), 49.1 (CH_2), 48.4 (CH), 45.1 (CH), 27.4 (CH_2), 10.8 (CH_3); MS (ES+) m/z 437 (100); HRMS calcd for $\text{C}_{24}\text{H}_{28}\text{O}_5\text{S}$ (M+Na): 451.1550. Found: 451.1555.



Compound **2-7e** (crude, 10.6 g, 24.3 mmol) was dissolved in ethanol (300 mL). Benzylamine (8.4 mL, 77.29 mmol) was added in one portion and heated for 72 h at 80 °C. The solution was cooled to room temperature then concentrated in vacuo. The crude product was dissolved in a minimum amount of methanol and dichloromethane and was cooled to 0 °C. After 72 h the light-brown solid was filtered and washed with diethyl ether (2 x 100 mL) to afford 3.1 g of **5-6** (23% from **2-1a**).

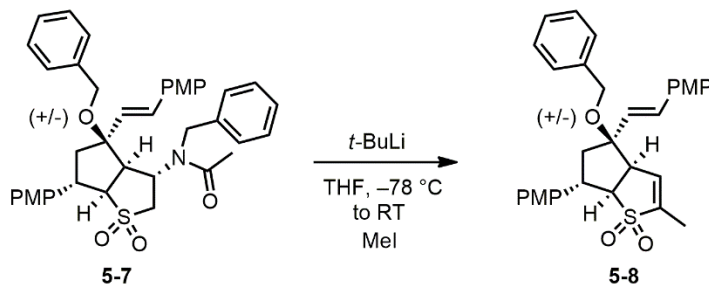
5-6: brown solid; $R_f = 0.5$ (dichloromethane:ethyl acetate, 10:1); $^1\text{H NMR}$ (CDCl_3 300 MHz) δ 7.36-7.17 (m, 9 H), 6.88 (d, $J = 8.4$ Hz, 2 H), 6.18 (d, $J = 8.4$ Hz, 2 H), 6.63 (d, $J = 16$ Hz, 1 H), 6.18 (d, $J = 16$ Hz, 1 H), 4.10 (q, $J = 8.9$ Hz, 1 H), 3.85 (s, 3 H), 3.80 (s, 3 H), 3.71 (dd, $J = 11, 9.0$ Hz, 1 H), 3.64 (dd, $J = 13, 6.5$ Hz, 1 H), 3.59-3.54 (m, 1 H), 3.26-3.12 (m, 2 H), 2.27-2.19 (m, 2 H).



Compound **5-6** (1.81 g, 3.49 mmol) was dissolved in dimethylformamide (10 mL). The solution was cooled to 0 °C. NaH (209 mg, 60% in mineral oil, 5.23 mmol) was added in one portion. The solution was stirred at 0 °C for 20 min. Benzyl bromide (621 μL , 5.23 mmol) was added. The solution was then warmed to room temperature and stirred for 16 h. The reaction mixture was partitioned between dichloromethane and saturated aqueous NH_4Cl . The aqueous layer was washed with dichloromethane, and the combined organic

fractions were dried with Na_2SO_4 and concentrated in vacuo. Flash column chromatography (50:0 to 5:1 dichloromethane:ethyl acetate gradient) afforded 850 mg of *O*-benzylated product (40%). The *O*-benzylated product (281 mg, 0.461 mmol) was dissolved in 20 mL dichloromethane. DMAP (11 mg, 0.092 mmol) followed by acetic anhydride (131 μL , 1.38 mmol) was added. The reaction mixture was stirred at room temperature for 16 h. The reaction mixture was partitioned between 10% aqueous NaHCO_3 and dichloromethane. The aqueous layer was washed with dichloromethane, and the combined organic extracts were dried with Na_2SO_4 and concentrated in vacuo. Flash column chromatography (100:0 to 5:1 dichloromethane:ethyl acetate gradient) afforded 165 mg (55% from **5-6**) of **5-7**.

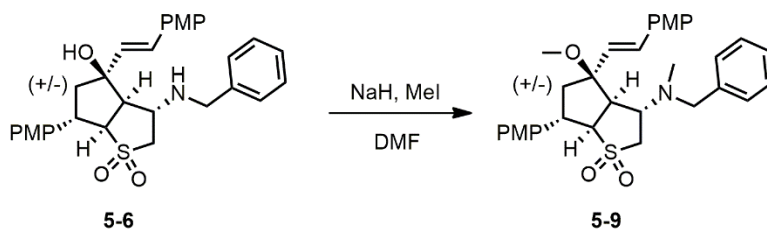
5-7: off-white solid, $R_f = 0.3$ (dichloromethane:ethyl acetate, 25:1); ^1H NMR (CDCl_3 300 MHz) δ 7.46-7.29 (m, 7 H), 7.25-7.19 (m, 5 H), 7.02-6.97 (m, 2 H), 6.92 (d, $J = 8.4$ Hz, 2 H), 6.87 (d, $J = 8.4$ Hz, 2 H), 6.60 (d, $J = 16$ Hz), 6.07 (d, $J = 16$ Hz), 4.72 (d, $J = 18$ Hz, 1 H), 4.55 (d, $J = 11$ Hz, 1 H), 4.43 (d, $J = 18$ Hz, 1 H), 4.43 (d, $J = 11$ Hz, 1 H), 4.09-3.98 (m, 1 H), 3.85 (s, 3 H), 3.85-3.78 (m, 2 H), 3.80 (s, 3 H), 3.63-3.54 (m, 1 H), 3.47-3.31 (m, 2 H), 2.74 (dd, $J = 13, 6.1$ Hz, 1 H), 2.14-2.08 (m, 1 H), 2.08 (s, 3 H).



Compound **5-7** (71 mg, 0.109 mmol) was dissolved in tetrahydrofuran (5 mL). The solution was cooled to -78°C . $t\text{-BuLi}$ (192 μL , 1.5 M in pentane, 0.327 mmol) was added in one portion and stirred for 20 min at -78°C . Methyl iodide (16 μL , 0.262 mmol) was added. The solution was stirred for 5 min at -78°C then warmed to room temperature and stirred for 16 h. The reaction mixture was partitioned between ethyl acetate and saturated aqueous NH_4Cl . The aqueous layer was washed with ethyl acetate, and the combined organic

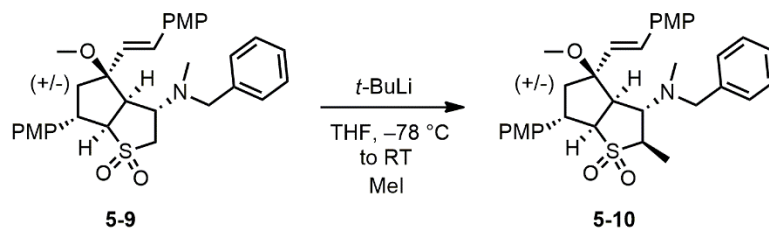
fractions were washed with brine then dried with Na_2SO_4 and concentrated in vacuo. Flash column chromatography (100:1 to 25:1 dichloromethane:ethyl acetate) afforded 25 mg of **5-8** (44% from **5-7**).

5-8: white solid, $R_f = 0.4$ (dichloromethane:ethyl acetate, 50:1); ^1H NMR (CDCl_3 300 MHz) δ 7.30-7.19 (m, 9 H), 6.82 (d, $J = 8.5$ Hz, 2 H), 6.81 (d, $J = 8.5$ Hz, 2 H), 6.54 (d, $J = 16$ Hz, 1 H), 6.15 (dd, $J = 3.5, 1.7$ Hz, 1 H), 6.08 (d, $J = 16$ Hz, 1 H), 4.40 (d, $J = 12$ Hz, 1 H), 4.41 (d, $J = 12$ Hz, 1 H), 4.00-3.89 (m, 1 H), 3.74 (s, 3 H), 3.72 (s, 3 H), 3.63 (dd, $J = 9.9, 8.2$ Hz, 1 H), 3.54-3.47 (m, 1 H), 2.70 (dd, $J = 13, 5.7$ Hz, 1 H), 2.22 (t, $J = 13$ Hz, 1 H), 2.02 (t, $J = 1.7$ Hz, 3 H).



Compound **5-6** (228 g, 0.439 mmol) was dissolved in dimethylformamide (5 mL). The solution was cooled to 0 °C. NaH (209 mg, 60% in mineral oil, 5.23 mmol) was added in one portion. The solution was stirred at 0 °C for 20 min. Methyl iodide (68 μL , 1.09 mmol) was added. The solution was then warmed to room temperature and stirred for 16 h. The reaction mixture was partitioned between ethyl acetate and saturated aqueous NH_4Cl . The aqueous layer was washed with ethyl acetate, and the combined organic fractions were dried with Na_2SO_4 and concentrated in vacuo. Flash column chromatography (25:1 to 5:1 dichloromethane:ethyl acetate gradient) afforded 44 mg of **5-9** (40% from **5-6**).

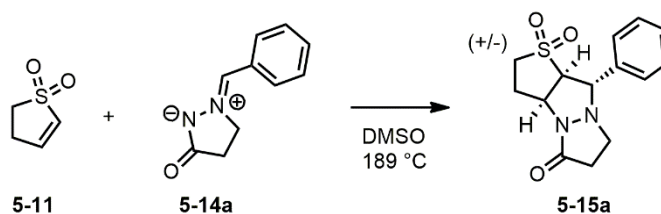
5-9: off-white solid; $R_f = 0.3$ (dichloromethane:ethyl acetate, 25:1); ^1H NMR (CDCl_3 300 MHz) δ 7.26-7.33 (d, $J = 8.8$ Hz, 2 H), 7.29 (d, $J = 8.8$ Hz, 2 H), 7.21 (m, 5 H), 6.91 (d, $J = 8.8$ Hz, 2 H), 6.48 (d, $J = 8.5$ Hz, 2 H), 6.52 (d, $J = 16$ Hz, 1 H), 6.02 (d, $J = 16$ Hz, 1 H), 4.04-3.89 (m, 2 H), 3.85 (s, 3 H), 3.81 (s, 3 H), 3.66 (dd, $J = 11, 7.3$ Hz, 1 H), 3.56 (s, 2 H), 3.48 (dd, $J = 14, 8.3$ Hz, 1 H), 3.39 (dd, $J = 14, 3.7$ Hz, 1 H), 3.20 (s, 3 H), 3.14 (dd, $J = 11, 2.1$ Hz, 1 H), 2.69 (dd, $J = 13, 6.4$ Hz, 1 H), 2.29 (s, 3 H), 2.09 (t, $J = 13$ Hz, 1 H).



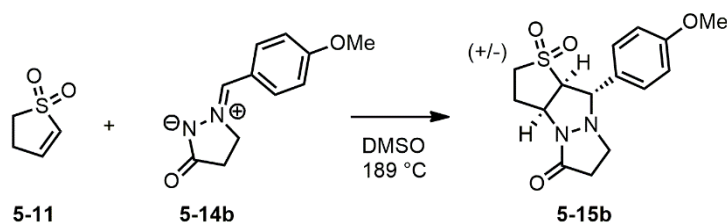
Compound **5-9** (42 mg, 0.077 mmol) was dissolved in tetrahydrofuran (5 mL). The solution was cooled to $-78\text{ }^{\circ}\text{C}$. *t*-BuLi (68 μL , 1.7 M in hexanes, 0.115 mmol) was added in one portion and stirred for 20 min at $-78\text{ }^{\circ}\text{C}$. Methyl iodide (9 μL , 0.14 mmol) was added. The solution was stirred for 5 min at $-78\text{ }^{\circ}\text{C}$ then warmed to room temperature and stirred for 16 h. The reaction mixture was partitioned between dichloromethane and saturated aqueous NH_4Cl . The aqueous layer was washed with dichloromethane, and the combined organic fractions were washed with brine then dried with Na_2SO_4 and concentrated in vacuo. Flash column chromatography (25:1 to 10:1 dichloromethane:ethyl acetate gradient) afforded 13 mg of **5-10** (30% from **5-9**) and 5 mg unreacted **5-9**. A single crystal suitable for X-ray crystallographic analysis was obtained from slow evaporation of **5-10** dissolved in a mixture of dichloromethane and ethyl acetate.

5-10: white solid, $R_f = 0.6$ (dichloromethane:ethyl acetate, 25:1); ^1H NMR (CDCl_3 300 MHz) δ 7.38-7.20 (m, 9 H), 6.90 (d, $J = 8.8$ Hz, 4 H), 6.50 (d, $J = 16$ Hz, 1 H), 6.26 (d, $J = 16$ Hz, 1 H), 4.04-3.89 (m, 2 H), 3.85 (s, 3 H), 3.81 (s, 3 H), 3.78-3.70 (m, 3 H), 3.43 (dd, $J = 9.9, 6.7$ Hz, 1 H), 3.26 (s, 3 H), 3.02 (dd, $J = 12, 7.2$ Hz, 1 H), 2.71 (dd, $J = 13, 6.0$ Hz, 1 H), 2.29 (s, 3 H), 2.18 (t, $J = 13$ Hz, 1 H), 1.52 (d, $J = 6.7$ Hz, 3 H). ^{13}C NMR (CDCl_3 75 MHz) δ 159.7 (C), 158.0 (C), 139.4 (C), 133.0 (C), 130.2 (CH), 129.2 (C), 128.7 (CH), 128.4 (CH), 128.4 (CH), 128.1 (CH), 127.9 (CH), 127.2 (CH), 114.4 (CH), 114.3 (CH), 83.9 (C), 70.5 (CH), 63.5 (CH), 60.4 (CH), 59.4 (CH_2), 55.5 (CH_3), 55.5 (CH_3), 55.2 (CH_3), 50.3 (CH), 41.5 (CH), 40.4 (CH_2), 37.0 (CH_3), 11.5 (CH_3).

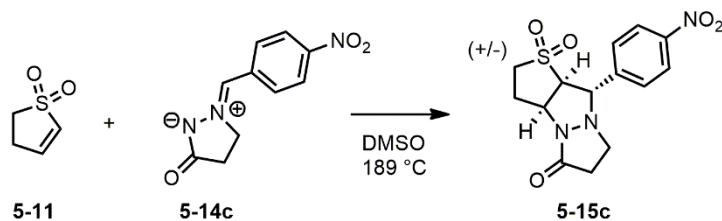
General procedure for the dipolar cycloaddition: The vinyl sulfone **5-11**, **5-16**, **5-18**, **5-19** or **2-7e** (0.5 mmol) and 1,3-dipole **5-15a**, **5-15b** or **5-15c** (3 equiv.) were combined in dry 2.0 mL DMSO (or bromobenzene), and the resulting solution was heated under reflux in a sand bath. After 24 h, the solution was concentrated under vacuum at 50 °C. Flash column chromatography (98:2 to 90:10 methanol:dichloromethane gradient) afforded the desired adduct. Yields reported are calculated from the initial 2-sulfolene starting material.



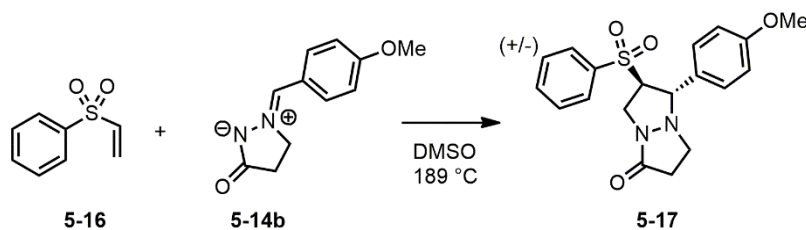
5-15a: brown solid (86% yield); Mp 189–192 °C; IR (film) 1694, 1514, 1302, 1254, 1112 cm^{-1} ; ^1H NMR (CDCl_3 300 MHz) δ 7.17–7.07 (m, 2 H), 6.92 (d, $J = 8.8$ Hz, 2 H), 5.01 (br s, 1 H), 4.46 (br s, 1 H), 3.81 (s, 3 H), 3.75 (dd, $J = 7.8, 1.9$ Hz, 1 H), 3.34–3.08 (m, 4 H), 2.80 (br s, 1 H), 2.59–2.27 (m, 2 H), 1.80 (br s, 1 H); ^{13}C NMR (CDCl_3 , 75 MHz) δ 160.3 (C), 129.7 (CH), 125.9 (C), 114.7 (CH), 70.4 (br CH), 69.0 (br CH), 55.3 (CH), 55.2 (CH_3), 48.2 (CH_2), 44.6 (br, CH_2), 32.8 (br, CH_2), 25.8 (br, CH_2); HRMS calcd for $\text{C}_{15}\text{H}_{18}\text{N}_2\text{O}_4\text{S}$ (M^+): 322.0987. Found: 322.0983.



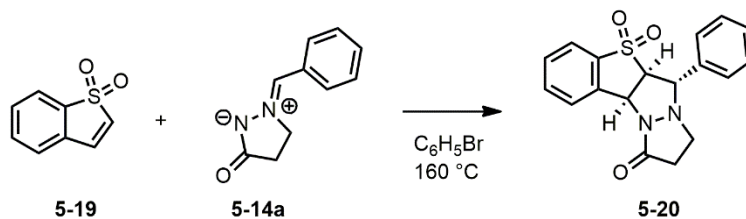
5-15b: brown solid (84% yield); Mp 134–137 °C; IR (film) 1693, 1303, 1114 cm^{-1} ; ^1H NMR (CDCl_3 300 MHz) δ 7.43–7.37 (m, 3 H), 7.27–7.20 (m, 2 H), 5.00 (br s, 1 H), 4.46 (br s, 1 H), 3.79 (dd, $J = 7.8, 2.6$ Hz, 1 H), 3.33–3.12 (m, 4H), 2.87 (br s, 1 H), 2.58–2.34 (m, 2 H), 2.01 (br s, 1 H); ^{13}C NMR (CDCl_3 75 MHz) δ 134.3 (C), 129.2 (CH), 129.2 (CH), 128.3 (CH), 70.5 (CH), 69.3 (CH), 55.2 (CH), 48.1 (CH_2), 44.9 (br, CH_2), 33.4 (br, CH_2), 25.4 (br, CH_2); HRMS calcd for $\text{C}_{14}\text{H}_{16}\text{N}_2\text{O}_3\text{S}$ (M^+): 292.0882. Found: 292.0883.



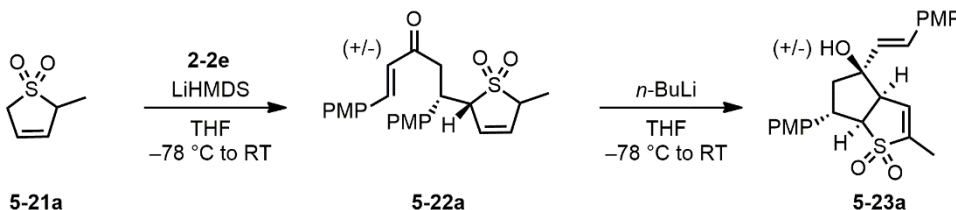
5-15c: brown solid (56% yield); Mp 201–203 °C; IR (film) 1694, 1520, 1349, 1305, 1113 cm^{-1} ; ^1H NMR (CDCl_3 300 MHz) δ 8.27 (d, $J = 8.8$ Hz, 2 H), 7.61 (d, $J = 8.6$ Hz, 2 H), 4.81 (br t, $J = 6.4$ Hz, 1 H), 4.32 (br d, $J = 4.9$ Hz, 1 H), 3.69 (dd, $J = 7.8, 5.8$ Hz, 1 H), 3.40–2.94 (m, 5 H), 2.77–2.36 (m, 3 H); ^{13}C NMR (CDCl_3 75 MHz) δ 148.4 (C), 142.4 (C), 128.9 (CH), 124.4 (CH), 69.6 (CH), 55.3 (CH), 47.9 (CH_2); HRMS calcd for $\text{C}_{14}\text{H}_{15}\text{N}_3\text{O}_5\text{S}$ (M^+): 337.0732. Found: 337.0730.



5-17: brown solid (68% yield); Mp 184–186 °C; IR (film) 1708, 1515, 1307, 1251, 1149 cm^{-1} ; ^1H NMR (CDCl_3 300 MHz) δ 7.80, (d, $J = 7.3$ Hz, 2 H), 7.60 (t, $J = 7.4$ Hz, 1 H), 7.48 (t, $J = 7.6$ Hz, 2 H), 7.25 (d, $J = 8.7$ Hz, 2 H), 6.81 (d, $J = 8.7$ Hz, 2 H), 4.35 (dd, $J = 13, 3.7$ Hz, 1 H), 4.05–3.95 (m, 2 H), 3.79 (s, 3 H), 3.54 (dd, $J = 12, 8.0$ Hz, 1 H), 3.47 (dt, $J = 12, 9.1$ Hz, 1 H), 3.10 (ddd, $J = 12, 9.5, 4.7$ Hz, 1 H), 2.80 (dt, $J = 18, 8.9$ Hz, 1 H), 2.61 (ddd, $J = 18, 9.3, 4.8$ Hz, 1 H); ^{13}C NMR (CDCl_3 75 MHz) δ 174.2 (C), 160.1 (C), 137.5 (C), 134.2 (CH), 129.4 (CH), 128.6 (CH), 127.3 (C), 114.3 (CH), 72.0 (CH), 68.5 (CH), 55.3 (CH_3), 45.3 (CH_2), 42.6 (CH_2), 30.0 (CH_2); HRMS calcd for $\text{C}_{19}\text{H}_{20}\text{N}_2\text{O}_4\text{S}$ ($\text{M}+\text{H}$), 373.1217. Found: 373.1214.



5-20: oil (95% yield); IR (film) 1698, 1304, 1150 cm^{-1} ; ^1H NMR (CDCl_3 300 MHz) δ 7.96–7.84 (m, 1 H), 7.81 (d, $J = 7.7$ Hz, 1 H), 7.73 (td, $J = 7.5, 1.2$ Hz, 1 H), 7.64 (br t, $J = 7.7$, 1 H), 7.47–7.40 (m, 3 H), 7.32–7.22 (m, 2 H), 6.06 (d, $J = 8.1$ Hz, 1 H), 4.78 (br s, 1 H), 4.42 (dd, $J = 8.2, 2.5$ Hz, 1 H), 3.34–3.17 (m, 1 H), 3.15–3.02 (m, 1 H), 2.36–2.18 (m, 1 H), 1.94–1.62 (m, 1 H); ^{13}C NMR (CDCl_3 75 MHz) δ 172.4 (C), 138.9 (C), 134.5 (CH), 134.2 (C), 134.1 (C), 131.0 (CH), 129.4 (CH), 129.4 (CH), 128.9 (CH), 121.2 (CH), 70.1 (CH), 68.1 (CH), 56.1 (CH), 43.8 (CH_2), 32.6 (CH_2); HRMS calcd for $\text{C}_{18}\text{H}_{16}\text{N}_2\text{O}_3\text{S}$ ($\text{M}+\text{Na}$): 363.0774. Found: 363.0771.



reaction was quenched by the addition of saturated aqueous NH_4Cl (10 mL), and the resulting solution was concentrated in vacuo. The residue was partitioned between dichloromethane extracted twice with dichloromethane. The organic fraction was dried with Na_2SO_4 then concentrated in vacuo at 30 °C. Flash column chromatography of a 2.71 g sample of crude material (50:1 to 10:1 dichloromethane:tetrahydrofuran gradient) afforded 920 mg of **5-23a** (34% from **5-21a**).

5-23a: yellow solid; $R_f = 0.2$ (dichloromethane:ethyl acetate, 50:1); IR (film) 3477, 1277, 1108 cm^{-1} ; ^1H NMR (CDCl_3 500 MHz) δ 7.33 (d, $J = 8.6$ Hz, 2 H), 7.26 (d, $J = 8.8$ Hz, 2 H), 6.88 (d, $J = 8.6$ Hz, 2 H), 6.87 (d, $J = 8.7$ Hz, 2 H), 6.71 (d, $J = 16$ Hz, 1 H), 6.20 (d, $J = 16$ Hz, 1 H) 6.11 (q, $J = 1.7$ Hz, 1 H), 4.16 (dt, $J = 12, 7.3$ Hz, 1 H), 3.82 (s, 3 H), 3.70 (s, 3 H), 3.73 (dd, $J = 9.6, 8.3$ Hz, 1 H), 3.62-3.47 (m, 1 H), 2.39 (dd, $J = 13, 6.7$ Hz, 1 H), 2.34 (t, $J = 13$ Hz, 1 H), 2.10 (br s, 3 H); ^{13}C NMR (CDCl_3 125 MHz) δ 159.7 (C), 158.8 (C), 142.6 (C), 132.9 (C), 129.4 (CH), 129.1 (CH), 128.8 (C), 128.7 (CH), 128.4 (CH), 127.9 (CH), 114.4 (CH), 114.3 (CH), 80.7 (C), 67.8 (CH), 55.4 (CH_3), 55.4 (CH_3), 55.4 (CH), 50.2 (CH_2), 42.6 (CH), 9.5 (CH_3); HRMS (ESI) calcd for $\text{C}_{24}\text{H}_{26}\text{O}_5\text{S}$ (M+Na): 449.1393. Found: 449.1388.

Bibliography

1. N. J. Cox and K. Subbarao, *Annual Review of Medicine*, **2000**, 51, 407-421.
2. E. D. Kilbourne, *Emerging Infectious Diseases*, **2006**, 12, 9-14.
3. F. S. Dawood, A. D. Luliano, C. Reed, M. I. Meltzer, D. K. Shay, P.-Y. Cheng, D. Bandaranayake, R. F. Breiman, W. A. Brooks, P. Buchy, D. R. Feikin, K. B. Fowler, A. Gordon, N. T. Hien, P. Horby, Q. S. Huang, M. A. Katz, A. Krishnan, R. Lal, J. M. Montgomery, K. Mølbak, R. Pebody, A. M. Presanis, H. Razuri, A. Steens, Y. O. Tinoco, J. Wallinga, H. Yu, S. Vong, J. Bresee and M.-A. Widdowson, *The Lancet Infectious Diseases*, **2012**, 12, 687-695.
4. J. Taubenberger and D. Morens, *Emerging Infectious Diseases*, **2006**, 12, 15-22.
5. R. G. Webster, W. J. Bean, O. T. Gorman, T. M. Chambers and Y. Kawaoka, *Microbiological Reviews*, **1992**, 56, 152-179.
6. G. Karl, M. John and Z. Maria, *The Lancet*, **2003**, 362, 1733-1745.
7. G. Brankston, L. Gitterman, Z. Hirji, C. Lemieux and M. Gardam, *The Lancet Infectious Diseases*, **2007**, 7, 257-265.
8. J. K. Taubenberger and D. M. Morens, *Annual Review of Pathology*, **2008**, 3, 499-522.
9. Influenza (Seasonal) Fact sheet N°211 March 2014. Accessed February 4th, 2015.
10. K. G. Nicholson, J. M. Wood and M. Zambon, *The Lancet*, **2003**, 362, 1733-1745.
11. R. J. Russell, L. F. Haire, D. J. Stevens, P. J. Collins, Y. P. Lin, G. M. Blackburn, A. J. Hay, S. J. Gamblin and J. J. Skehel, *Nature*, **2006**, 443, 45-49.
12. J. K. Taubenberger and D. M. Morens, *Annual Review of Pathology: Mechanisms of Disease*, **2008**, 3, 499-522.
13. Y. Wu, Y. Wu, B. Tefsen, Y. Shi and G. F. Gao, *Trends in Microbiology*, **2014**, 22, 183-191.
14. L. Glaser, J. Stevens, D. Zamarin, I. A. Wilson, A. García-Sastre, T. M. Tumpey, C. F. Basler, J. K. Taubenberger and P. Palese, *Journal of Virology*, **2005**, 79, 11533-11536.
15. W. Laver, J. C. Downie and R. Webster, *Virology*, **1974**, 59, 230-244.
16. P. Palese, *Cell*, **1977**, 10, 1-10.

17. J. J. Skehel and D. C. Wiley, *Annual Review of Biochemistry*, **2000**, 69, 531-569.
18. R. Ruigrok, P. Andree, R. H. Van Huysduynen and J. Mellema, *Journal of General Virology*, **1984**, 65, 799-802.
19. R. G. Webster, W. J. Bean, O. T. Gorman, T. M. Chambers and Y. Kawaoka, *Microbiological Reviews*, **1992**, 56, 152-179.
20. H. Leonov, P. Astrahan, M. Krugliak and I. T. Arkin, *Journal of the American Chemical Society*, **2011**, 133, 9903-9911.
21. W. Chen, P. A. Calvo, D. Malide, J. Gibbs, U. Schubert, I. Bacik, S. Basta, R. O'Neill, J. Schickli and P. Palese, *Nature Medicine*, **2001**, 7, 1306-1312.
22. H. M. Wise, A. Foeglein, J. Sun, R. M. Dalton, S. Patel, W. Howard, E. C. Anderson, W. S. Barclay and P. Digard, *Journal of Virology*, **2009**, 83, 8021-8031.
23. B. Jagger, H. Wise, J. Kash, K.-A. Walters, N. Wills, Y.-L. Xiao, R. Dunfee, L. Schwartzman, A. Ozinsky and G. Bell, *Science*, **2012**, 337, 199-204.
24. H. M. Wise, E. C. Hutchinson, B. W. Jagger, A. D. Stuart, Z. H. Kang, N. Robb, L. M. Schwartzman, J. C. Kash, E. Fodor and A. E. Firth, *PLOS Pathogens*, **2012**, 8.
25. R. E. O'Neill, J. Talon and P. Palese, *The EMBO Journal*, **1998**, 17, 288-296.
26. M. R. Hilleman, *Vaccine*, **2002**, 20, 3068-3087.
27. C. A. Russell, T. C. Jones, I. G. Barr, N. J. Cox, R. J. Garten, V. Gregory, I. D. Gust, A. W. Hampson, A. J. Hay and A. C. Hurt, *Vaccine*, **2008**, 26, D31-D34.
28. J. A. Wilde, J. A. McMillan, J. Serwint, J. Butta, M. A. O'Riordan and M. C. Steinhoff, *The Journal of the American Medical Association*, **1999**, 281, 908-913.
29. K. Fukuda, D. O'Mara and J. A. Singleton, *Pharmacy and Therapeutics*, **2002**, 27, 235-242.
30. A. Hay, A. Wolstenholme, J. Skehel and M. H. Smith, *The EMBO journal*, **1985**, 4, 3021-3024.
31. M. Khan, N. T. Rangari, T. Kalyankar and P. C. Agarwal, *International Journal of Research in Pharmaceutical and Biomedical Sciences*, **2011**, 2, 52-58.
32. R. M. Pielak, J. R. Schnell and J. J. Chou, *Proceedings of the National Academy of Sciences*, **2009**, 106, 7379-7384.

33. V. M. Deyde, X. Xu, R. A. Bright, M. Shaw, C. B. Smith, Y. Zhang, Y. Shu, L. V. Gubareva, N. J. Cox and A. I. Klimov, *Journal of Infectious Diseases*, **2007**, 196, 249-257.
34. R. A. Bright, D. K. Shay, B. Shu, N. J. Cox and A. I. Klimov, *The Journal of the American Medical Association*, **2006**, 295, 891-894.
35. J. Wang, Y. Wu, C. Ma, G. Fiorin, J. Wang, L. H. Pinto, R. A. Lamb, M. L. Klein and W. F. DeGrado, *Proceedings of the National Academy of Sciences*, **2013**, 110, 1315-1320.
36. J. Wang, C. Ma, G. Fiorin, V. Carnevale, T. Wang, F. Hu, R. A. Lamb, L. H. Pinto, M. Hong, M. L. Klein and W. F. DeGrado, *Journal of the American Chemical Society*, **2011**, 133, 12834-12841.
37. V. Balannik, J. Wang, Y. Ohigashi, X. Jing, E. Magavern, R. A. Lamb, W. F. DeGrado and L. H. Pinto, *Biochemistry*, **2009**, 48, 11872-11882.
38. R. B. Moss, C. Hansen, R. L. Sanders, S. Hawley, T. Li and R. T. Steigbigel, *The Journal of Infectious diseases*, **2012**, 206, 1844-1851.
39. M. P. Malakhov, L. M. Aschenbrenner, D. F. Smee, M. K. Wandersee, R. W. Sidwell, L. V. Gubareva, V. P. Mishin, F. G. Hayden, D. H. Kim, A. Ing, E. R. Campbell, M. Yu and F. Fang, *Antimicrobial Agents and Chemotherapy*, **2006**, 50, 1470-1479.
40. Y. Furuta, B. B. Gowen, K. Takahashi, K. Shiraki, D. F. Smee and D. L. Barnard, *Antiviral Research*, **2013**, 100, 446-454.
41. S. J. Smither, L. S. Eastaugh, J. A. Steward, M. Nelson, R. P. Lenk and M. S. Lever, *Antiviral Research*, **2014**, 104, 153-155.
42. T. Baranovich, S.-S. Wong, J. Armstrong, H. Marjuki, R. J. Webby, R. G. Webster and E. A. Govorkova, *Journal of Virology*, **2013**, 87, 3741-3751.
43. R. Y. Kao, D. Yang, L.-S. Lau, W. H. W. Tsui, L. Hu, J. Dai, M.-P. Chan, C.-M. Chan, P. Wang, B.-J. Zheng, J. Sun, J.-D. Huang, J. Madar, G. Chen, H. Chen, Y. Guan and K.-Y. Yuen, *Nature Biotechnology*, **2010**, 28, 600-605.
44. J. Yang, M. Li, X. Shen and S. Liu, *Viruses*, **2013**, 5, 352-373.
45. A. Basu, A. Antanasijevic, M. Wang, B. Li, D. M. Mills, J. A. Ames, P. J. Nash, J. D. Williams, N. P. Peet, D. T. Moir, M. N. Prichard, K. A. Keith, D. L.

- Barnard, M. Caffrey, L. Rong and T. L. Bowlin, *Journal of Virology*, **2014**, 88, 1447-1460.
46. M. P. Walkiewicz, D. Basu, J. J. Jablonski, H. M. Geysen and D. A. Engel, *Journal of General Virology*, **2011**, 92, 60-70.
47. Center for Disease Control and Prevention, *Morbidity and Mortality Weekly Report*, **2006**, 55, 44-46.
48. Y. Abed, M. Baz and G. Boivin, *Antiviral Therapy*, **2006**, 11, 971-976.
49. R. Schauer, in *Advances in Carbohydrate Chemistry and Biochemistry*, Academic Press, **1982**, 40, 131-234.
50. Z. Huang, A. Panda, S. Elankumaran, D. Govindarajan, D. D. Rockemann and S. K. Samal, *Journal of Virology*, **2004**, 78, 4176-4184.
51. C. W. Cairo, *Medicinal Chemistry Communications*, **2014**, 5, 1067-1074.
52. H. Streicher, *Current Medicinal Chemistry-Anti-Infective Agents*, **2004**, 3, 149-161.
53. G. Harth, C. G. Haidaris and M. So, *Proceedings of the National Academy of Sciences*, **1987**, 84, 8320-8324.
54. J. C. Telford, J. H. F. Yeung, G. Xu, M. J. Kiefel, A. G. Watts, S. Hader, J. Chan, A. J. Bennet, M. M. Moore and G. L. Taylor, *Journal of Biological Chemistry*, **2011**, 286, 10783-10792.
55. R. Schauer, *Trends in Biochemical Sciences*, **1985**, 10, 357-360.
56. W. Colli, *The FASEB Journal*, **1993**, 7, 1257-1264.
57. A. Buschiazzo, M. F. Amaya, M. L. Cremona, A. C. Frasch and P. M. Alzari, *Molecular Cell*, **2002**, 10, 757-768.
58. G. Xu, M. J. Kiefel, J. C. Wilson, P. W. Andrew, M. R. Oggioni and G. L. Taylor, *Journal of the American Chemical Society*, **2011**, 133, 1718-1721.
59. J. N. Varghese, J. L. McKimm-Breschkin, J. B. Caldwell, A. A. Kortt and P. M. Colman, *Proteins: Structure, Function, and Bioinformatics*, **1992**, 14, 327-332.
60. M. R. Lentz, R. G. Webster and G. M. Air, *Biochemistry*, **1987**, 26, 5351-5358.
61. D. Kobasa, S. Kodihalli, M. Luo, M. R. Castrucci, I. Donatelli, Y. Suzuki, T. Suzuki and Y. Kawaoka, *Journal of Virology*, **1999**, 73, 6743-6751.

62. A. Albohy, M. D. Li, R. B. Zheng, C. Zou and C. W. Cairo, *Glycobiology*, **2010**, 1127-1138.
63. A. K. Chong, M. S. Pegg, N. R. Taylor and M. von Itzstein, *European Journal of Biochemistry*, **1992**, 207, 335-343.
64. J. Chan, A. R. Lewis, M. Gilbert, M.-F. Karwaski and A. J. Bennet, *Nature Chemical Biology*, **2010**, 6, 405-407.
65. A. G. Watts, I. Damager, M. L. Amaya, A. Buschiazzo, P. Alzari, A. C. Frasch and S. G. Withers, *Journal of the American Chemical Society*, **2003**, 125, 7532-7533.
66. J. Chan and A. J. Bennet, in *Influenza Virus Sialidase-A Drug Discovery Target*, Springer, **2012**, 47-66.
67. J.-H. Kim, R. Resende, T. Wennekes, H.-M. Chen, N. Bance, S. Buchini, A. G. Watts, P. Pilling, V. A. Streltsov and M. Petric, *Science*, **2013**, 340, 71-75.
68. J. Chan, J. N. Watson, A. Lu, V. C. Cerda, T. J. Borgford and A. J. Bennet, *Biochemistry*, **2011**, 51, 433-441.
69. J. N. Varghese, W. G. Laver and P. M. Colman, *Nature*, **1983**, 303, 35-40.
70. A. P. Corfield, H. Higa, J. C. Paulson and R. Schauer, *Biochimica et Biophysica Acta - Protein Structure and Molecular Enzymology*, **1983**, 744, 121-126.
71. B. Dale, R. Brown, J. Miller, R. T. White, G. M. Air and B. Cordell, *Virology*, **1986**, 155, 460-468.
72. C. Liu, M. C. Eichelberger, R. W. Compans and G. M. Air, *Journal of Virology*, **1995**, 69, 1099-1106.
73. P. Palese, K. Tobita, M. Ueda and R. W. Compans, *Virology*, **1974**, 61, 397-410.
74. P. Meindl and H. Tuppy, *Monatshefte für Chemie/Chemical Monthly*, **1969**, 100, 1295-1306.
75. P. Meindl, G. Bodo, P. Palese, J. Schulman and H. Tuppy, *Virology*, **1974**, 58, 457-463.
76. C. T. Holzer, M. von Itzstein, B. Jin, M. S. Pegg, W. P. Stewart and W. Y. Wu, *Glycoconjugate Journal*, **1993**, 10, 40-44.
77. P. Palese and R. Compans, *Journal of General Virology*, **1976**, 33, 159-163.

78. U. Nöhle, J. M. Beau and R. Schauer, *European Journal of Biochemistry*, **1982**, 126, 543-548.
79. M. von Itzstein, W. Y. Wu, G. B. Kok, M. S. Pegg, J. C. Dyason, B. Jin, T. Van Phan, M. L. Smythe, H. F. White, S. W. Oliver, P. M. Colman, J. N. Varghese, D. Michael Ryan, J. M. Woods, R. C. Bethell, V. J. Hotman, J. M. Cameron and C. R. Penn, *Nature*, **1993**, 363, 418-423.
80. L. R. Cass, C. Efthymiopoulos and A. Bye, *Clinical Pharmacokinetics*, **1999**, 36, 1-11.
81. A. S. Monto, D. M. Fleming, D. Henry, R. de Groot, M. Makela, T. Klein, M. Elliott, O. N. Keene and C. Y. Man, *The Journal of Infectious Diseases*, **1999**, 180, 254-261.
82. M. Yamashita, T. Tomozawa, M. Kakuta, A. Tokumitsu, H. Nasu and S. Kubo, *Antimicrobial Agents and Chemotherapy*, **2009**, 53, 186-192.
83. S. J. Macdonald, K. G. Watson, R. Cameron, D. K. Chalmers, D. A. Demaine, R. J. Fenton, D. Gower, J. N. Hamblin, S. Hamilton, G. J. Hart, G. G. Inglis, B. Jin, H. T. Jones, D. B. McConnell, A. M. Mason, V. Nguyen, I. J. Owens, N. Parry, P. A. Reece, S. E. Shanahan, D. Smith, W. Y. Wu and S. P. Tucker, *Antimicrobial Agents and Chemotherapy*, **2004**, 48, 4542-4549.
84. S. Ogawa, M. Yoshikawa and T. Taki, *Journal of the Chemical Society, Chemical Communications*, **1992**, 406-408.
85. M. Chandler, R. Conroy, A. W. J. Cooper, R. B. Lamont, J. J. Scicinski, J. E. Smart, R. Storer, N. G. Weir, R. D. Wilson and P. G. Wyatt, *Journal of the Chemical Society, Perkin Transactions 1*, **1995**, 1189-1197.
86. C. U. Kim, W. Lew, M. A. Williams, H. Liu, L. Zhang, S. Swaminathan, N. Bischofberger, M. S. Chen, D. B. Mendel, C. Y. Tai, W. G. Laver and R. C. Stevens, *Journal of the American Chemical Society*, **1997**, 119, 681-690.
87. B. E. Davies, *Journal of Antimicrobial Chemotherapy*, **2010**, 65, ii5-ii10.
88. W. Lew, X. Chen and C. U. Kim, *Current Medicinal Chemistry*, **2000**, 7, 663-672.
89. B. E. Davies, *The Journal of Antimicrobial Chemotherapy*, **2010**, 65, Suppl 2, ii5-ii10.

90. W. Li, P. A. Escarpe, E. J. Eisenberg, K. C. Cundy, C. Sweet, K. J. Jakeman, J. Merson, W. Lew, M. Williams, L. Zhang, C. U. Kim, N. Bischofberger, M. S. Chen and D. B. Mendel, *Antimicrobial Agents and Chemotherapy*, **1998**, 42, 647-653.
91. J. Sun, J. M. Miller, A. Beig, L. Rozen, G. L. Amidon and A. Dahan, *Expert Opinion on Drug Metabolism and Toxicology*, **2011**, 7, 313-323.
92. T. Yamamoto, H. Kumazawa, K. Inami, T. Teshima and T. Shiba, *Tetrahedron Letters*, **1992**, 33, 5791-5794.
93. Y. S. Babu, P. Chand, S. Bantia, P. Kotian, A. Dehghani, Y. El-Kattan, T. H. Lin, T. L. Hutchison, A. J. Elliott, C. D. Parker, S. L. Ananth, L. L. Horn, G. W. Laver and J. A. Montgomery, *Journal of Medicinal Chemistry*, **2000**, 43, 3482-3486.
94. P. Chand, P. L. Kotian, A. Dehghani, Y. El-Kattan, T. H. Lin, T. L. Hutchison, Y. S. Babu, S. Bantia, A. J. Elliott and J. A. Montgomery, *Journal of Medicinal Chemistry*, **2001**, 44, 4379-4392.
95. P. Paolo, *Expert Opinion on Pharmacotherapy*, **2011**, 12, 1523-1549.
96. D. Zhang, A. Du, L. Zhang, J. Ma, L. Meng, M. Deng, J. Xu and H. Liu, *Xenobiotica*, **2015**, 45, 239-243.
97. D. Birnkrant and E. Cox, *New England Journal of Medicine*, **2009**, 361, 2204-2207.
98. M. Abramowicz, G. Zuccotti and J.-M. Pflomm, *The Journal of the American Medical Association*, **2015**, 313, 413-414.
99. G. T. Wang, Y. Chen, S. Wang, R. Gentles, T. Sowin, W. Kati, S. Muchmore, V. Giranda, K. Stewart and H. Sham, *Journal of Medicinal Chemistry*, **2001**, 44, 1192-1201.
100. V. Stoll, K. D. Stewart, C. J. Maring, S. Muchmore, V. Giranda, Y.-G. Y. Gu, G. Wang, Y. Chen, M. Sun and C. Zhao, *Biochemistry*, **2003**, 42, 718-727.
101. C. J. Maring, V. S. Stoll, C. Zhao, M. Sun, A. C. Krueger, K. D. Stewart, D. L. Madigan, W. M. Kati, Y. Xu and R. J. Carrick, *Journal of Medicinal Chemistry*, **2005**, 48, 3980-3990.

102. A. C. Krueger, Y. Xu, W. M. Kati, D. J. Kempf, C. J. Maring, K. F. McDaniel, A. Molla, D. Montgomery and W. E. Kohlbrenner, *Bioorganic & Medicinal Chemistry Letters*, **2008**, 18, 1692-1695.
103. M. Baz, Y. Abed, B. Nehme and G. Boivin, *Antimicrobial Agents and Chemotherapy*, **2009**, 53, 791-793.
104. E. Sudbeck, M. Jedrzejewski, S. Singh, W. Brouillette, G. Air, W. Laver, Y. Babu, S. Bantia, P. Chand and N. Chu, *Journal of Molecular Biology*, **1997**, 267, 584-594.
105. M. Williams, N. Bischofberger, S. Swaminathan and C. U. Kim, *Bioorganic & Medicinal Chemistry Letters*, **1995**, 5, 2251-2254.
106. V. R. Atigadda, W. J. Brouillette, F. Duarte, Y. S. Babu, S. Bantia, P. Chand, N. Chu, J. A. Montgomery, D. A. Walsh and E. Sudbeck, *Bioorganic & Medicinal Chemistry*, **1999**, 7, 2487-2497.
107. W. J. Brouillette, S. N. Bajpai, S. M. Ali, S. E. Velu, V. R. Atigadda, B. S. Lommer, J. B. Finley, M. Luo and G. M. Air, *Bioorganic & Medicinal Chemistry*, **2003**, 11, 2739-2749.
108. P. J. P. Adabala, E. B. LeGresley, N. Bance, M. Niikura and B. M. Pinto, *The Journal of Organic Chemistry*, **2013**, 78, 10867-10877.
109. N. J. Dharan, L. V. Gubareva, J. J. Meyer, M. Okomo-Adhiambo, R. C. McClinton, S. A. Marshall, K. St. George, S. Epperson, L. Brammer, A. I. Klimov, J. S. Bresee and A. M. Fry, *The Journal of the American Medical Association*, **2009**, 301, 1034-1041.
110. D. M. Weinstock and G. Zuccotti, *The Journal of the American Medical Association*, **2009**, 301, 1066-1069.
111. J. McKimm-Breschkin, A. Sahasrabudhe, T. Blick and M. McDonald, *International Congress Series*, **2001**, 1219, 855-861.
112. M. Baz, Y. Abed, B. Nehmé and G. Boivin, *Antimicrobial Agents and Chemotherapy*, **2009**, 53, 791-793.
113. T. Zürcher, P. J. Yates, J. Daly, A. Sahasrabudhe, M. Walters, L. Dash, M. Tisdale and J. L. McKimm-Breschkin, *Journal of Antimicrobial Chemotherapy*, **2006**, 58, 723-732.

114. A. C. Hurt, J. K. Holien, M. Parker, A. Kelso and I. G. Barr, *Journal of Virology*, **2009**, 83, 10366-10373.
115. L. V. Gubareva, M. N. Matrosovich, M. K. Brenner, R. C. Bethell and R. G. Webster, *The Journal of Infectious Diseases*, **1998**, 178, 1257-1262.
116. B. J. Smith, J. L. McKimm-Breshkin, M. McDonald, R. T. Fernley, J. N. Varghese and P. M. Colman, *Journal of Medicinal Chemistry*, **2002**, 45, 2207-2212.
117. Y. Abed, B. Nehme, M. Baz and G. Boivin, *Antiviral Research*, **2008**, 77, 163-166.
118. T. Miyagi and K. Yamaguchi, *Glycobiology*, **2012**, 22, 880-896.
119. Y. Pilatte, J. Bignon and C. R. Lambré, *Glycobiology*, **1993**, 3, 201-218.
120. N. M. Stamatou, F. Liang, X. Nan, K. Landry, A. S. Cross, L.-X. Wang and A. V. Pshezhetsky, *FEBS Journal*, **2005**, 272, 2545-2556.
121. N. Papini, L. Anastasia, C. Tringali, L. Dileo, I. Carubelli, M. Sampaolesi, E. Monti, G. Tettamanti and B. Venerando, *Journal of Cellular Biochemistry*, **2012**, 113, 2967-2978.
122. A. Fanzani, A. Zanola, F. Faggi, N. Papini, B. Venerando, G. Tettamanti, M. Sampaolesi and E. Monti, *Skeletal Muscle*, **2012**, 2, 23-33.
123. S. Ueno, S. Saito, T. Wada, K. Yamaguchi, M. Satoh, Y. Arai and T. Miyagi, *Journal of Biological Chemistry*, **2006**, 281, 7756-7764.
124. T. Miyagi, T. Wada, K. Yamaguchi and K. Hata, *Glycoconjugate Journal*, **2003**, 20, 189-198.
125. M. Arabkhari, S. Bunda, Y. Wang, A. Wang, A. V. Pshezhetsky and A. Hinek, *Glycobiology*, **2010**, 20, 603-616.
126. Y. Natori, N. Ohkura, M. Nasui, G.-i. Atsumi and F. Kihara-Negishi, *Biological and Pharmaceutical Bulletin*, **2013**, 36, 1027-1031.
127. Y. Kakugawa, T. Wada, K. Yamaguchi, H. Yamanami, K. Ouchi, I. Sato and T. Miyagi, *Proceedings of the National Academy of Sciences*, **2002**, 99, 10718-10723.
128. H. Yamanami, K. Shiozaki, T. Wada, K. Yamaguchi, T. Uemura, Y. Kakugawa, T. Hujjiya and T. Miyagi, *Cancer Science*, **2007**, 98, 299-307.

129. V. Seyrantepe, H. Poupetova, R. Froissart, M.-T. Zabet, I. Maire and A. V. Pshezhetsky, *Human Mutation*, **2003**, 22, 343-352.
130. A. J. G. Jansen, E. C. Josefsson, V. Rumjantseva, Q. P. Liu, H. Falet, W. Bergmeier, S. M. Cifuni, R. Sackstein, U. H. von Andrian, D. D. Wagner, J. H. Hartwig and K. M. Hoffmeister, *Blood*, **2012**, 119, 1263-1273.
131. L. M. G. Chavas, C. Tringali, P. Fusi, B. Venerando, G. Tettamanti, R. Kato, E. Monti and S. Wakatsuki, *Journal of Biological Chemistry*, **2005**, 280, 469-475.
132. S. Magesh, T. Suzuki, T. Miyagi, H. Ishida and M. Kiso, *Journal of Molecular Graphics and Modelling*, **2006**, 25, 196-207.
133. A. Albohy, M. D. Li, R. B. Zheng, C. Zou and C. W. Cairo, *Glycobiology*, **2010**, 20, 1127-1138.
134. A. Albohy, S. Mohan, R. B. Zheng, B. M. Pinto and C. W. Cairo, *Bioorganic & Medicinal Chemistry*, **2011**, 19, 2817-2822.
135. S. Magesh, V. Savita, S. Moriya, T. Suzuki, T. Miyagi, H. Ishida and M. Kiso, *Bioorganic & Medicinal Chemistry*, **2009**, 17, 4595-4603.
136. Y. Zhang, A. Albohy, Y. Zou, V. Smutova, A. V. Pshezhetsky and C. W. Cairo, *Journal of Medicinal Chemistry*, **2013**, 56, 2948-2958.
137. Y. Zou, A. Albohy, M. Sandbhor and C. W. Cairo, *Bioorganic & Medicinal Chemistry Letters*, **2010**, 20, 7529-7533.
138. K. Hata, K. Koseki, K. Yamaguchi, S. Moriya, Y. Suzuki, S. Yingsakmongkon, G. Hirai, M. Sodeoka, M. von Itzstein and T. Miyagi, *Antimicrobial Agents and Chemotherapy*, **2008**, 52, 3484-3491.
139. S. Magesh, S. Moriya, T. Suzuki, T. Miyagi, H. Ishida and M. Kiso, *Bioorganic & Medicinal Chemistry Letters*, **2008**, 18, 532-537.
140. A. Albohy, Y. Zhang, V. Smutova, A. V. Pshezhetsky and C. W. Cairo, *ACS Medicinal Chemistry Letters*, **2013**, 4, 532-537.
141. S. Kim, D.-B. Oh, H. A. Kang and O. Kwon, *Applied Microbiology and Biotechnology*, **2011**, 91, 1-15.
142. G. Soong, A. Muir, M. I. Gomez, J. Waks, B. Reddy, P. Planet, P. K. Singh, Y. Kanetko, M. C. Wolfgang and Y.-S. Hsiao, *The Journal of Clinical Investigation*, **2006**, 116, 2297-2305.

143. D. Parker, G. Soong, P. Planet, J. Brower, A. J. Ratner and A. Prince, *Infection and Immunity*, **2009**, 77, 3722-3730.
144. L. Rohmer, D. Hocquet and S. I. Miller, *Trends in Microbiology*, **2011**, 19, 341-348.
145. Cholera Fact sheet N°107 Reviewed February 2014. Accessed February 2015.
146. J. A. McCullers and K. C. Bartmess, *The Journal of Infectious Diseases*, **2003**, 187, 1000-1009.
147. C. T. Holzer, M. Itzstein, B. Jin, M. S. Pegg, W. P. Stewart and W.-Y. Wu, *Glycoconjugate Journal*, **1993**, 10, 40-44.
148. S. L. Newstead, J. A. Potter, J. C. Wilson, G. Xu, C.-H. Chien, A. G. Watts, S. G. Withers and G. L. Taylor, *Journal of Biological Chemistry*, **2008**, 283, 9080-9088.
149. G. Xu, X. Li, P. W. Andrew and G. L. Taylor, *Acta Crystallographica Section F: Structural Biology and Crystallization Communications*, **2008**, 64, 772-775.
150. S. Crennell, E. Garman, G. Laver, E. Vimr and G. Taylor, *Structure*, **1994**, 2, 535-544.
151. H. Gut, G. Xu, G. L. Taylor and M. A. Walsh, *Journal of Molecular Biology*, **2011**, 409, 496-503.
152. T. Jefferson, M. A. Jones, P. Doshi, C. B. Del Mar, R. Hama, M. J. Thompson, E. A. Spencer, I. Onakpoya, K. R. Mahtani, D. Nunan, J. Howick and C. J. Heneghan, *Cochrane Database of Systematic Review*, **2014**, 4, Cd008965.
153. I. Torjesen, *The British Medical Journal: Cochrane Review Questions Effectiveness of Neuraminidase Inhibitors*, **2014**, 348.
154. M. G. Brant, C. M. Bromba and J. E. Wulff, *The Journal of Organic Chemistry*, **2010**, 75, 6312-6315.
155. J. M. McIntosh, 3-Sulfolene in *Encyclopedia of Reagents for Organic Synthesis*, John Wiley & Sons, Ltd., **2001**.
156. L. R. Drake, S. C. Stowe and A. M. Partansky, *Journal of the American Chemical Society*, **1946**, 68, 2521-2524.
157. W. L. Mock, *Journal of the American Chemical Society*, **1975**, 97, 3673-3680.
158. W. L. Mock, *Journal of the American Chemical Society*, **1970**, 92, 3807-3808.

159. N. S. Isaacs and A. A. R. Laila, *Journal of the Chemical Society, Perkin Transactions 2*, **1976**, 1470-1475.
160. H. J. Backer and T. A. H. Blaas, *Recueil des Travaux Chimiques des Pays-Bas*, **1942**, 61, 785-801.
161. D. Craig, *Journal of the American Chemical Society*, **1943**, 65, 1006-1013.
162. T. E. Sample and L. F. Hatch, *Journal of Chemical Education*, **1968**, 45, 55-56.
163. C.-T. Lin and T.-C. Chou, *Synthesis*, **1988**, 1988, 628-630.
164. C. Kaneko, R. Hayashi, H. Fujii and A. Yamamoto, *Chemical and Pharmaceutical Bulletin* **1978**, 26, 3582-3584.
165. S. Yamada, T. Suzuki and H. Takayama, *Tetrahedron Letters*, **1981**, 22, 3085-3088.
166. S. Yamada, T. Suzuki, H. Takayama, K. Miyamoto, I. Matsunaga and Y. Nawata, *The Journal of Organic Chemistry*, **1983**, 48, 3483-3488.
167. K. C. Nicolaou, W. E. Barnette and P. Ma, *The Journal of Organic Chemistry*, **1980**, 45, 1463-1470.
168. T.-S. Chou and S.-S. P. Chou, *Journal of the Chinese Chemical Society*, **1992**, 39, 625-633.
169. R. B. Woodward and R. Hoffmann, *Angewandte Chemie International Edition*, **1969**, 8, 781-853.
170. S. D. McGregor and D. M. Lemal, *Journal of the American Chemical Society*, **1966**, 88, 2858-2859.
171. W. L. Mock, *Journal of the American Chemical Society*, **1975**, 97, 3666-3672.
172. W. L. Mock and J. H. McCausland, *The Journal of Organic Chemistry*, **1976**, 41, 242-247.
173. G. R. Knox and I. G. Thom, *Journal of the Chemical Society, Chemical Communications*, **1981**, 373-374.
174. R. Bloch and J. Abecassis, *Tetrahedron Letters*, **1983**, 24, 1247-1250.
175. H.-H. Tso, T.-S. Chou and Y.-L. Lai, *Journal of the Chinese Chemical Society*, **1989**, 36, 367-369.
176. T. Subramanian, R. Padmakumar and S. V. Bhat, *Tetrahedron Letters*, **1997**, 38, 2585-2586.

177. T. Subramanian, R. Padmakumar and S. V. Bhat, *Tetrahedron Letters*, **1997**, 38, 2585-2586.
178. T.-S. Chou, S.-J. Lee and N.-K. Yao, *Tetrahedron*, **1989**, 45, 4113-4124.
179. H. H. Tso, L. J. Chang, L. C. Lin and T. S. Chou, *Journal of the Chinese Chemical Society*, **1985**, 32, 333-340.
180. T. Subramanian, R. Padmakumar and S. V. Bhat, *Synthetic Communications*, **1997**, 27, 4067-4072.
181. K.-I. Takao, R. Munakata and K.-I. Tadano, *Chemical Reviews*, **2005**, 105, 4779-4807.
182. K. C. Nicolaou, S. A. Snyder, T. Montagnon and G. Vassilikogiannakis, *Angewandte Chemie International Edition*, **2002**, 41, 1668-1698.
183. S. V. Bhat, *Journal of the Indian Institute of Science*, **1994**, 74.
184. E. V. Polunin, I. M. Zaks, A. M. Moiseenkov and A. V. Semenovskii, *Bulletin of the Academy of Sciences of the USSR Division of Chemical Science*, **1979**, 28, 594-596.
185. R. C. Krug, J. A. Rigney and G. R. Tichelaar, *The Journal of Organic Chemistry*, **1962**, 27, 1305-1309.
186. R. Block and J. Abecassis, *Tetrahedron Letters*, **1982**, 23, 3277-3280.
187. S. Yamada, H. Ohsawa, T. Suzuki and H. Takayama, *Chemistry Letters*, **1983**, 12, 1003-1006.
188. T.-S. Chou, H.-H. Tso and L.-J. Chang, *Journal of the Chemical Society, Perkin Transactions 1*, **1985**, 515-519.
189. C. D. Broaddus, *Journal of the American Chemical Society*, **1966**, 88, 3863-3865.
190. L. K. Brice, W.-M. Chang, J. E. Smith and S. M. Sullivan, *The Journal of Physical Chemistry*, **1967**, 71, 2814-2819.
191. M. Lusinchi, T. V. Stanbury and S. Z. Zard, *Chemical Communications*, **2002**, 1532-1533.
192. T. S. Chou, H. H. Tso and L. C. Lin, *The Journal of Organic Chemistry*, **1986**, 51, 1000-1002.
193. T.-S. Chou and H.-J. Tseng, *Tetrahedron Letters*, **1995**, 36, 7105-7108.

194. T.-S. Chou and C.-J. Chang, *Journal of the Chinese Chemical Society*, **1998**, 45, 529-533.
195. S. F. Martin, S. R. Desai, G. W. Philips and A. C. Miller, *Journal of the American Chemical Society*, **1980**, 102, 3294-3296.
196. J. Leonard, A. B. Hague and M. F. Jones, *Tetrahedron Letters*, **1997**, 38, 3071-3074.
197. T. S. Chou, S. J. Lee, H. H. Tso and C. F. Yu, *The Journal of Organic Chemistry*, **1987**, 52, 5082-5085.
198. T.-S. Chou, L.-J. Chang and H.-H. Tso, *Journal of the Chemical Society, Perkin Transactions I*, **1986**, 1039-1042.
199. T. S. Chou and C. Y. Chang, *The Journal of Organic Chemistry*, **1991**, 56, 4560-4563.
200. S. Yamada, H. Suzuki, H. Naito, T. Nomoto and H. Takayama, *Journal of the Chemical Society, Chemical Communications*, **1987**, 332-333.
201. H. Won, W. B. Lee and I.-Y. C. Lee, *Bulletin of the Korean Chemical Society*, **1994**, 15, 448-452.
202. R. Padmakumar, T. Subramanian and S. Bhat, *Organic Preparations and Procedures International*, **1995**, 27, 463-467.
203. R. P. Welcher, *The Journal of Organic Chemistry*, **1963**, 28, 1712-1713.
204. L. A. Paquette, *Tetrahedron*, **1997**, 53, 13971-14020.
205. R. Chuard, A. Giraud and P. Renaud, *Angewandte Chemie International Edition*, **2002**, 41, 4321-4323.
206. L. A. Paquette, *Angewandte Chemie International Edition*, **1990**, 29, 609-626.
207. M. R. Richards, M. G. Brant, M. J. Boulanger, C. W. Cairo and J. E. Wulff, *Medicinal Chemistry Communications*, **2014**, 5, 1483-1488.
208. M. G. Brant and J. E. Wulff, *Organic Letters*, **2012**, 14, 5876-5879.
209. Z. Fang, Y. n. Song, P. Zhan, Q. Zhang and X. Liu, *Future Medicinal Chemistry*, **2014**, 6, 885-901.
210. D. F. Veber, S. R. Johnson, H.-Y. Cheng, B. R. Smith, K. W. Ward and K. D. Kopple, *Journal of Medicinal Chemistry*, **2002**, 45, 2615-2623.
211. E. Keller and V. Kraemer, *Zeitschrift für Naturforschung B*, **2007**, 62, 983-987.

212. M. Karplus, *Journal of the American Chemical Society*, **1963**, 85, 2870-2871.
213. D. A. DeGoey, W. J. Flosi, V. L. Giranda, D. J. Kempf, A. Kennedy, L. L. Klein, A. C. Krueger, C. J. Maring, K. F. Mcdaniel and V. S. Stoll, WO2001029050 A2, **2001**.
214. P. S. Jones, P. W. Smith, G. W. Hardy, P. D. Howes, R. J. Upton and R. C. Bethell, *Bioorganic & Medicinal Chemistry Letters*, **1999**, 9, 605-610.
215. M. J. Bamford, J. C. Pichel, W. Husman, B. Patel, R. Storer and N. G. Weir, *Journal of the Chemical Society, Perkin Transactions 1*, **1995**, 1181-1187.
216. P. W. Smith, N. Trivedi, P. D. Howes, S. L. Sollis, G. Rahim, R. C. Bethell and S. Lynn, *Bioorganic & Medicinal Chemistry Letters*, **1999**, 9, 611-614.
217. P. Gerber and K. Müller, *Journal of Computer-Aided Molecular Design*, **1995**, 9, 251-268.
218. T. Curtius, *Berichte der Deutschen Chemischen Gesellschaft*, **1890**, 23, 3023-3033.
219. P. Chand, Y. S. Babu, S. Bantia, S. Rowland, A. Dehghani, P. L. Kotian, T. L. Hutchison, S. Ali, W. Brouillette, Y. El-Kattan and T.-H. Lin, *Journal of Medicinal Chemistry*, **2004**, 47, 1919-1929.
220. C. M. Bromba, J. W. Mason, M. G. Brant, T. Chan, M. D. Lunke, M. Petric, M. J. Boulanger and J. E. Wulff, *Bioorganic & Medicinal Chemistry Letters*, **2011**, 21, 7137-7141.
221. H. Lineweaver and D. Burk, *Journal of the American Chemical Society*, **1934**, 56, 658-666.
222. J. Sun, J. M. Miller, A. Beig, L. Rozen, G. L. Amidon and A. Dahan, *Expert Opinion on Drug Metabolism & Toxicology*, **2011**, 7, 313-323.
223. M. J. Jedrzejewski, S. Singh, W. J. Brouillette, W. G. Laver, G. M. Air and M. Luo, *Biochemistry*, **1995**, 34, 3144-3151.
224. M. G. Brant, J. N. Friedmann, C. G. Bohlken, A. G. Oliver and J. E. Wulff, *Organic & Biomolecular Chemistry*, **2015**, 13, 4581-4588.
225. Y. T. Tao, C. L. Liu, S. J. Lee and S. S. P. Chou, *The Journal of Organic Chemistry*, **1986**, 51, 4718-4721.

226. T. S. Chou, C. Y. Tsai and L. J. Huang, *The Journal of Organic Chemistry*, **1990**, 55, 5410-5413.
227. S.-S. P. Chou, C.-C. Sung and D.-J. Sun, *Journal of the Chinese Chemical Society*, **1992**, 39, 333-338.
228. S.-S. P. Chou and C.-C. Sung, *Journal of the Chinese Chemical Society*, **1989**, 36, 601-607.
229. E. G. Cox and G. A. Jeffrey, *Rubber Chemistry and Technology*, **1943**, 16, 486-492.
230. P. B. Hopkins and P. L. Fuchs, *The Journal of Organic Chemistry*, **1978**, 43, 1208-1217.
231. T. S. Chou, S. C. Hung and H. H. Tso, *The Journal of Organic Chemistry*, **1987**, 52, 3394-3399.
232. P. G. Baraldi, A. Barco, S. Benetti, S. Manfredini, G. P. Pollini, D. Simoni and V. Zanirato, *Tetrahedron*, **1988**, 44, 6451-6454.
233. H. Bader, H. Hopf and K. Sieper, *Chemische Berichte*, **1989**, 122, 383-384.
234. W.-C. Cheng, M. M. Olmstead and M. J. Kurth, *The Journal of Organic Chemistry*, **2001**, 66, 5528-5533.
235. T. S. Chou, H. H. Tso, Y. T. Tao and L. C. Lin, *The Journal of Organic Chemistry*, **1987**, 52, 244-246.
236. V. Berestovitskaya, E. Speranskii and V. Perekalin, *Zhurnal Organicheskoi Khimii*, **1977**, 13, 1934-1944.
237. S. S. Y. Wong, M. G. Brant, C. Barr, A. G. Oliver and J. E. Wulff, *Beilstein Journal of Organic Chemistry*, **2013**, 9, 1419-1425.
238. W. Chen, X. H. Yuan, R. Li, W. Du, Y. Wu, L. S. Ding and Y. C. Chen, *Advanced Synthesis & Catalysis*, **2006**, 348, 1818-1822.
239. M. P. Sibi, D. Rane, L. M. Stanley and T. Soeta, *Organic Letters*, **2008**, 10, 2971-2974.
240. H. Suga, T. Arikawa, K. Itoh, Y. Okumura, A. Kakehi and M. Shiro, *Heterocycles*, **2010**, 81, 1669-1688.
241. N. D. Shapiro, Y. Shi and F. D. Toste, *Journal of the American Chemical Society*, **2009**, 131, 11654-11655.

242. M. M. Efremova, A. P. Molchanov, A. V. Stepakov, R. R. Kostikov, V. S. Shcherbakova and A. V. Ivanov, *Tetrahedron*, **2015**, 71, 2071–2078.
243. H. O. Krabbenhoft, *The Journal of Organic Chemistry*, **1979**, 44, 4285-4294.
244. C. Conard and M. Dolliver, *Organic Syntheses Collective*, **1943**, 2, 167-168.
245. W. J. Bailey and E. W. Cummins, *Journal of the American Chemical Society*, **1954**, 76, 1932-1936.
246. Y. Xin, J. Zhao, J. Gu and S. Zhu, *Journal of Fluorine Chemistry*, **2011**, 132, 402-408.

Appendix A: NMR Data for Selected Compounds

Figure A-1. ^1H NMR (CDCl_3 500 MHz) of vinyl-sulfone 2-7a.

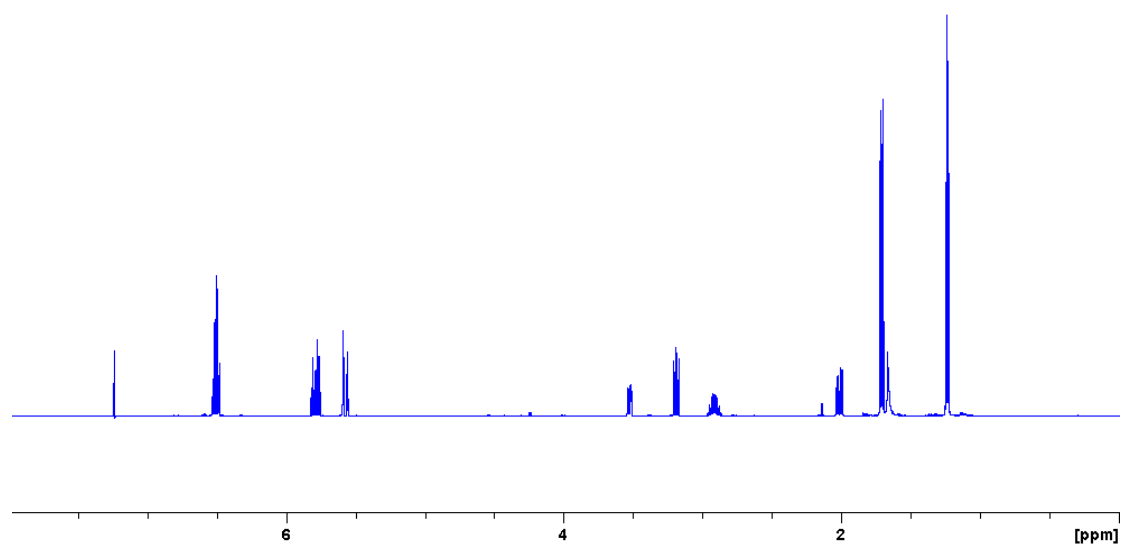


Figure A-2. ^{13}C NMR (CDCl_3 500 MHz) of vinyl sulfone 2-7a.

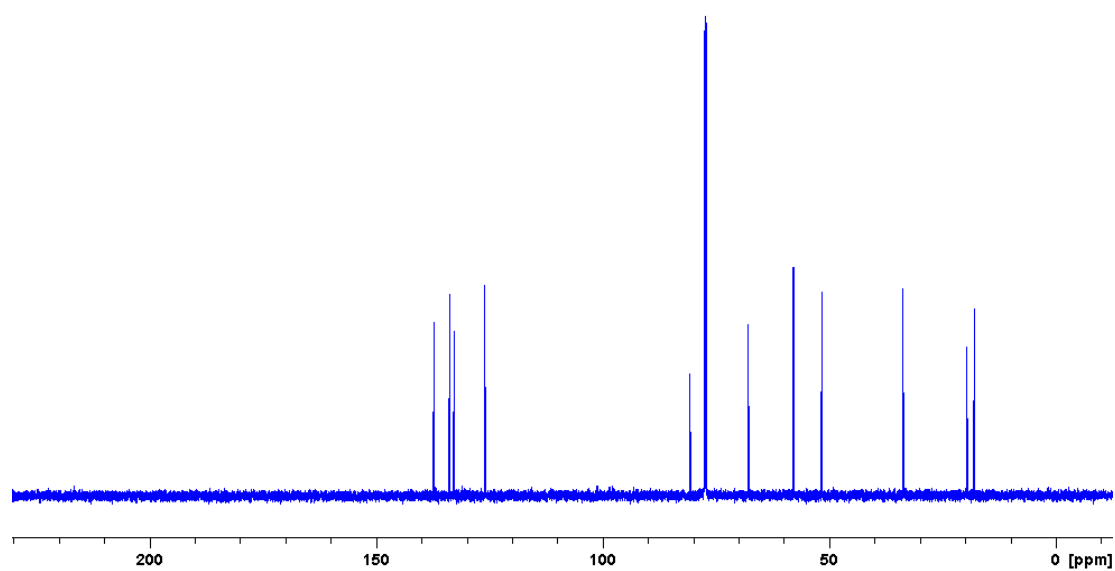


Figure A-3. ^1H NMR (D_2O 300 MHz) of amino-acid 3-34.

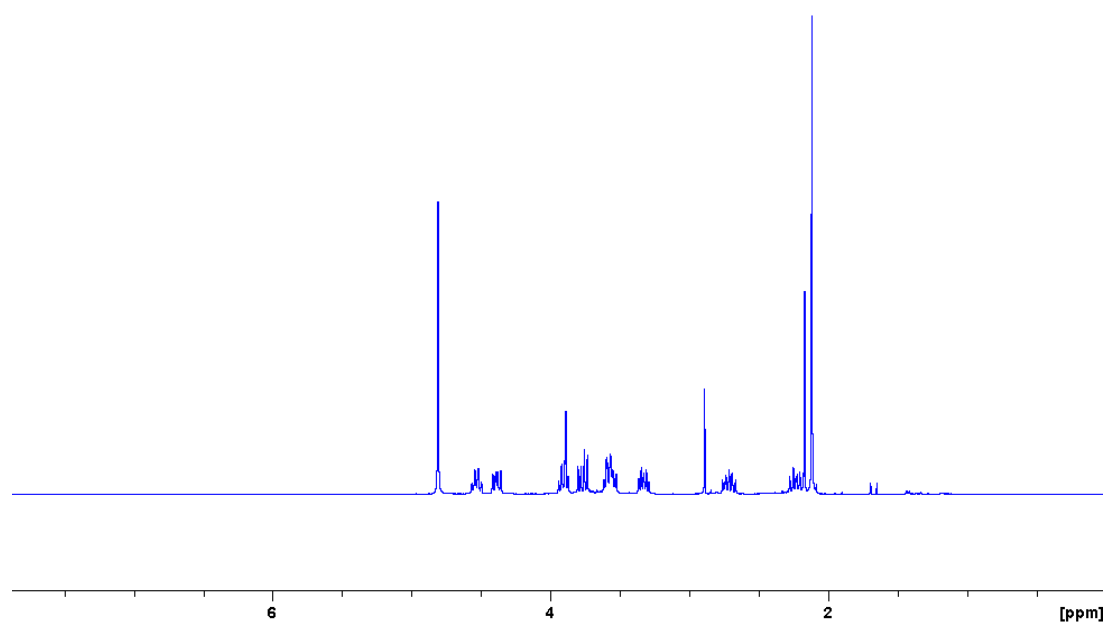


Figure A-4. ^{13}C NMR (D_2O 300 MHz) of amino-acid 3-34.

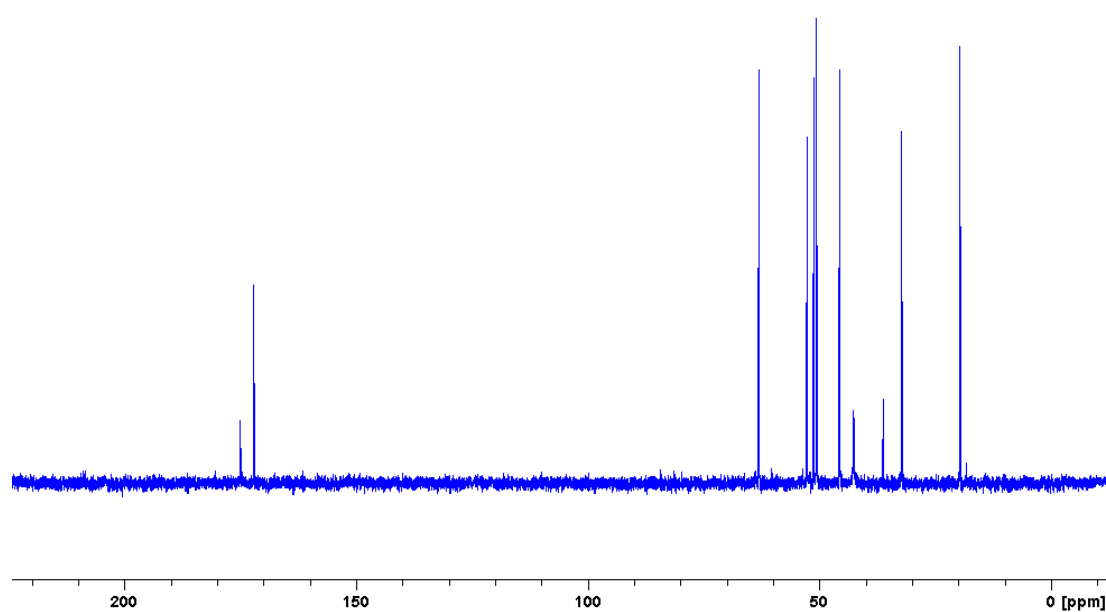


Figure A-5. ^1H NMR (D_2O 500 MHz) of guanidino-acid 3-27.

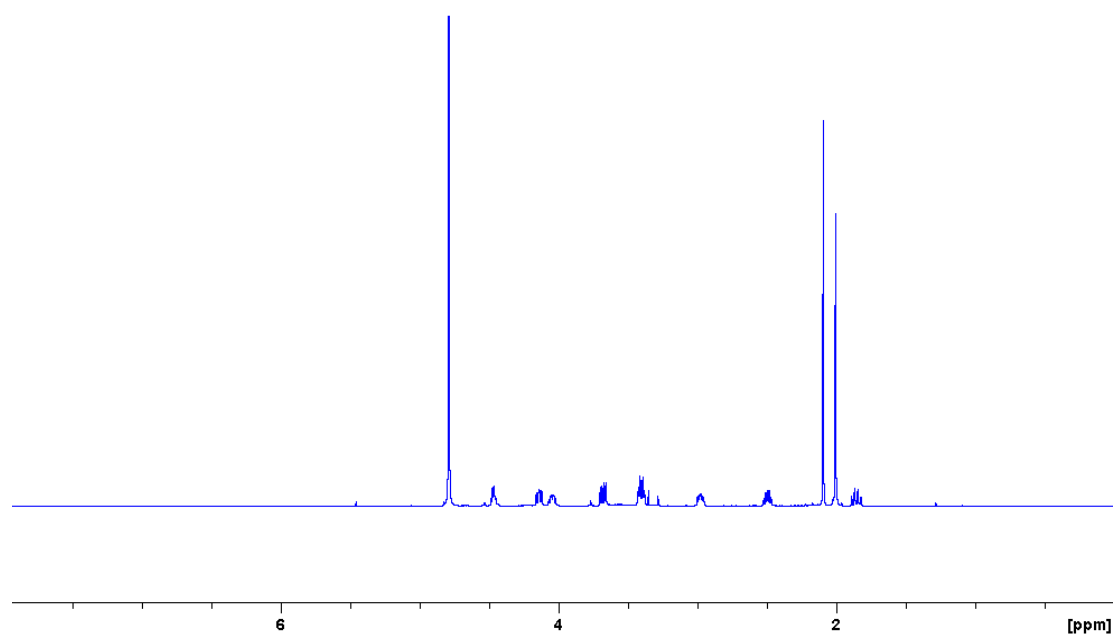


Figure A-6. ^{13}C NMR (D_2O 500 MHz) of guanidino-acid 3-27.

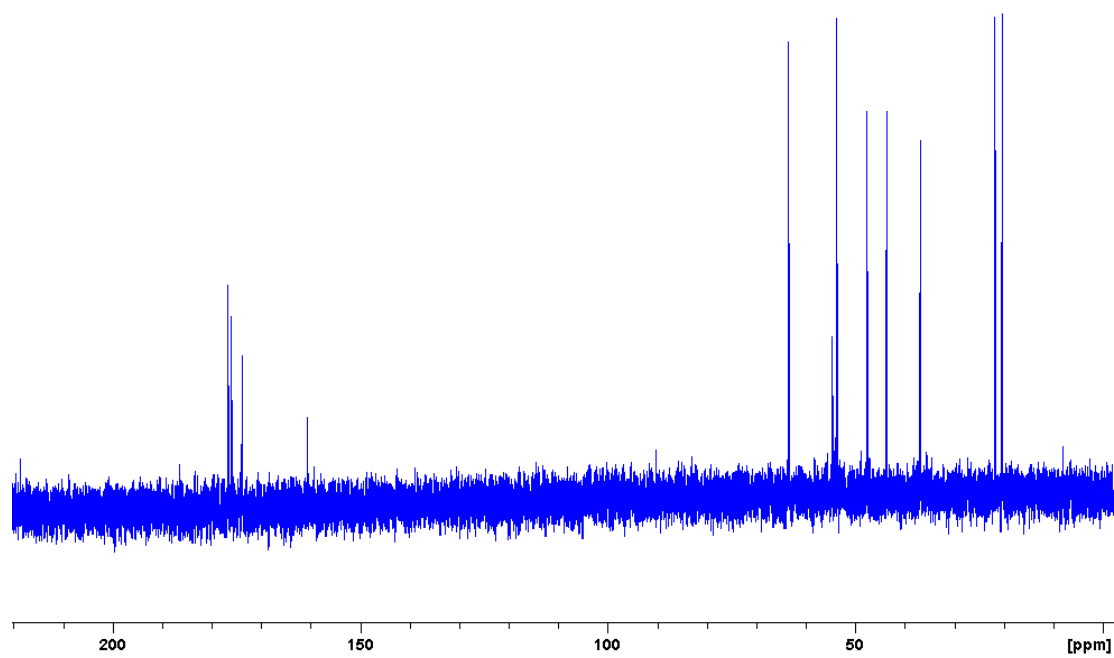


Figure A-7. ^1H NMR (CDCl_3 300 MHz) of [3.2.1]bicycle 4-5b.

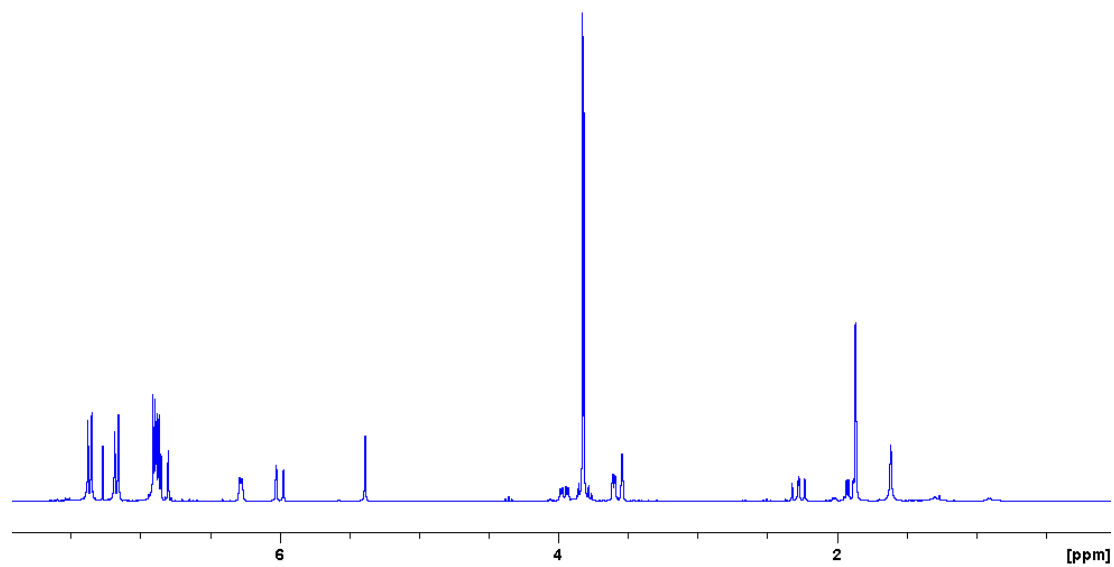


Figure A-8. ^{13}C NMR (CDCl_3 300 MHz) of [3.2.1]bicycle 4-5b.

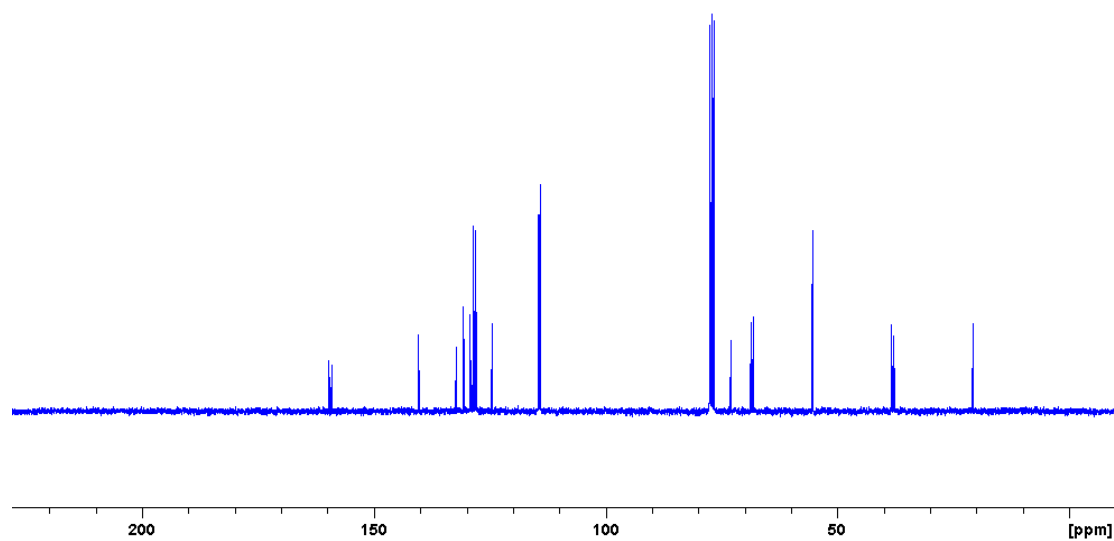


Figure A-9. ^1H NMR (CDCl_3 300 MHz) of [5.4]spirocycle 4-6f.

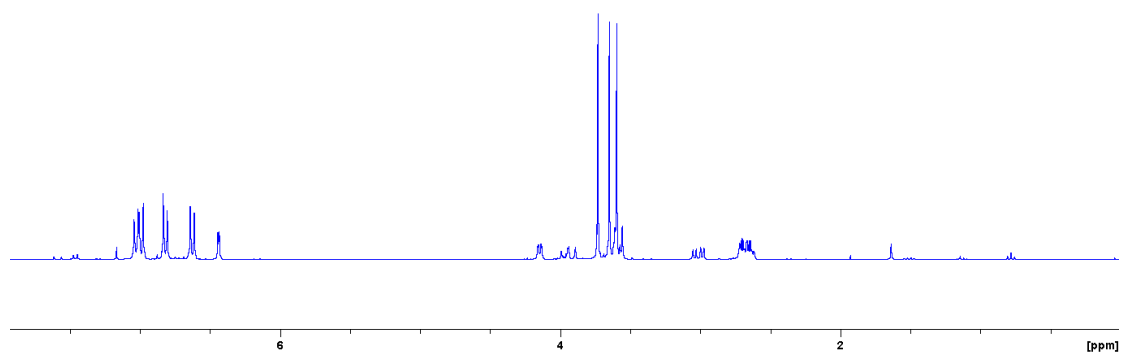


Figure A-10. ^{13}C NMR (CDCl_3 300 MHz) of [5.4]spirocycle 4-6f.

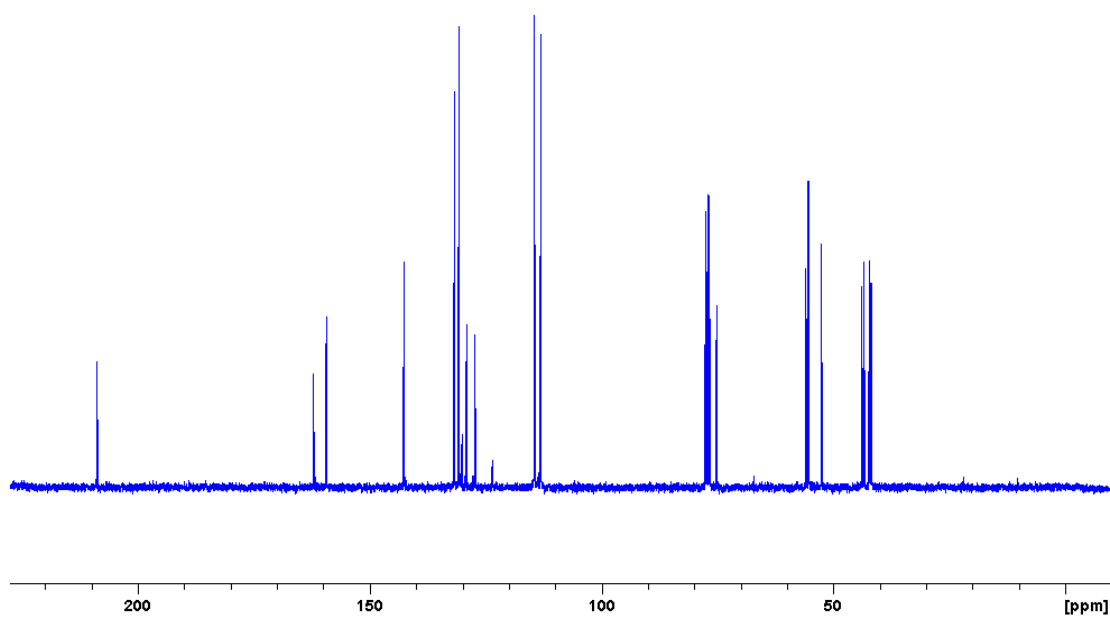


Figure A-11. ^1H NMR (CDCl_3 500 MHz) of benzyl-sulfone 5-4.

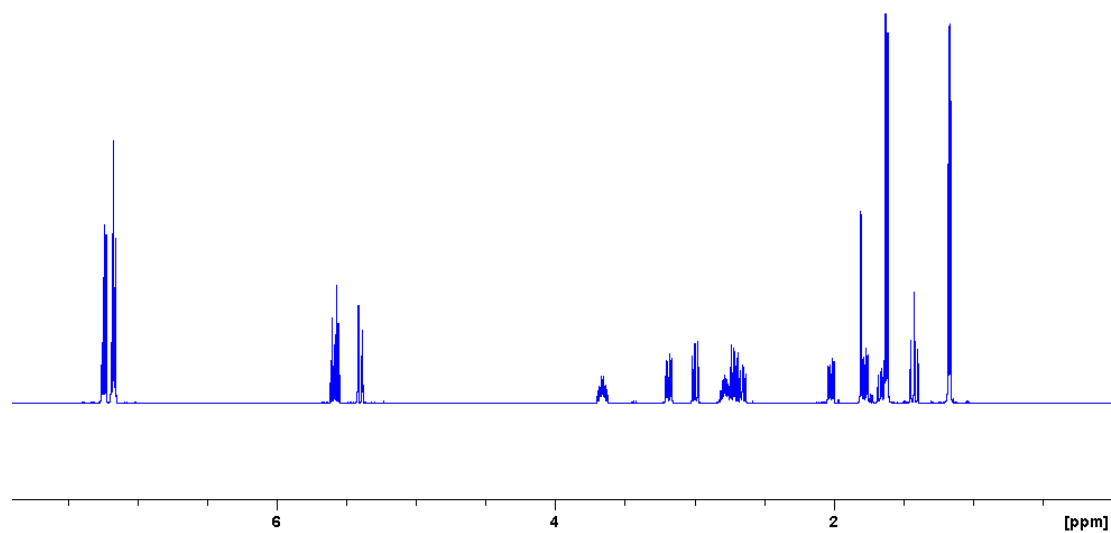
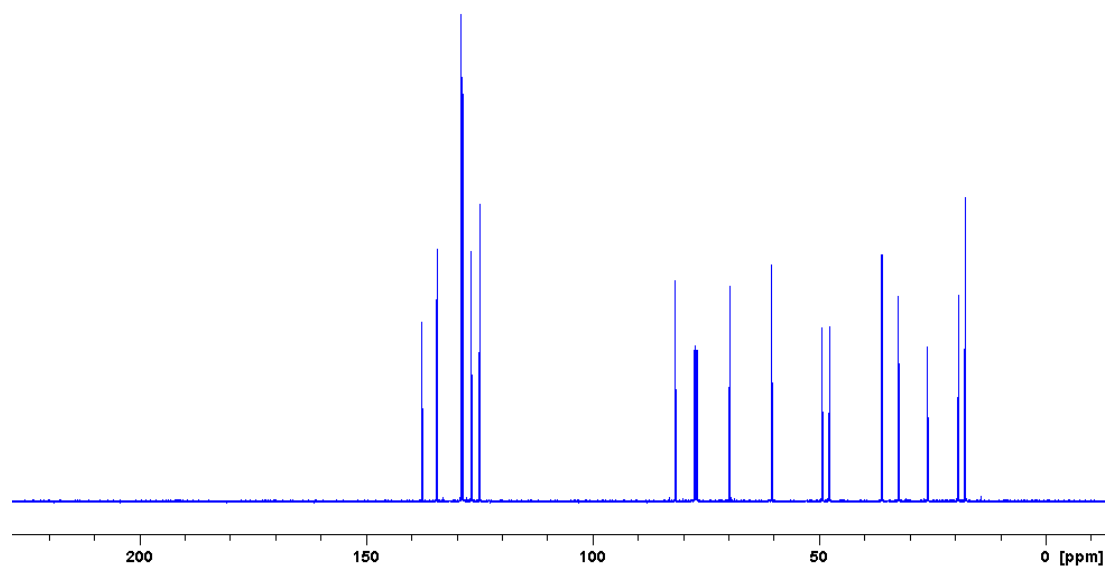


Figure A-12. ^{13}C NMR (CDCl_3 500 MHz) of benzyl-sulfone 5-4.



Appendix B: Crystallographic Parameters

Table B-1. Crystallographic parameters for 2-7a, 2-9b and 3-20.

	2-7a	2-9b	3-20
CCDC #	766248	1025141	-
Formula	C ₁₁ H ₁₆ O ₃ S	C ₂₆ H ₂₈ O ₅ S	C ₁₁ H ₂₀ ClN ₃ O ₅ S
Formula weight	228.30	452.54	341.81
Appearance	colourless, block	colourless, block	colourless, block
Crystal dimensions (mm)	0.24 × 0.18 × 0.15	0.134 × 0.098 × 0.084	0.14 × 0.09 × 0.06
a (Å)	12.0282(1)	9.0583(6)	10.2150(2)
b (Å)	34.3106(6)	29.646(2)	13.9710(3)
c (Å)	11.2526(1)	8.5818(6)	10.5413(2)
α (deg)	90	90	90
β (deg)	90	106.748(2)	94.9290(10)
γ (deg)	90	90	90
Volume (Å ³)	4643.89(10)	2206.8(3)	1498.83(5)
ρ (calc) (g/cm ³)	1.306	1.362	1.515
Crystal system	Orthorhombic	Monoclinic	Monoclinic
Space group	Fdd2	P2 ₁ /c	P2 ₁ /n
Z	16	4	4
Absorption coefficient μ (mm ⁻¹)	2.371	0.183	3.803
Temperature (K)	100(2)	120(2)	100(2)
Unique reflections	2113 [R _{int} = 0.0263]	5530 [R _{int} = 0.0366]	2776 [R _{int} = 0.0323]
Refinement method	Full-matrix least-squares on F ²	Full-matrix least-squares on F ²	Full-matrix least-squares on F ²
Data/restraints/parameters	2113 / 1 / 138	5530 / 0 / 295	2776 / 0 / 192
Goodness-of-fit on F ²	1.077	1.019	1.051
Final R indices [I > 2σ(I)]	R ₁ = 0.0260 wR ₂ = 0.0666	R ₁ = 0.0374 wR ₂ = 0.0901	R ₁ = 0.0392 wR ₂ = 0.1021
R indices (all data)	R ₁ = 0.0264 wR ₂ = 0.0669	R ₁ = 0.0485 wR ₂ = 0.0957	R ₁ = 0.0458 wR ₂ = 0.1073

$$R_1 = \frac{\sum ||F_o| - |F_c||}{\sum |F_o|}$$

$$wR_2 = \left[\frac{\sum (w (F_o^2 - F_c^2)^2)}{\sum w(F_o^2)^2} \right]^{1/2}$$

Table B-2. Crystallographic parameters for 3-29, 3-33 and 3-37.

	3-29	3-33	3-37
CCDC #	-	-	-
Formula	C ₂₅ H ₂₉ NO ₆ S	C ₁₀ H ₁₄ N ₄ O ₅ S	C _{11.50} H ₂₀ N ₄ O _{5.50} S
Formula weight	471.55	302.31	334.38
Appearance	colourless, block	colourless, block	colourless, columnar
Crystal dimensions (mm)	0.13 × 0.08 × 0.06	0.25 × 0.18 × 0.13	0.28 × 0.09 × 0.07
a (Å)	14.0982(3)	10.6331(4)	9.2307(4)
b (Å)	17.0726(4)	10.5343(4)	11.5963(5)
c (Å)	10.3466(2)	12.5500(5)	14.4409(6)
α (deg)	90	90	104.5160(10)
β (deg)	105	111.0190(10)	93.990(2)
γ (deg)	90	90	97.106(2)
Volume (Å ³)	2397.85(9)	1312.22(9)	1476.78(11)
ρ (calc) (g/cm ³)	1.306	1.530	1.504
Crystal system	Monoclinic	Monoclinic	Triclinic
Space group	P2 ₁ /c	P2 ₁ /c	P-1
Z	4	4	4
Absorption coefficient μ (mm ⁻¹)	1.540	2.466	2.270
Temperature (K)	120(2)	120(2)	120(2)
Unique reflections	4531 [R _{int} = 0.0386]	2523 [R _{int} = 0.0181]	5489 [R _{int} = 0.0256]
Refinement method	Full-matrix least-squares on F ²	Full-matrix least-squares on F ²	Full-matrix least-squares on F ²
Data/restraints/parameters	4531 / 0 / 303	2523 / 0 / 183	5489 / 0 / 398
Goodness-of-fit on F ²	1.052	1.048	1.120
Final R indices [I > 2σ(I)]	R ₁ = 0.0341 wR ₂ = 0.0889	R ₁ = 0.0280 wR ₂ = 0.0739	R ₁ = 0.0490 wR ₂ = 0.1489
R indices (all data)	R ₁ = 0.0383 wR ₂ = 0.0919	R ₁ = 0.0280 wR ₂ = 0.0739	R ₁ = 0.0516 wR ₂ = 0.1520

$$R_1 = \sum ||F_o| - |F_c|| / \sum |F_o|$$

$$wR_2 = [\sum (w (F_o^2 - F_c^2)^2) / \sum w(F_o^2)^2]^{1/2}$$

Table B-3. Crystallographic parameters for 4-4c, 4-5b and 4-4e'.

	4-4c	4-5b	4-4e'
CCDC #	1025137	1025139	1025138
Formula	C ₂₃ H ₂₃ ClO ₅ S	C ₂₄ H ₂₆ O ₅ S	C ₂₉ H ₂₈ O ₅ S
Formula weight	446.92	426.51	488.57
Appearance	colourless, tablet	colourless, rod	colourless, block
Crystal dimensions (mm)	0.085 × 0.065 × 0.037	0.163 × 0.080 × 0.060	0.147 × 0.122 × 0.120
a (Å)	21.4489(15)	9.7206(4)	7.3355(3)
b (Å)	15.1178(15)	14.2444(5)	27.2184(11)
c (Å)	14.8599(12)	15.3744(5)	12.3978(5)
α (deg)	90	95.0350(14)	90
β (deg)	120.899	95.5230(15)	106.5590(11)
γ (deg)	90	96.4600(15)	90
Volume (Å ³)	4134.6(6)	2094.98(13)	2372.69(17)
ρ (calc) (g/cm ³)	1.436	1.352	1.368
Crystal system	Monoclinic	Triclinic	Monoclinic
Space group	C2/c	P-1	P2 ₁ /c
Z	8	4	4
Absorption coefficient μ (mm ⁻¹)	0.320	0.188	0.176
Temperature (K)	120(2)	120(2)	120(2)
Unique reflections	4240 [R _{int} = 0.0713]	9304 [R _{int} = 0.0420]	5935 [R _{int} = 0.0249]
Refinement method	Full-matrix least-squares on F ²	Full-matrix least-squares on F ²	Full-matrix least-squares on F ²
Data/restraints/parameters	4240 / 0 / 282	9304 / 0 / 555	5935 / 0 / 322
Goodness-of-fit on F ²	1.018	1.014	1.016
Final R indices [I > 2σ(I)]	R ₁ = 0.0383 wR ₂ = 0.0819	R ₁ = 0.0402 wR ₂ = 0.0910	R ₁ = 0.0352 wR ₂ = 0.0887
R indices (all data)	R ₁ = 0.0614 wR ₂ = 0.0898	R ₁ = 0.0609 wR ₂ = 0.1013	R ₁ = 0.0421 wR ₂ = 0.0932

$$R_1 = \sum ||F_o| - |F_c|| / \sum |F_o|$$

$$wR_2 = [\sum (w (F_o^2 - F_c^2)^2) / \sum w(F_o^2)^2]^{1/2}$$

Table B-4. Crystallographic parameters for 4-6f, 5-5 and 5-10.

	4-6f	5-5	5-10
CCDC #	1025140	766249	-
Formula	C ₂₅ H ₂₆ O ₇ S	C ₁₈ H ₂₄ O ₃ S	C ₃₃ H ₃₉ NO ₅ S
Formula weight	470.52	320.43	561.71
Crystal Appearance	yellow, block	colourless, block	colourless, tablet
Crystal dimensions (mm)	0.170 × 0.130 × 0.050	0.22 × 0.18 × 0.12	0.165 × 0.087 × 0.026
a (Å)	10.6137(10)	12.2547(2)	23.9783(6)
b (Å)	15.5004(14)	27.5395(5)	7.2669(2)
c (Å)	13.2501(12)	9.9291(2)	34.2194(8)
α (deg)	90	90	90
β (deg)	92.946(3)	90	99.079(2)
γ (deg)	90	90	90
Volume (Å ³)	2177.0(3)	3350.96(11)	5888.0(3)
ρ (calc) (g/cm ³)	1.436	1.270	1.267
Crystal system	Monoclinic	Orthorhombic	Monoclinic
Space group	P2 ₁ /c	Pccn	C2/c
Z	4	8	8
Absorption coefficient, μ (mm ⁻¹)	0.195	1.794	1.312
Temperature (K)	120(2)	100(2)	120(2)
Unique reflections	5447 [R _{int} = 0.0401]	3131 [R _{int} = 0.0466]	5687 [R _{int} = 0.0404]
Refinement method	Full-matrix least-squares on F ²	Full-matrix least-squares on F ²	Full-matrix least-squares on F ²
Data/restraints/parameters	5447 / 0 / 301	3131 / 0 / 201	5687 / 0 / 361
Goodness-of-fit on F ²	1.023	1.028	1.024
Final R indices [I > 2σ(I)]	R ₁ = 0.0348 wR ₂ = 0.0816	R ₁ = 0.0400 wR ₂ = 0.0980	R ₁ = 0.0379 wR ₂ = 0.0930
R indices (all data)	R ₁ = 0.0476 wR ₂ = 0.0884	R ₁ = 0.0498 wR ₂ = 0.1044	R ₁ = 0.0482 wR ₂ = 0.0991

$$R_1 = \sum ||F_o| - |F_c|| / \sum |F_o|$$

$$wR_2 = [\sum (w (F_o^2 - F_c^2)^2) / \sum w(F_o^2)^2]^{1/2}$$

Appendix C: Complete Listing of Bond Lengths and Angles

Figure C-1: ORTEP diagram of **2-7a** with thermal ellipsoids shown at the 50% probability level.

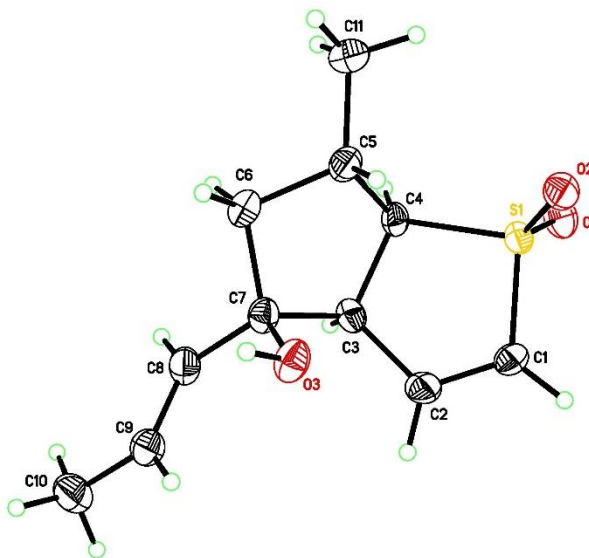


Table C-1: Bond Lengths (Å) and Angles (°) for **2-7a**.

S(1)-O(1)	1.4451(12)	S(1)-O(2)	1.4492(12)	S(1)-C(1)	1.7504(18)
S(1)-C(4)	1.8017(16)	O(3)-C(7)	1.4263(19)	C(1)-C(2)	1.325(3)
C(2)-C(3)	1.502(2)	C(3)-C(4)	1.543(2)	C(3)-C(7)	1.567(2)
C(4)-C(5)	1.525(2)	C(5)-C(11)	1.522(2)	C(5)-C(6)	1.536(3)
C(6)-C(7)	1.531(2)	C(7)-C(8)	1.508(2)	C(8)-C(9)	1.310(3)
C(9)-C(10)	1.503(3)				
O(1)-S(1)-O(2)	116.56(8)	O(1)-S(1)-C(1)	110.62(8)		
O(2)-S(1)-C(1)	110.14(8)	O(1)-S(1)-C(4)	110.13(7)		
O(2)-S(1)-C(4)	111.79(8)	C(1)-S(1)-C(4)	95.65(9)		
C(2)-C(1)-S(1)	111.50(14)	C(1)-C(2)-C(3)	117.37(15)		
C(2)-C(3)-C(4)	108.99(13)	C(2)-C(3)-C(7)	114.01(13)		
C(4)-C(3)-C(7)	105.86(13)	C(5)-C(4)-C(3)	106.53(13)		
C(5)-C(4)-S(1)	115.18(11)	C(3)-C(4)-S(1)	105.88(11)		
C(11)-C(5)-C(4)	113.47(15)	C(11)-C(5)-C(6)	114.90(15)		
C(4)-C(5)-C(6)	101.87(14)	C(7)-C(6)-C(5)	103.84(14)		
O(3)-C(7)-C(8)	112.42(14)	O(3)-C(7)-C(6)	110.52(13)		
C(8)-C(7)-C(6)	113.50(14)	O(3)-C(7)-C(3)	106.36(13)		
C(8)-C(7)-C(3)	110.66(13)	C(6)-C(7)-C(3)	102.73(13)		
C(9)-C(8)-C(7)	126.29(17)	C(8)-C(9)-C(10)			

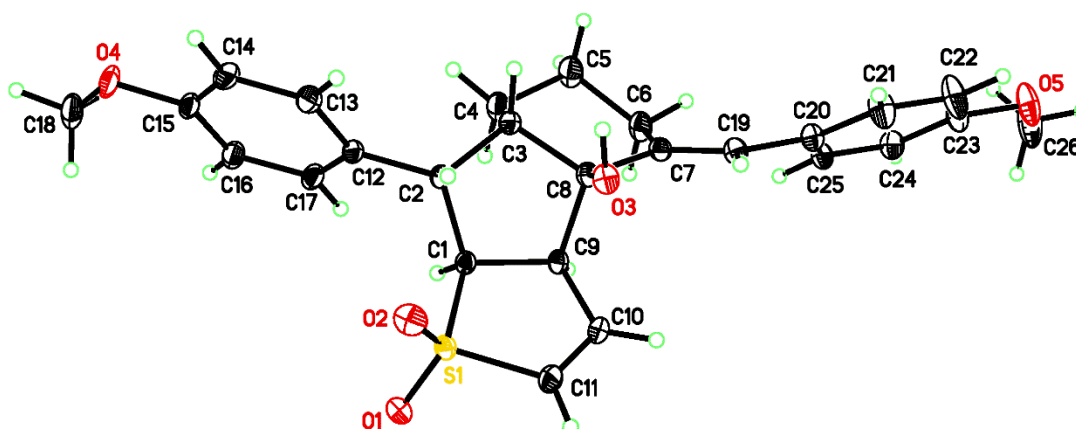


Figure C-2: ORTEP diagram of **2-9b** with thermal ellipsoids shown at the 50% probability level.

Table C-2: Bond Lengths (Å) and Angles (°) for **2-9b**.

S(1)-O(2)	1.4340(10)	S(1)-O(1)	1.4433(10)	S(1)-C(11)	1.7416(14)
S(1)-C(1)	1.7907(13)	O(3)-C(8)	1.4206(16)	O(4)-C(15)	1.3616(16)
O(4)-C(18)	1.423(2)	O(5)-C(23)	1.3764(17)	O(5)-C(26)	1.404(2)
C(1)-C(2)	1.5359(17)	C(1)-C(9)	1.5403(17)	C(2)-C(12)	1.5098(18)
C(2)-C(3)	1.5455(18)	C(3)-C(4)	1.5201(19)	C(3)-C(8)	1.5411(18)
C(4)-C(5)	1.5170(19)	C(5)-C(6)	1.524(2)	C(6)-C(7)	1.5031(19)
C(7)-C(19)	1.3380(18)	C(7)-C(8)	1.5220(18)	C(8)-C(9)	1.5545(18)
C(9)-C(10)	1.4967(19)	C(10)-C(11)	1.315(2)	C(12)-C(17)	1.383(2)
C(12)-C(13)	1.3939(19)	C(13)-C(14)	1.379(2)	C(14)-C(15)	1.383(2)
C(15)-C(16)	1.385(2)	C(16)-C(17)	1.3940(18)	C(19)-C(20)	1.4709(18)
C(20)-C(25)	1.3870(19)	C(20)-C(21)	1.399(2)	C(21)-C(22)	1.378(2)
C(22)-C(23)	1.385(2)	C(23)-C(24)	1.379(2)	C(24)-C(25)	1.3853(19)
O(3)-H(3O)	0.82(2)				
O(2)-S(1)-O(1)	116.48(6)	O(2)-S(1)-C(11)	111.60(7)		
O(1)-S(1)-C(11)	109.34(6)	O(2)-S(1)-C(1)	112.18(6)		
O(1)-S(1)-C(1)	109.66(6)	C(11)-S(1)-C(1)	95.61(6)		
C(15)-O(4)-C(18)	117.35(12)	C(23)-O(5)-C(26)	117.44(12)		
C(2)-C(1)-C(9)	107.35(10)	C(2)-C(1)-S(1)	114.13(9)		
C(9)-C(1)-S(1)	106.26(9)	C(12)-C(2)-C(1)	115.35(11)		
C(12)-C(2)-C(3)	117.40(11)	C(1)-C(2)-C(3)	102.29(10)		
C(4)-C(3)-C(8)	112.38(11)	C(4)-C(3)-C(2)	113.90(11)		
C(8)-C(3)-C(2)	102.01(10)	C(5)-C(4)-C(3)	110.86(11)		
C(4)-C(5)-C(6)	111.50(12)	C(7)-C(6)-C(5)	111.91(12)		

C(19)-C(7)-C(6)	125.10(12)	C(19)-C(7)-C(8)	119.56(12)
C(6)-C(7)-C(8)	115.32(11)	O(3)-C(8)-C(7)	112.41(10)
O(3)-C(8)-C(3)	109.30(10)	C(7)-C(8)-C(3)	115.19(11)
O(3)-C(8)-C(9)	104.76(10)	C(7)-C(8)-C(9)	111.61(10)
C(3)-C(8)-C(9)	102.65(10)	C(10)-C(9)-C(1)	108.80(11)
C(10)-C(9)-C(8)	113.44(11)	C(1)-C(9)-C(8)	104.91(10)
C(11)-C(10)-C(9)	117.53(12)	C(10)-C(11)-S(1)	111.79(11)
C(17)-C(12)-C(13)	117.46(12)	C(17)-C(12)-C(2)	124.09(12)
C(13)-C(12)-C(2)	118.45(12)	C(14)-C(13)-C(12)	121.21(14)
C(13)-C(14)-C(15)	120.55(13)	O(4)-C(15)-C(14)	115.64(13)
O(4)-C(15)-C(16)	124.88(14)	C(14)-C(15)-C(16)	119.48(13)
C(15)-C(16)-C(17)	119.22(14)	C(12)-C(17)-C(16)	122.05(13)
C(7)-C(19)-C(20)	129.31(13)	C(25)-C(20)-C(21)	117.21(13)
C(25)-C(20)-C(19)	123.56(12)	C(21)-C(20)-C(19)	119.07(13)
C(22)-C(21)-C(20)	121.66(14)	C(21)-C(22)-C(23)	119.51(14)
O(5)-C(23)-C(24)	123.42(13)	O(5)-C(23)-C(22)	116.23(13)
C(24)-C(23)-C(22)	120.34(13)	C(23)-C(24)-C(25)	119.34(13)
C(24)-C(25)-C(20)	121.91(12)	C(8)-O(3)-H(30)	106.8(13)

Figure C-3: ORTEP diagram of **3-20** with thermal ellipsoids shown at the 50% probability level.

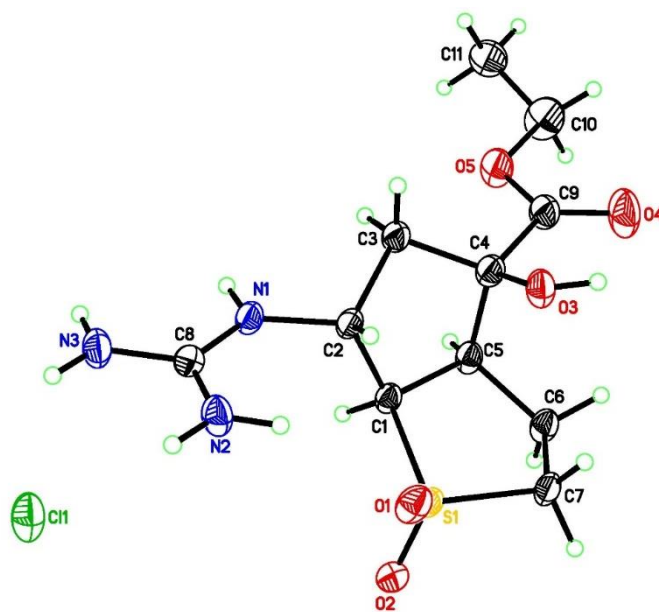


Table C-3: Bond Lengths (Å) and Angles (°) for **3-20**.

S(1)-O(1)	1.4504(17)	S(1)-O(2)	1.4524(17)	S(1)-C(7)	1.785(2)
S(1)-C(1)	1.809(2)	O(3)-C(4)	1.414(3)	O(4)-C(9)	1.209(3)
O(5)-C(9)	1.317(3)	O(5)-C(10)	1.467(3)	N(1)-C(8)	1.338(3)
N(1)-C(2)	1.460(3)	N(2)-C(8)	1.317(3)	N(3)-C(8)	1.333(3)
C(1)-C(5)	1.547(3)	C(1)-C(2)	1.552(3)	C(2)-C(3)	1.537(3)
C(3)-C(4)	1.528(3)	C(4)-C(9)	1.522(3)	C(4)-C(5)	1.553(3)
C(5)-C(6)	1.546(3)	C(6)-C(7)	1.530(3)	C(10)-C(11)	1.463(4)
O(1)-S(1)-O(2)	117.07(10)	O(1)-S(1)-C(7)	111.28(10)		
O(2)-S(1)-C(7)	109.62(10)	O(1)-S(1)-C(1)	111.09(10)		
O(2)-S(1)-C(1)	107.84(10)	C(7)-S(1)-C(1)	98.27(10)		
C(9)-O(5)-C(10)	115.2(2)	C(8)-N(1)-C(2)	123.88(19)		
C(5)-C(1)-C(2)	107.07(17)	C(5)-C(1)-S(1)	106.02(14)		
C(2)-C(1)-S(1)	115.04(15)	N(1)-C(2)-C(3)	112.52(17)		
N(1)-C(2)-C(1)	112.93(18)	C(3)-C(2)-C(1)	103.60(17)		
C(4)-C(3)-C(2)	101.97(17)	O(3)-C(4)-C(9)	109.58(19)		
O(3)-C(4)-C(3)	107.87(18)	C(9)-C(4)-C(3)	116.85(19)		
O(3)-C(4)-C(5)	111.09(18)	C(9)-C(4)-C(5)	108.93(19)		
C(3)-C(4)-C(5)	102.33(18)	C(6)-C(5)-C(1)	110.16(18)		
C(6)-C(5)-C(4)	116.13(18)	C(1)-C(5)-C(4)	103.15(17)		
C(7)-C(6)-C(5)	109.57(17)	C(6)-C(7)-S(1)	104.56(15)		
N(2)-C(8)-N(3)	118.9(2)	N(2)-C(8)-N(1)	122.3(2)		
N(3)-C(8)-N(1)	118.8(2)	O(4)-C(9)-O(5)	124.9(2)		
O(4)-C(9)-C(4)	121.2(2)	O(5)-C(9)-C(4)	113.8(2)		
C(11)-C(10)-O(5)	107.9(2)				

Figure C-4: ORTEP diagram of **3-29** with thermal ellipsoids shown at the 50% probability level.

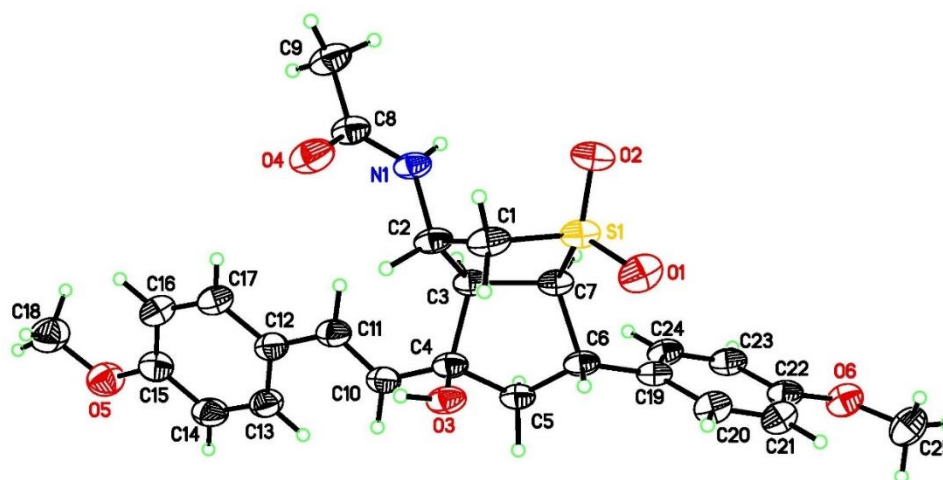


Table C-4: Bond Lengths (Å) and Angles (°) for **3-29**.

S(1)-O(2)	1.4413(11)	S(1)-O(1)	1.4453(11)	S(1)-C(1)	1.7781(17)
S(1)-C(7)	1.7917(13)	O(3)-C(4)	1.4354(16)	O(4)-C(8)	1.2283(18)
O(5)-C(15)	1.368(2)	O(5)-C(18)	1.426(2)	O(6)-C(22)	1.3698(19)
O(6)-C(25)	1.429(2)	N(1)-C(8)	1.3403(19)	N(1)-C(2)	1.4631(16)
C(1)-C(2)	1.534(2)	C(2)-C(3)	1.5542(19)	C(3)-C(7)	1.553(2)
C(3)-C(4)	1.5605(18)	C(4)-C(10)	1.499(2)	C(4)-C(5)	1.528(2)
C(5)-C(6)	1.529(2)	C(6)-C(19)	1.509(2)	C(6)-C(7)	1.5518(18)
C(8)-C(9)	1.509(2)	C(10)-C(11)	1.325(2)	C(11)-C(12)	1.469(2)
C(12)-C(17)	1.389(2)	C(12)-C(13)	1.399(2)	C(13)-C(14)	1.379(3)
C(14)-C(15)	1.396(2)	C(15)-C(16)	1.382(2)	C(16)-C(17)	1.389(2)
C(19)-C(20)	1.382(2)	C(19)-C(24)	1.397(2)	C(20)-C(21)	1.390(2)
C(21)-C(22)	1.384(2)	C(22)-C(23)	1.390(2)	C(23)-C(24)	1.379(2)
O(2)-S(1)-O(1)	117.83(7)	O(2)-S(1)-C(1)	108.90(7)		
O(1)-S(1)-C(1)	111.67(7)	O(2)-S(1)-C(7)	107.63(6)		
O(1)-S(1)-C(7)	111.73(7)	C(1)-S(1)-C(7)	97.03(7)		

C(15)-O(5)-C(18)	116.84(14)	C(22)-O(6)-C(25)	116.33(12)
C(8)-N(1)-C(2)	121.12(12)	C(2)-C(1)-S(1)	105.03(10)
N(1)-C(2)-C(1)	113.50(12)	N(1)-C(2)-C(3)	110.44(11)
C(1)-C(2)-C(3)	107.50(12)	C(7)-C(3)-C(2)	112.14(12)
C(7)-C(3)-C(4)	104.28(11)	C(2)-C(3)-C(4)	113.88(11)
O(3)-C(4)-C(10)	110.88(12)	O(3)-C(4)-C(5)	105.09(11)
C(10)-C(4)-C(5)	112.77(12)	O(3)-C(4)-C(3)	110.00(11)
C(10)-C(4)-C(3)	115.24(12)	C(5)-C(4)-C(3)	102.11(11)
C(4)-C(5)-C(6)	103.88(11)	C(19)-C(6)-C(5)	115.75(11)
C(19)-C(6)-C(7)	115.40(11)	C(5)-C(6)-C(7)	100.98(11)
C(6)-C(7)-C(3)	107.56(11)	C(6)-C(7)-S(1)	115.33(9)
C(3)-C(7)-S(1)	105.46(9)	O(4)-C(8)-N(1)	121.30(13)
O(4)-C(8)-C(9)	121.95(14)	N(1)-C(8)-C(9)	116.75(13)
C(11)-C(10)-C(4)	126.00(14)	C(10)-C(11)-C(12)	126.92(14)
C(17)-C(12)-C(13)	117.30(15)	C(17)-C(12)-C(11)	119.50(14)
C(13)-C(12)-C(11)	123.20(14)	C(14)-C(13)-C(12)	121.35(15)
C(13)-C(14)-C(15)	120.32(15)	O(5)-C(15)-C(16)	124.75(16)
O(5)-C(15)-C(14)	115.98(15)	C(16)-C(15)-C(14)	119.26(16)
C(15)-C(16)-C(17)	119.72(15)	C(12)-C(17)-C(16)	122.04(15)
C(20)-C(19)-C(24)	117.10(14)	C(20)-C(19)-C(6)	120.63(12)
C(24)-C(19)-C(6)	122.26(13)	C(19)-C(20)-C(21)	122.30(14)
C(22)-C(21)-C(20)	119.30(14)	O(6)-C(22)-C(21)	124.09(14)
O(6)-C(22)-C(23)	116.26(13)	C(21)-C(22)-C(23)	119.64(14)
C(24)-C(23)-C(22)	119.93(13)	C(23)-C(24)-C(19)	121.70(14)

Figure C-5: ORTEP diagram of **3-33** with thermal ellipsoids shown at the 50% probability level.

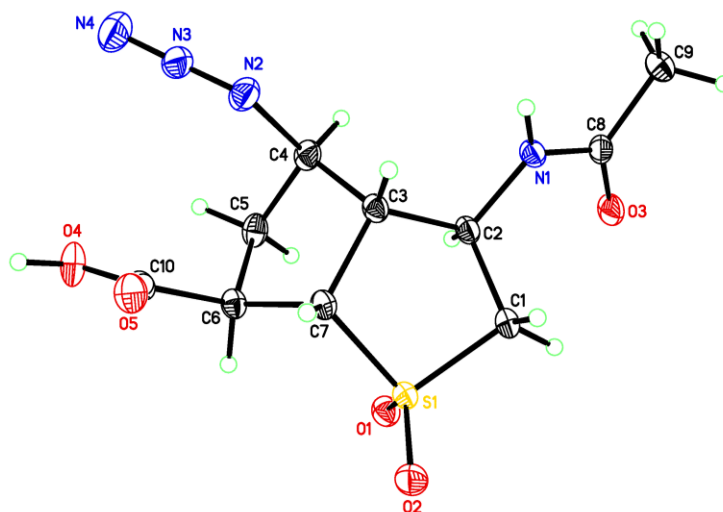


Table C-5: Bond Lengths (Å) and Angles (°) for 3-33.

S(1)-O(2)	1.4404(10)	S(1)-O(1)	1.4433(10)	S(1)-C(1)	1.7741(13)
S(1)-C(7)	1.8062(13)	O(3)-C(8)	1.2397(18)	O(4)-C(10)	1.3141(16)
O(5)-C(10)	1.2161(17)	N(1)-C(8)	1.3371(17)	N(1)-C(2)	1.4499(16)
N(2)-N(3)	1.2451(17)	N(2)-C(4)	1.5014(17)	N(3)-N(4)	1.1338(19)
C(1)-C(2)	1.5353(18)	C(2)-C(3)	1.5477(17)	C(3)-C(4)	1.5376(18)
C(3)-C(7)	1.5599(17)	C(4)-C(5)	1.5286(19)	C(5)-C(6)	1.5429(18)
C(6)-C(10)	1.5236(17)	C(6)-C(7)	1.5346(17)	C(8)-C(9)	1.4941(18)
O(2)-S(1)-O(1)	118.07(6)	O(2)-S(1)-C(1)	111.83(6)		
O(1)-S(1)-C(1)	108.29(6)	O(2)-S(1)-C(7)	111.55(6)		
O(1)-S(1)-C(7)	109.43(6)	C(1)-S(1)-C(7)	95.29(6)		
C(8)-N(1)-C(2)	120.56(11)	N(3)-N(2)-C(4)	113.40(12)		
N(4)-N(3)-N(2)	174.11(15)	C(2)-C(1)-S(1)	101.78(8)		
N(1)-C(2)-C(1)	112.75(10)	N(1)-C(2)-C(3)	110.47(10)		
C(1)-C(2)-C(3)	107.04(10)	C(4)-C(3)-C(2)	112.72(10)		
C(4)-C(3)-C(7)	105.28(10)	C(2)-C(3)-C(7)	109.00(10)		
N(2)-C(4)-C(5)	111.61(11)	N(2)-C(4)-C(3)	106.55(10)		

C(5)-C(4)-C(3)	103.73(11)	C(4)-C(5)-C(6)	103.99(10)
C(10)-C(6)-C(7)	111.51(10)	C(10)-C(6)-C(5)	113.89(11)
C(7)-C(6)-C(5)	103.81(10)	C(6)-C(7)-C(3)	107.09(10)
C(6)-C(7)-S(1)	112.54(9)	C(3)-C(7)-S(1)	105.76(8)
O(3)-C(8)-N(1)	120.75(12)	O(3)-C(8)-C(9)	122.22(12)
N(1)-C(8)-C(9)	117.02(12)	O(5)-C(10)-O(4)	124.45(12)
O(5)-C(10)-C(6)	124.01(12)	O(4)-C(10)-C(6)	111.50(11)

Figure C-6: ORTEP diagram of **3-37** with thermal ellipsoids shown at the 50% probability level.

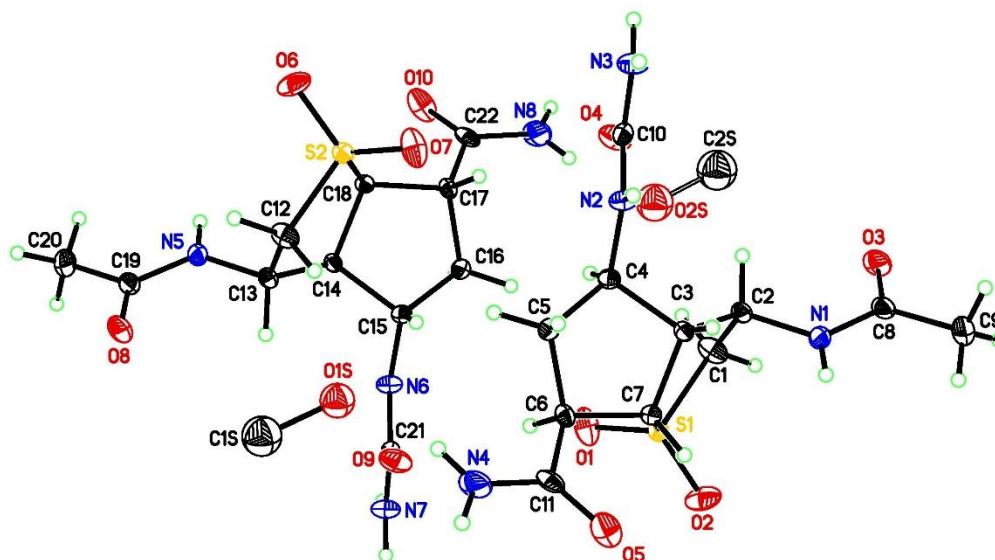


Table C-6: Bond Lengths (Å) and Angles (°) for 3-37.

S(1)-O(1)	1.4388(15)	S(1)-O(2)	1.4486(14)	S(1)-C(1)	1.7915(19)
S(1)-C(7)	1.8107(18)	O(3)-C(8)	1.235(3)	O(4)-C(10)	1.238(3)
O(5)-C(11)	1.236(3)	N(1)-C(8)	1.341(2)	N(1)-C(2)	1.457(2)
N(2)-C(10)	1.356(2)	N(2)-C(4)	1.448(2)	N(3)-C(10)	1.350(3)
N(4)-C(11)	1.322(3)	C(1)-C(2)	1.537(3)	C(2)-C(3)	1.536(2)
C(3)-C(7)	1.533(2)	C(3)-C(4)	1.541(2)	C(4)-C(5)	1.533(2)
C(5)-C(6)	1.548(2)	C(6)-C(7)	1.541(2)	C(6)-C(11)	1.528(3)
C(8)-C(9)	1.508(3)	S(2)-O(7)	1.4375(15)	S(2)-O(6)	1.4507(14)
S(2)-C(12)	1.7856(18)	S(2)-C(18)	1.8126(18)	O(8)-C(19)	1.241(3)
O(9)-C(21)	1.239(2)	O(10)-C(22)	1.223(3)	N(5)-C(19)	1.337(2)
N(5)-C(13)	1.459(2)	N(6)-C(21)	1.351(2)	N(6)-C(15)	1.449(2)
N(7)-C(21)	1.350(3)	N(8)-C(22)	1.333(3)	C(12)-C(13)	1.538(3)
C(13)-C(14)	1.536(2)	C(14)-C(18)	1.537(2)	C(14)-C(15)	1.544(2)
C(15)-C(16)	1.532(2)	C(16)-C(17)	1.548(2)	C(17)-C(22)	1.522(3)

C(17)-C(18) 1.538(2) C(19)-C(20) 1.504(3) O(1S)-C(1S) 1.427(4)
 O(2S)-C(2S) 1.430(15)

O(1)-S(1)-O(2)	118.05(10)	O(1)-S(1)-C(1)	110.33(10)
O(2)-S(1)-C(1)	109.54(9)	O(1)-S(1)-C(7)	110.84(8)
O(2)-S(1)-C(7)	108.33(9)	C(1)-S(1)-C(7)	97.86(8)
C(8)-N(1)-C(2)	122.19(16)	C(10)-N(2)-C(4)	123.73(16)
C(2)-C(1)-S(1)	107.07(12)	N(1)-C(2)-C(3)	108.47(15)
N(1)-C(2)-C(1)	113.79(15)	C(3)-C(2)-C(1)	108.32(14)
C(7)-C(3)-C(2)	110.86(14)	C(7)-C(3)-C(4)	103.99(13)
C(2)-C(3)-C(4)	115.67(14)	N(2)-C(4)-C(5)	112.67(15)
N(2)-C(4)-C(3)	112.59(14)	C(5)-C(4)-C(3)	102.37(14)
C(4)-C(5)-C(6)	104.74(14)	C(11)-C(6)-C(7)	111.53(15)
C(11)-C(6)-C(5)	112.83(15)	C(7)-C(6)-C(5)	105.00(13)
C(3)-C(7)-C(6)	107.21(13)	C(3)-C(7)-S(1)	105.24(12)
C(6)-C(7)-S(1)	113.94(12)	O(3)-C(8)-N(1)	121.70(18)
O(3)-C(8)-C(9)	122.17(17)	N(1)-C(8)-C(9)	116.04(18)
O(4)-C(10)-N(3)	122.45(17)	O(4)-C(10)-N(2)	122.52(17)
N(3)-C(10)-N(2)	115.03(18)	O(5)-C(11)-N(4)	122.33(19)
O(5)-C(11)-C(6)	121.48(16)	N(4)-C(11)-C(6)	116.18(18)
O(7)-S(2)-O(6)	117.75(10)	O(7)-S(2)-C(12)	110.69(9)
O(6)-S(2)-C(12)	109.54(9)	O(7)-S(2)-C(18)	111.06(8)
O(6)-S(2)-C(18)	107.99(8)	C(12)-S(2)-C(18)	98.00(8)
C(19)-N(5)-C(13)	121.79(16)	C(21)-N(6)-C(15)	124.23(16)
C(13)-C(12)-S(2)	106.79(12)	N(5)-C(13)-C(14)	108.89(14)
N(5)-C(13)-C(12)	113.60(15)	C(14)-C(13)-C(12)	108.60(14)
C(13)-C(14)-C(18)	110.92(14)	C(13)-C(14)-C(15)	115.35(14)
C(18)-C(14)-C(15)	104.23(13)	N(6)-C(15)-C(16)	112.61(15)
N(6)-C(15)-C(14)	112.38(14)	C(16)-C(15)-C(14)	102.62(13)
C(15)-C(16)-C(17)	104.51(14)	C(22)-C(17)-C(18)	111.82(15)
C(22)-C(17)-C(16)	111.37(15)	C(18)-C(17)-C(16)	104.96(13)
C(14)-C(18)-C(17)	107.43(13)	C(14)-C(18)-S(2)	105.60(12)
C(17)-C(18)-S(2)	113.62(12)	O(8)-C(19)-N(5)	121.54(18)
O(8)-C(19)-C(20)	121.85(17)	N(5)-C(19)-C(20)	116.55(18)
O(9)-C(21)-N(7)	121.51(17)	O(9)-C(21)-N(6)	122.61(17)
N(7)-C(21)-N(6)	115.88(18)	O(10)-C(22)-N(8)	123.40(19)
O(10)-C(22)-C(17)	122.04(17)	N(8)-C(22)-C(17)	114.53(18)

Figure C-7: ORTEP diagram of **4-4c** with thermal ellipsoids shown at the 50% probability level.

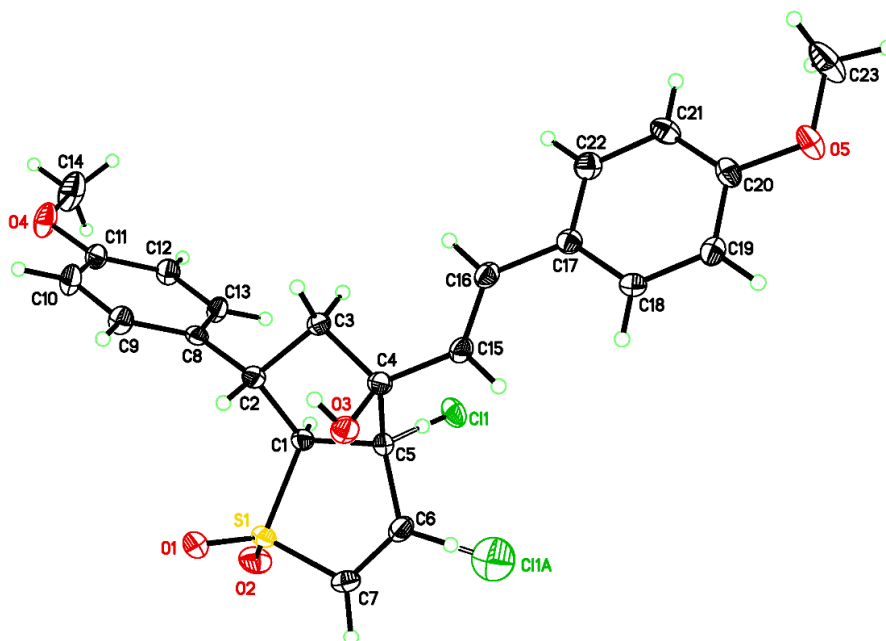


Table C-7: Bond Lengths (Å) and Angles (°) for **4-4c**.

Cl(1)-C(5)	1.791(2)	Cl(1A)-C(6)	1.630(13)	S(1)-O(1)	1.4319(15)
S(1)-O(2)	1.4357(15)	S(1)-C(7)	1.744(2)	S(1)-C(1)	1.7956(19)
O(3)-C(4)	1.435(2)	O(4)-C(11)	1.367(2)	O(4)-C(14)	1.416(3)
O(5)-C(20)	1.377(2)	O(5)-C(23)	1.422(3)	C(1)-C(2)	1.535(3)
C(1)-C(5)	1.544(3)	C(2)-C(8)	1.507(3)	C(2)-C(3)	1.530(3)
C(3)-C(4)	1.518(3)	C(4)-C(15)	1.488(3)	C(4)-C(5)	1.564(3)
C(5)-C(6)	1.493(3)	C(6)-C(7)	1.314(3)	C(8)-C(13)	1.383(3)
C(8)-C(9)	1.386(3)	C(9)-C(10)	1.375(3)	C(10)-C(11)	1.380(3)
C(11)-C(12)	1.385(3)	C(12)-C(13)	1.381(3)	C(15)-C(16)	1.322(3)
C(16)-C(17)	1.467(3)	C(17)-C(22)	1.384(3)	C(17)-C(18)	1.395(3)
C(18)-C(19)	1.372(3)	C(19)-C(20)	1.386(3)	C(20)-C(21)	1.384(3)
C(21)-C(22)	1.383(3)	O(3)-H(3O)	0.81(3)		
O(1)-S(1)-O(2)	117.42(9)	O(1)-S(1)-C(7)	109.99(9)		
O(2)-S(1)-C(7)	110.87(9)	O(1)-S(1)-C(1)	111.56(9)		
O(2)-S(1)-C(1)	109.29(9)	C(7)-S(1)-C(1)	95.55(9)		
C(11)-O(4)-C(14)	117.10(16)	C(20)-O(5)-C(23)	117.05(17)		

C(2)-C(1)-C(5)	107.19(15)	C(2)-C(1)-S(1)	115.27(13)
C(5)-C(1)-S(1)	105.70(13)	C(8)-C(2)-C(3)	114.91(16)
C(8)-C(2)-C(1)	115.71(16)	C(3)-C(2)-C(1)	101.49(15)
C(4)-C(3)-C(2)	103.89(15)	O(3)-C(4)-C(15)	109.12(15)
O(3)-C(4)-C(3)	109.99(16)	C(15)-C(4)-C(3)	117.27(16)
O(3)-C(4)-C(5)	104.06(15)	C(15)-C(4)-C(5)	114.13(16)
C(3)-C(4)-C(5)	101.33(15)	C(6)-C(5)-C(1)	109.42(16)
C(6)-C(5)-C(4)	115.84(16)	C(1)-C(5)-C(4)	104.87(15)
C(6)-C(5)-Cl(1)	108.18(13)	C(1)-C(5)-Cl(1)	109.46(13)
C(4)-C(5)-Cl(1)	108.94(13)	C(7)-C(6)-C(5)	117.10(18)
C(7)-C(6)-Cl(1A)	117.7(5)	C(5)-C(6)-Cl(1A)	119.1(5)
C(6)-C(7)-S(1)	112.08(16)	C(13)-C(8)-C(9)	118.06(18)
C(13)-C(8)-C(2)	122.74(18)	C(9)-C(8)-C(2)	119.12(18)
C(10)-C(9)-C(8)	121.54(19)	C(9)-C(10)-C(11)	119.53(19)
O(4)-C(11)-C(10)	115.71(18)	O(4)-C(11)-C(12)	124.13(18)
C(10)-C(11)-C(12)	120.16(18)	C(13)-C(12)-C(11)	119.38(19)
C(12)-C(13)-C(8)	121.32(19)	C(16)-C(15)-C(4)	125.77(18)
C(15)-C(16)-C(17)	126.72(19)	C(22)-C(17)-C(18)	117.70(18)
C(22)-C(17)-C(16)	119.81(18)	C(18)-C(17)-C(16)	122.49(18)
C(19)-C(18)-C(17)	121.10(19)	C(18)-C(19)-C(20)	120.12(19)
O(5)-C(20)-C(21)	124.53(18)	O(5)-C(20)-C(19)	115.43(18)
C(21)-C(20)-C(19)	120.03(18)	C(22)-C(21)-C(20)	118.93(19)
C(21)-C(22)-C(17)	122.09(19)	C(4)-O(3)-H(3O)	110(2)

Figure C-8: ORTEP diagram of **4-5b** with thermal ellipsoids shown at the 50% probability level.

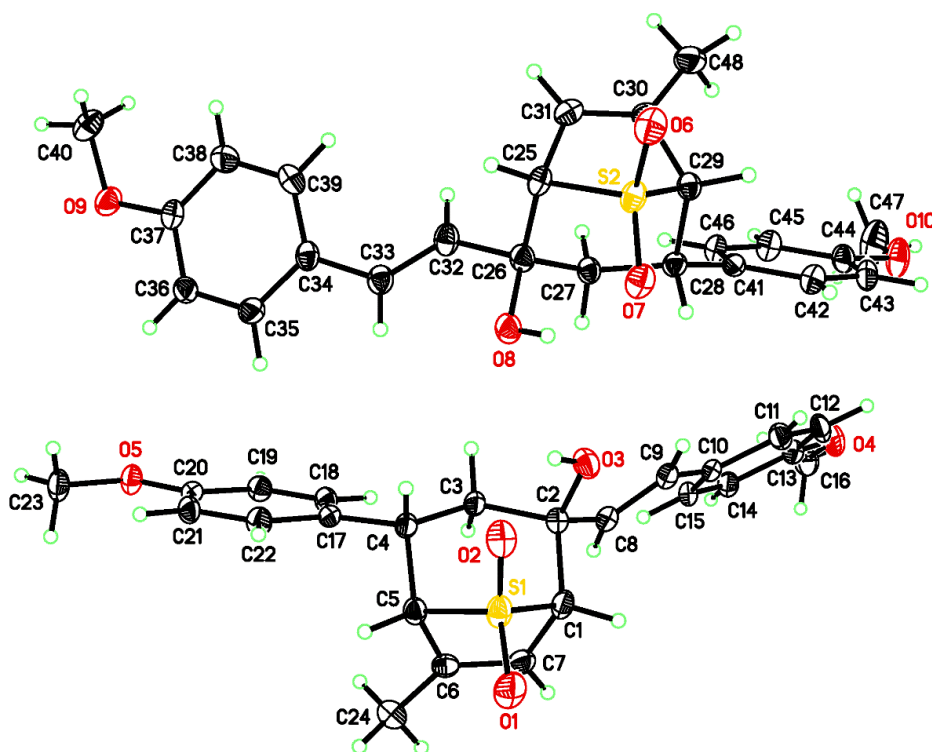


Table C-8: Bond Lengths (Å) and Angles (°) for **4-5b**.

S(1)-O(1)	1.4341(14)	S(1)-O(2)	1.4389(14)	S(1)-C(5)	1.8004(18)
S(1)-C(1)	1.8022(18)	O(3)-C(2)	1.413(2)	O(4)-C(13)	1.367(2)
O(4)-C(16)	1.427(2)	O(5)-C(20)	1.370(2)	O(5)-C(23)	1.423(2)
C(1)-C(7)	1.505(3)	C(1)-C(2)	1.565(2)	C(2)-C(8)	1.505(2)
C(2)-C(3)	1.547(2)	C(3)-C(4)	1.539(2)	C(4)-C(17)	1.523(2)
C(4)-C(5)	1.557(2)	C(5)-C(6)	1.507(3)	C(6)-C(7)	1.330(3)
C(6)-C(24)	1.495(3)	C(8)-C(9)	1.326(2)	C(9)-C(10)	1.468(2)
C(10)-C(15)	1.390(3)	C(10)-C(11)	1.400(2)	C(11)-C(12)	1.375(3)
C(12)-C(13)	1.383(3)	C(13)-C(14)	1.390(2)	C(14)-C(15)	1.381(3)
C(17)-C(18)	1.391(2)	C(17)-C(22)	1.393(2)	C(18)-C(19)	1.380(2)
C(19)-C(20)	1.381(2)	C(20)-C(21)	1.386(2)	C(21)-C(22)	1.393(2)
S(2)-O(6)	1.4378(13)	S(2)-O(7)	1.4443(13)	S(2)-C(29)	1.7863(17)
S(2)-C(25)	1.7964(17)	O(8)-C(26)	1.422(2)	O(9)-C(37)	1.362(2)
O(9)-C(40)	1.421(2)	O(10)-C(44)	1.366(2)	O(10)-C(47)	1.433(2)
C(25)-C(31)	1.510(2)	C(25)-C(26)	1.567(2)	C(26)-C(32)	1.504(2)
C(26)-C(27)	1.547(2)	C(27)-C(28)	1.537(2)	C(28)-C(41)	1.518(2)
C(28)-C(29)	1.560(2)	C(29)-C(30)	1.512(2)	C(30)-C(31)	1.331(2)

C(30)-C(48)	1.485(3)	C(32)-C(33)	1.315(3)	C(33)-C(34)	1.473(2)
C(34)-C(39)	1.385(3)	C(34)-C(35)	1.391(2)	C(35)-C(36)	1.379(2)
C(36)-C(37)	1.385(3)	C(37)-C(38)	1.384(3)	C(38)-C(39)	1.386(3)
C(41)-C(46)	1.382(2)	C(41)-C(42)	1.398(2)	C(42)-C(43)	1.379(2)
C(43)-C(44)	1.386(3)	C(44)-C(45)	1.384(2)	C(45)-C(46)	1.385(2)

O(1)-S(1)-O(2)	117.02(9)	O(1)-S(1)-C(5)	111.98(8)
O(2)-S(1)-C(5)	111.46(8)	O(1)-S(1)-C(1)	110.51(8)
O(2)-S(1)-C(1)	113.20(8)	C(5)-S(1)-C(1)	89.43(8)
C(13)-O(4)-C(16)	117.37(14)	C(20)-O(5)-C(23)	116.87(14)
C(7)-C(1)-C(2)	111.71(14)	C(7)-C(1)-S(1)	98.57(12)
C(2)-C(1)-S(1)	109.28(12)	O(3)-C(2)-C(8)	107.23(14)
O(3)-C(2)-C(3)	112.69(14)	C(8)-C(2)-C(3)	107.67(14)
O(3)-C(2)-C(1)	110.42(14)	C(8)-C(2)-C(1)	108.07(14)
C(3)-C(2)-C(1)	110.56(14)	C(4)-C(3)-C(2)	117.57(14)
C(17)-C(4)-C(3)	112.55(14)	C(17)-C(4)-C(5)	110.56(14)
C(3)-C(4)-C(5)	111.02(14)	C(6)-C(5)-C(4)	113.37(14)
C(6)-C(5)-S(1)	99.75(11)	C(4)-C(5)-S(1)	106.57(12)
C(7)-C(6)-C(24)	126.69(18)	C(7)-C(6)-C(5)	112.52(16)
C(24)-C(6)-C(5)	120.79(16)	C(6)-C(7)-C(1)	114.61(16)
C(9)-C(8)-C(2)	124.29(17)	C(8)-C(9)-C(10)	126.71(17)
C(15)-C(10)-C(11)	117.03(16)	C(15)-C(10)-C(9)	124.10(16)
C(11)-C(10)-C(9)	118.82(16)	C(12)-C(11)-C(10)	121.89(17)
C(11)-C(12)-C(13)	119.80(17)	O(4)-C(13)-C(12)	115.93(16)
O(4)-C(13)-C(14)	124.28(17)	C(12)-C(13)-C(14)	119.78(17)
C(15)-C(14)-C(13)	119.61(17)	C(14)-C(15)-C(10)	121.89(16)
C(18)-C(17)-C(22)	117.00(16)	C(18)-C(17)-C(4)	123.43(15)
C(22)-C(17)-C(4)	119.53(15)	C(19)-C(18)-C(17)	121.58(16)
C(18)-C(19)-C(20)	120.35(16)	O(5)-C(20)-C(19)	115.30(15)
O(5)-C(20)-C(21)	124.76(15)	C(19)-C(20)-C(21)	119.93(16)
C(20)-C(21)-C(22)	118.79(16)	C(17)-C(22)-C(21)	122.32(16)
O(6)-S(2)-O(7)	116.58(8)	O(6)-S(2)-C(29)	111.70(8)
O(7)-S(2)-C(29)	111.73(8)	O(6)-S(2)-C(25)	111.47(8)
O(7)-S(2)-C(25)	112.67(8)	C(29)-S(2)-C(25)	89.62(8)
C(37)-O(9)-C(40)	117.58(15)	C(44)-O(10)-C(47)	116.58(15)
C(31)-C(25)-C(26)	111.26(14)	C(31)-C(25)-S(2)	98.38(11)
C(26)-C(25)-S(2)	109.52(12)	O(8)-C(26)-C(32)	107.40(14)
O(8)-C(26)-C(27)	112.25(14)	C(32)-C(26)-C(27)	110.21(14)
O(8)-C(26)-C(25)	110.93(14)	C(32)-C(26)-C(25)	104.97(14)
C(27)-C(26)-C(25)	110.78(14)	C(28)-C(27)-C(26)	116.22(14)
C(41)-C(28)-C(27)	114.57(14)	C(41)-C(28)-C(29)	107.90(13)
C(27)-C(28)-C(29)	111.17(14)	C(30)-C(29)-C(28)	112.93(14)
C(30)-C(29)-S(2)	99.81(11)	C(28)-C(29)-S(2)	107.26(11)
C(31)-C(30)-C(48)	128.04(17)	C(31)-C(30)-C(29)	112.03(16)
C(48)-C(30)-C(29)	119.93(16)	C(30)-C(31)-C(25)	114.54(16)

C(33)-C(32)-C(26)	126.50(17)	C(32)-C(33)-C(34)	125.50(18)
C(39)-C(34)-C(35)	117.41(17)	C(39)-C(34)-C(33)	122.37(16)
C(35)-C(34)-C(33)	120.19(16)	C(36)-C(35)-C(34)	121.33(17)
C(35)-C(36)-C(37)	120.29(17)	O(9)-C(37)-C(38)	124.62(17)
O(9)-C(37)-C(36)	115.93(16)	C(38)-C(37)-C(36)	119.46(17)
C(37)-C(38)-C(39)	119.44(18)	C(34)-C(39)-C(38)	122.04(18)
C(46)-C(41)-C(42)	117.34(16)	C(46)-C(41)-C(28)	124.08(15)
C(42)-C(41)-C(28)	118.48(15)	C(43)-C(42)-C(41)	121.44(17)
C(42)-C(43)-C(44)	120.02(16)	O(10)-C(44)-C(45)	124.59(17)
O(10)-C(44)-C(43)	115.87(16)	C(45)-C(44)-C(43)	119.52(16)
C(44)-C(45)-C(46)	119.68(17)	C(41)-C(46)-C(45)	121.98(16)
C(2)-O(3)-H(3O)	107.4(19)		

Figure C-9: ORTEP diagram of **4-4e'** with thermal ellipsoids shown at the 50% probability level.

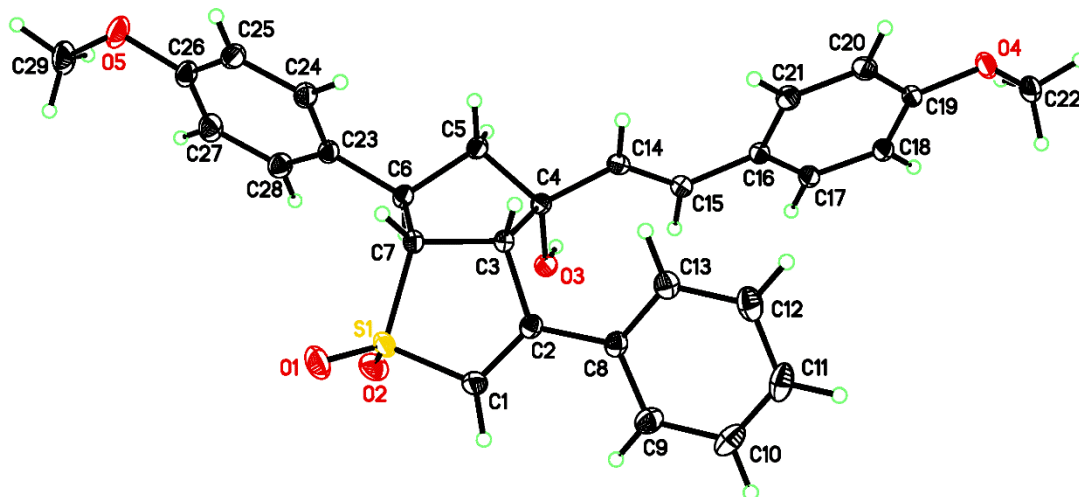


Table C-9: Bond Lengths (Å) and Angles (°) for **4-4e'**.

S(1)-O(2)	1.4413(10)	S(1)-O(1)	1.4417(10)	S(1)-C(1)	1.7326(13)
S(1)-C(7)	1.7937(12)	O(3)-C(4)	1.4255(14)	O(4)-C(19)	1.3640(14)
O(4)-C(22)	1.4254(15)	O(5)-C(26)	1.3669(15)	O(5)-C(29)	1.4202(18)
C(1)-C(2)	1.3303(17)	C(2)-C(8)	1.4733(16)	C(2)-C(3)	1.5105(16)
C(3)-C(7)	1.5438(16)	C(3)-C(4)	1.5542(16)	C(4)-C(14)	1.5007(16)
C(4)-C(5)	1.5312(16)	C(5)-C(6)	1.5337(16)	C(6)-C(23)	1.5046(16)
C(6)-C(7)	1.5443(16)	C(8)-C(9)	1.3941(17)	C(8)-C(13)	1.3949(17)
C(9)-C(10)	1.3805(18)	C(10)-C(11)	1.378(2)	C(11)-C(12)	1.384(2)
C(12)-C(13)	1.3864(18)	C(14)-C(15)	1.3251(16)	C(15)-C(16)	1.4620(16)
C(16)-C(17)	1.3913(16)	C(16)-C(21)	1.4005(16)	C(17)-C(18)	1.3856(16)
C(18)-C(19)	1.3815(16)	C(19)-C(20)	1.3918(17)	C(20)-C(21)	1.3767(17)
C(23)-C(28)	1.3850(17)	C(23)-C(24)	1.3937(17)	C(24)-C(25)	1.3773(17)
C(25)-C(26)	1.3869(19)	C(26)-C(27)	1.3812(19)	C(27)-C(28)	1.3962(17)
O(3)-H(3O)	0.83(2)				
O(2)-S(1)-O(1)	116.12(6)	O(2)-S(1)-C(1)	110.45(6)		
O(1)-S(1)-C(1)	110.89(6)	O(2)-S(1)-C(7)	112.14(6)		
O(1)-S(1)-C(7)	110.08(6)	C(1)-S(1)-C(7)	95.24(6)		
C(19)-O(4)-C(22)	116.85(9)	C(26)-O(5)-C(29)	117.35(12)		
C(2)-C(1)-S(1)	113.11(10)	C(1)-C(2)-C(8)	123.35(11)		
C(1)-C(2)-C(3)	115.57(11)	C(8)-C(2)-C(3)	121.08(10)		
C(2)-C(3)-C(7)	109.12(9)	C(2)-C(3)-C(4)	116.02(9)		
C(7)-C(3)-C(4)	104.30(9)	O(3)-C(4)-C(14)	112.33(9)		
O(3)-C(4)-C(5)	109.95(9)	C(14)-C(4)-C(5)	112.92(10)		

O(3)-C(4)-C(3)	105.17(9)	C(14)-C(4)-C(3)	114.35(10)
C(5)-C(4)-C(3)	101.35(9)	C(4)-C(5)-C(6)	103.44(9)
C(23)-C(6)-C(5)	115.78(10)	C(23)-C(6)-C(7)	113.68(10)
C(5)-C(6)-C(7)	101.72(9)	C(3)-C(7)-C(6)	107.74(9)
C(3)-C(7)-S(1)	106.17(8)	C(6)-C(7)-S(1)	114.79(8)
C(9)-C(8)-C(13)	118.47(11)	C(9)-C(8)-C(2)	120.00(11)
C(13)-C(8)-C(2)	121.53(11)	C(10)-C(9)-C(8)	121.15(13)
C(11)-C(10)-C(9)	119.92(13)	C(10)-C(11)-C(12)	119.82(12)
C(11)-C(12)-C(13)	120.55(13)	C(12)-C(13)-C(8)	120.08(12)
C(15)-C(14)-C(4)	123.14(11)	C(14)-C(15)-C(16)	128.65(11)
C(17)-C(16)-C(21)	117.39(11)	C(17)-C(16)-C(15)	118.31(10)
C(21)-C(16)-C(15)	124.29(11)	C(18)-C(17)-C(16)	122.37(11)
C(19)-C(18)-C(17)	118.92(11)	O(4)-C(19)-C(18)	123.98(11)
O(4)-C(19)-C(20)	115.94(10)	C(18)-C(19)-C(20)	120.08(11)
C(21)-C(20)-C(19)	120.29(11)	C(20)-C(21)-C(16)	120.94(11)
C(28)-C(23)-C(24)	118.03(11)	C(28)-C(23)-C(6)	120.93(11)
C(24)-C(23)-C(6)	121.01(11)	C(25)-C(24)-C(23)	121.00(12)
C(24)-C(25)-C(26)	120.14(12)	O(5)-C(26)-C(27)	124.91(12)
O(5)-C(26)-C(25)	114.89(12)	C(27)-C(26)-C(25)	120.20(12)
C(26)-C(27)-C(28)	118.94(12)	C(23)-C(28)-C(27)	121.66(12)
C(4)-O(3)-H(3O)	108.1(13)		

Figure C-10: ORTEP diagram of **4-6f** with thermal ellipsoids shown at the 50% probability level.

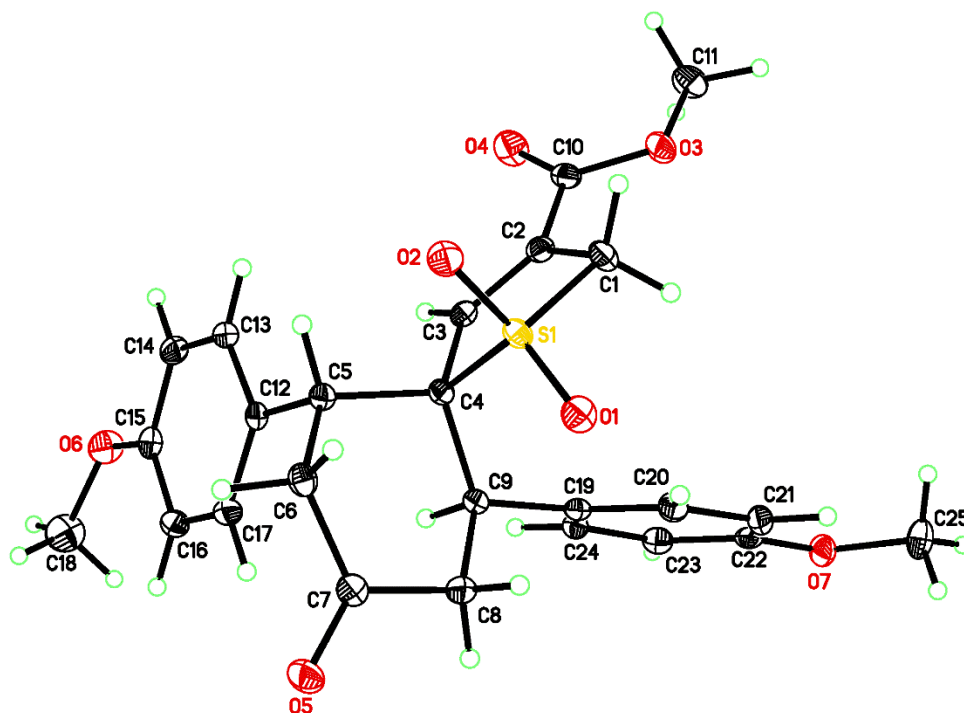


Table C-10: Bond Lengths (Å) and Angles (°) for **4-6f**.

S(1)-O(2)	1.4358(11)	S(1)-O(1)	1.4377(10)	S(1)-C(1)	1.7845(14)
S(1)-C(4)	1.8478(13)	O(3)-C(10)	1.3380(17)	O(3)-C(11)	1.4472(17)
O(4)-C(10)	1.2011(17)	O(5)-C(7)	1.2153(17)	O(6)-C(15)	1.3673(17)
O(6)-C(18)	1.4221(19)	O(7)-C(22)	1.3643(16)	O(7)-C(25)	1.4276(18)
C(1)-C(2)	1.4985(19)	C(2)-C(3)	1.3313(18)	C(2)-C(10)	1.4836(18)
C(3)-C(4)	1.5041(18)	C(4)-C(9)	1.5553(18)	C(4)-C(5)	1.5637(18)
C(5)-C(12)	1.5172(18)	C(5)-C(6)	1.5376(18)	C(6)-C(7)	1.5018(19)
C(7)-C(8)	1.5048(19)	C(8)-C(9)	1.5372(18)	C(9)-C(19)	1.5190(18)
C(12)-C(17)	1.3890(19)	C(12)-C(13)	1.3931(19)	C(13)-C(14)	1.378(2)
C(14)-C(15)	1.389(2)	C(15)-C(16)	1.3834(19)	C(16)-C(17)	1.3892(19)
C(19)-C(20)	1.3874(19)	C(19)-C(24)	1.3935(19)	C(20)-C(21)	1.3907(19)
C(21)-C(22)	1.386(2)	C(22)-C(23)	1.3882(19)	C(23)-C(24)	1.3784(19)
O(2)-S(1)-O(1)	117.74(6)	O(2)-S(1)-C(1)	107.85(7)		
O(1)-S(1)-C(1)	111.39(6)	O(2)-S(1)-C(4)	107.54(6)		
O(1)-S(1)-C(4)	113.37(6)	C(1)-S(1)-C(4)	96.82(6)		
C(10)-O(3)-C(11)	114.94(11)	C(15)-O(6)-C(18)	117.34(12)		

C(22)-O(7)-C(25)	117.35(11)	C(2)-C(1)-S(1)	102.10(9)
C(3)-C(2)-C(10)	122.35(12)	C(3)-C(2)-C(1)	117.16(12)
C(10)-C(2)-C(1)	120.49(12)	C(2)-C(3)-C(4)	117.80(12)
C(3)-C(4)-C(9)	111.62(11)	C(3)-C(4)-C(5)	113.64(11)
C(9)-C(4)-C(5)	108.56(10)	C(3)-C(4)-S(1)	99.94(9)
C(9)-C(4)-S(1)	115.58(9)	C(5)-C(4)-S(1)	107.39(9)
C(12)-C(5)-C(6)	113.56(11)	C(12)-C(5)-C(4)	112.33(11)
C(6)-C(5)-C(4)	109.70(11)	C(7)-C(6)-C(5)	115.56(11)
O(5)-C(7)-C(6)	121.44(13)	O(5)-C(7)-C(8)	121.25(13)
C(6)-C(7)-C(8)	117.25(12)	C(7)-C(8)-C(9)	114.43(11)
C(19)-C(9)-C(8)	111.52(11)	C(19)-C(9)-C(4)	117.70(11)
C(8)-C(9)-C(4)	112.82(11)	O(4)-C(10)-O(3)	124.26(13)
O(4)-C(10)-C(2)	125.10(13)	O(3)-C(10)-C(2)	110.64(12)
C(17)-C(12)-C(13)	117.53(12)	C(17)-C(12)-C(5)	123.05(12)
C(13)-C(12)-C(5)	119.41(12)	C(14)-C(13)-C(12)	121.30(13)
C(13)-C(14)-C(15)	120.19(13)	O(6)-C(15)-C(16)	124.50(13)
O(6)-C(15)-C(14)	115.75(12)	C(16)-C(15)-C(14)	119.75(13)
C(15)-C(16)-C(17)	119.25(13)	C(12)-C(17)-C(16)	121.92(13)
C(20)-C(19)-C(24)	117.69(12)	C(20)-C(19)-C(9)	123.93(12)
C(24)-C(19)-C(9)	118.24(12)	C(19)-C(20)-C(21)	121.48(13)
C(22)-C(21)-C(20)	119.65(13)	O(7)-C(22)-C(21)	124.73(13)
O(7)-C(22)-C(23)	115.65(12)	C(21)-C(22)-C(23)	119.62(13)
C(24)-C(23)-C(22)	119.96(13)	C(23)-C(24)-C(19)	121.58(13)

Figure C-11: ORTEP diagram of **5-5** with thermal ellipsoids shown at the 50% probability level.

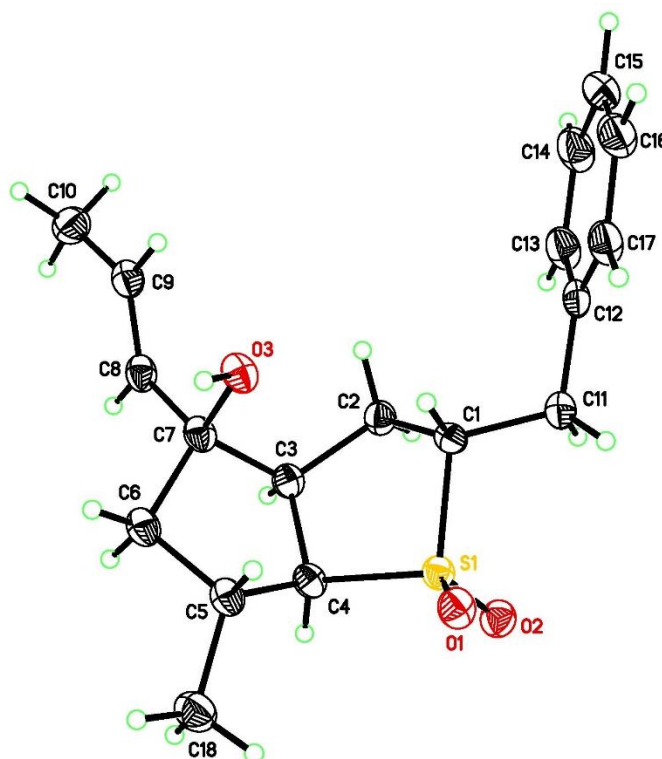


Table C-11: Bond Lengths (Å) and Angles (°) for 5-5.

S(1)-O(2)	1.4492(14)	S(1)-O(1)	1.4517(13)	S(1)-C(4)	1.7927(19)
S(1)-C(1)	1.7980(18)	O(3)-C(7)	1.435(2)	C(1)-C(2)	1.530(3)
C(1)-C(11)	1.536(3)	C(2)-C(3)	1.545(3)	C(3)-C(7)	1.554(3)
C(3)-C(4)	1.561(3)	C(4)-C(5)	1.542(3)	C(5)-C(6)	1.529(3)
C(5)-C(18)	1.526(3)	C(6)-C(7)	1.531(3)	C(7)-C(8)	1.508(3)
C(8)-C(9)	1.322(3)	C(9)-C(10)	1.498(3)	C(11)-C(12)	1.513(3)
C(12)-C(13)	1.394(3)	C(12)-C(17)	1.394(3)	C(13)-C(14)	1.386(3)
C(14)-C(15)	1.376(3)	C(15)-C(16)	1.382(3)	C(16)-C(17)	1.387(3)
O(2)-S(1)-O(1)	116.69(8)	O(2)-S(1)-C(4)	108.78(9)		
O(1)-S(1)-C(4)	112.39(8)	O(2)-S(1)-C(1)	108.56(8)		
O(1)-S(1)-C(1)	111.12(9)	C(4)-S(1)-C(1)	97.56(9)		
C(2)-C(1)-C(11)	116.22(16)	C(2)-C(1)-S(1)	103.03(13)		
C(11)-C(1)-S(1)	110.41(13)	C(1)-C(2)-C(3)	109.12(15)		
C(2)-C(3)-C(7)	115.07(15)	C(2)-C(3)-C(4)	110.89(15)		
C(7)-C(3)-C(4)	104.48(15)	C(5)-C(4)-C(3)	107.46(15)		
C(5)-C(4)-S(1)	115.77(13)	C(3)-C(4)-S(1)	105.52(12)		
C(18)-C(5)-C(6)	114.55(17)	C(18)-C(5)-C(4)	113.23(16)		

C(6)-C(5)-C(4)	102.03(15)	C(5)-C(6)-C(7)	104.19(15)
O(3)-C(7)-C(8)	111.02(15)	O(3)-C(7)-C(6)	110.72(15)
C(8)-C(7)-C(6)	113.80(16)	O(3)-C(7)-C(3)	107.34(14)
C(8)-C(7)-C(3)	111.44(15)	C(6)-C(7)-C(3)	102.03(15)
C(9)-C(8)-C(7)	126.04(18)	C(8)-C(9)-C(10)	125.60(19)
C(12)-C(11)-C(1)	112.05(16)	C(13)-C(12)-C(17)	118.35(19)
C(13)-C(12)-C(11)	121.91(19)	C(17)-C(12)-C(11)	119.74(18)
C(14)-C(13)-C(12)	120.5(2)	C(15)-C(14)-C(13)	120.7(2)
C(14)-C(15)-C(16)	119.5(2)	C(15)-C(16)-C(17)	120.3(2)
C(16)-C(17)-C(12)	120.7(2)		

Figure C-12: ORTEP diagram of **5-10** with thermal ellipsoids shown at the 50% probability level.

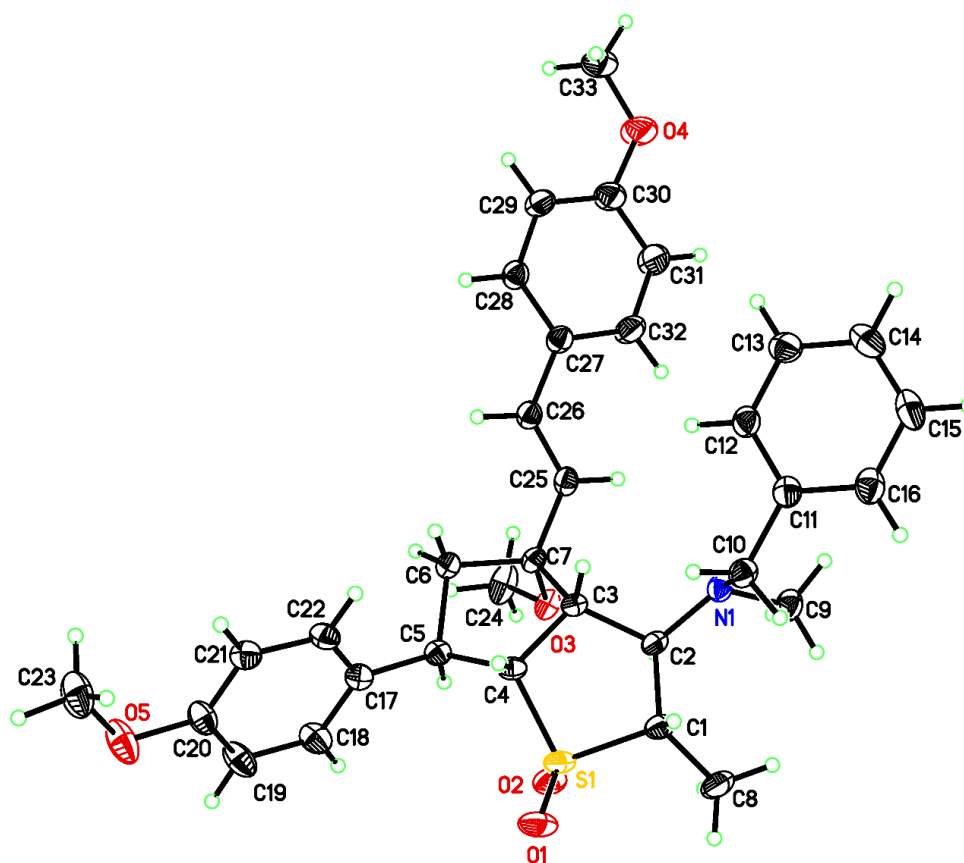


Table C-12: Bond Lengths (Å) and Angles (°) for **5-10**.

S(1)-O(2)	1.4442(12)	S(1)-O(1)	1.4496(12)	S(1)-C(4)	1.7826(16)
S(1)-C(1)	1.7922(17)	O(3)-C(24)	1.4293(19)	O(3)-C(7)	1.4467(18)
O(4)-C(30)	1.369(2)	O(4)-C(33)	1.420(2)	O(5)-C(20)	1.373(2)
O(5)-C(23)	1.426(2)	N(1)-C(2)	1.4595(19)	N(1)-C(10)	1.4649(19)
N(1)-C(9)	1.466(2)	C(1)-C(8)	1.524(2)	C(1)-C(2)	1.554(2)
C(2)-C(3)	1.552(2)	C(3)-C(7)	1.551(2)	C(3)-C(4)	1.551(2)
C(4)-C(5)	1.543(2)	C(5)-C(17)	1.514(2)	C(5)-C(6)	1.541(2)
C(6)-C(7)	1.533(2)	C(7)-C(25)	1.502(2)	C(10)-C(11)	1.515(2)
C(11)-C(16)	1.391(2)	C(11)-C(12)	1.394(2)	C(12)-C(13)	1.387(2)
C(13)-C(14)	1.388(3)	C(14)-C(15)	1.379(3)	C(15)-C(16)	1.393(3)
C(17)-C(22)	1.386(2)	C(17)-C(18)	1.394(2)	C(18)-C(19)	1.384(2)
C(19)-C(20)	1.388(3)	C(20)-C(21)	1.393(2)	C(21)-C(22)	1.389(2)

C(25)-C(26)	1.329(2)	C(26)-C(27)	1.472(2)	C(27)-C(28)	1.384(2)
C(27)-C(32)	1.401(2)	C(28)-C(29)	1.393(2)	C(29)-C(30)	1.383(2)
C(30)-C(31)	1.391(3)	C(31)-C(32)	1.378(3)		

O(2)-S(1)-O(1)	117.45(7)	O(2)-S(1)-C(4)	110.14(7)
O(1)-S(1)-C(4)	111.15(8)	O(2)-S(1)-C(1)	108.38(8)
O(1)-S(1)-C(1)	111.80(8)	C(4)-S(1)-C(1)	95.76(7)
C(24)-O(3)-C(7)	114.89(12)	C(30)-O(4)-C(33)	117.06(15)
C(20)-O(5)-C(23)	116.83(14)	C(2)-N(1)-C(10)	115.90(12)
C(2)-N(1)-C(9)	114.34(13)	C(10)-N(1)-C(9)	110.45(12)
C(8)-C(1)-C(2)	115.77(14)	C(8)-C(1)-S(1)	110.17(11)
C(2)-C(1)-S(1)	102.45(10)	N(1)-C(2)-C(3)	110.83(12)
N(1)-C(2)-C(1)	117.09(12)	C(3)-C(2)-C(1)	107.62(12)
C(7)-C(3)-C(4)	104.46(12)	C(7)-C(3)-C(2)	116.51(12)
C(4)-C(3)-C(2)	111.70(12)	C(5)-C(4)-C(3)	107.51(12)
C(5)-C(4)-S(1)	115.36(11)	C(3)-C(4)-S(1)	105.15(10)
C(17)-C(5)-C(6)	116.04(13)	C(17)-C(5)-C(4)	115.40(12)
C(6)-C(5)-C(4)	100.71(12)	C(7)-C(6)-C(5)	102.94(12)
O(3)-C(7)-C(25)	108.56(12)	O(3)-C(7)-C(6)	110.20(12)
C(25)-C(7)-C(6)	117.24(13)	O(3)-C(7)-C(3)	105.82(12)
C(25)-C(7)-C(3)	113.01(12)	C(6)-C(7)-C(3)	101.32(12)
N(1)-C(10)-C(11)	110.16(13)	C(16)-C(11)-C(12)	118.73(16)
C(16)-C(11)-C(10)	121.53(16)	C(12)-C(11)-C(10)	119.73(14)
C(13)-C(12)-C(11)	120.74(16)	C(12)-C(13)-C(14)	119.94(17)
C(15)-C(14)-C(13)	119.87(17)	C(14)-C(15)-C(16)	120.24(17)
C(11)-C(16)-C(15)	120.48(18)	C(22)-C(17)-C(18)	117.70(15)
C(22)-C(17)-C(5)	121.71(14)	C(18)-C(17)-C(5)	120.56(14)
C(19)-C(18)-C(17)	121.48(16)	C(18)-C(19)-C(20)	119.84(16)
O(5)-C(20)-C(19)	115.93(15)	O(5)-C(20)-C(21)	124.25(16)
C(19)-C(20)-C(21)	119.81(15)	C(22)-C(21)-C(20)	119.19(15)
C(17)-C(22)-C(21)	121.93(15)	C(26)-C(25)-C(7)	126.58(14)
C(25)-C(26)-C(27)	126.66(15)	C(28)-C(27)-C(32)	117.24(16)
C(28)-C(27)-C(26)	119.52(15)	C(32)-C(27)-C(26)	123.21(16)
C(27)-C(28)-C(29)	122.56(15)	C(30)-C(29)-C(28)	119.12(16)
O(4)-C(30)-C(29)	124.74(17)	O(4)-C(30)-C(31)	115.96(17)
C(29)-C(30)-C(31)	119.29(17)	C(32)-C(31)-C(30)	120.93(18)
C(31)-C(32)-C(27)	120.85(17)		